

**POLYCAPROLACTONE BLOCK COPOLYMER  
NANOSCAFFOLDS FOR DRUG DELIVERY TO  
CANCER CELLS**

A THESIS

SUBMITTED IN PARTIAL FULFILMENT OF THE REQUIREMENTS  
OF THE DEGREE OF

**DOCTOR OF PHILOSOPHY**

BY

**BAPURAO SURNAR**

**Reg No: 20103066**



**DEPARTMENT OF CHEMISTRY  
INDIAN INSTITUTE OF SCIENCE EDUCATION AND  
RESEARCH PUNE – 411 008**

**ARPIL 2016**

*Dedicated to*  
*My Parents*



भारतीय विज्ञान शिक्षा एवं अनुसंधान संस्थान पुणे  
INDIAN INSTITUTE OF SCIENCE EDUCATION AND RESEARCH PUNE  
(An Autonomous Institution of Ministry of Human Resource Development, Govt. of India)  
Dr. Homi Bhabha Road, Pune - 411 008.

**Dr. M. Jayakannan**  
Department of Chemistry

**CERTIFICATE**

Certified that the work incorporated in the thesis entitled “*Polycaprolactone Block Copolymer Nanoscaffolds for Drug Delivery to Cancer Cells*” Submitted by Mr. Bapurao Surnar was carried out by the candidate under my supervision. The work presented here or any part of it has not been included in any other thesis submitted previously for the award of any degree or diploma from any other University or Institution.

Date: 15<sup>th</sup> April 2016  
Pune (MH) India

  
**Dr. M. Jayakannan**  
(Thesis Supervisor) 15/4/2016

## DECLARATION

I affirm that this written thesis document represents my own ideas in words and the ideas that I adopted from others' have been adequately cited and referenced the original sources. I also declare that I have obeyed to all principles of scientific honesty, integrity and have not misrepresented or fabricated or falsified any idea/data/fact/source in my submission. I understand that violation of the above will be cause for disciplinary action by the institute and can also suggest penal action from the sources which have thus not been properly cited or from whom proper permission has not been taken when desired.

**Date: 15<sup>th</sup> APRIL 2016**

**Pune (MH) India**

  
**Bapurao Surnar** 15/4/2016

**Roll No: 20103666**



## **ACKNOWLEDGEMENTS**

The journey of PhD would not have been possible without exclusive of help and support of the kind of peoples around me. Foremost, I wish to thank my supervisor **Dr. M. Jayakannan**, for his exceptional guidance, invaluable suggestions, constant encouragement, and support during these past five years. His observations and comments assisted to set up the overall direction of my research and to move ahead with investigation profoundly. I always ended up with confidence and full of energy after discussion with him. His encouragement and help made me feel confident to overcome every difficulty I encountered. I had a great liberty to plan and execute my ideas in research without any pressure. I believe from my heart that he is dream supervisor for a student who desire to perform research and I am blessed to be one of those who had an opportunity to work with him.

I would like to thank **Dr. Harinath Chakrapani (HC)** and **Dr. K. krishnamoorthy** for being my research advisory committee (RAC) members and providing me valuable comments during RAC meetings, which enabled me to notice the shortcomings of work and make necessary improvements. I am extremely thankful to **HC** for his extensive discussions, constructive criticism, valuable suggestions and all the freedom given me to access instruments and culture room facilities.

I would like to express my sincere thanks to **Prof. K.N. Ganesh**, Director, IISER-Pune for providing world class research facility at IISER Pune carrying out this research work.

I am grateful to **Dr. Asha, S. K.** for her constant support and for extending research facilities in her laboratory.

I would like to thank all the faculty members in the department of chemistry, IISER Pune for interactive scientific discussions and teaching me various chemistry courses.

Special thanks to my present and former lab mates for their support and cooperation which made my life memorable at IISER, Pune especially, Mahima, Bala, Smita, Ananthraj, Pramod, Narsimha, Rajendra, Bhagyashree, Sonashree, Nilesh, Mehak, Moumita, Harpreeth, Anuj, Uma, Vikas, Thameez, Maithreyi, Lipi, Khushboo, Shraddha, Nithish, Hemlatha, Rekha, Kaushal, Nagesh, Chinmay, Shekar, Nisha, Senthil, Saibal, Prajitha, Swapnil, Sandeep and Sarabhjoth.

I take this occasion to say my earnest thanks to Kavita Sharma for providing me experimental hands-on-training on different aspects of cell culture methods and MTT assays. I owe gratitude to all **HC** lab members.

I would like to thank all instruments' technicians of IISER Pune for their support: Pooja, Deepali (NMR), Swati (MALDI), Neetha (HRMS), Meghna (AFM), Anil, Yatish (FE-SEM) and Vijay (CLSM). I thank National Chemical Laboratory (NCL) Pune for HR TEM and SLS facilities.

I am indebted to many other friends for providing an inspiring and fun filled environment in IISER Pune, especially Rajendra, Sharad, Ravikiiran, Krishna, Somu, Arindam, Venki (Noble), Kishor, Manna, Dinesh, Reman, Pallu, Rana, all other friends. I also thank all the staff members in administration, finance, accounts, stores, library, canteen especially, Ms. Naina, Mr. Mayuresh, Mr. Nitin and Mr. Ankush for their immediate help whenever I needed them. I also thank the entire cleaning depot to keeping campus clean and clear.

I would like to acknowledge with tremendous and deep thanks to my Parents, my brothers (Srinivas, Ganesh and Ashish) and my sisters (Ashwini and Megha) for their whole hearted support and encouragement.

Financial support from UGC and IISER Pune is greatly acknowledged.

Bapu

## **SYNOPSIS**

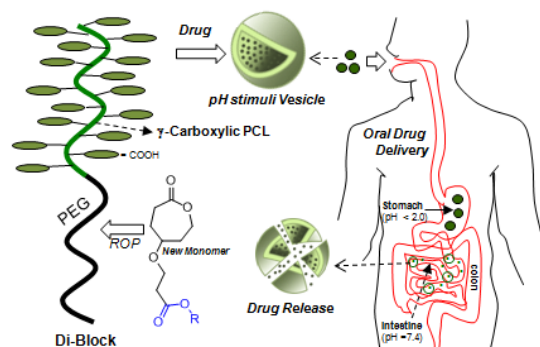
Polymer nano-assemblies are emerging as important nano-scaffolds for loading and delivering anticancer drugs and genes in cancer treatment. Among the diverse synthetic polymers, well defined hydrophilic and hydrophobic block copolymers are excellent candidates to precisely control the size and shape of the self-assembled nano-carriers such as micelles and vesicles. These block copolymers can be synthesized in a controlled way to result in narrow polydisperse polymers with high molecular weight as well as bearing pH, enzyme, temperature etc. stimuli in order to disassemble for delivering the loaded cargoes. In this aspect, the development of biodegradable block copolymers is particularly important since the degraded small oligomers or monomeric units after the delivery of the cargoes could be readily excreted from the biological system. The present thesis has aimed to develop new classes of biodegradable block copolymer nano-assemblies based on carboxylic functionalized polycaprolactones (PCL) and demonstrate their delivering capabilities for wide ranges of anticancer drugs such as doxorubicin (DOX), cisplatin, camptothecin and Ibuprofen, etc. The new polymer scaffolds were employed as oral delivery vehicles under gastrointestinal (GI) tract and also deliver of drugs at the intracellular level in cancer cells. The thesis has been divided into following five chapters:

- (i) Chapter 1: The introduction chapter provides complete literature survey on block copolymers synthesis and self-assembly, application in biomedical field and describe the aim of the thesis work.
- (ii) Chapter 2: New classes of *pH responsive carboxylic substituted polycaprolactones* were designed and developed. Synthesis of new monomers by multi-step reactions, block copolymer synthesis via ring opening polymerization methodology, self-assembly of block copolymers into vesicles and study their *in vitro* drug delivering capabilities under gastrointestinal tract (GI).
- (iii) Chapter 3: *Hydrogen-bond controlled anticancer drug delivery* strategy was developed for intracellular delivery of drugs. Enzyme-responsiveness of the hydrogen bonded biodegradable diblock copolymers were programmed for “burst” versus “controlled” release of drugs at the intracellular level.
- (iv) Chapter 4: PCL *diblock copolymer-cisplatin core-shell nanoparticles* were developed to overcome the detoxification of cisplatin drugs against cytoplasmic thiol residues such as glutathione and cysteine. The core-shell nanoparticles were very

stable in saline, phosphate saline buffer (PBS) and blood serum (FBS) and exclusively cleaved at the intracellular level by enzymes to deliver the Pt-drugs.

- (v) Chapter 5: New classes of triple layer nano-particles were developed to achieve the combination therapy of DOX and cisplatin together from single nano-carrier. This method accomplished the synergistic killing of breast cancer cells via combination therapy.

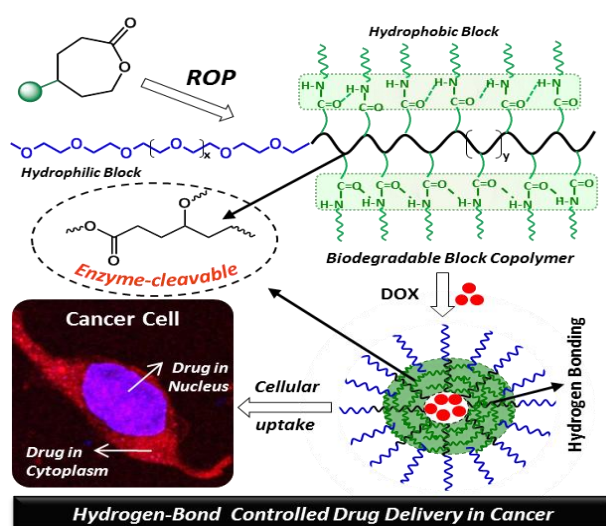
In chapter 2, new carboxylic functionalized poly(caprolactone) (PCL) block copolymer vesicles was developed as novel dual drug delivery pH responsive vehicles for oral administration under gastrointestinal (GI) tract. New carboxylic functionalized caprolactone monomer was custom designed through multi-step organic reactions and



polymerized under controlled ROP conditions using polyethylene glycol as initiator. These carboxylic PCL block copolymers were self-organized into 100-250 nm vesicular assemblies. The size and shape of the vesicular assemblies were confirmed by light scattering, Zeta potential and electron microscopy. These vesicles were capable of loading both hydrophilic molecules (like rhodamine B, Rh-B) and hydrophobic drugs such as Ibuprofen (IBU) and camptothecin (CPT) in the core and layer, respectively. These pH responsive PCL vesicles were stable in strong acidic conditions ( $\text{pH} < 2.0$ , stomach) and ruptured to release the loaded cargoes under neutral or basic pH ( $\text{pH} = 7.0$ , similar to that of small intestine). The drug release kinetics under simulated GI tract revealed that the individual drug loaded vesicles followed the combination of diffusion and erosion pathway whereas the stable dual drug loaded vesicles predominantly followed the diffusion controlled process.

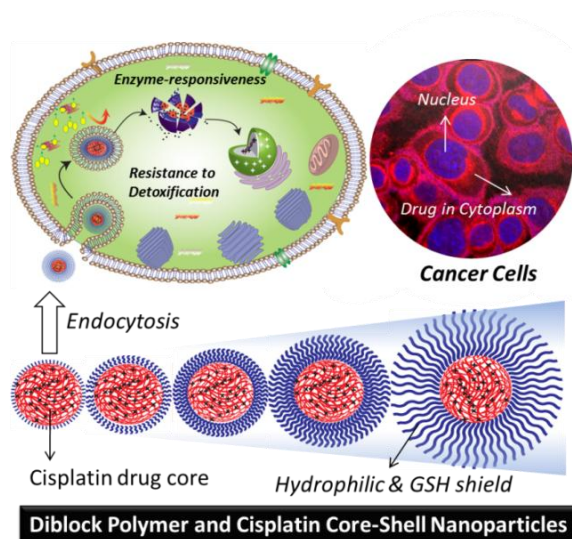
In chapter 3, hydrogen-bond controlled drug delivery strategy has been designed to programme the enzymatic degradation of block copolymer nano-assemblies at the intracellular compartments to deliver drugs to cancer cells. Hydrogen bonded polycaprolactone-block-polyethylene glycol copolymers were custom designed and self-assembled as aqueous micellar aggregates of  $\sim 90$ -160 nm. These diblock polymer nanoparticles exhibited excellent capability for loading doxorubicin (DOX) and stabilized the drugs against leaching at extracellular circularly conditions ( $37^\circ\text{C}$  in PBS). At the intracellular level, lysosomal-esterase enzyme degraded the aliphatic polyester PCL backbone

to release DOX in steady and controlled profiles. Cytotoxicity studies in cervical cancer (HeLa) and breast cancer (MCF 7) cell lines revealed that the newly engineered hydrogen bonded diblock copolymers are non-toxic to cells. In vitro cytotoxicity experiments pointed out that the controlled DOX release from hydrogen bonded nanoparticles exhibited slow and steady cell killing compared to that of their non-hydrogen



bonded analogues. *In vivo* mimicking cell line experiments were designed to study the action of drug on breast and cervical cancer cells by programmed incubation period. These cell line experiments provided direct evidence for hydrogen-bond controlled lysosomal enzymatic cleavage of polymer-drug scaffolds at the intracellular level on their cell killing ability.

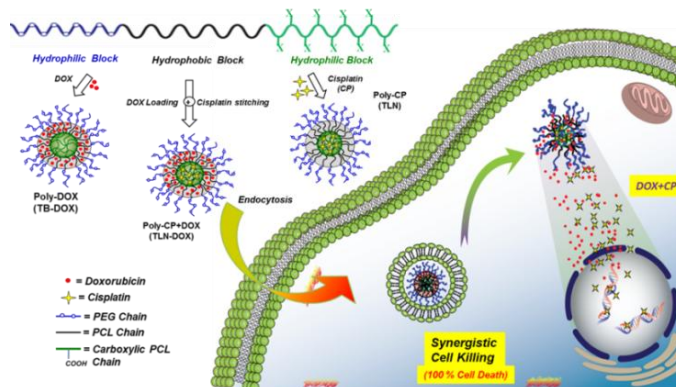
In chapter 4, glutathione resistant polymer-cisplatin core shell nanoparticles were custom designed based on biodegradable carboxylic functional polycaprolactone (PCL)-block- polyethylene glycol diblock copolymers. The core of the nanoparticle was fixed as 100 carboxylic units and shell part was varied using various molecular weight polyethylene glycol monomethyl ethers (MW of PEGs =100 to 5000 g/mol) as initiator in the ring opening polymerization. The complexation of cisplatin aquo species with the diblocks produced core-shell nanoparticles of 75 nm core with precise size control of the particles from 1 to 190 nm. The core-shell nanoparticles were found to be stable in saline and PBS and they exhibited enhanced stability with increase in the PEG shell at the periphery. The hydrophobic PCL layer on the periphery of the cisplatin core has behaved as protecting layer against the cytoplasmic thiol residues (GSH and cysteine) and exhibited < 5 % of drug detoxification. *In vitro* drug release studies revealed that the core-shell nanoparticles were ruptured upon exposure to lysosomal enzymes like esterase at the intracellular compartments. Cytotoxicity studies were performed both in normal wild



type mouse embryonic fibroblasts (Wt-MEFs) cells, breast cancer (MCF 7) and cervical cancer (HeLa) cell lines. Free cisplatin and polymer drug core-shell nanoparticles showed similar cytotoxicity effect in the HeLa cells. In MCF 7 cells, the free cisplatin drug exhibited 50 % cell death whereas complete cell death (100 %) was accomplished by the polymer cisplatin core-shell nanoparticles. Confocal microscopic images confirmed that the core-shell nanoparticles were taken up by the MCF 7 and HeLa cells and they were accumulated both at the cytoplasm as well at peri-nuclear environments.

In chapter 5, combination chemotherapy is developed to overcome the drug GSH-detoxification and DNA repair based on new triple layer nanoparticles (TLNs). These TLNs were custom designed based on polyethylene glycol-*block*-polycaprolactone-*block*-carboxylic functional polycaprolactone triblock copolymers PEG-PCL-CPCL (TBs). The complexation of cisplatin aquo species with the triblock copolymers fabricated triple layer nanoparticles (TLNs) of  $150\pm 10$  nm size. The hydrophobic anticancer drug DOX was encapsulated in middle PCL layer of TLNs to achieve synergistic cell killing in breast cancer cells. These dual loaded nanoparticles were found to be stable in PBS; they exhibited ~ 90 % cisplatin stability due to subsumed PCL layer between PEG shell and CPCL core. The hydrophobic PCL layer also behaved as a protecting layer against the cytoplasmic GSH and completely inhibited the drug detoxification. *In vitro* drug release studies revealed that the dual loaded nanoparticles ruptured upon exposure to

lysosomal enzymes and showed controlled release up to 2 days. Cytotoxicity studies were performed both in normal wild-type mouse embryonic fibroblasts (Wt-MEFs) cells, breast cancer (MCF 7) and cervical cancer (HeLa) cell lines. In MCF 7 cells, the free cisplatin drug exhibited 50 % cell death whereas complete cell death (100 %) with synergistic killing was accomplished by the TLNs.



The overall conclusion of the thesis work revealed that the tailor-made carboxylic acid substitute caprolactones are potential block copolymer biomaterial candidates and also they exhibited excellent drug loading and delivering capabilities for DOX, cisplatin, camptothecin and Ibuprofen, etc. The last chapter summarized the thesis work with future perspectives.

## TABLE OF CONTENTS

<b>Chapter 1: Introduction</b>	<b>1-47</b>
1.1. Introduction to Block Copolymer	2
1.2. Applications of the Block Copolymer	6
1.3. Self-assembly of Amphiphilic Block Copolymers	9
1.3.1. Block Copolymer Micelles	11
1.3.2. Block Copolymer Nanospheres	12
1.3.3. Block Copolymer Nnanocapsules	13
1.3.4. Block Copolymer Vesicles	14
1.4. Bio-degradable Block Copolymers	16
1.4.1. Ring-Opening Polymerization	17
1.4.2. Polyglycolide or poly(glycolic acid) (PGA)	20
1.4.3. Polylactide (PLA)	20
1.4.4. Poly(lactide- <i>co</i> -glycolide) (PLGA)	21
1.4.5. Polycaprolactone (PCL)	22
1.5. Funtional Polycaprolactone as Drug Carriers	29
1.6. Aim of the Thesis	38
1.7. References	40
<b>Chapter 2: Stimuli-responsive Poly(caprolactone) Vesicles for Dual Drug Delivery under GI Tract</b>	<b>48-83</b>
2.1. Introduction	50
2.2. Experimental Methods	54
2.2.1 Materials	54
2.2.2. General Procedures	54
2.3. Results and Discussion	61
2.3.1. Synthesis and Characterization of Polymers	61
2.3.2. Self Assemblies of Substituted PCL	66
2.3.3. Encapsulation Capabilities of the PCL Vesicles	69
2.3.4. pH Response and Zeta potential of the PCL Vesicles	73
2.3.5. <i>In vitro</i> delivery under simulated GI tract	74

2.4. Conclusion	77
2.5. References	79

**Chapter 3: Hydrogen-Bond Controlled Drug Delivery to Cancer Cells by  
Programming the Enzyme Degradation in Block Copolymer**

**Nano-assemblies 84-119**

3.1. Introduction	86
3.2. Experimental Methods	91
3.2.1. Materials	91
3.2.2. General procedures	91
3.3. Results and Discussion	100
3.3.1. Synthesis and Characterization of Di-block Copolymers	100
3.3.2. Self-assembly of Amphiphilic Di-blocks	102
3.3.3. Variable temperature <sup>1</sup> H-NMR analysis	105
3.3.4. DOX Encapsulation in Di-blocks	106
3.3.5. <i>In vitro</i> DOX release studies	108
3.3.6. Cytotoxicity of DOX-loaded nanoparticles	110
3.3.7. Confocal Imaging and Cellular Uptake	114
3.4. Conclusion	116
3.5. References	118

**Chapter 4: Core-Shell Polymer Nanoparticles for Prevention of GSH**

**Drug Detoxification and Cisplatin Delivery 120-162**

4.1. Introduction	122
4.2. Experimental Methods	127
4.2.1. Materials	127
4.2.2. General Procedures	127
4.3. Results and Discussion	136
4.3.1. Synthesis of Block Copolymer-Cisplatin prodrug	136
4.3.2. Cisplatin chelation with polymers	140
4.3.3. Size and shape of the Polymer-Cisplatin prodrug	144



4.3.4. Core-shell nanoparticle stability	147
4.3.5. GSH Resistance and Enzyme-responsive cleavage	149
4.3.6. Cellular Uptake and Cytotoxicity	152
4.4. Conclusion	158
4.5. References	160

**Chapter 5: Triple Layer Nanoparticle Approach for Cisplatin-Doxorubicin  
Combination Therapy** **163-202**

5.1. Introduction	165
5.2. Experimental Methods	170
5.2.1. Materials	170
5.2.2. General Procedures	170
5.3. Results and Discussion	177
5.3.1. Synthesis and Characterization of triblocks	177
5.3.2. Cisplatin chelation with triblocks	181
5.3.3. Size and shape of the polymer-cisplatin prodrug	183
5.3.4. Stability of triple layer nanoparticles in PBS	184
5.3.5. Stability of triple layer nanoparticles against esterase	186
5.3.6. GSH Detoxification	187
5.3.7. Cytotoxicity of TLNs	188
5.3.8. DOX Encapsulation	190
5.3.9. Cytotoxicity of TB-DOX	193
5.3.10. Cytotoxicity of TLN-DOX	195
5.3.11. Cellular Uptake of TLN-DOX	197
5.4. Conclusion	198
5.5. References	200

***Summary and Future Directions*** **203-208**

***List of Publications*** **209-210.**

*Chapter 1*

---

---

*Introduction*

## 1.1. Introduction to Block Copolymer

Prior to 1920's the chemists disbelieved the existence of molecules with higher than a few thousand molecular weights.<sup>1-2</sup> Hermann Staudinger, whose revelation about the polymeric structure of rubber, based on an isoprene repeating unit, challenged this limiting view.<sup>3</sup> From this point forth there was an exponential growth in the field of polymer chemistry and enormous efforts went into achieving more controlled polymerization kinetics.<sup>4</sup> After the invention of the living character of polymerization in the mid-1950s by Szwarc, the anionic polymerization process on copolymers (mainly block copolymers) becomes one of the major areas of research in the polymer science and technology.<sup>5</sup>

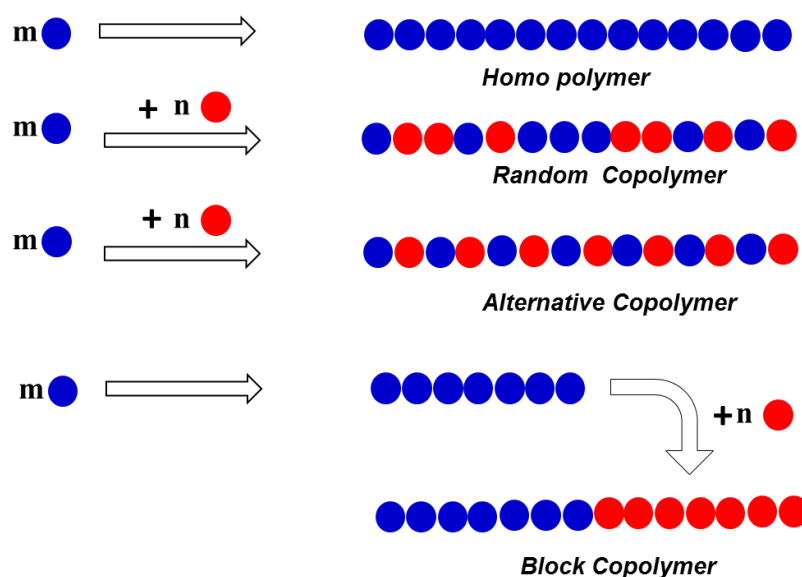


**Figure 1.1.** *Types of different copolymers.*

Polymers are formed by attaching of similar or different monomers together, these results in the homo and copolymers respectively.<sup>6</sup> As shown in figure 1.1 similar monomer units come together to form homopolymers and two or more monomers come together to form copolymers. For example two monomers stitch together to form copolymer, hence depending on the monomer arrangement they were divided as follows. In random copolymers monomers are arranged in random fashion, and in alternating copolymers they occur in a regular alternating fashion. On the other hand, block copolymers involve two or more homopolymer parts connected together through covalent bonds. The synthesis of these block copolymers (see figure 1.1) primarily involves the homo polymerization of a single monomer

and subsequently another monomer is added which grows beside the homopolymer to yield a block copolymer. In this process, depending on the monomers used, polymers can be subdivided into diblock (two monomers) and triblock (three different monomers). In the introduction chapter the synthesis, applications of the block copolymers are discussed in detail.<sup>7-8</sup>

Block copolymers are a distinct type of polymers in which each chain consists of two or more different segments of varying monomers joined in certain architecture by a covalent bond. Henceforth, these block copolymers are classified by the number of blocks and their arrangement.<sup>9</sup> Block copolymers with two, three, or more blocks are called as di, tri, and multi block copolymers respectively. If considering the block copolymer topology it can be linear or star. In linear arrangement the blocks are linked end-to-end, and in star topology they are connected through one of their ends at a single junction. The higher order arrangements like brushes and miktoarm stars are also possible.<sup>10-11</sup> The different types of block copolymer arrangements are schematically presented in Figure 1.2.

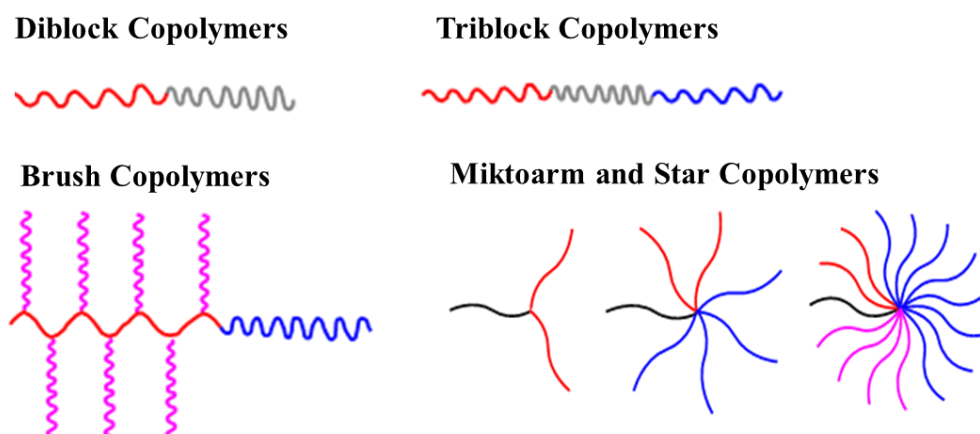


**Figure 1.2.** Various block copolymer architectures (adapted from England et al. *Polym. Chem.* **2010**, *1*, 1533–1544).

Block copolymers have attracted enormous interest due to their capacity to self-assemble into nano-sized assemblies.<sup>12-15</sup> The molecular architecture of the block copolymer, which consists of two or more chemically distinct homopolymers tied to each other, so the strength of the repulsive interaction between blocks is sufficiently large, leads to microphase separation of dissimilar polymer chains into periodic domains whether in the solid or solution state.<sup>16-17</sup> Typical dimensions of these micro-aggregates (micro-domains) range from 5 to 100 nm usually, a range that encompasses the sizes needed by the semiconductor industry for the construction of future integrated circuits (ICs).<sup>1-20</sup> The rate of progression of modern

semiconductor devices is ruled by the ability to generate high-resolution patterns on substrates of electronic materials. Consideration of these issues has heightened an already growing interest in the use of self-assembly of materials as a means for patterning solid surfaces.<sup>21</sup> Self-assembly, in principle, offers well-organized structures with molecular level precision. In an ultimate application of self-assembly, nanoscale device components might be directly deposited on a substrate in a self-organized fashion to form a functioning circuit. This strategy creates opportunity to utilize the profits of self-assembly in an evolutionary way.<sup>22</sup> In order to pursue this goal, a huge amount of efforts were taken to understand the self-assembly of the block copolymers.

Many synthesis strategies have been widely employed to prepare block copolymers with well-defined structure, molecular weight, and composition. Besides classical synthetic routes such as living anionic and cationic polymerization, in recent years, new polymerization methods have engendered intense interest among polymer chemists.<sup>23-25</sup> The arrival of controlled radical polymerization (CRP) started through the invention of nitroxide mediated polymerization (NMP) and furthered by the expansion of atom transfer radical polymerization (ATRP) and reversible addition fragmentation chain transfer (RAFT) polymerization has initiated a resurgence in the use of free radical polymerization for the preparation of functional polymeric materials (see figure 1.3 – 1.5).<sup>26-27</sup>

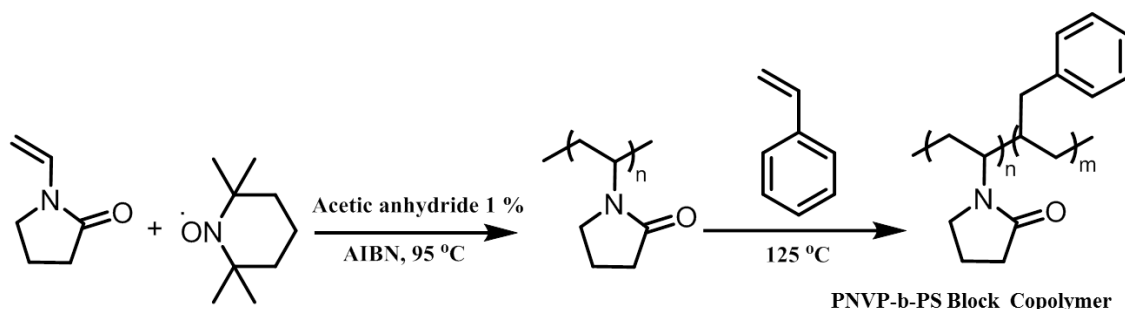
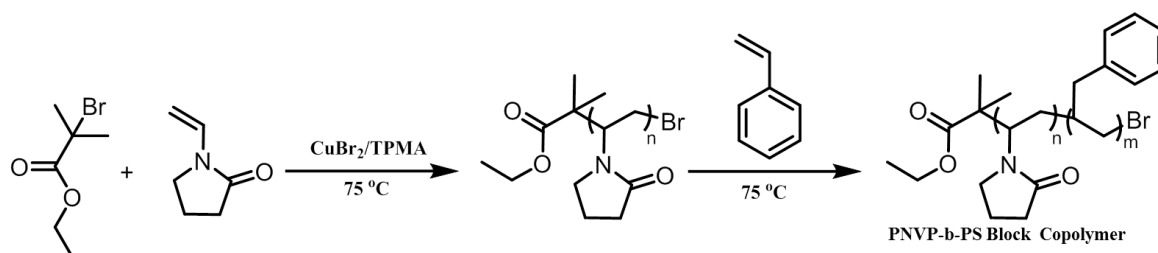


**Figure 1.3.** Synthesis of PNVP-*b*-PS block copolymer using nitroxide mediated polymerization (NMP) (adapted from Bilalis et al. *J. Polym. Sci. A Polym Chem.* **2006**, *44*, 659–665).

These techniques provided ease of synthesis in functional polymers with controlled molar mass, narrow polydispersities (PDI) and defined molecular architecture including block, gradient, graft and star copolymers.<sup>27</sup> These methods combine the aids of the robust nature of conventional radical polymerization with the capability to prepare well-defined macromolecular architectures common to living polymerization techniques.<sup>28</sup> These

polymerization techniques facilitated the growth of the block copolymer area in manifolds. These controlled radical polymerization techniques (CRP) have been described in detail in these reviews Matyjaszewski et al.<sup>29-30</sup>

**Figure 1.4.** Synthesis of polystyrene using (adapted from Bilalis et al. *J. Polym. Sci. A Polym Chem.* **2006**, *44*, 659–665).



Nitroxide-mediated radical polymerization (NMP) is a protocol that makes use of an alkoxy amine initiator to produce polymers with well controlled and defined stereochemistry and narrow polydispersity index. As an example the synthesis of PNVP-*b*-PS using NMP technique is depicted in figure 1.3, where using alkoxy amine initiator homopolymer was prepared and second monomer styrene was added to generate the block copolymer.<sup>30</sup> ATRP is one of the examples of reversible-deactivation radical polymerization i.e. polymerization processes by formation of the carbon-carbon bond through a transition metal catalyst (see figure 1.4).<sup>31</sup>

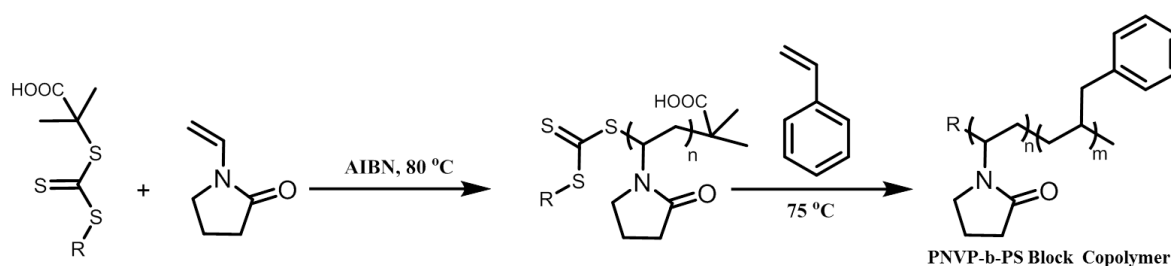
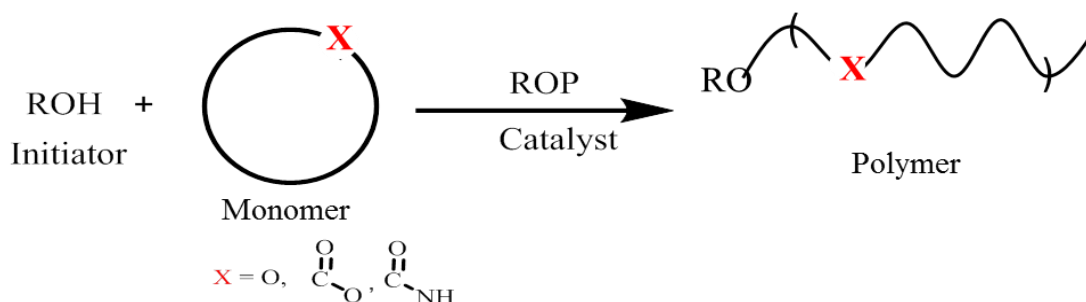


**Figure 1.5.** Synthesis of PNVP-*b*-PS block copolymer using RAFT polymerization. (adapted from Bilalis et al. *J. Polym. Sci. A Polym Chem.* **2006**, *44*, 659–665).

The atom transfer is a key step in the polymerization responsible for defined polymer chain development. In the RAFT technique thio-carbonyl-thio compounds were used as initiator, where chain transfer agent is in the form of an initiator to achieve control over the produced molecular weight and polydispersity index during polymerization (see figure 1.5).<sup>32</sup>



**Scheme 1.1.** Schematic representation of ROP of cyclic ethers ( $X=O$ ), lactones ( $X=COO$ ), lactams ( $X=CONH$ ).

Ring opening polymerization (ROP) also popularized in producing controlled and narrow dispersed molecular weights. The major benefit of these methods is their tolerance to a large variety of functional groups, with the additional advantage of controlled polymerization (see scheme 1.1). The block copolymers produced from these techniques are known to have narrow polydispersity with controlled molecular weights, which means the properties achieved from these polymers will be highly accurate.<sup>33</sup> Block copolymers can also be synthesized by coupling end-functionalized polymers or for instance chemical modification of a given homopolymer by hydrogenation (discussed in detail below).

## 1.2. Applications of the Block Copolymer

Over the last two decades, incredible research efforts have been taken to study the potential applications of block copolymers in advanced technologies, such as information storage, drug delivery, photonic crystals, etc. These studies have shown that block copolymers are very important candidates for applications in these areas.<sup>34</sup>

The most important and popular application of block copolymers is their use as thermoplastic elastomers (TPEs). TPEs were considered to be one of the major breakthroughs in rubber technology.<sup>35</sup> Thermo plasticity and elasticity these are two conflicting terms. At the molecular level, non-cross linked chains brings the thermo plasticity, whereas elasticity is reliable with cross linked chains. These materials are so versatile that they are widely used in wine bottle stoppers, outer coverings for optical fibre cables, jelly candles, adhesives, bitumen modifiers and in artificial synthetic organ technology.<sup>36</sup> The first commercially available TPEs were produced by B. F. Goodrich Co. in the late fifties and were based on polyurethanes (TPU).<sup>37</sup> These polymers have excellent strength, wear, and oil resistance and

are used in automotive bumpers, snowmobile treads, etc. Later on, styrenic TPEs (Shell, as Kratton) based on polyesters, TPEs (du Pont) based on polyamides were introduced into the market.<sup>38</sup> Furthermore, unlike vulcanized rubber, they can be reused.

The applications of block copolymers in Conventional and potential high-technology are completely based on their ability to self-assemble, in bulk and in selective solvents, into ordered nanostructures. By changing the molecular weight, chemical structure, molecular architecture, and composition of block copolymers, the size scale, the type of ordering, and the features of these nanostructures can be tuned.<sup>39</sup>

Nanometre-scale patterning of materials is an important objective of current science and technology due to the miniaturization of electronic,<sup>40</sup> optoelectronic,<sup>41</sup> and magnetic devices.<sup>43</sup> Block copolymers, which have the ability to self-assemble into periodic ordered microstructures in bulk, are found to be useful candidates for patterning nanostructures. The bulk self-assembly of block copolymers leads to the formation of higher aggregates structures such as body-centered-cubic spheres, hexagonally packed cylinders, bi-continuous gyroids and lamellae as shown in figure 1.6.<sup>44</sup> A few examples of nano patterning by using block copolymers are presented below.

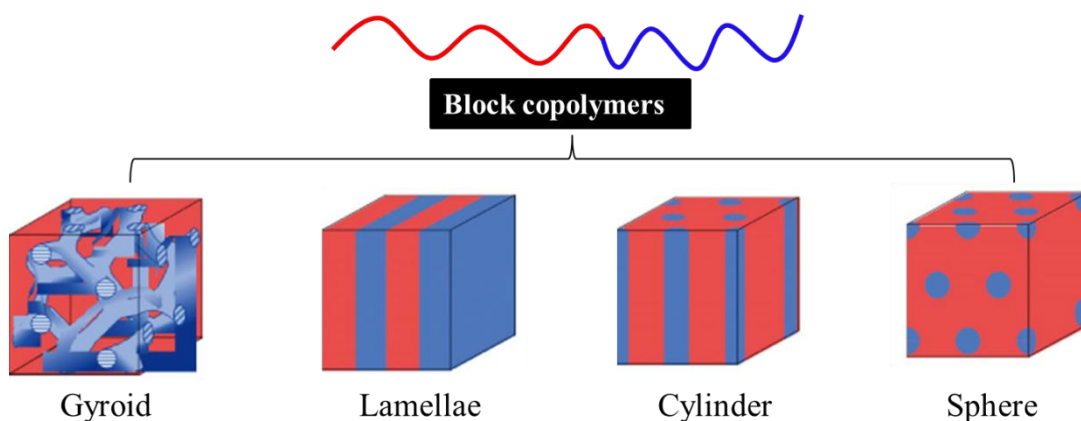


**Figure 1.6.** Block copolymer based self-assemblies in bulk and solution (adapted from Mai *et al. Chem. Soc. Rev.* **2012**, *41*, 5969–5985).

Nano patterning is a very important technique for lithography. The sizes greater than 150 nm can be precisely created by photolithography.<sup>45</sup> The sizes achievable in photolithography are possible due to the tuning of wavelength of light used in the exposure. Electron beam lithography (EBL) is commonly used to access feature sizes between 150 nm and 30 nm. However, sizes less than 30 nm are not easily obtained by standard lithography.



This obstacle can be overcome by using block copolymers, wherein periodic arrays of patterns have been fabricated on silicon wafer using block copolymers.<sup>46</sup> Later on polymer not filled in patterns will be removed; this provides the nanoscale patterns. This technique accesses a length scale difficult to attain by conventional lithography and opens up new routes for the micro patterning domain.

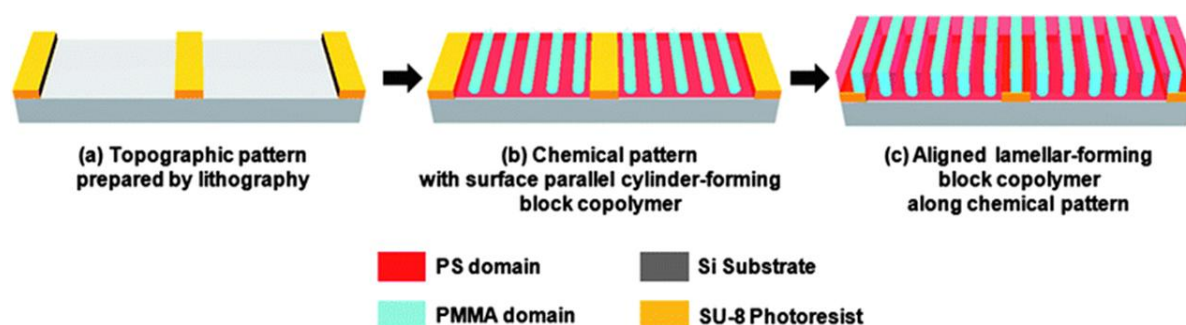


**Figure 1.7.** Nano patterning on silicon substrate using polystyrene-block-PMMA diblock copolymers (adapted from Kim et al. *Soft Matter* **2013**, 9, 2780-2786).

The fabrication of nano patterning using polystyrene-block-PMMA diblock copolymers is shown schematically in figure 1.7.<sup>47</sup> By using the same principle, various dense nano meter patterns can be produced by employing block copolymers. For example, parallel lines can be produced either by a film of lamellae, which are oriented normal to the substrate or by cylinders that lie parallel to the surface. Deep UV exposure degrades the PMMA domains and simultaneously crosslinks the PS matrix.<sup>47-48</sup> By using block copolymers, monoporous and nano-relief ceramic films can be prepared with important applications to address such as next generation catalysts, and photonic materials.

These block copolymers are partially solubilised in solvents to self-aggregate as spherical micelles, vesicles, nano-capsules and nanoparticles.<sup>49</sup> This phenomenon can be used in water purification,<sup>50</sup> tissue engineering,<sup>51-52</sup> bone engineering<sup>53-54</sup> and most importantly, in drug delivery.<sup>55</sup> The selective delivery of drugs to malicious tissues or cells is a very exigent task in medical and pharmaceutical sciences. This is because most of the drugs are toxic to healthy cells and produce side effects, or face solubility problems in the blood plasma, if they are released in non-target systems. Most of the drugs present in the market are hydrophobic compounds, and they are usually subjected to patient through the blood stream. The blood plasma consists of water and a wide variety of dissolved proteins as well as other substances

which the drugs can come in contact with, that eventually decrease the half-life of these drugs.<sup>56</sup>

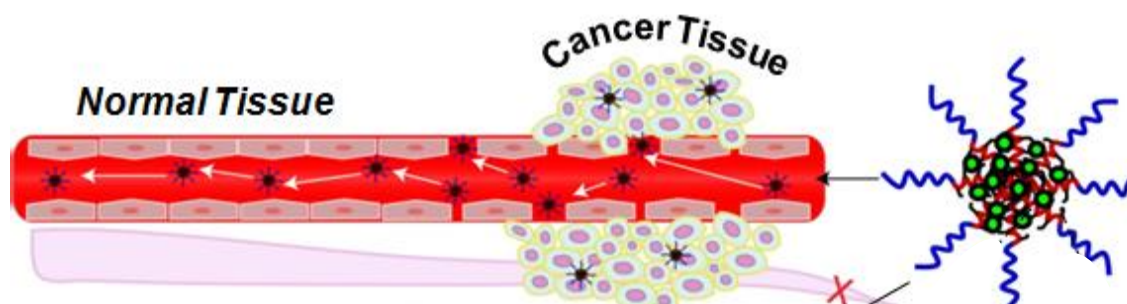


**Figure 1.8.** Illustration of passive targeting of Polymer Drug conjugate by EPR Effect to tumor tissue.

In order to overcome these barriers, block copolymers self-assembled as nano containers act as delivery vehicle for drugs. Block copolymer amphiphiles self-organize in solution to give rise to various morphologies such as micelles, nanoparticles, nanocapsules, polymeric vesicles or polymerosomes and so on.<sup>57</sup> Such nanometer sized (1 to 500 nm) polymeric structures retard the adverse effects associated with the encapsulated drug by controlling the delivery of drug via diffusion or polymer degradation mechanism, long exposure of drug at target site through EPR effect (see figure 1.8), protecting drug from harsh physiological conditions, increasing circulatory longevity with slow rate of renal clearance, enhanced aqueous solubility etc.<sup>58</sup>

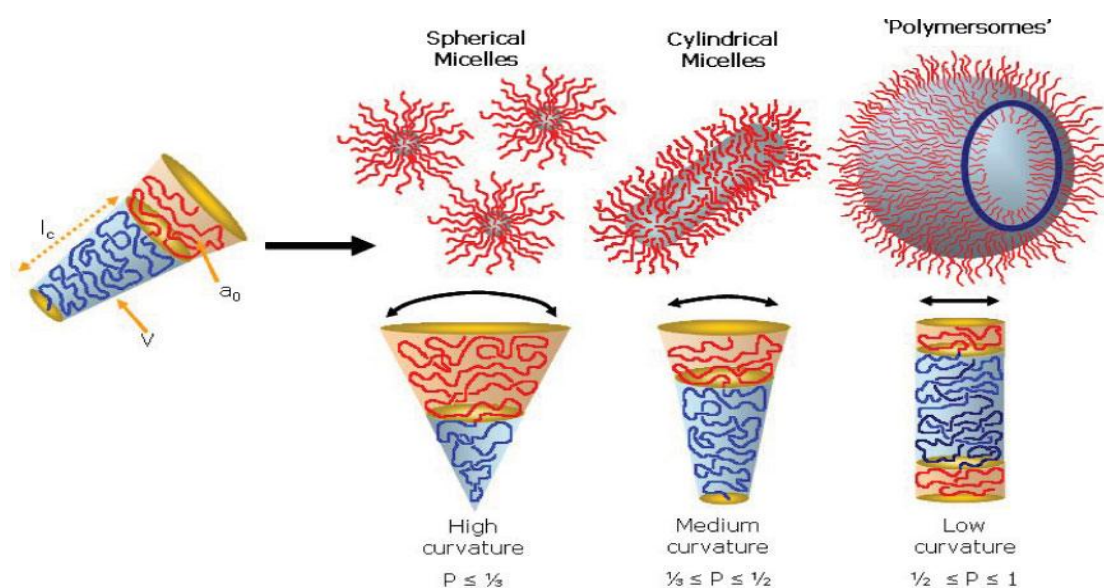
### 1.3. Self-assembly of Amphiphilic Block Copolymers

Block copolymers are made up of two or more fragments of distinct chemical nature that undergo phase separation in water which leads to selective solubility of one of the blocks. During the self-organization process, the hydrophobic blocks tend to be in inner side of the aggregates, whereas the hydrophilic segments position between the inner core and the external aqueous medium.<sup>59-60</sup> These blocks can self-assemble as micelles, vesicles and nano capsules.<sup>57</sup> These unique architectures of block copolymers in water enable the loading and stabilization of hydrophobic and hydrophilic drugs depending upon the self-assembly. As per the general rule proposed by Prof. Israelachvili, the type of supramolecular self-assembly can tentatively be predicted.<sup>61</sup> The various reported morphologies such as spherical micelles, cylindrical micelles and polymerosomes are primarily a result of the inherent molecular curvature and how this influences the packing of the copolymer chains; specific self-

assembled nanostructures can be predicted according to a ‘packing parameter’,  $p$ , which is defined by the equation below:

$$p = n/a_0l_c$$

where  $n$  is the volume of the hydrophobic chains,  $a_0$  is the optimal area of the head group, and  $l_c$  is the length of the hydrophobic tail. Therefore, the packing parameter of a given molecule usually provides its possible self-assembled morphology. As a general rule, spherical micelles are favoured when  $p = 1/3$ , cylindrical micelles when  $1/3 \leq p \leq 1/2$ , and polymersomes when it is  $1/2 \leq p \leq 1$  (see figure 1.9).

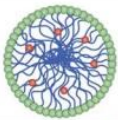
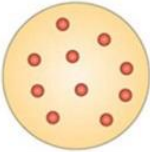
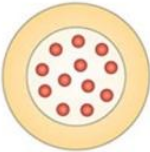



**Figure 1.9.** Various self-aggregated structures created by amphiphilic block copolymers in solvent. (adapted from Armes and co-workers *Macromol. Rapid Commun.* **2009**, 30, 267–277).

Scaffold to be used as a drug delivery vehicle must consist of a water-soluble block (hydrophilic), in order to impart solubility to the container under blood plasma conditions and a water insoluble block (hydrophobic) compatible with the drug to be carried.<sup>62</sup> The water-soluble block, that constitutes the outer shell of the carrier, should be biologically inert towards interactions with the antibodies of the organism. In order to achieve selective localization at some specific site or cell in the “vector”, a targeting moiety should be covalently attached to the outer hydrophilic block.<sup>63</sup> In most of the cases, poly ethylene glycol (PEG), a synthetic block, serves the aforementioned purpose. Block copolymers of ethylene oxide with propylene oxide (hydrophobic block), like PEG-*b*-PPO-*b*-PEO triblocks;<sup>64</sup> with benzyl-L-aspartate (BAsp), like PEG-*b*-PBAsp<sup>65</sup> or with caprolactone<sup>66</sup> as PEG-*b*-PCL are

potential candidates for delivery of anticancer drugs that are water-insoluble, for example Doxorubicin (DOX) or Adriamycin (ADN). In aqueous solution these blocks form nano aggregates, with the hydrophobic PPG, PBAsp and PCL chain in the core, surrounded by the hydrophilic PEG corona.

**Table 1.1.** Table shows polymeric self organized structures and its characteristics features (Adapted from Letchford et al. *Eur.J.Pharm. Biopharm.* **2007**, 65, 259-265).

Block Copolymer Based Self-Assembly	Representation	Size (nm)	Characteristics
<b>Micelle</b>		10-100	Hydrophobic core and stabilizes hydrophobic drugs. Low CMC
<b>Nanoparticles (Nanospheres)</b>		10-200	Solid colloidal particle Hydrophobic drug entrapped, encapsulated or chemically bound to the polymer matrix.
<b>Nanoparticles</b>		100-300	Single layer polymer membrane surrounding an oily core or drug reservoir. Encapsulate hydrophobic drug in the core
<b>Vesicles</b>		5 -500	Bilayer polymer membrane surrounds an aqueous reservoir. Encapsulate hydrophilic drugs in core and hydrophobic drugs in membrane. Dual drug loading carriers

### 1.3.1. Block Copolymer Micelles

In aqueous solutions, amphiphilic molecules orient themselves so that the hydrophobic blocks are away from the aqueous environment in order to achieve a state of minimum free energy.<sup>67</sup> There has been great interest in the use of polymeric micelles as drug carriers. The size of the aggregates can be tuned by varying the molecular characteristics of the copolymer. A convenient size range, which can be easily obtained, is 10 to 200 nm; these sizes are acceptable for pharmaceutical applications (table 1.1).<sup>68</sup> At a specific and narrow concentration range of amphiphile in solution, termed the critical micelle concentration (CMC), several amphiphiles will self-assemble into colloidal-sized particles termed micelles. The formation of micelles effectively removes the hydrophobic portion of the amphiphile

from solution minimizing unfavourable interactions between the surrounding water molecules and the hydrophobic groups of the amphiphiles. At concentrations above the CMC value, micelle formation is thermodynamically favourable and stable against disassembly. However, these micelles rapidly disassemble upon dilution to values lower than CMC and the rate at which disassembly takes place depends upon the amphiphiles' structure as well as inter-chain interactions. The core region is encapsulated by a corona composed of the hydrophilic part of the amphiphiles. This outer corona renders advantages like suppression of opsonisation by blood components, thus retarding phagocytosis by macrophages and decreasing clearance by the reticuloendothelial system (RES), resulting in prolonged circulation times.<sup>69-70</sup>

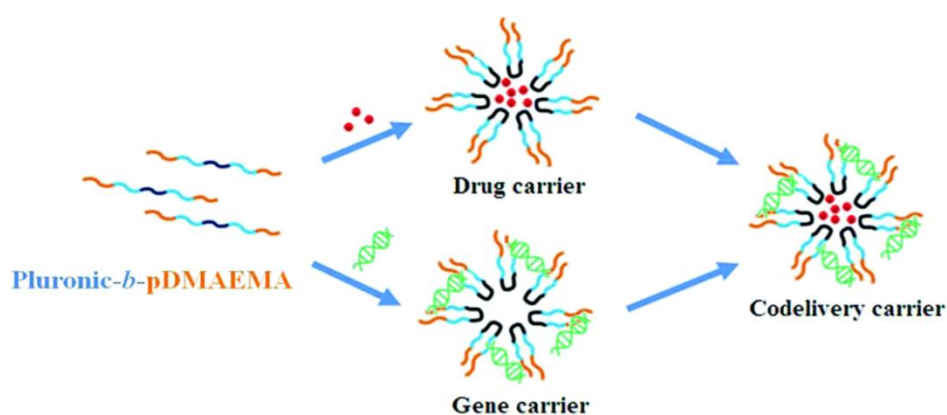


**Figure 1.10.** Pluronic based micellar structure for drug and gene delivery. (adapted from Haung et al. *RSC Adv.* **2014**, *4*, 31552-31563)

Emphasis will be given to three explicit categories of poly(ethylene oxide)-based block copolymers, which are classified according to the chemical nature of the core forming hydrophobic blocks. Therefore, the blocks will be grouped as poly(ethylene oxide)-block-poly(propylene oxide)-block-poly(ethylene oxide), i.e., the Pluronics (see figure 1.10).<sup>71</sup>

### 1.3.2. Block Copolymer Nanospheres

A polymeric nano sphere is defined as a solid colloidal matrix particle in which cargoes are encapsulated or chemically bound to the constituent polymer matrix. These particles are usually larger than micellar aggregates with diameters of 100 to 250 nm and also display significantly high polydispersity.<sup>72</sup> It is shown that the hydrophobic surfaces of these sub-micron nano-aggregates are highly vulnerable to opsonisation and clearance by the RES. Thus, it became clearer that in order to prolong the circulation of nanoparticles in blood plasma, surface needs to be pegylated to resemble water.<sup>73</sup> Various surfactants, such as

poloxamine and poloxame, are used to modify the nanoparticles surface by adsorbing onto it in order to improve its half-life.<sup>74</sup> Nanospheres prepared using amphiphilic copolymers such as MePEG-*b*-PLA with high molecular weight blocks conjugated with PEG coatings provided greater stability. A phase-separated structure for the diblock copolymer nanospheres was observed with a solid core. A clear distinction between micelles and nanospheres formed from diblock copolymers is not always possible, or desirable.<sup>75</sup>

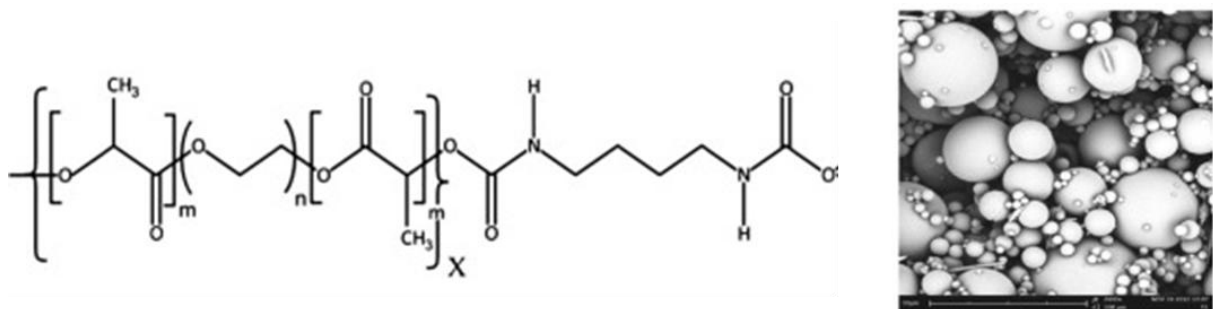


**Figure 1.11:** PEG-*b*-PDLLA block copolymer based suitinib loaded nanospheres. (adapted from Ramazani et al. *Eur. J. Pharm. Biopharm.* **2015**, 95, 368–377).

Experimental studies using a series of PEG-*b*-PDLLA block copolymers, by Riley et al.<sup>76</sup> and Heald et al.<sup>77</sup> investigated the effects of increasing hydrophobicity on the physicochemical properties of nanoparticles manufactured (see figure 1.11). The study revealed that the aggregation behaviour and copolymer architecture of these blocks were entirely dependent on copolymer composition. With increase in the molecular weight of the PDLLA block, the core of the nanoparticles became more solid-like, resembling nanospheres, whereas smaller PDLLA blocks resulted in micelle-like nanoparticle assemblies.

### 1.3.3. Block Copolymer Nanocapsules

Nanocapsule is a vesicle, where an oily liquid constitutes the core surrounded by a single layer of polymer. These systems proved to be useful in the encapsulation and delivery of hydrophobic drugs such as methotrexate, xanthone and 3-methylxanthone.<sup>79</sup> Polymers used for the preparation of nanocapsules includes polyester homopolymers such as PLA, PLGA and PCL.<sup>80-81</sup> Nanocapsules composed of a copolymer of PEG and chitosan have recently been used for the oral delivery of salmon calcitonin, where PEG increased the stability of the nanocapsules in gastrointestinal fluid while reducing their cytotoxicity (see figure 1.12).<sup>82</sup>



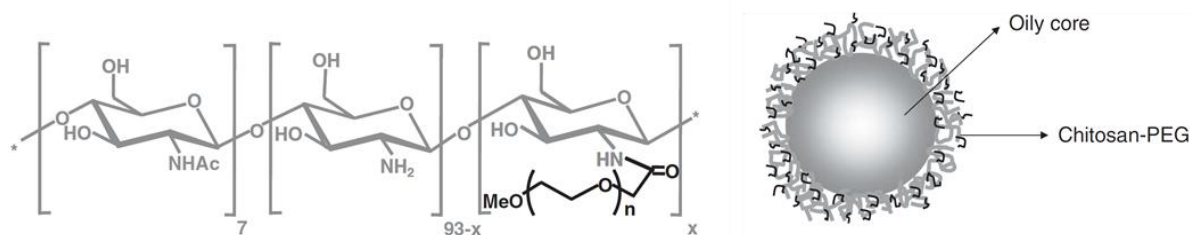


**Figure 1.12.** PEG-g-Chitosan polymer structure and its self-assembly as nanocapsules (adapted from Prego et al. *Journal of Controlled Release* **2006**, *11*, 299–308).

Polymeric micelles, nanospheres and nanocapsules provide opportunity for loading and delivering hydrophobic drug molecules. However, hydrophilic therapeutics such as drug, gene (DNA) and proteins were not possible to load in the above carriers.

#### 1.3.4. Block Copolymer Vesicles

Vesicles with an aqueous reservoir enclosed by a hydrophobic bilayer membrane serve the purpose of dual delivery of the hydrophilic and hydrophobic molecules. Vesicles are ubiquitous higher order self-organized systems that exist in all living organisms from archae-bacteria to human cells.<sup>83-84</sup> These are special assemblies that are self-directed by the association of hydrophobic chains of amphiphilic molecules with the presence of hydrophilic segments on both sides of the membrane. Structurally, it has a hydrophilic hollow cavity along with a hydrophobic membrane as seen in the Table 1.1. Vesicles found in cells are composed of amphiphilic lipid molecules (phospholipids) and are termed as lipid vesicles.<sup>85</sup> The diblock copolymers PEG-*b*-PBD (polybutadiene)<sup>86</sup> and PEG-*b*-PEE (polyethylene)<sup>87</sup> have a high tendency to form vesicle or polymerosomes. Pioneering work in the area of polymerosomes was extensively carried out by Discher and co-workers using the block copolymer, poly (ethylene oxide)-*b*-poly-(ethyl ethylene) (PEO-*b*-PEE).<sup>87</sup> Later, numerous polymers were explored in the literature for the preparation of polymeric vesicles. Block copolymers known to form vesicles have identical amphiphilic character as that of lipids, but instead are composed of covalently connected two or more distinct polymer segments. As shown in figure 1.13, Chen et al. synthesised PEG-*b*-p(DEA-stat-TMA47) block copolymer dual responsive vesicles, capable of loading delivering DOX.HCl.<sup>88</sup>

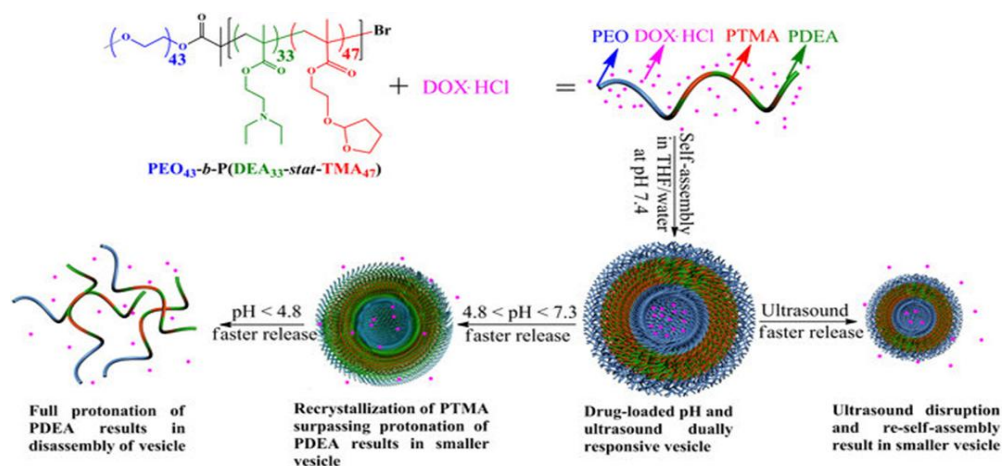


**Figure 1.13.** DOX loaded PEG-*b*-p(DEA-*stat*-TMA<sub>47</sub>) block copolymer vesicles and stimuli responsive drug release (adapted from Chen *et al. Scientific Reports* doi:10.1038/srep02162).

The drug, which is physically trapped inside or covalently bound to the polymer scaffolds, can be released in its active form, when these nano aggregates undergo structural changes or cleavage upon encounter with the tumor environments. To achieve this goal, polymer scaffold should have some kind of stimuli which brings about structural changes in the scaffold at the tumor environment. Some of the stimuli responsive block copolymers have been discussed below.

Stimuli responsive aggregates are capable of showing structural changes within upon exposure to harsh tumor conditions. Stimuli-responsive drug delivery is quintessential since controlled and targeted delivery is required in order to avoid systemic side effects and resistance to drug molecules.<sup>89</sup> In the recent years, research focussed on stimuli responsive block copolymers (smart polymers) involves the preparation of intelligent polymeric micelles, nano capsules and vesicles that respond to biological, physical and chemical stimulus. These can be internal stimuli such as pH,<sup>90</sup> temperature,<sup>91</sup> enzymes,<sup>92</sup> redox potential,<sup>93</sup> and external stimuli such as light, ultrasound and magnetic field.<sup>94</sup> Stimuli responsiveness with examples has been described in review by Alvarez-Lorenzo<sup>95</sup> and Zhuang.<sup>96</sup>

The self-assembly of block copolymers has been discussed at length above; however, an extremely important point needs to be addressed. That is in order for these block copolymers to be of relevance for biomedical applications they are required to be biodegradable, i.e. after completing their task of delivering the cargo at the tumor site they



should, over a period of time, degrade within the body and get cleared from the system. A few reviews talk extensively about biodegradable block copolymers such as Kumar et al.<sup>97</sup> Some of the biodegradable block copolymers have been discussed in brief in the further section.

#### 1.4. Bio-degradable Block Copolymers

The biodegradability of the polymers is of utmost importance, since these biomaterials are required to break down in to small fragments and subsequently be removed or resorbed.<sup>98</sup> Collagen, a natural polymer have been used for years in biomedical applications, however few years back synthetic biodegradable block copolymers came in to picture.<sup>99</sup> In the last 5 decades, the successes have been plentiful, but grand challenges still exist in both the basic and translational arena of biomaterial design. As these materials are applied in the clinical setting, numerous issues arise that could not be adequately identified and addressed in previous *in vitro* and *in vivo* model experiments. The host response to both drug delivery and tissue engineering scaffolds depends on the chemical, physical and biological properties of these biomaterials. When it is said that these materials are biodegradable, there is an issue of continuous changes in the material properties persuaded by degradation over a period of time. This issue is non-trivial and has contributed to the slow evolution of biodegradable polymer biomaterials as a field of research.<sup>100</sup>

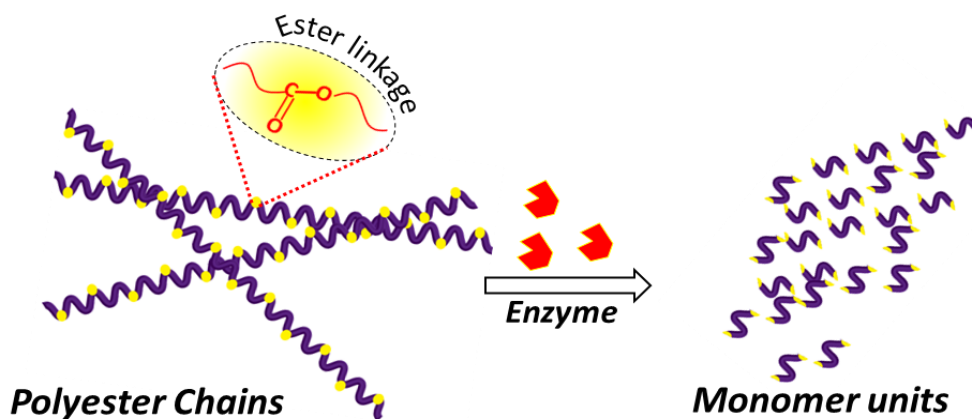


**Figure 1.14.** Illustration of enzyme degradation polyesters.

These biodegradable polymers own enzymatically or hydrolytically reactive chemical bonds in their backbone and can be broken down without secondary influence. There are large number of degradable polymers known in the literature that have bonds that are vulnerable to enzyme degradation and water hydrolysis including esters, anhydrides, acetals,

carbonates, amides, urethanes and phosphates reviewed by Kumar et al.<sup>97</sup> The following text only talks about ester group containing polymers i.e. polyesters.

Poly( $\alpha$ -esters) are a class of polymers that contain an aliphatic ester bond in their backbone which can be easily cleaved in the presence of enzyme as shown in figure 1.14. While a number of polyesters are commercially available and all are theoretically degradable too, these are some of the degradable polymers utilized for biomedical applications. These polymers are usually mildly hydrophobic, undergo bulk erosion due to ester bond reactivity. Due to the relative ease of their synthesis and commercial availability, poly( $\alpha$ -esters) have been the most heavily researched degradable biomaterials to date.<sup>101</sup>

The synthesis of bio-degradable polyesters through condensation polymerization primarily appeared in the literature in late 1920s by Carothers et al.<sup>102</sup> This technique provides opportunity to synthesize a wide range of degradable polymers whose properties can be easily tuned by varying the starting material. However this approach needs the mechanistic features such as long reaction times and high conversion to achieve high molecular weight polymers, which leads to highly dispersed polymers. This hampers the industrial usage where amount of material per unit time is vital as this technique requires longer polymerization time and with broad polydispersity.

In this respect, chain growth polymerization such as ring opening polymerization (ROP) offers the advantages such as (i) high control over the polymer molecular weight structure, (ii) high control over the rate of polymerization which leads to narrow dispersed polymers. Along with the aforementioned advantages it also gives the opportunity to use wide range of initiators and catalysts. These advantages help to achieve control on molecular weights and macromolecular structure, thus it is easy to synthesize refined macromolecular architectures including block copolymers, branched and star-shaped polymers with high accuracy. ROP of various monomers at different conditions is discussed in more detail in the following section.

#### **1.4.1. Ring-Opening Polymerization**

The polymerization of lactones is generally performed in bulk as well as in solution route. In bulk (melt route) it is usually carried out in highly inert conditions and temperature is usually maintained between 100-150 °C depending on the monomer being used.<sup>110</sup> The reaction kinetics of melt route is very high. The polymers synthesized using this route are

highly pure as it is carried out in solvent free conditions. On the other hand in solution route ROP, performed in THF, dioxane and toluene, the range of low temperatures has been used ( $< 60\text{ }^{\circ}\text{C}$ ) to produce the narrow disperse polymers.<sup>103</sup>

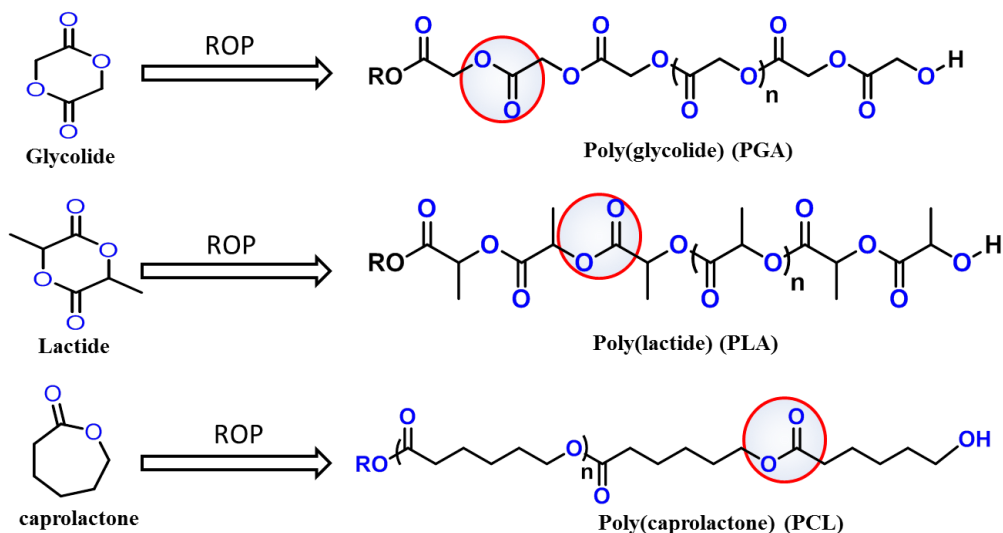


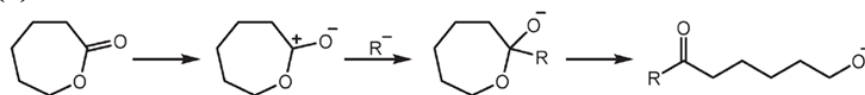
**Figure 1.15.** Biodegradable polymers prepared using ROP.

The pharmaceutically important polyesters including PGA, PLA, PBL and PCL are derived by ROP from cyclic esters such as glycolide (GA), lactide (LA),  $\alpha$ -butyrolactone ( $\alpha$ -BL) and  $\epsilon$ -caprolactone ( $\epsilon$ -CL) respectively (see figure 1.15). The random copolymers such as poly(lactic acid-co-glycolic acid) (PLGA) and block copolymers poly(lactic acid)-*b*-poly(ethylene oxide) (PLA-PEG) have been extensively explored for their degradability and drug delivery applications. ROP of lactones has four main mechanisms depending on the catalyst including (i) anionic, (ii) cationic, (iii) monomer-activated and (iv) coordination–insertion mechanism (see figure 1.16).

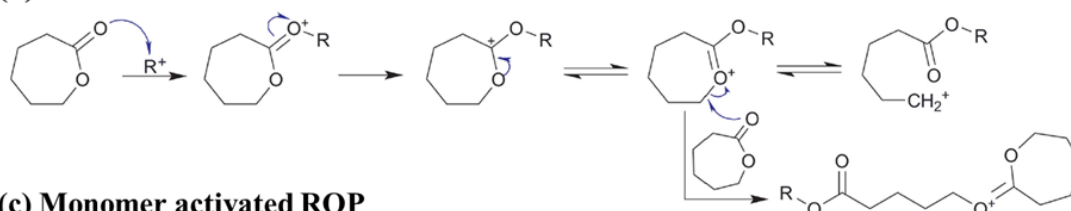
Anionic ROP involves the formation of an anionic species which further attacks the carbonyl group of the monomer. The growing species is an alkoxide as the monomer is ring opened at the acyl–oxygen bond (see figure 1.16).<sup>104-105</sup> The main drawback of this method is the back-biting that is intramolecular trans-esterification; this causes the formation of low molecular weight polymers. The cationic ROP involves the formation of a cationic species which is attacked by the carbonyl oxygen of the monomer through a nucleophilic substitution reaction.<sup>104-105</sup> The monomer-activated ROP involves the activation of the monomer molecules by a catalyst, followed by the attack of the activated monomer onto the polymer chain end (see figure 1.16).<sup>106</sup> The various ROP mechanisms for caprolactone as a model

monomer are depicted in figure 1.16, similar mechanism are followed for other monomers such as lactides and glycolides.

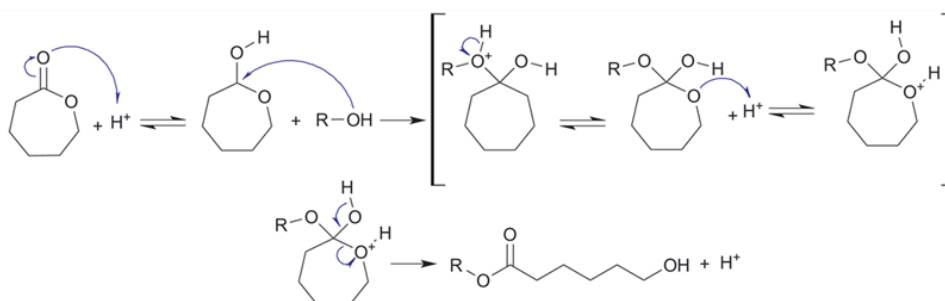
**(a) Anionic ROP**



**(b) Cationic ROP**



**(c) Monomer activated ROP**



**(d) Coordination–insertion ROP**

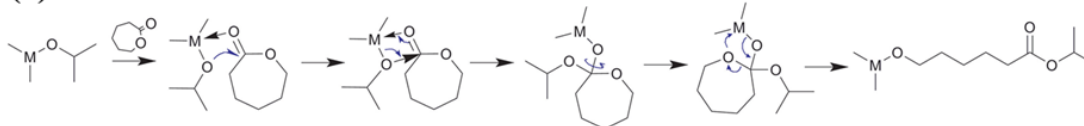


**Figure 1.16.** Various types of ROP mechanisms (adapted from A. Khanna, Y. Sudha, S. Pillai and S. Rath, *J. Mol. Model.*, 2008,14, 367–374., K. M. Stridsberg, M. Ryner and A.-C. Albertsson, *Adv. Polym. Sci.*, 2002, 157, 41–65M. S. Kim, K. S. Seo, G. Khang and H. B. Lee, *Macromol. Rapid Commun.*, 2005, 26, 643–648.T. Endo, in *Handbook of Ring-Opening Polymerization*, ed. P. Dubois, O. Coulembier and J.-M. Raquez, Wiley-VCH, Weinheim, 2009, pp. 53–63.).

The coordination insertion ROP is the very common procedure of this polymerization technique. It is also known as a pseudo-anionic ROP. In this mechanism ROP propagates through the monomer coordination to the catalyst and it's insertion into a metal oxygen bond of the catalyst (see figure 1.16).<sup>104-105</sup> Throughout propagation, the increasing chain is attached to the metal by an alkoxide bond. Many organometallics, such as carboxylates, oxides, and alkoxides are employed as effective initiators for the controlled ROP of lactones to result in the synthesis of polyesters. Mostly high molecular weight and narrow dispersed polyesters have been synthesized by using coordination-insertion or anionic ROP.

For ROP, amine and alcohols are usually employed as initiators, and three different types of catalysts are employed including metal based, inorganic acid and enzymatic catalyst. Metal based catalyst such as *alkali* (lithium diisopropylamide, Phenyl lithium, potassium tert-butoxide), *Alkaline earth* (magnesium aryl oxide, calcium alkoxide, calcium aluminate and strontium ammoniates etc), poor metal based aluminium alkoxide are used. Along with this tin octanoate, scandium triflate, transition metal based zinc alkoxides, iron alkoxides, molybdenum (IV) complexes, rare earth metals such as yttrium (III) and neodymium (III), series of lipase enzymes are also used as catalysts. Some of these catalysts are mentioned, their activity, conditions and reaction kinetics have been discussed in detail in a review by Labet et al. Some of the very important polyesters are described below which are synthesized employing ROP.<sup>103</sup>

#### 1.4.2. Polyglycolide or poly(glycolic acid) (PGA)

PGA is one of the very first degradable block copolymers ever explored for biomedical application.<sup>104</sup> These polymers are usually synthesized from ROP of glycolide as shown in figure 1.15. These polymers have  $> 200$  °C melting point ( $T_m$ ), 40 °C glass transition temperature ( $T_g$ ) and very high tensile strength of 12.5 GPa.<sup>105</sup> PGA found application as the degradable suture DEXON which has been actively used since 1970.<sup>107</sup> Due to PGA's fast degradation and insolubility in many common solvents, limited research has been conducted with PGA-based drug delivery devices. Instead, mostly research has focussed on manufacturing of tissue engineering scaffolds. PGA is often fabricated into a mesh network and has been used as a scaffold for bone, cartilage, tooth, vaginal, intestinal and spinal regeneration.<sup>108-112</sup> While there has been research conducted into a wide range of applications, there exists significant issues with PGA. Rapid degradation leads to loss of mechanical strength and significant local production of glycolic acid. While glycolic acid is bio-resorbable by cells via the citric acid cycle, high level of glycolic acid has been linked to a strong, undesired inflammatory response.<sup>113</sup>

#### 1.4.3. Polylactide (PLA)

Since the PLA possesses chiral molecules, they are found in four forms such as poly(D-lactic acid) (PDLA), poly(L-lactic acid) (PLLA), poly(D, L-lactic acid) (PDLLA) a racemic mixture of PLLA and PDLA and meso-poly(lactic acid).<sup>114</sup> Mostly PLLA and PDLLA have found promising applications and have been extensively studied as in

biomaterials. PLLA has a  $T_g$  of 60 - 65 °C, a melting temperature of around 175 °C and a mechanical strength of 4.8 GPa.

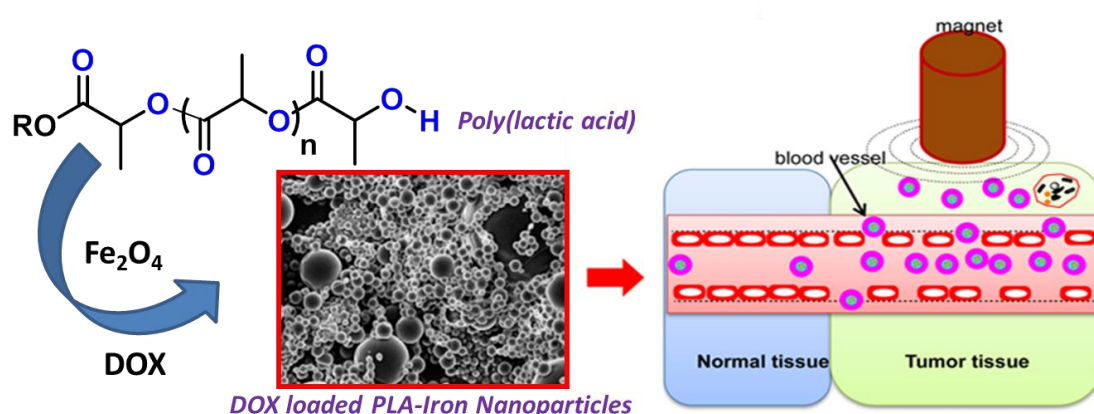


**Figure 1.17.** Synthesis of PLA/DOX/Fe<sub>2</sub>O<sub>4</sub> nanoparticles for magnetic targeting to the tumorous tissues (adapted from Mhlanga et al. *ACS Appl. Mater. Interfaces* **2015**, 7, 22692–22701).

The additional methyl group in PLA causes the polymer to be much more hydrophobic and stable against hydrolysis as compared to PGA. Due to the slow degradation time, limited research has been recently conducted into drug delivery by PLLA systems alone. As shown in figure 1.17, Mhlanga developed PLA based DOX and iron nanoparticles loaded nanospheres to magnetic targeted delivery to the tumor tissues over healthy tissues.<sup>115</sup> In order to reduce degradation time, investigators have either developed modification techniques or have blended or copolymerized PLLA with other degradable polymers. It is also widely used in tissue engineering applications ranging from scaffolds for bone, cartilage, tendon, neural, and vascular regeneration.<sup>116-117</sup>

#### 1.4.4. Poly(lactide-co-glycolide) (PLGA)

Random copolymerization of PLA and PGA, known as poly(lactide-co-glycolide) (PLGA), is the most investigated degradable polymer for biomedical applications and has been used in sutures, drug delivery devices and tissue engineering scaffolds. One particular advantage is that since PLA and PGA have significantly different properties, careful choice of copolymer composition allows for optimization of PLGA for intended applications.<sup>118</sup> Property modulation is even more significant for PLGA copolymers since with 25 – 75 % lactide composition, PLGA forms amorphous polymers which are very hydrolytically unstable compared to the more stable homopolymers. This is evident in the degradation times

of 50:50 PLGA, 75:25 PLGA, and 85:15 PLGA being 1–2 months, 4–5 months and 5–6 months, respectively.<sup>119-120</sup>

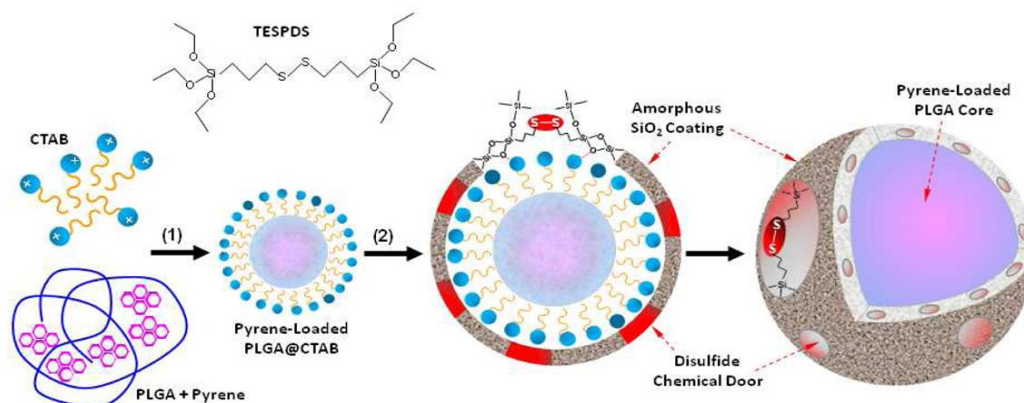


**Figure 1.18.** Schematic illustration of pyrene loaded PLGA-silica nanoparticles for targeted delivery (adapted from Quesada et al. *Chem. Mater.* **2013**, 25, 2597–2602).

With rapid degradation compared to other polyesters, PLGA has been utilized extensively in drug delivery applications. PLGA has been used to deliver chemotherapeutics, proteins, vaccines, antibiotics, analgesics, anti-inflammatory drugs and siRNA.<sup>120</sup> Most often PLGA is fabricated into microspheres, microcapsules, nano-spheres to facilitate controlled delivery of encapsulated or adsorbed payloads. As shown in figure 1.18 Quesada et al. manufactured, glutathione sensitive disulphide coated PLGA nanoparticles to deliver pyrene as model cargoes deliver to the tumour tissues.<sup>121</sup> Unfortunately, it has seen a significant drop in recent use due to public concern that it induces significant inflammation after implantation even though a recent report refutes this argument.

#### 1.4.5. Polycaprolactone (PCL)

Polycaprolactone (PCL) is one of the very earliest polymers produced by the Carothers group in the early 1930s.<sup>102</sup> After identification of microorganism degradation of this synthetic polymer it became commercially available. PCL is usually prepared via ring opening polymerization (ROP) of caprolactone using a variety of aforementioned anionic, cationic and co-ordination insertion mechanism based catalysts. This polymer can be also synthesized by free radical ring-opening polymerization of 2-methylene-1, 3-dioxepane.<sup>122</sup>

It is a semi crystalline polyester with 55-60 °C as the melting point ( $T_m$ ) and -54 °C glass transition temperature ( $T_g$ ) value which also has great solubility in wide range of

organic solvent. Polycaprolactone has a very low bio degradability and high permeability or solubility for hydrophobic drugs. This answers that why PCL is one of the very popular polymeric materials to be used as long term implant devices and drug delivery vehicles.<sup>123</sup> Capronor is a PCL based commercial contraceptive product that has shown to have the capability of delivering levonorgestrel *in vivo* for years and it is available in market for over 25 years. PCL biodegradation completely depends on the molecular weight, degree of crystallinity of the polymer and also on the conditions of degradation. Many microbes can degrade PCL which are present in nature; it is known that these microbes degrade the amorphous portion of the polymer first and followed by the crystalline domain.<sup>124</sup> This results in increase in the crystallinity whilst by keeping molecular weights constant. In this process finally ester bonds get chopped out which leads to complete decrease in overall mass.

The superior viscoelastic and rheological properties of PCL over many other aliphatic polyester counter parts render PCL the advantage of easy production and manipulation for applications in a large range of devices and implants. These interesting facts about PCL made it a very important material in the biomaterial arena. As said above it has FDA approval and inexpensive synthetic protocol (ROP). PCL's high processability allows the development of new scaffolds composed of microspheres, electro spun fibres and porous networks. PCL homopolymers, copolymers or blended materials have been employed as tissue engineering scaffolds for regeneration of bone, cartilage, ligament and vascular tissue.<sup>125-127</sup>

The pure PCL usage in the field of drug delivery is stemmed by its high hydrophobicity and its slow degradation. Along with this it's non-functionality also provides less opportunity to improve it's aforementioned properties. However, it has best hydrophobicity which encapsulates most of the hydrophobic drugs and creates stable nano-aggregates in water. This polymer needs to be manipulated in such a way that one could improve and make usage of its unique properties. To do this multiple ways have been employed in the literature, two of them are described below. First polycaprolactone could be coupled with hydrophilic or functional block polymer in order to improve amphiphilicity and its properties. This was achieved by either the copolymerization of caprolactone with monomer of interest or one end of the PCL coupled to other block. The second method being the making of a functional monomer, the ROP of this monomer provided the functionality and amphiphilicity to polymer (this will be discussed later). As mentioned above PCL



segments are heavily used with other blocks to construct drug delivery nano-devices; this PCL block has been coupled with PEG, polylactides, polypeptides, polysaccharides etc.

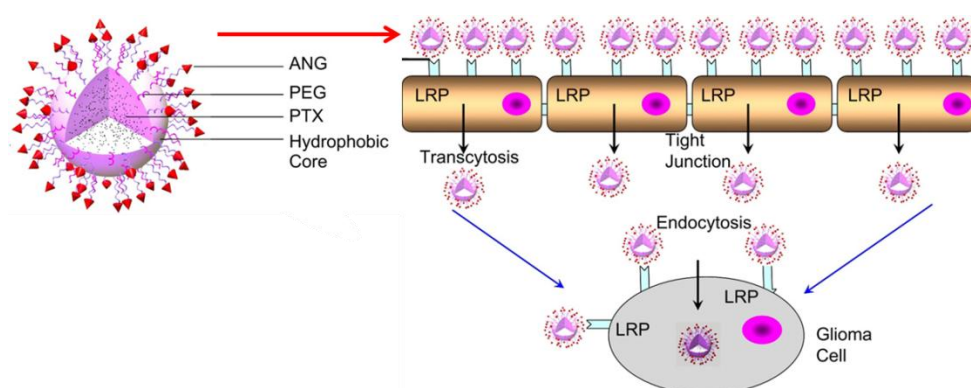


**Figure 1.19.** Strategy of PTX loaded Angiopep-conjugated polymer nanoaggregates as dual targeting drug delivery system for glioma via LRP mediated endocytosis. (adapted from Xin et al. *Biomaterials* 2012, 33, 8167-8176)

Xin et al. carried out ROP of PCL using PEG as initiator/hydrophilic block, where they have synthesized Angiopep-conjugated PEG-PCL nanoparticles (ANG-PEG-NP) as a dual targeting drug delivery system for glioma (tumor to glial cells) treatment (see figure 1.19) based on low density lipoprotein related protein (LRP) receptor that is not only over-expressed on BBB but also on glioma cells. It is known that the therapeutic effect on glioma is very less due to low permeability of delivery systems through the Blood-Brain Barrier (BBB) and poor diffusion into the tumor tissue. In this study they have shown that paclitaxel (PTX) loaded 90 nm size nanoparticles were able to overcome the aforementioned two barriers. They have prepared 3D glioma spheroids where they were able to achieve the selective tumor regression compared with non-targeted (PEG-NP) nanoparticles. Results showed that no critical toxicity to hematological system, liver, kidney and brain tissue was observed after intravenous administration with a dose of 100 mg/kg blank ANG-PEG-NP per day for a week in glioma mice model.<sup>128</sup>

Veena koul and co-workers fabricated amphiphilic triblock copolymer (pPEGMA-PCL-S-S-PCL-pPEGMA) based redox sensitive polymerosomes (see figure 1.20). To minimize cardiotoxicity and to increase the bioavailability of doxorubicin, redox sensitive linkage (-S-S-) were designed and developed.

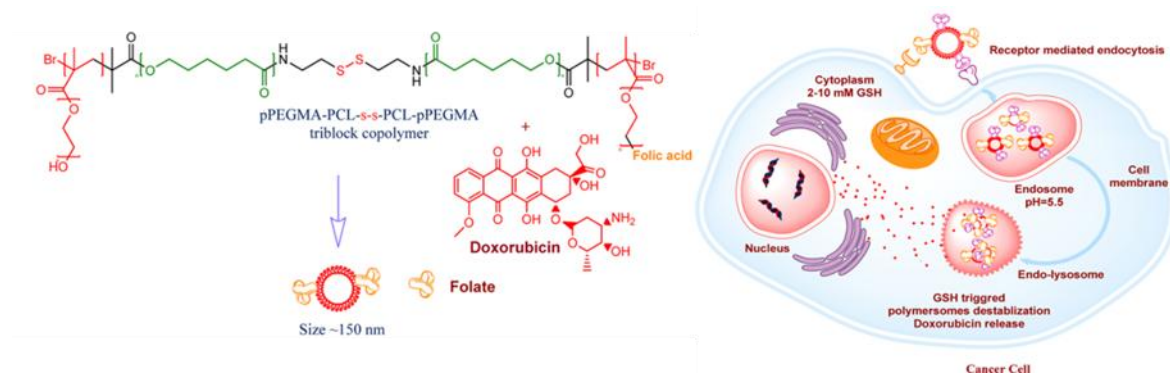


**Figure 1.20.** Schematic Illustration of Dual Targeted (Folic Acid and Trastuzumab) Redox Sensitive pPEGMA-PCL-ss-PCLpPEGMA Polymerosomes for Cancer Targeting. (adapted from Koul et al. *ACS Appl. Mater. Interfaces* **2015**, 7, 9211–9227)

The polymers were prepared via ROP of  $\epsilon$ -caprolactone and followed by atom transfer radical polymerization (ATRP) of PEGMA. This triblock copolymer undergoes self-assembly with DOX to form polymerosomes in the size range of  $\sim 150$  nm. Disulphide linkages favored nano aggregates to release the cargo at the GSH over expression conditions in the breast cancer cell line (MCF 7). *In vivo* studies on Ehrlich's ascites tumor (EAT) bearing Swiss albino mouse model showed  $\sim 85\%$  tumor regression as compared to free doxorubicin without any significant cardiotoxicity associated with doxorubicin.<sup>129</sup>

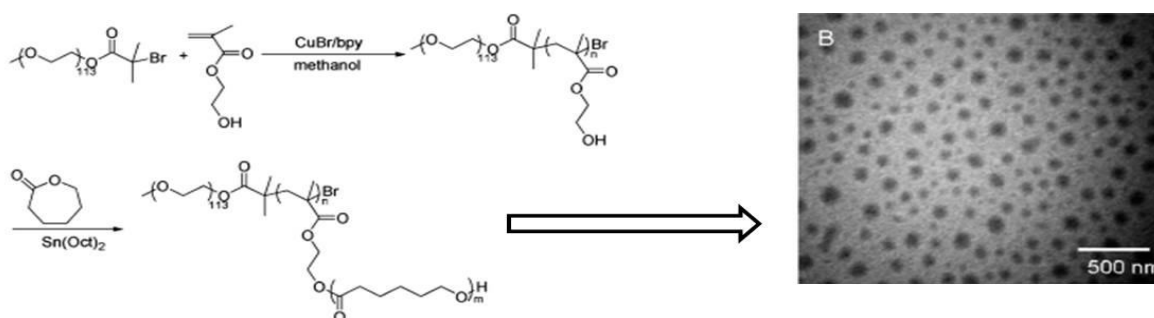


**Figure 1.21.** Synthesis of amphiphilic PEG-*b*-P(HEMA-*g*-PCL) blocks and its micellar aggregation. (adapted from Chen and coworkers *Biomacromolecules* **2010**, 11, 1331–1338)

Chen and coworkers prepared PCL block grafted on PEG-*b*-HEMA block copolymer to achieve amphiphilic PEG-*b*-P(HEMA-*g*-PCL) tooth brush like copolymers. Also the micellization properties of tooth brush like polymers with DOX loading was studied in aqueous solution (see figure 1.21). *In vitro* DOX release data and confocal laser scanning microscopy (CLSM) studies showed that DOX-loaded tooth brush like copolymer micelles

could be effectively internalized by bladder carcinoma cells (EJ cell line), and the DOX could be released into cytoplasmic compartments and finally travelled to the nucleus.<sup>130</sup>

Discher and co-workers reported the very first protocol for preparation of giant and flexible worm micelles self-assembled from degradable copolymer PEG-*b*-PCL. They have described that these worm micelles impulsively shorten to produce spherical micelles, triggered by degradable PCL hydrolysis (refer to figure 1.22.).<sup>131</sup>

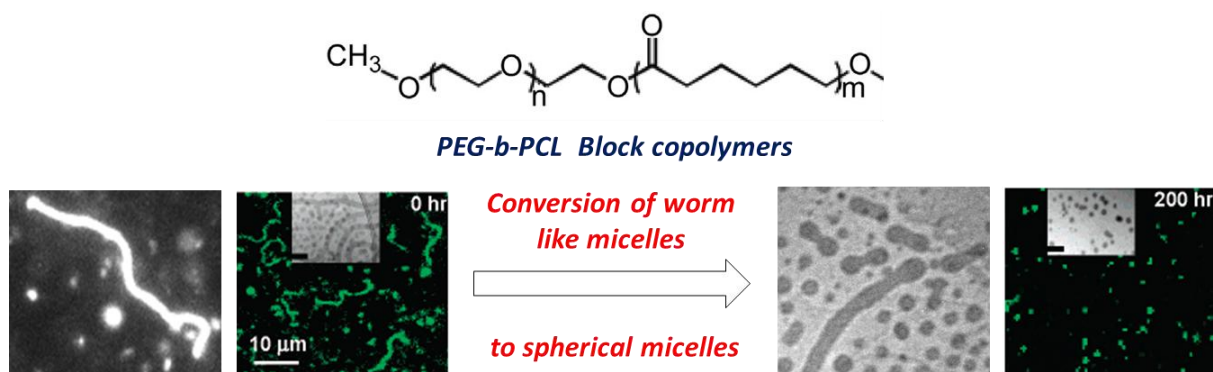


**Figure 1.22.** CLSM and microscopic images of PEG-*b*-PCL block copolymer worm micelles spontaneously shorten with time to spherical micelles in water (adapted from Discher et al. *J. Am. Chem. Soc.* **2005**, 127, 12780-12781).

Dong and coworkers studied mPEG-*b*-PCL-*b*-PDMAEMA triblock copolymer nanoparticles as the co-delivery vector for hydrophobic drug PTX and pDNA as shown in figure 1.23. Importantly, they have showed that the introduction of hydrophobic segment between mPEG and PDMAEMA segments can lead to 15 fold improvement in the gene transfection efficiency compared to mPEG-*b*-PDMAEMA. These dual loaded particles efficiently internalized into HEK 293T cells after transfection for 2 h. They have mentioned that this approach could help to improve the anti-tumor efficacy and patient compliance.<sup>132</sup>

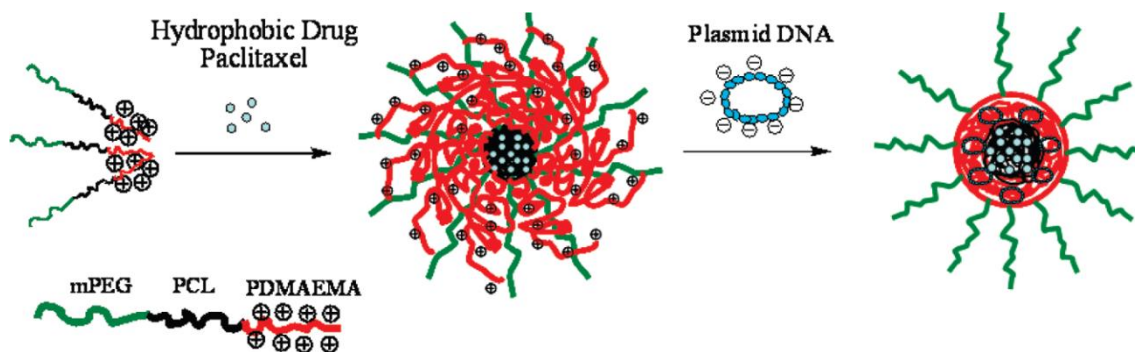


**Figure 1.23.** Preparation of mPEG-*b*-PCL-*b*-PDMAEMA NPs to codeliver hydrophobic Drug and DNA (adapted from Dong and coworkers *Biomacromolecules* **2010**, 11, 2306–2312)

Jin et al prepared the triblock PEG-*b*-PCL-*b*-PEG copolymer by embedding PCL into two PEG blocks with oxime linkages to achieve pH sensitive micellar assemblies. DOX was physically loaded and anti-tumor efficiency was tested in NIH/3T3 cells (see figure 1.24).<sup>133</sup>

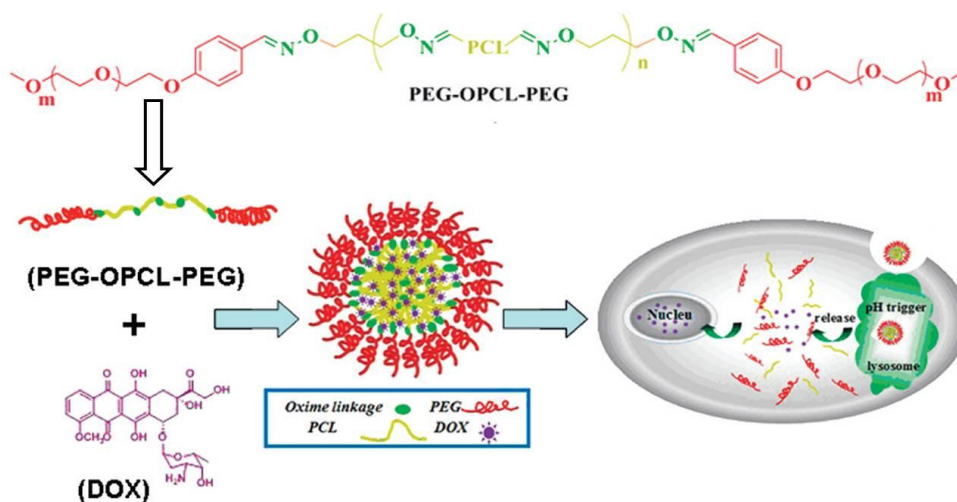


**Figure 1.24.** Synthetic Route of PEG-OPCL-PEG and Schematic Illustration of Intracellular Drug Release (adapted from Jin et al. *Biomacromolecules* **2011**, 12, 3460-3468)

Song et al. proposed a new strategy for nano-vehicle construction to load DOX based on PCL and poly lysine (see figure 1.25). This is bearing a redox responsive disulfide bond and clickable alkynyl groups to couple detachable PEG chain with a highly pH-sensitive benzoic-imine linkage. Furthermore, folic acid (FA) as a model targeting ligand was conjugated and successfully selective targeting was achieved.<sup>134</sup>

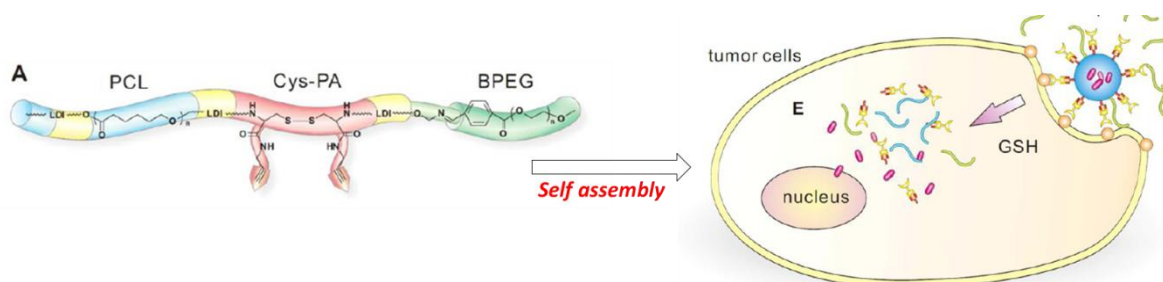


**Figure 1.25.** Design and Construction of Targeting-Clickable and Tumor-Cleavable Polyurethane Nano-micelles: Schematic molecular structure of 27 multiblocks polyurethanes; Intracellular drug release triggered by the cleavage of disulfide bond in response to GSH (adapted from Song et al. *Biomacromolecules* **2013**, 14, 4407-4419)



Park and coworkers developed tumor-targeted robust nanoparticles based on an amphiphilic hyaluronic acid (HA)-polycaprolactone (PCL) block copolymer, in which the HA shell was cross-linked via a disulfide linkage (see figure 1.26). These blocks were loaded with Doxorubicin (DOX) (DOX-HA-ss-NPs) that greatly retarded the drug release under physiological conditions (pH 7.4), whereas the drug release rate was markedly enhanced in the presence of glutathione at cytoplasmic conditions of SCC7 cells.<sup>135</sup>

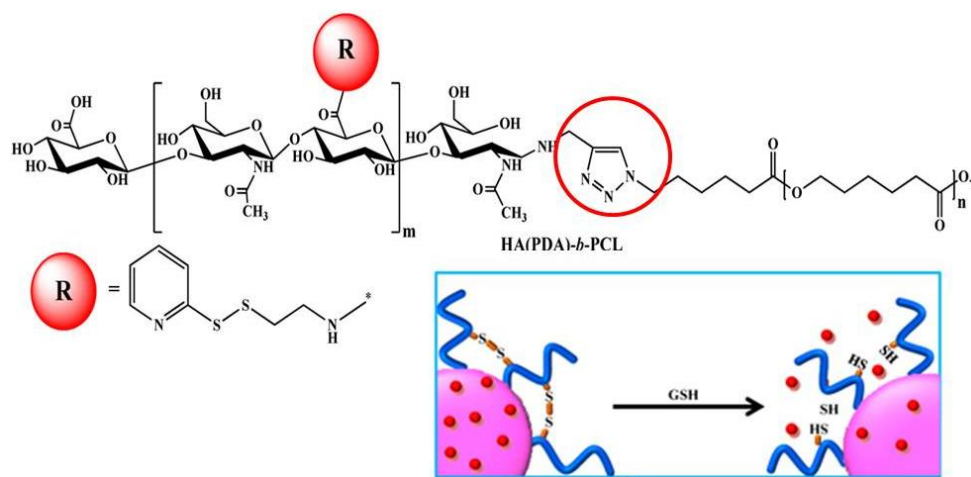


**Figure 1.26.** Synthetic route for the PDA-conjugated HA-*b*-PCL copolymer and intracellular drug release triggered by the cleavage of disulfide bond in response to GSH (adapted from Park and coworkers. *Biomacromolecules* 2015, 16, 447–456)

Gong and coworkers prepared hydrophilic doxorubicin (DOX) and hydrophobic curcumin (CUR) loaded biodegradable poly(ethylene glycol)–poly(3-caprolactone) (mPEG-*b*-PCL) based micelles for combination chemotherapy (see figure 1.27). Furthermore, they have found that these co-delivery vehicles exhibited remarkable progress in either cytotoxic activities or apoptotic effects compared with free drugs alone. This micellar co-delivery of DOX and Cur could synergistically potentiate antitumor effects on breast tumor.<sup>136</sup>

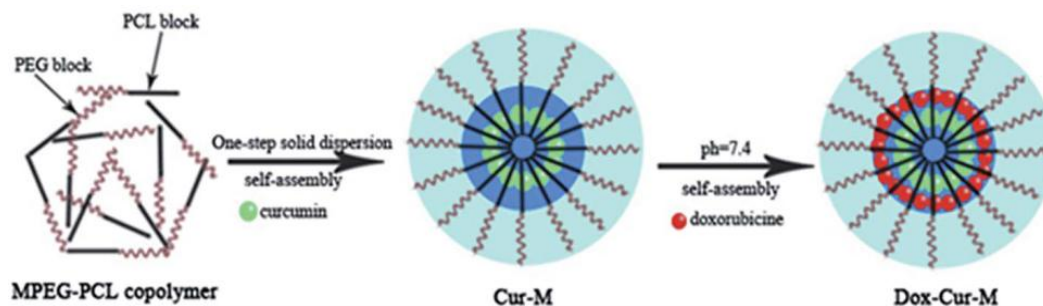
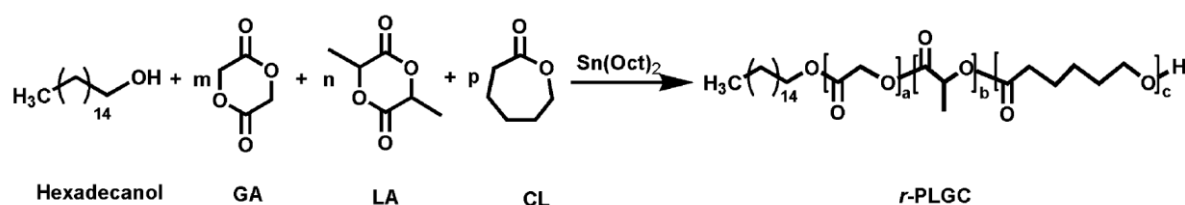


**Figure 1.27.** Preparation of Dox–Cur-micelles; schematic illustration of self-assembly of Dox–Cur-micelles (adapted from Gong and co-workers *RSC Adv.* 2014, 4, 46737–46750).

Zhao et al. showed that an anti-tuberculosis drug (rifampicin, RFP) was loaded into a porous scaffold, which was composed of caprolactone and lactide copolymerization (see scheme 1.2). During the *in vivo* experimental period, the drug concentration in tissues surrounding implants was much higher than that in blood which was still superior to the effective value to kill mycobacterium tuberculosis. The results of a rabbit radius repair experiment displayed that scaffolds have good bone regeneration capacity. The RFP composite scaffold thus could be envisioned to be a potential and promising substrate in clinical treatment of bone tuberculosis.<sup>137</sup>



**Scheme 1.2.** Preparation of PLGC triblock copolymers (adapted from Zhao et al. *J. Mater. Chem. B* **2015**, 3, 6885).

These approaches which make PCL amphiphilic, such as where these polymers were grown as block, or grafted on to various other block hydrophilic polymers seem to be important. Even though these scaffolds showed potential as drug delivery vehicles, there are some unaddressed problems such as non-functionality which hinders the opportunity of covalent drugs conjugation to increase loading content, to attach targeting moiety for site specific drug delivery. In order to overcome this, scientists adapted the approach of substituted (or) functional polycaprolactone that offer amphiphilicity, functional group availability to conjugate drug or target specific moieties as well as render 100 % biodegradable systems.

### 1.5. Functional Polycaprolactone as Drug Carriers

As mentioned above, the polyester PCL has excellent physical properties along with good biocompatibility and bio degradability which stands them in the first row of biomaterials in pharmaceutical industry. In recent ages the usage of this polymer got hampered by its non-functionality along with high hydrophobicity and crystallinity which renders the slow biodegradation. To achieve this substitution of monomer came into picture which upon polymerization provides substituted (or) functional polymers. This provides

advantages over non substituted or non-functional PCL such as (i) solubility of polymer in water can be enhanced, (ii) drug solubility of hydrophobic drugs can be tuned, (iii) packing or crystallinity in the scaffold can be varied, (iv) site specific drug delivery can be achieved, (v) stimuli responsive nano-carriers can be prepared, (vi) substituents can provide the opportunity to deliver genes, and (vii) finally, drugs can be covalently attached to the polymer. The aforementioned properties are completely reliant on the kind of substitution on the polymer.

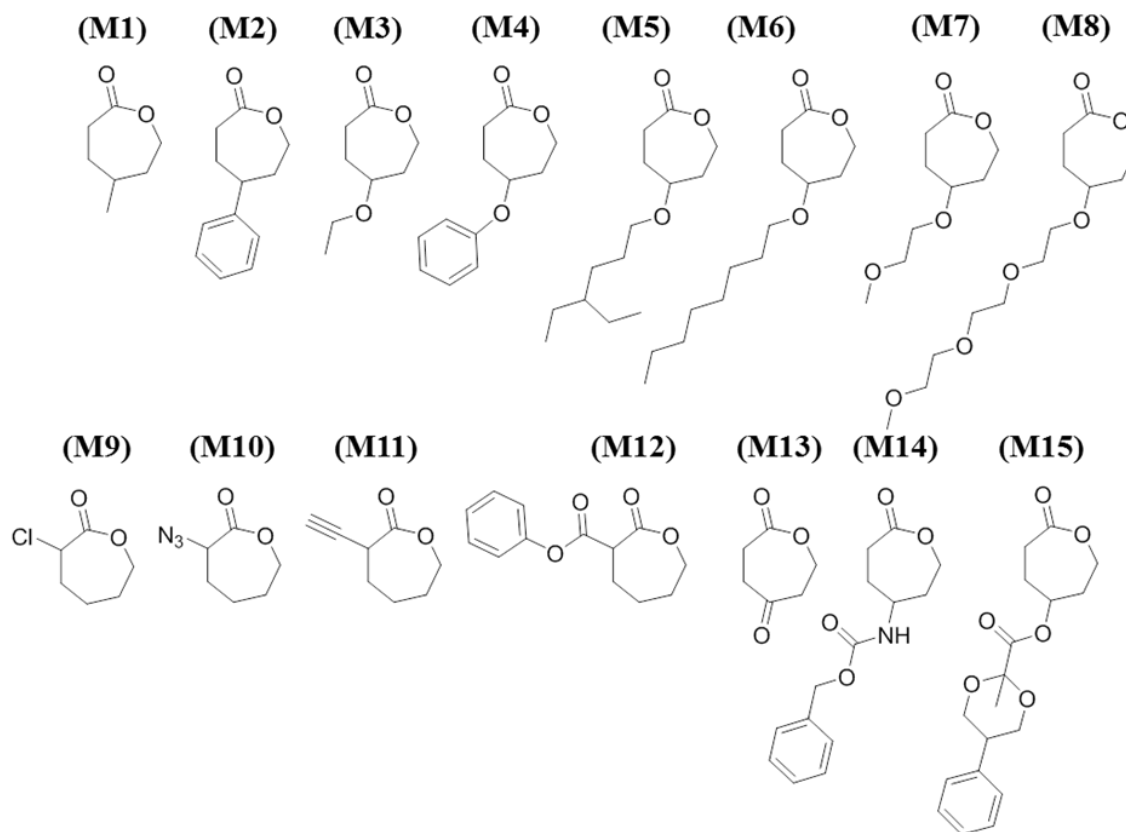


**Figure 1.28.** *Substituted caprolactone monomers.*

SPCL is usually synthesized from corresponding substituted caprolactone monomer using ring opening polymerization (ROP). In literature various types of substituted monomers have been synthesized and employed for ROP by using various initiators and catalysts. Most of the monomers have substituents at  $\alpha$  and  $\gamma$  positions. The  $\alpha$ -substituted caprolactone monomers were usually synthesized from caprolactone itself. Electrophilic substitution of monomer was carried out with electrophile of interest. The  $\gamma$ -substituted caprolactone monomers were usually synthesized from 1, 4-cyclohexane diol or 1, 4-cyclohexanone. For example in the case of diol one of the  $-OH$  groups was coupled with the moiety of interest

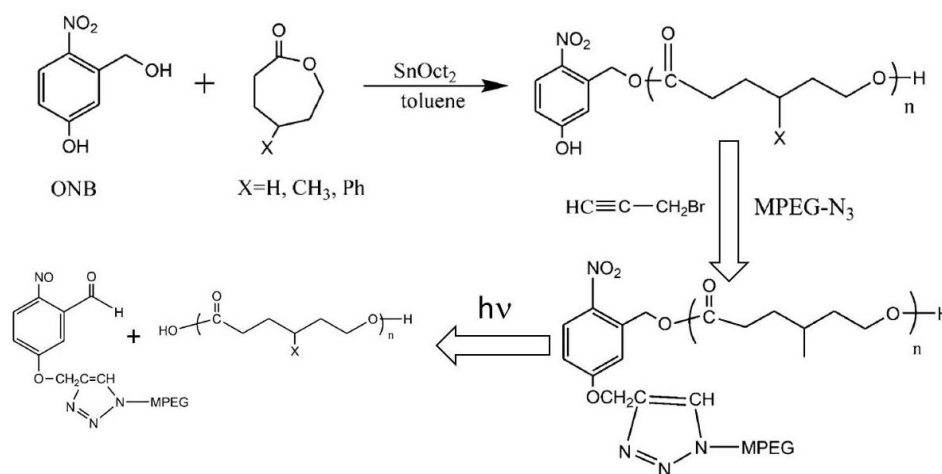
and subsequent free OH converted to keto group, followed by Baeyer villiger oxidation to achieve the monomer.<sup>138</sup>

The various monomers known in the literature are listed in figure 1.28, these were prepared using above mentioned techniques. The synthesis of polymers from these monomers and polymer usage as biomaterial has been discussed in detail. SPCL can be synthesized by ROP of these substituted caprolactone monomers. The typical route to poly( $\epsilon$ -caprolactone)s is the ROP of caprolactone monomer, often catalyzed by stannous 2-ethylhexanoate ( $\text{Sn}(\text{Oct})_2$ ), with a small alcohol or other hydroxy-terminated macro initiator like mPEG-OH.<sup>138</sup>

As said above  $\alpha$  and  $\gamma$  substituted polycaprolactones are available in the literature. These monomers depending on the nature of the substituent we have classified and categorized them as described below.

### Alky or phenyl substituted polycaprolactone

Methyl and phenyl substituted polycaprolactone were prepared from monomer M1 and M2 by Li and coworkers, where they have prepared methyl/phenyl substituted caprolactone, carried out ROP using PEG which has a photo degradable linker, this provided amphiphilic block copolymer (PEG-ONB-PCL) (scheme 1.3). From this block they have prepared Indomethacin (IMC) loaded micellar structures of 100 nm size. When polymer solutions were exposed to UV, significant changes were observed in the morphology of particles. After 30 min of UV radiation it showed light-triggered burst drug release in PBS at ambient temperature. No significant toxicity of these nanoparticles was found, at concentrations up to 1000 mg/mL before or after light irradiation.<sup>139</sup>



**Scheme 1.3.** Photo cleavable mPEG-b-PXCL block copolymers (adapted from Li and coworkers RSC Adv. 2013, 3, 18453)



### Alkoxy substituted polycaprolactone

These substituents are connected to the caprolactone monomer with ether moiety. Ethoxy (M3), Benzyloxy (M4), ethyl hexyl oxy (M5), Octyloxy (M6), ethylene glycol (M7) and triethylene glycol (M8) etc. moieties were attached using various chemical reactions. The polymerization of these monomers, their properties and application as drug delivery vehicles (if any) are explained in detail below.

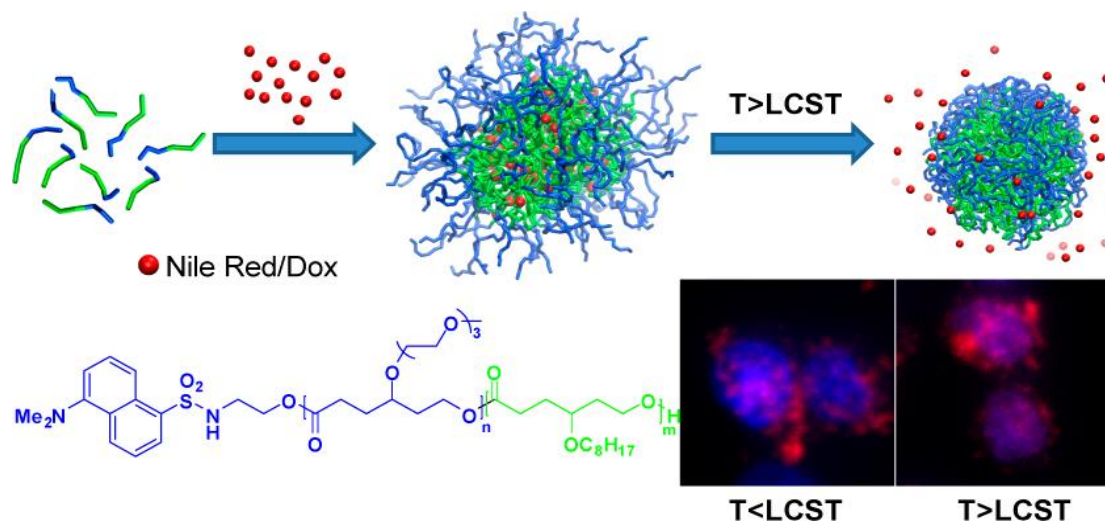
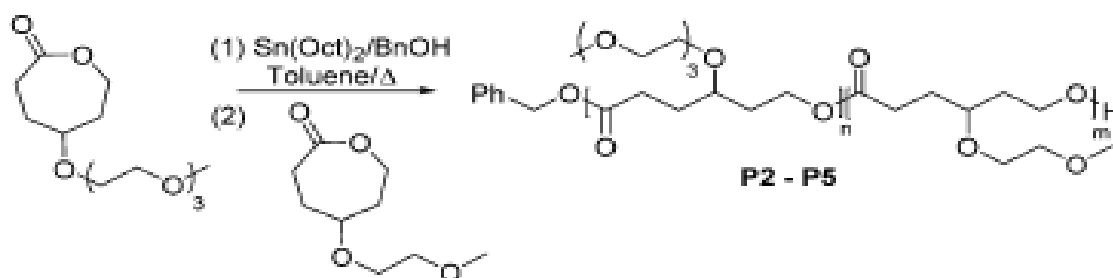


**Figure 1.29.** Synthesis of Nile Red loaded PMEEECL-*b*-POCTCL diblock micelles and its LCST properties (adapted from Stefan and co-workers *Biomacromolecules* **2012**, *13*, 2163–2173).

Stefan and coworkers prepared a thermo-responsive poly{ $\gamma$ -2-[2-(2-methoxyethoxy)-ethoxy]ethoxy- $\epsilon$ -caprolactone}-*b*-poly( $\gamma$ -octyloxy- $\epsilon$ -caprolactone) (PMEEECL-*b*-OCTCL) diblock copolymer and employed for delivery of DOX and Nile Red (NR) to MCF 7 human breast cancer cell lines (see figure 1.29). For this they have prepared two new octyl ether and triethylene glycol (TEG) substituted monomers and carried out ROP using tin octanoate (Sn(Oct)<sub>2</sub>) as catalyst and a fluorescent dansyl initiator. The PMEEECL-*b*-POCTCL had a lower critical solution temperature (LCST) of 38 °C, and it was employed to prepare thermally responsive micelles. At this temperature they have incubated DOX loaded micelles, and obtained elevated toxicity and better cellular uptake in MCF 7 cells.<sup>140</sup>

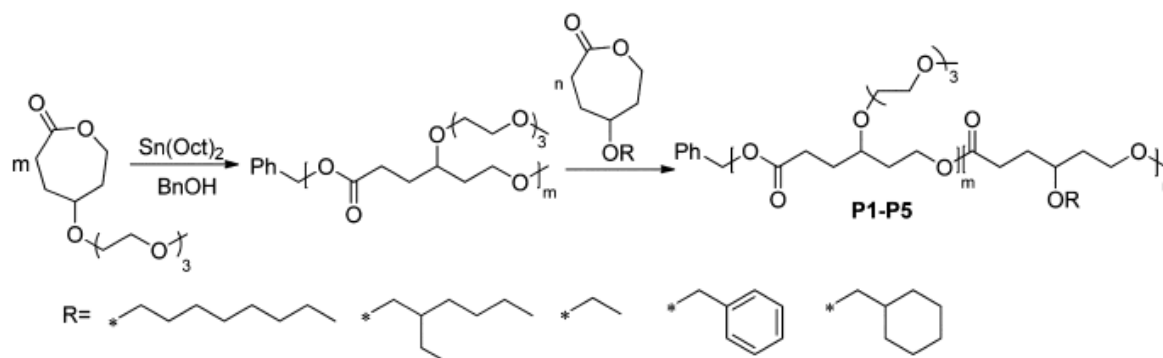
Same authors prepared one more new monomer  $\gamma$ -2-(methoxyethoxy)-3-caprolactone (MECL) and copolymerized with already synthesized TEG coupled monomer ( $\gamma$ -2-[2-(2-methoxyethoxy)-ethoxy]ethoxy- $\epsilon$ -caprolactone) to have an amphiphilic block polymer (see

scheme 1.4). By varying the composition of both the monomers they were accurately able to tune LCST values (31–43 °C).<sup>141</sup>



**Scheme 1.4.** Synthesis of  $\gamma$ -2-(methoxyethoxy)-3-caprolactone-block-( $\gamma$ -2-[2-(2-methoxyethoxy)-ethoxy]ethoxy- $\epsilon$ -caprolactone) diblocks. (adapted from Rainbolt et al. *J. Mater. Chem. B*, **2013**, 16532)

Continuation of the above shown work, authors prepared five new monomers using the earlier protocols. Wherein, they have substituted monomers with five different alkyl units and these monomers were copolymerized with TEG substituted caprolactone individually, and provided five random copolymers with different hydrophobicity (see scheme 1.5). In this work they have shown that increase in hydrophobic nature of the micellar core increases the hydrophobic drug loading.<sup>142</sup>



**Scheme 1.5.** Synthesis of various alkyl substituted polycaprolactones (SPCLs) (adapted from Hao et al. *Macromolecules* **2013**, 46, 4829-4838)

Functional groups such as chloro (M9), azido (M10), alkynyl (M11), benzyloxy (M12), keto (M13), di hydroxy (M14), amino (M15) functional substituted polycaprolactones were prepared from respective functional group protected monomers. The

polymerization of these monomers, their properties and application as drug delivery vehicles (if any) are explained in detail below.

The Lavasanifar group recently prepared  $\alpha$ -alkynyl substituted caprolactone using above mentioned protocol and carried out the ROP using PEG as initiator. Further alkynyl groups reacted with azide ( $N_3$ ) end having PEG chains, which bring polymer chains together to form micelles in water. Loading and delivering capabilities of PTX were tested in these micellar structures (see figure 1.30).<sup>143</sup>

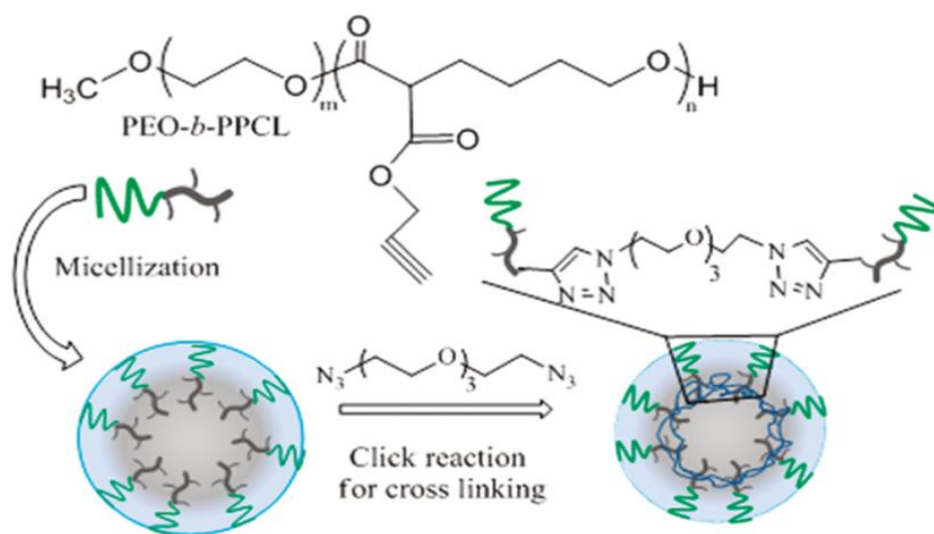
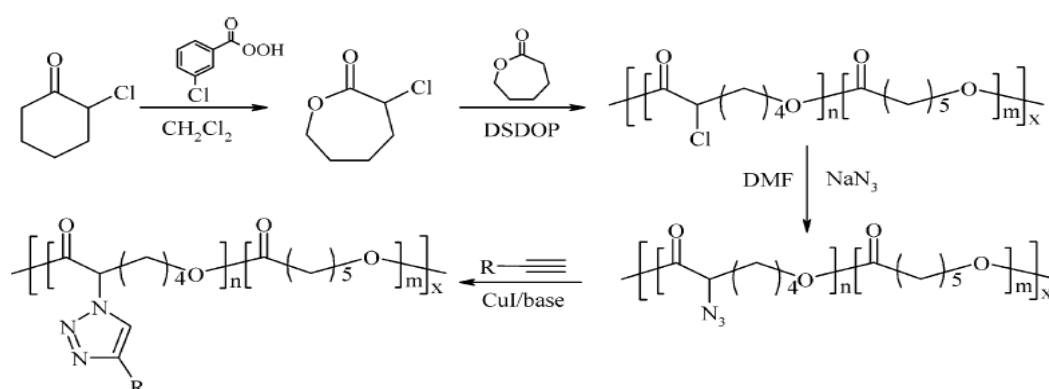


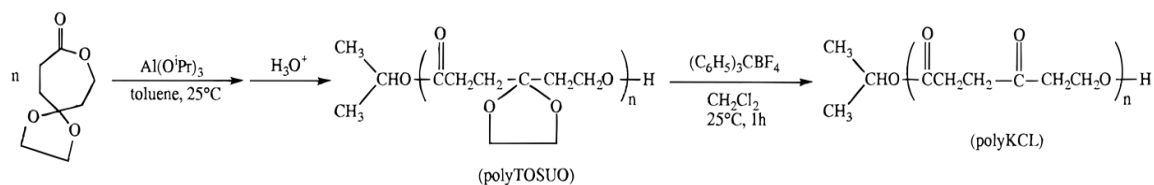
**Figure 1.30.** Synthesis of clickable micelles based on PEG-b-PPCL block copolymers (adapted from Lavasanifar and co-workers *Macromolecules* **2011**, 44, 2058–2066).



**Scheme 1.6.** Strategy for the chemical modification and grafting of PCL by click chemistry (adapted from Jerome and co-workers *Macromolecules* **2007**, 40, 796-803)

Robert Jerome and Philippe Lecomte firstly created  $\alpha$ -chloro and  $\alpha$ -azido substituted caprolactones as shown in scheme 1.6. Further they have carried out the ROP of azide

substituted caprolactone. They have proposed that this azide group grafted PCL provides huge number of opportunities to attach various functional groups through click chemistry<sup>144</sup>



**Scheme 1.7.** Synthesis of 5-keto functionalized PCL (KCL) (adapted from Jerome et al. *Macromolecules* **1998**, 31, 924-927).

Jerome and coworkers prepared  $\gamma$ -keto substituted caprolactone (see scheme 1.7), and they have standardized the ROP using PEG as initiator at ambient temperature using  $\text{Al}(\text{iOPr})_3$  as a catalyst. This block copolymer was thoroughly characterized using NMR, SEC and FTIR techniques. Continuation to this work they carried out the anionic ROP of epoxides on caprolactones  $\gamma$  position. This offered the caprolactone monomer with PEG chain on the  $\gamma$  position; they believed that this monomer may help in preparing new polymers that will help in drug delivery.<sup>145</sup>

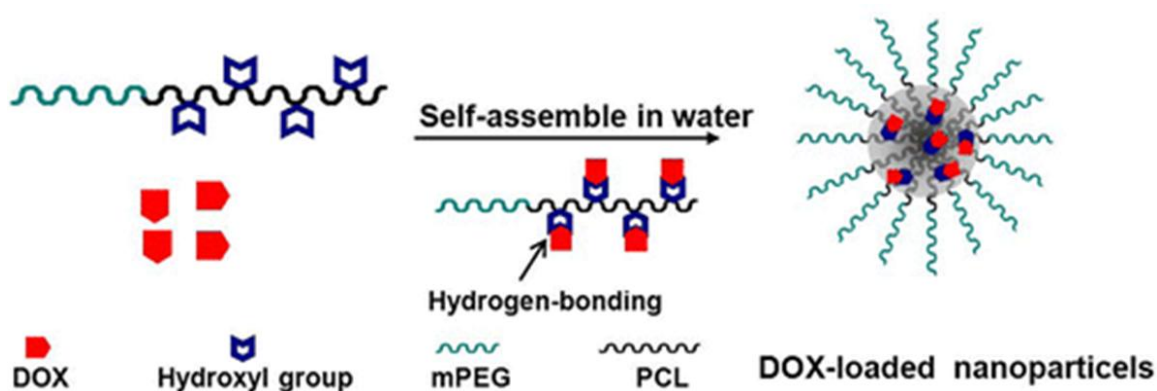
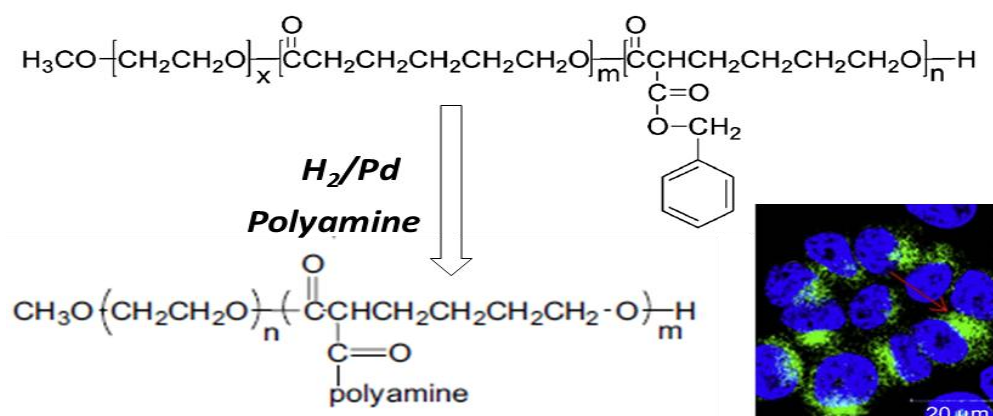


**Figure 1.31.** Synthesis of DOX loaded micelles based on hydroxy PEG-*b*-PPCL block copolymers (adapted from Chang et al. *Biomacromolecules*, **2012**, 13, 3301-3310).

This approach was further adapted by Chang et al. to synthesized methoxy poly(ethylene glycol)-*b*-poly( $\epsilon$ -caprolactone-co- $\gamma$ -hydroxyl- $\epsilon$ -caprolactone) (mPEG-*b*-P(CL-co-HCL)) bearing pendant hydroxyl groups on the PCL block (see figure 1.31). The hydroxyl groups were formed through the reduction of the above shown KCL, a keto substituted polycaprolactone by sodium borohydride. These polymers self-assembled along with DOX in water to form NPs of 140 nm. They have demonstrated that for loading and delivering DOX

the hydroxyl groups play very important role as they form H-bonding with the DOX molecule. They have also performed cytotoxicity assay and cellular uptake studies in HepG2 cells.<sup>146</sup>

Lavasanifar and coworkers synthesized, for the first time,  $\alpha$ -benzyl ester substituted caprolactone. They have synthesized this monomer in two steps, in first step caprolactone's  $\alpha$  position was activated and the second step followed the benzoyl chloroformate substitution. This monomer was subjected to ROP with PEG as initiator to get poly(ethylene oxide)-*block*-benzoyl poly(caprolactone) (PEO-*b*-BnPCL) based block copolymers which provided micelles in water (see scheme 1.8). They haven't shown any loading capabilities of the block copolymer. In the next work these particular block copolymers were loaded with curcumin and used as drug delivery vehicles for anticancer drugs.<sup>147</sup>



**Scheme 1.8.** Synthesis of PEO-*b*-BPCL diblock copolymer and its post-polymerization to polyamine grafted diblock copolymer; in inset CLSM image of MDA435/LCC6 cells shows transfection. (adapted from Lavasanifar and co-workers *Macromolecules* **2006**, *39*, 9419-9428, *Biomaterials* **2009**, *30*, 242-253)

Same authors later on carried out the post polymerization of above synthesized block copolymers (PEO-*b*-BPCL). Where they have substituted the hanging benzoyl groups with polyamine, this provides the cationic charged micellar structures in water (see scheme 1.8). Further, these nano-aggregates were employed to deliver siRNA to specific site.<sup>148</sup>

Hedrick and coworkers prepared series of  $\gamma$ -substituted monomers, with various functional groups including benzyl, di-alcohol, trifluoroacetamide, t-butyl ester group (see figure 1.32). They have carried out the ROP of these monomers individually and together in order to achieve homo and block copolymers. Further they were able to succeed in post polymerization to deprotect t-butyl and trifluoroacetamide to have corresponding polymers.

Unfortunately they were unable to achieve high molecular weights in the case of t-butyl grafted polymers.<sup>149</sup>

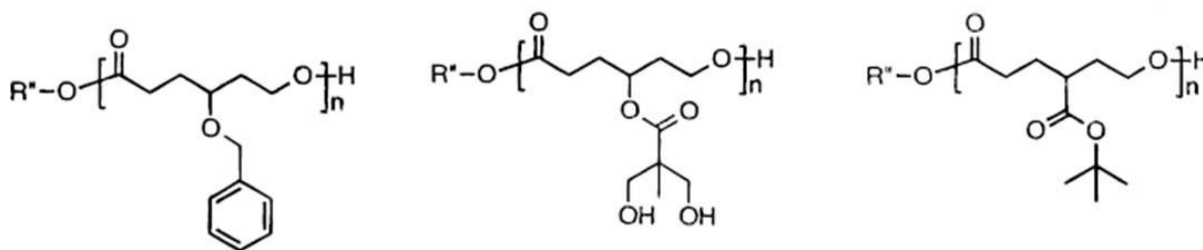


**Figure 1.32.** Substituted polycaprolactones synthesized by Hedrick and coworkers. (adapted from *Macromolecules* **2000**, 33, 4619-4627).

The aforementioned examples clearly outlined about the substituted caprolactone monomers and how these substitutions led to changes in the properties of the subsequent polymers. Scientists were able to tune the amphiphilicity, the drug or cargo loading abilities and target specific delivery of the polymeric scaffolds. However, among these examples there is no mention of carboxylic substituted polycaprolactone. The carboxylic group, in itself, is a diverse functionality in terms of the opportunities it offers to a chemist to bring about further modification by carrying out various coupling reactions. It can offer the advantages of enhanced water solubility, developing vesicular assemblies, bring about pH responsiveness, as well as offer the advantage of covalently binding drugs or targeting moieties in order to enhance the efficiency of polymers for biomedical applications.

## 1.6. Aim of the thesis

The detailed review of the block copolymers clearly demonstrates the several technological advantages behind the design and development of functional polycaprolactones. Unfortunately, the carboxylic polycaprolactones are not applied in the drug delivery applications. The development of new carboxylic polycaprolactone would provide the opportunity to create pH-responsive nano-scaffolds like micelles and vesicles to load various drug molecules. Further, the carboxylic acid groups can be employed for conjugation of drug molecules to increase the drug loading as well as blood plasma stability. Thus both stimuli responsiveness as well as drug conjugation can be achieved by preparing carboxylic functional PCL systems.

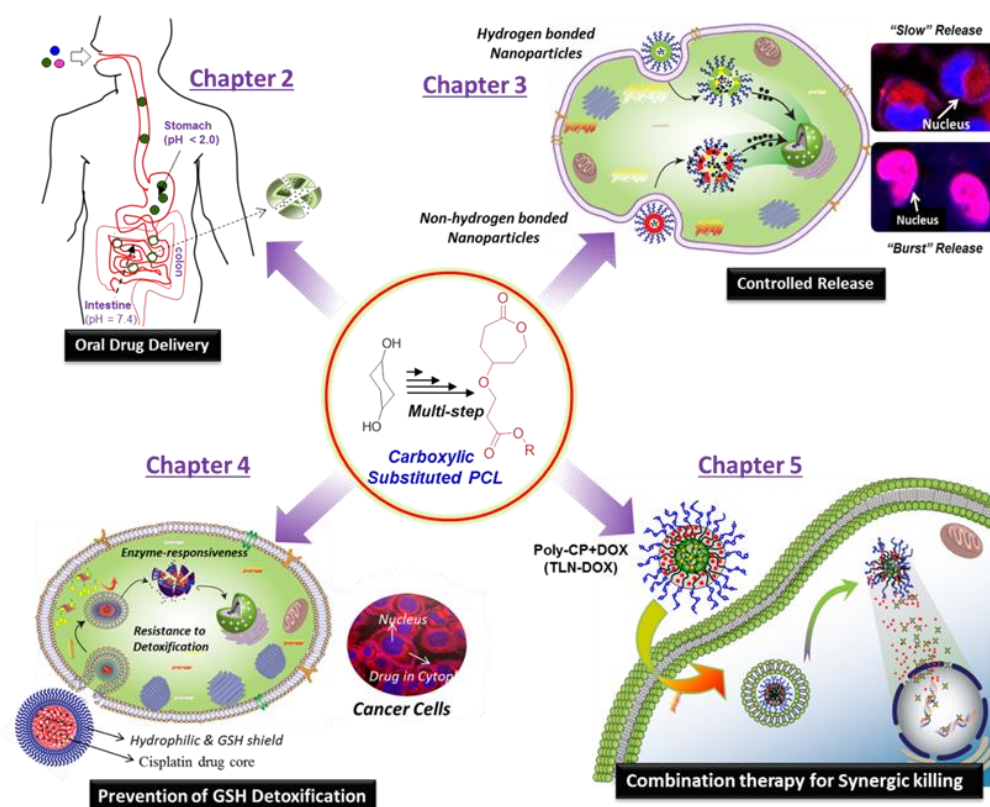


**Figure 1.33.** Carboxylic polycaprolactone based scaffolds for various applications.

This thesis work is focused on design and development of new carboxylic substituted caprolactone monomer and its ring opening polymerization with PEG in very controlled manner to achieve narrow dispersed polymers with high molecular weights. These polymers formed pH responsive vesicles, which were further loaded with ibuprofen, camptothecin and rhodamine-B and employed as oral delivery vehicles under gastrointestinal (GI) tract. Further these carboxylic units were substituted with various alcohols and amine to tune the



biodegradability of polymer, which controls the release rate of the loaded cargo and its cellular uptake. Efforts were also put to anchor the cisplatin drug to the carboxylic groups of the polycaprolactone to form core-shell nanoparticles which delivers the drug to the resistant breast cancer cells by preventing GSH detoxification. This approach extended to the development of the triblock polymer based dual drug loaded (cisplatin and DOX) nanoparticles to achieve synergistic cell killing in resistant breast cancer cells.

The thesis work is focused on the design and development of biocompatible and biodegradable carboxylic functionalised polycaprolactone nano-aggregates for physical loading and chemical anchoring of chemotherapeutics to achieve complete cell killing in various cell lines. The thesis work is divided into four chapters and the scientific outcome has been reported below in detail:

- (vi) New classes of *pH responsive carboxylic substituted polycaprolactones* were designed and developed. Synthesis of new monomers by multi-step reactions, block copolymer synthesis via ring opening polymerization methodology, self-assembly of block copolymers into vesicles and study the *in vitro* drug delivering capabilities under the gastrointestinal tract (GI).
- (vii) *Hydrogen-bond controlled anticancer drug delivery* approach was developed for intracellular delivery of chemotherapeutics. Enzyme-responsiveness of the hydrogen bonded biodegradable diblock copolymers were programmed for “burst” versus “controlled” release of drugs at the intracellular level.
- (viii) PCL *diblock copolymer-cisplatin core-shell nanoparticles* were made to overcome the detoxification of cisplatin drugs against cytoplasmic thiol residues such as glutathione and cysteine. The core-shell nanoparticles were very stable in saline, phosphate saline buffer (PBS) and bovine serum (FBS) and exclusively cleaved at the intracellular compartment by enzymes to deliver the Pt-drug.
- (ix) New classes of *triblock copolymer based triple layer nano-particles (TLNs)* were developed to achieve the combination therapy of cisplatin, DOX and together from single nano-carrier. This method accomplished the synergistic killing of breast cancer cells (MCF 7) by the combination therapy.

Finally, the overall conclusion of the thesis has been summarized in the last chapter with future perspectives.



## 1.7. References

1. Williams, David J. "*Polymer Science and Engineering.*" Englewood Cliffs, NJ, **1971**, 19.
2. Ferdinand, R. "*Principles of Polymer Systems.* McGraw-Hill, NY, **1970**. 35.
3. Ruzette1, A-V.; Leibler, L. *Nat. Mat.* **2005**, *4*, 19 – 31.
4. Lin, Y.; Stansbury, J.W. *Polymer***2003**, *44*, 4781-4789.
5. Szwarc M. *Nature***1956**, *176*, 1168.
6. Davis, K. A.; Matyjaszewski, K. *Adv. Polym. Sci.***2002**, *159*, 2-166.
7. Li, M.; Jahed, N. M.; Min, K.; Matyjaszewski, K. *Macromolecules***2004**, *37*, 2434-2441.
8. Matyjaszewski, K. *Polym. Inter.***2003**, *52*, 1559-1565.
9. Hawker, C. J. *Angew. Chem., Int. Ed. Engl.* **1995**, *34*, 1456-1459.
10. Quirk, R. P.; Kim, J. *Rubber Chemistry and Technology* **1991**, *64*, 450-468.
11. Hadjichristidis, N.; Pitsikalis, M.; Pispas, S.; Iatrou, H. *Chem. Rev.* **2001**, *101*, 3747-3792.
12. Israelachvili, J. N. *Intermolecular and Surface Forces*, Elsevier, Amsterdam**2011**.
13. Fong, C.; Le, T.; Drummond, C. J. *Chem. Soc. Rev.*,**2012**, *41*, 1297–1322.
14. Alexandridis, P.; Lindman, B. *Amphiphilic Block Copolymers: Self-Assembly and Applications*, Elsevier, Amsterdam**2000**.
15. Thomas, E. L.; Anderson, D. M.; Henkee C. S.; Hoffman, D. *Nature*, **1988**,*334*, 598–601.
16. Bates, F. S. *Science* **1991**, *251*, 898–905.
17. Bates, F. S.; Fredrickson, G. H. *Phys. Today***1999**,*52*, 32–38.
18. Craver, C. D.; Carraher, C. E. Jr. *Applied Polymer Science. 21st Century*, Elsevier Science Ltd. **2000**.
19. Black, C. T. *J. Res. Dev.***2007**, *51*, 605–633.
20. Black, C. T. *Appl. Phys. Lett.* **2005**, *87*, 163116.
21. Hua, B.; Lin, Q.; Zhang, Q.; Fan, Z. *Nanoscale***2013**, *5*, 6627–6640.
22. Naito, K.; Hieda, H.; Sakurai, M.; Kamata, Y.; Asakawa, K. *IEEE Trans. Magn.* **2002**, *38*, 1949–1951.
23. Matyjaszewski, K.; Davis, T. P., *Handbook of Radical Polymerization*, 1st ed.; Eds.; Wiley-Interscience:New York, **2002**.

24. Matyjaszewski, K. *Controlled Radical Polymerization*; Ed.; ACS Symposium Series 685; American Chemical Society: Washington, DC, **1998**.
25. Matyjaszewski, K. *Controlled/Living Radical Polymerization: Progress in ATRP, NMP and RAFT*; ACS Symposium Series 768; American Chemical Society: Washington, DC, **2000**.
26. Matyjaszewski, K. *Advances in Controlled/Living Radical Polymerization*; Ed.; ACS Symposium Series 854; American Chemical Society: Washington, DC, 2003.
27. Jakubowski, W.; Tsarevsky, N. V.; McCarthy, P. *ACS Symp. Ser.* **2009**, *1023*, 343.
28. Goto, A.; Fukuda, T. *Prog. Polym. Sci.* **2004**, *29*, 329.
29. Braunecker, W. A.; Matyjaszewski, K. *Prog. Polym. Sci.* **2007**, *32*, 93–146.
30. Matyjaszewski, K.; Xia, J. *Chem Rev* **2001**, *101*, 2921.
31. Hawker, C. J.; Bosman, A. W.; Harth, E. *Chem Rev* **2001**, *101*, 3661.
32. Chiefari, J.; Chong, Y. K.; Ercole, F.; Krstina, J.; Jeffery, J.; Le, T. P. T.; Mayadunne, R. T. A.; Meijs, G. F.; Moad, C. L.; Moad, E.; Rizzardo, E.; Thang, S. H. *Macromolecules* **1998**, *31*, 5559.
33. Kamber, N. E.; Jeong, W.; Waymouth, R. M.; Pratt, R. C.; Lohmeijer, B. G. G.; Hedrick, J. L. *Chem. Rev.* **2007**, *107*, 5813–5840.
34. Legge, N. R.; Holden, G.; Schroeder H. E. *J. Polym. Sci. Polym. Lett. Ed.* **1989**, *27*, 243.
35. Leone, G.; Mauri, M.; Bertini, F.; Canetti, M.; Piovani, D.; Ricci, G. *Macromolecules*, **2015**, *48*, 1304–1312.
36. Banerjee, S. S.; Bhowmick, A. K. *Ind. Eng. Chem. Res.* **2015**, *54*, 8137–8146.
37. Schollenberger, C. S. *Advances in Chemistry, Chapter 5*, **2009**, *176*, 83–96.
38. Shell Co. *Chem. Eng. News*, **1969**, *47*, 24–25.
39. Fong, C.; Le, T.; Drummond, C. J. *Chem. Soc. Rev.* **2012**, *41*, 1297–1322.
40. Whitesides, G. M., *Science* **1991**, *254*, 1312.
41. Javier, A. E.; Patel, S. N.; Hallinan, D. T.; Srinivasan, V.; Balsara, N. P. *Angew. Chem. Int. Ed.* **2011**, *50*, 9848–9851.
42. Qiang, L. *Macromol. Rapid Commun.* **2006**, *27*, 1779.
43. AL-Badri, M. H.; Maddikeri, R.R.; Zha, Y.; Thaker, H.D.; Dobriyal, P. Shunmugam, R.; Russell, T. P.; Tew, G. N. *Nat. Commun.* DOI: 10.1038/ncomms1485.
44. Mai, Y.; Eisenberg, A. *Chem. Soc. Rev.* **2012**, *41*, 5969–5985.
45. Ramanathan, M.; Nettleton, E.; Darling, S. B. *Thin Solid Films* **2009**, *517*, 4474.

46. Yang, J.; Jung, Y. S.; Chang, J-B.; Mickiewicz, R. A.; Alexander-Katz, A.; Ross, C. A.; Berggren, K. K. *Nat. Nanotechnol.* **2010**, *5*, 256 – 260.
47. Kim, B.H.; Kim, J.Y.; Kim, S. O. *Soft Matter.* **2013**, *9*, 2780.
48. Ramanathan, M.; Kilbey, S. M.; Ji, Q.; Hillcd, J. P.; Ariga, K. *J. Mater. Chem.* **2012**, *22*, 10389.
49. Letchford, K.; Burt, H. *Eur.J.Pharm. Biopharm.* **2007**, *65*, 259-265.
50. Wang, G.; Henselwood, F.; Liu, G. *Langmuir* **1998**, *14*, 1554-1559.
51. Drury, J. L.; Mooney, D. J.; *Biomaterials* **2003**, *24*, 4337–4351.
52. Tessmar, J.K.; Gopferich, A.M.; *Macromol. Biosci.* **2007**, *7*, 23–39.
53. Khan, F.; Tanaka, M.; Ahmad, A. R. *J. Mater. Chem. B* **2015**, *3*, 8224.
54. Chen, X.; Wang, W.; Cheng, S.; Dong, B.; Li, C. Y. *ACS Nano* **2013**, *7*, 8251–8257.
55. Adams, M. L.; Lavasanifar, A.; Kwon, G. S. *J. Pharm.Sci* **2003**, *92*, 1343.
56. Jones, M-C.; Leroux, J-C. *Eur. J. Pharm. Biopharm.* **1999**, *48*, 101–111.
57. Torchilin, V. P.; Levchenko T.S.; Yaroslavov, A. A.; Michailova, E.V.; Shtilman, M. I. *Biomaterials* **2001**, *22*, 3035–3044.
58. Matsumura, Y.; Maeda, H. *Cancer Res.* **1986**, *46*, 6387-6392.
59. Thomas, E. L.; Anderson, D. M.; Henkee, C. S.; Hoffman, D. *Nature* **1988**, *334*, 598–601.
60. Hest, J. C. M.; Delnoye, D. A. P.; Baars, M. W. P. L.; Meijer, E. W. *Science* **1995**, *268*, 1592–1595.
61. Israelachvili, J. ‘‘*Intermolecular & Surface Forces*’’, 2nd ed., Academic Press, London **1991**.
62. Yokoyama, M.; Miyauchi, M.; Yamada, N.; Okano, T.; NSakurai, Y.; Kataoka, K.; Lnoue, S. *J. Controlled Release* **1990**, *11*, 269–278.
63. Ogris, M. *J. Controlled Release* **2003**, *91*, 173-181.
64. Lin, J.; Chen, T.; Lin, S.; Cai, C.; Zhang, L.; Zhuang, Y.; Wang, X-S. *Biomaterials* **2009**, *30*, 108–117.
65. Yokoyama, M.; Lnoue, S.; Kataoka, K.; Yui, N.; Sakurai, Y.; *Makromol. Chem., Rapid Commun.* **1987**, *8*, 431–435.
66. Zhu, X.; Fryd, M.; Tran, B.D.; Ilies, M. A.; Wayland, B. B. *Macromolecules* **2012**, *45*, 660–665.
67. Ahmad, Z.; Shah, A.; Siddiq, M.; Kraatz, H.-B., *RSC Adv.* **2014**, *4*, 17028-17038.

- 
68. Maity, A. R.; Chakraborty, A.; Mondal, A.; Jana, N. R., *Nanoscale* **2014**, *6*, 2752-2758.
69. Torchilin, V. P., *Nat. Rev. Drug Discov.* **2014**, *13*, 813-827.
70. Brinkhuis, R. P.; Rutjes, F. P. J. T.; van Hest, J. C. M., *Polym. Chem.* **2011**, *2*, 1449-1462.
71. Haung, S-J.; Hsu, Z. R.; Wang, L-F. *RSC Adv.* **2014**, *4*, 31552-31563.
72. Kwon, G.S.; *Crit. Rev. Ther. Drug Carrier. Syst.* **1998**, *15*, 481-512.
73. Illum, L.; Davis, S. S. *FEBS Lett.* **1984**, *167*, 79-82.
74. Allen, T.M. *Adv. Drug Deliv. Rev.* **1994**, *13*, 285-309.
75. Troester, S.D.; Kreuter, J. *J. Microencapsulation* **1992**, *9*, 19-28.
76. Riley, T.; Stolnik, S.; Heald, C.R.; Xiong, C.D.; Garnett, M.C.; Illum, L.; Davis, S.S.; Gellert, P.R. *Langmuir* **2001**, *17*, 3168-3174.
77. Heald, C.R.; Stolnik, S.; Kujawinski, K.S.; De Matteis, C.; Garnett, M.C.; Illum, L.; Barlow, R.J.; Gellert, P.R. *Langmuir* **2002**, *18*, 3669-3675.
78. Soppimath, K.S.; Aminabhavi, T.M.; Kulkarni, A.R.; Rudzinski, W.E. *J. Controlled Release* **2001**, *70*, 1-20.
79. Ameller, T.; Marsaud, V.; Legrand, P.; Gref, R.; Barratt, G.; Renoir, J.-M. *Pharm. Res.* **2003**, *20*, 1063-1070.
80. De Faria, T.J.; Campos, A.; Senna, E.L. *Macromolecular Symposia* **2005**, *229*, 228-233.
81. Teixeira, M.; Alonso, M.J.; Pinto, M.M.M.; Barbosa, C.M. *Eur. J. Pharm. Biopharm.* **2005**, *59*, 491-500.
82. Prego, C.; Torres, D.; Fernandez-Megia, E.; Novoa-Carballal, R.; Quiñoá, E.; Alonso, M.J.. *J. Controlled Release* **2006**, *11*, 299-308.
83. Du, J.; O'Reilly, R. K., *Soft Matter* **2009**, *5*, 3544-3561.
84. Chang, H-I.; Yeh, M-K. *Int. J. Nanomedicine* **2012**, *7*, 49-60.
85. Bellomo, E. G.; Wyrsta, M. D.; Pakstis, L.; Pochan, D. J.; Deming, T. J.; *Nat. Mater.* **2004**, *3*, 244-248
86. Discher, D. E.; Eisenberg, A. *Science* **2002**, *297*, 967-973.
87. Discher, D. E.; Ahmed, F. *Annu. Rev. Biomed. Eng.* **2006**, *8*, 323-341
88. Chen et al. *Sci. Rep.* DOI:10.1038/srep02162.
89. Mura, S.; Nicolas, J.; Couvreur, P. *Nature Mater.* **2013**, *12*, 991-1003.
90. Gao, W.; Chan, J. M.; Farokhzad, O.C.; *Mol. Pharm.* **2010**, *7*, 1913-1920.

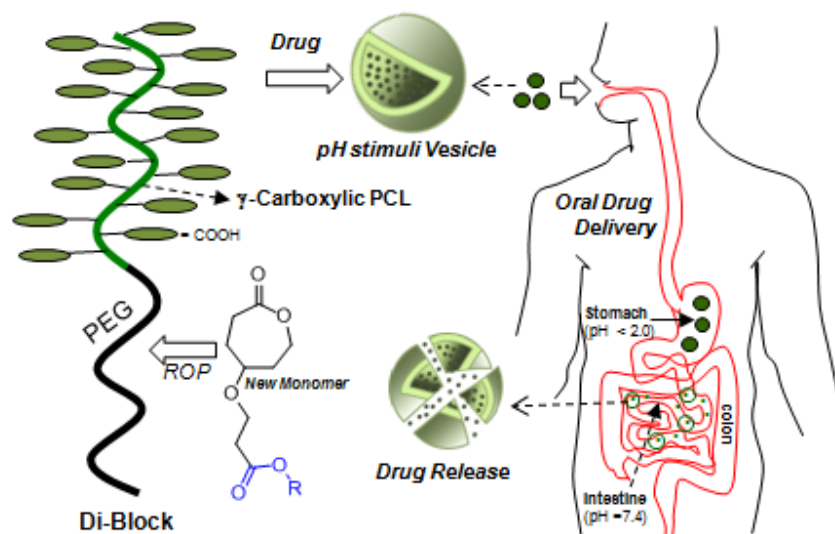
91. Hamner, K. L.; Alexander, C. M.; Coopersmith, K.; Reishofer, D.; Provenza, C.; Maye, M. M. *ACS Nano* **2013**, *7*, 7011-7020.
92. Guo, D-S.; Wang, K.; Wang, Y-X.; Liu, Y. *J. Am. Chem. Soc.* **2012**, *134*, 10244-10250.
93. Ren, T.; Wu, W.; Jia, M.; Dong, H.; Li, Ou, Z. *ACS Appl. Mater. Interfaces* **2013**, *5*, 10721-10730.
94. Meng, F.; Zhong, Z.; Feijen, J. *Biomacromolecules* **2009**, *10*, 197-209.
95. Alvarez-Lorenzo et al. *Chem. Commun.* **2014**, *50*, 7743-7765.
96. Zhuang et al. *Chem. Soc. Rev.* **2013**, *42*, 7421-7435.
97. Kumar et al. *Adv. Drug Deliv. Rev.* **2001**, *53*, 23-44.
98. Sato, N.; Okada, T.; Horiuchi, H.; Murakami, N.; Takakashi, J.; Nawata, M.; Ota, H.; Nozaki, K.; Takaoka, K. *Nat. Biotechnol.* **2001**, *19*, 332-335.
99. Izhar, U.; Schwalb, H.; Borman, J.B.; Hellener, G.R.; Hotoveli-Salomon, A.; Marom, G.; Stern, T.; Cohn, D.; *J. Surg. Res.* **2001**, *95*, 152-160.
100. Urich, K.E.; Cannizzaro, S.M.; Langer, R.S.; Shakesheff, K.M. *Chem. Rev.* **1999**, *99*, 3181-3198.
101. Ulery, B. D.; Nair, L. S.; Laurencin, C. T. *J. Polym. Sci. Part B Polym. Phys.* **2011**, *49*, 832-864
102. Van Natta, F.J.; Hill, J.W.; Carruthers, W.H. *J. Am. Chem. Soc.* **1934**, *56*, 455-9.
103. Labet, M.; Thielemans, W. Synthesis of polycaprolactone: a review. *Chem. Soc. Rev.* **2009**, *38*, 3484-3504.
104. Stridsberg, K. M.; Ryner M.; Albertsson, A.-C. *Adv. Polym. Sci.* **2002**, *157*, 41-65.
105. Khanna, A.; Sudha, Y.; Pillai S.; Rath, S. *J. Mol. Model.* **2008**, *14*, 367-374.
106. Kim, M. S.; Seo, K. S.; Khang G.; Lee, H. B.; *Macromol. Rapid Commun.* **2005**, *26*, 643-648.
107. Maurus, P. B.; Kaeding, C. C. *Oper. Techn. Sports Med.* **2004**, *12*, 158-160.
108. Knight, S.; Erggelet, C.; Endres, M.; Sittinger, M.; Kaps, C.; Stussi, E. *J. Biomed. Mater. Res. Part B: Appl. Biomater.* **2007**, *83*, 50-57.
109. Erggelet, C.; Neumann, K.; Endres, M.; Haberstroh, K.; Sittinger, M.; Kaps, C. *Biomaterials* **2007**, *28*, 5570-5580.
110. Pihlajamaki, H.; Tynninen, O.; Karjalainen, P.; Rokkanen, P. *J. Biomed. Mater. Res.* **2007**, *81*, 987-993.
111. Sayasneh, A.; Johnson, H. J. *Obstet. Gynaecol.* **2010**, *30*, 721-724.

112. Abbushi, A.; Endres, M.; Cabraja, M.; Kroppenstedt, S. N.; Thomale, U. W.; Sittinger, M.; Hegewald, A. A.; Morawietz, L.; Lemke, A.-J.; Bansemer, V.-G.; Kaps, C.; Woiciechowsky, C. *Spine* **2008**, *33*, 1527–1532.
113. Ceonzo, K.; Gaynor, A.; Shaffer, L.; Kojima, K.; Vacanti, C. A.; Stahl, G. L. *Tissue Eng.* **2006**, *12*, 301–308.
114. Middleton, J. C.; Tipton, A. J. *Biomaterials* **2000**, *21*, 2335–2346.
115. Mhlanga et al. *ACS Appl. Mater. Interfaces* **2015**, *7*, 22692–22701
116. Suuronen, R.; Pohjonen, T.; Hietanen, J.; Lindqvist, C. J. *Oral Maxillofac. Surg.* **1998**, *56*, 604–614.
117. Zielhuis, S. W.; Nijsen, J. F. W.; Seppenwoolde, J.-H.; Bakker, C. J. G.; Krijger, G. C.; Dullens, H. F. J.; Zonnenbery, B. A.; Rijk, P. P. V.; Hennink, W. E.; Schip, A. D. V. G. *Biomaterials* **2007**, *28*, 4591–4599.
118. Miller, R. A.; Brady, J. M.; Cutright, D. E. *J. Biomed. Mater. Res.* **1977**, *11*, 711–719.
119. Middleton, J. C.; Tipton, A. J. *Med. Plast. Biomater.* **1998**, 31–38.
120. Conn, J.; Oyasu, R.; Welsh, M.; Beal, J. M. *Am. J. Surg.* **1974**, *128*, 19–23.
121. Quesada et al. *Chem. Mater.* **2013**, *25*, 2597–2602.
122. Pitt CG. Polycaprolactone and its copolymers. In: Chasin M, Langer R, editors. *Biodegradable polymers as drug delivery systems*. New York: Marcel Dekker; **1990**. p. 71–120.
123. Patlolla, A.; Collins, G.; Arinze, T. L. *Acta Biomater.* **2010**, *6*, 90–101.
124. Darney, P. D.; Monroe, S. E.; Klaisle, C. M.; Alvarado, A. *Am. J. Obstet. Gynecol.* **1989**, *160*, 1292–1295.
125. Li, J.; Li, L.; Yu, H.; Cao, H.; Gao, C.; Gong, Y. *ASAIO J.* **2006**, *52*, 321–327.
126. Garkhal, K.; Verma, S.; Tikoo, K.; Kumar, N. *J. Biomed. Mater. Res. A* **2007**, *82*, 747–756.
127. Guarino, V.; Ambrosio, L. *Acta Biomater.* **2008**, *4*, 1778–1787.
128. Xin, H.; Sha, X.; Jiang, X.; Zhang, W.; Chen, L.; Fang, X. *Biomaterials* **2012**, *33*, 8167–8176.
129. Kumar, A.; Lale, V.; Mahajan, S.; Choudhary, V.; Koul, V. *ACS Appl. Mater. Interfaces* **2015**, *7*, 9211–9227.
130. Zhang, W.; Li, Y.; Liu, L.; Sun, Q.; Shuai, X.; Zhu, W.; Chen, Y. *Biomacromolecules* **2010**, *11*, 1331–1338
131. Geng, Y.; Discher, D. E. *J. Am. Chem. Soc.* **2005**, *127*, 12780–12781

132. Yue, X.; Qiao, Y.; Qiao, N.; Guo, S.; Xing, J.; Deng, L.; Xu, J.; Dong, A.; *Biomacromolecules* **2010**, *11*, 2306–2312
133. Jin, Y.; Lian, S.; Su, Y.; Zhu, L.; Pang, Y.; Qiu, F.; Tong, G.; Yan, D.; Zhu, B.; Zhu, X. *Biomacromolecules* **2011**, *12*, 3460–3468.
134. Song, N.; Ding, D.; Pan, Z.; Li, J.; Zhou, L.; Tan, H.; Fu, Q. *Biomacromolecules* **2013**, *14*, 4407–4419.
135. Han, H. S.; Thambi, T.; Choi, K. Y.; Son, S.; Ko, H.; Chae, Y. S.; Kang, Y. M.; Lee, J. Y.; Park, J. H. *Biomacromolecules* **2015**, *16*, 447–456.
136. Sun, L.; Deng, X.; Yang, X.; Li, Z.; Wang, Z.; Li, L. Wu, Q.; Peng, F.; Liu, L.; Gong, C. *RSC Adv.* **2014**, *4*, 46737–46750
137. Zhao, P.; Li, D.; Yang, F.; Ma, Y.; Wang, T.; Duan, S.; Shen, H.; Cai, Q.; Wu, D.; Yanga, X.; Wang, S. *J. Mater. Chem. B* **2015**, *3*, 6885
138. Rainbolt, E. A.; Washington, K. E.; Biewera, M. C.; Stefan, M. C. *Polym. Chem.* **2015**, *6*, 2369–2381.
139. Peng, P.-Y.; Wang, S.-W.; Huab, M.-Y.; Lee, R.-S. *RSC Adv.* **2013**, *3*, 18453.
140. Cheng, Y. Hao, J.; Lee, L. A.; Biewer, M. C.; Wang, Q.; Stefan, M. C. *Biomacromolecules* **2012**, *13*, 2163–2173.
141. Rainbolt, E. A.; Washington, K. E.; Biewer, M. C.; Stefan, M. C. *J. Mater. Chem. B*, **2013**, 16532.
142. Hao, H.; Cheng, Y.; Ranatunga, R. J. K. Y.; Senevirathne, S.; Biewer, M. C.; Nielsen, S. O.; Wang, Q.; Stefan, M. C. *Macromolecules* **2013**, *46*, 4829–4838.
143. Garg, S. M.; Xiong, X.-B.; Lu, C.; Lavasanifar, A. *Macromolecules* **2011**, *44*, 2058–2066.
144. Riva, R.; Schmeits, S.; Jerome, C.; Jerome, R.; Lecomte, P. R.; *Macromolecules* **2007**, *40*, 796–803.
145. Tian, D.; Halleux, O.; Dubois, P.; Jerome, R. *Macromolecules* **1998**, *31*, 924–927.
146. Chang, L.; Deng, L.; Wang, W.; Lv, Z.; Hu, F.; Dong, A.; Zhang, J. *Biomacromolecules*, **2012**, *13*, 3301–3310.
147. Mahmud, A.; Xiong, X.-B.; Lavasanifar, A. *Macromolecules* **2006**, *39*, 9419–9428,
148. Xiong, X.-B.; Uludağ, H.; Lavasanifar, A. *Biomaterials* **2009**, *30*, 242–253
149. Trollsås, M.; Lee, V.; Mecerreyes, D.; Moller, M.; Miller, R. D.; Hedrick, J. L. *Macromolecules* **2000**, *33*, 4619–4627

## Chapter 2

### *Stimuli-responsive Poly(caprolactone) Vesicles for Dual Drug Delivery under GI Tract*





---

## ***Stimuli-responsive Poly(caprolactone) Vesicles for Dual Drug Delivery under GI Tract***

---

*The present investigation reports the first example of carboxylic functionalized poly(caprolactone) (PCL) block copolymer vesicles as novel dual drug delivery pH responsive vehicles for oral administration under gastrointestinal (GI) tract. New carboxylic functionalized caprolactone monomer was custom designed through multi-step organic reactions and polymerized under controlled ROP conditions using polyethylene glycol (PEG-2000) as initiator to produce amphiphilic diblocks, PEG-*b*-CPCL<sub>*x*</sub>, with *x*= 25, 50, 75 and 100. These carboxylic PCL block copolymers were self-organized into 100-250 nm vesicular assemblies. The size and shape of the vesicular assemblies were confirmed by light scattering, Zeta potential and electron microscopy. These vesicles were capable of loading both hydrophilic molecules (like rhodamine B, Rh-B) and hydrophobic drugs such as Ibuprofen (IBU) and camptothecin (CPT) in the core and layer, respectively. These pH responsive PCL vesicles were stable in strong acidic conditions (pH < 2.0, stomach) and ruptured to release the loaded cargoes under neutral or basic pH (pH =7.0, similar to that of small intestine). The drug release kinetics under simulated GI tract revealed that the individual drug loaded vesicles followed the combination of diffusion and erosion pathway whereas the stable dual drug loaded vesicles predominantly followed the diffusion controlled process. Thus, the custom designed PCL vesicles open up a new area of pH stimuli responsive polymer vehicles for delivering multiple drugs via oral drug delivery route which is yet to be explored for biomedical applications.*

## 2.1. Introduction

Oral delivery under gastrointestinal (GI) tract is one of the most elegant methods for the administration of drug molecules with improved patient compliances, low cost and ease of treatment and so on so forth.<sup>1</sup> An oral delivery is a very challenging task because the drug molecules should be stable and retained in the active form under the harsh GI tract and be intact against the p-glycoprotein mediated efflux effect.<sup>2</sup> Today we have major hurdles in the oral delivery of NSAIDS (nonsteroidal anti-inflammatory drugs), anti-cancer drugs and protein based therapeutics (mainly insulin).

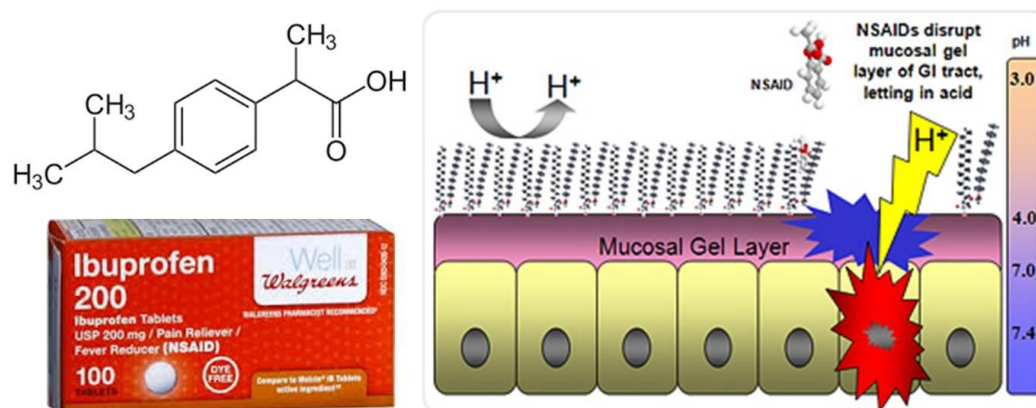


**Figure 2.1.** *Ibuprofen and schematic representation of disruption of mucosal layer by NSAIDS like IBU*

For example in the case of NSAIDS, such as Ibuprofen (IBU) that hinders the cyclooxygenase system and is used as an analgesic and antipyretic for a variety of inflammatory pathologies.<sup>3</sup> IBU can be used for a short and long duration therapy such as for headache and rheumatoid arthritis respectively. However, it is sparingly soluble in water<sup>4</sup>, and it is rapidly eliminated from systemic circulation displaying a relatively short half-life (1.7-2 h), and therefore, leading to several dosages for an effective and prolonged pharmacological activity<sup>5</sup>. The stomach's ability to protect itself from stomach acids gets interfered by these NSAIDS which lead to ulcers (see figure 2.1). As it is known that stomach has three defenses against digestive juices namely, mucus that coats the stomach lining and shields it from stomach acid, the bicarbonates that neutralize stomach acid, and blood circulation to the stomach lining that aids in cell renewal and repair; all of these all get hindered by NSAIDS. There are about some 20 different traditional drugs including aspirin, ibuprofen, naproxen, indomethacin, and piroxicam which are facing similar problems.<sup>5</sup> On the other hand, oral delivery of proteins such as insulin has received widest attention, however,

yet currently no oral insulin preparation exists. Oral administration of insulin was found to be ineffective for the treatment of insulin-dependent diabetes mellitus<sup>6</sup>. Since then the subcutaneous route has been the mainstay of insulin delivery until today. Hence, to achieve effective and prolonged drug levels for an extended period without having related gastric side effects, new polymer based formulations were urgently required for controlled and sustained release of various therapeutics.

pH-responsive synthetic polymers are particularly attractive for the above purpose since they can protect the drug molecules in the acidic stomach conditions (pH < 2.0) and burst instantaneously under neutral or basic pH (7.4 or > 7.4) in the small intestine to release the loaded cargoes.<sup>7-11</sup> Amphiphilic block copolymers<sup>12-14</sup>, random copolymers,<sup>15-19</sup> dendronized structures,<sup>20, 21</sup> polyacrylic acid<sup>22</sup>, polymethacrylic acid<sup>23, 24</sup>, poly(lactic-co-glutamic acid)<sup>25</sup> polycarboxylates<sup>26</sup>, amine functionalized polymers<sup>27-32</sup> and poly(trimethylene carbonate)-*b*-poly(L-glutamic acid)<sup>33,34</sup> are few important examples reported for releasing drugs under pH stimuli.

In general, among all the nano structures, vesicular assemblies are particularly important for drug delivery since they resemble the structure of the cell membrane and also provides features such as loading both water soluble and water insoluble drugs.<sup>35-37</sup> Most of the pH responsive polymer vesicles were employed for the administration of DNA,<sup>38</sup> gold nanoparticles,<sup>39</sup> MRI agents<sup>40,41</sup> and anticancer drug molecules<sup>42</sup> under *in vitro* conditions similar to that of intravenous delivery. It is rather surprising to notice that there is no report on pH stimuli-based polymer vesicles for oral drug delivery under GI tract. Thus, new efforts are required to explore pH responsive vesicular assemblies for both fundamental understanding as well as developing new scaffolds for oral drug delivery applications.

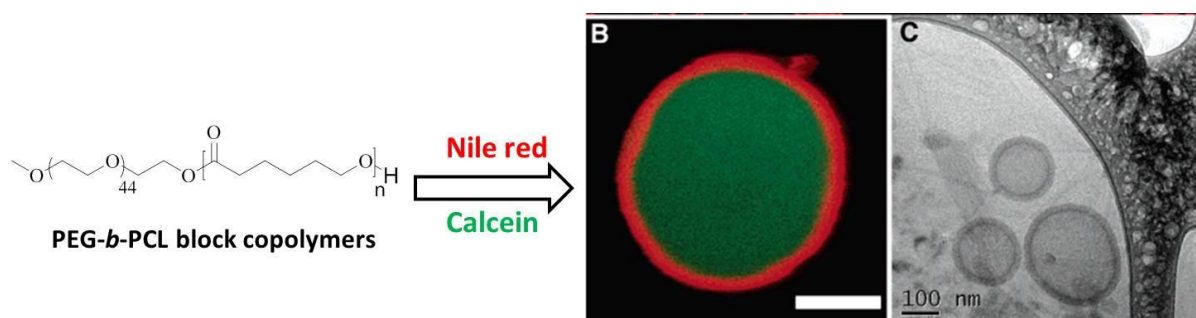


**Figure 2.2.** Preparation of PEG-*b*-PCL block copolymer based vesicles, and its CLSM and cryo-TEM images. (adapted from Ghoroghchain et al. *Macromolecules* **2006**,<sup>39</sup>, 1673-1675)

Poly(caprolactone) (PCL) is one of the most important commercial aliphatic polyester explored for biodegradable and biomedical applications.<sup>43</sup> PCL is water insoluble; however its block copolymer with hydrophilic polyethylene glycol (PEG) chains (PEG-*b*-PCL) provides appropriate hydrophilic and hydrophobic balance to self-organize in water.<sup>44, 45</sup> Typically, PEG-*b*-PCL block copolymers were known to produce only micelles (not vesicles) for delivering water insoluble hydrophobic drugs.<sup>46</sup> Few reports document the generation of these block copolymer vesicles under solvent assisted processing techniques.<sup>47-50</sup> For example, solvent combination of organic solvent + water is one of the methods used to produce vesicles. Ghoroghchain et al. reported the formation of PEG-*b*-PCL block copolymer vesicles via thin-film hydration method (see figure 2.2)<sup>49</sup> wherein, it is shown that by keeping PEG (2000) chain length constant and increasing the PCL chain length facilitates vesicle formation. In all the blocks the higher analogue PEG-*b*-PCL<sub>12K</sub> diblock copolymer showed the vesicular formation. Kurz et al. reported TOSUO substituted PEG-*block*-PCL for vesicle formation as shown in figure 2.3; however, they are not pH sensitive.<sup>50</sup> Unfortunately none of these conditions are suitable for delivering anticancer drugs using pH as stimuli. As a result, poly(caprolactone)s based pH responsive vesicles are not reported in the literature.

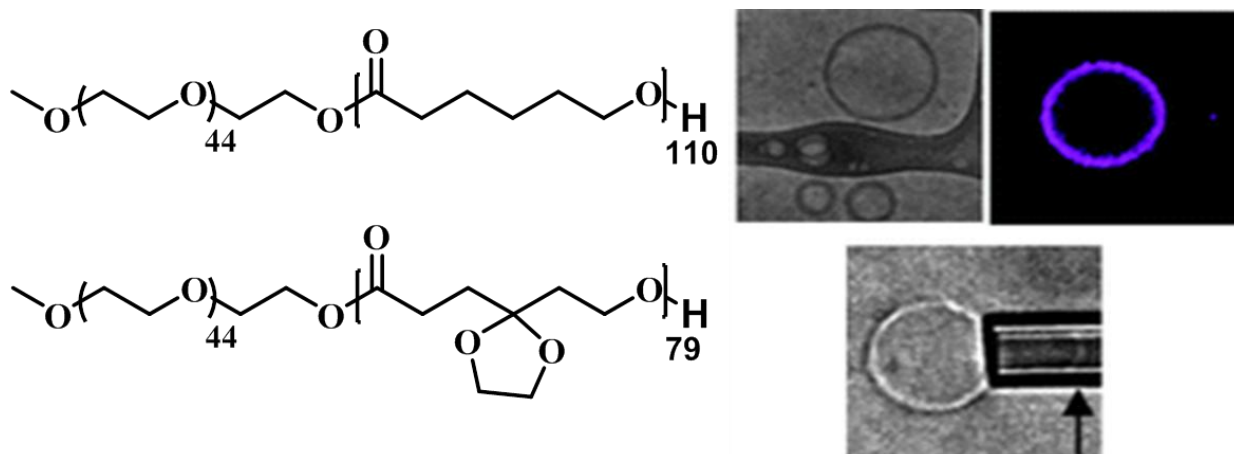


**Figure 2.3.** Preparation of PEG-*b*-PCL and PEG-*b*-PTOSUO block copolymer based vesicles, and its CLSM and cryo-TEM images. (adapted from Kurz et al. *Soft Matter*, **2012**, 8, 10853)

Functional Poly(caprolactone)s were also developed with hydroxyl<sup>51</sup>, alkyl<sup>52-55</sup>, azide<sup>56</sup>, and benzyl<sup>57,58</sup> or  $\alpha$ -cholesteryl<sup>59</sup> units and their micelles (or nanoparticles) were employed for drug delivery. Jerome and co-workers reported hydroxyl substituted and click chemistry based  $\alpha$ -position derivatives in poly(caprolactone)s.<sup>60-62</sup> Hedrick and co-workers

earlier attempted to make carboxylic poly(caprolactone)s; however, it was not successful since their monomer design was only capable of producing low molecular weight oligomers (no information is available on their molecular self-organization as well).<sup>63,64</sup> Thus, pH responsive PCL scaffolds are yet to be achieved for drug delivery both via oral and intravenous routes.

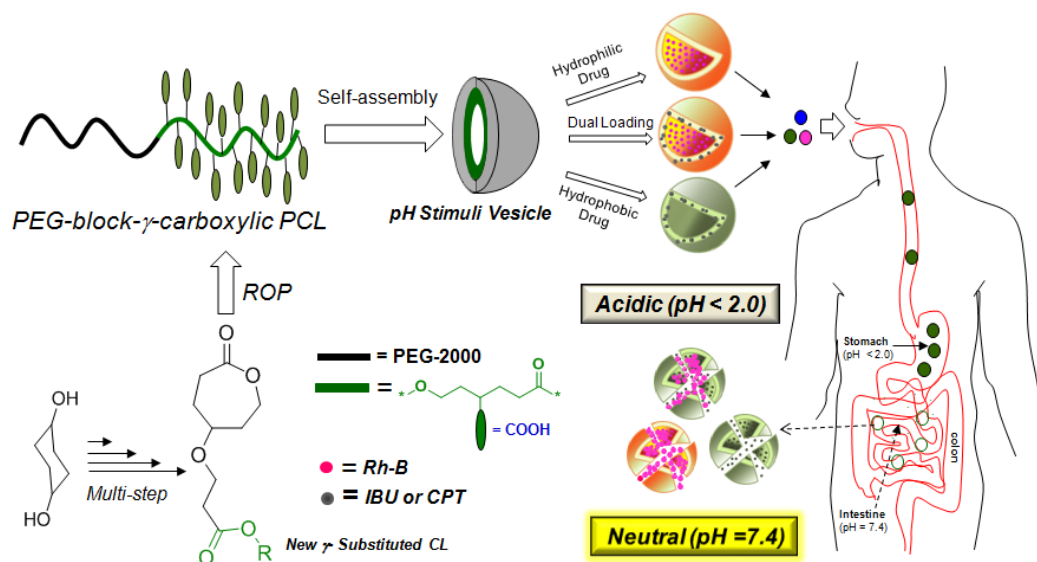


**Figure 2.4.** Carboxylic substituted PCL block copolymer vesicles and their pH stimuli rendered delivery under GI tract.

The present investigation is emphasized to address the two un-resolved problems in polymer drug delivery that are (i) design and development of pH responsive PCL block copolymers and (ii) investigation on the individual or dual drug loading and delivering capabilities of pH stimuli-based vesicular assemblies for oral delivery under GI tract. This new approach is schematically shown in figure 2.4. New substituted carboxylic acid caprolactone was synthesized through tailor-made approach and polymerized under controlled ROP conditions to produce series of PEG-*block*-carboxylic PCL (PEG-*b*-CPCL<sub>x</sub>, with x= 25 to 100). These new carboxylic functionalized block copolymers were completely water soluble and they self-organized into pH responsive polymer vesicles of 100 - 250 nm size. These pH stimuli PCL vesicles have unique ability to encapsulate both water soluble molecules such as Rhodamine-B (RhB) and insoluble anti-inflammatory drug Ibuprofen (IBU) and anticancer drugs like camptothecin (CPT). The *in vitro* release profiles of drug loaded vesicles were studied under simulated gastrointestinal conditions. The PCL vesicles were observed to stabilize the drug molecules under strong acidic conditions (like pH < 2.0 in stomach) and ruptured to release the cargoes under neutral pH, similar to that of small

intestine. Thus, the custom designed PCL vesicles open up new oral drug delivery approach for pH stimuli-incorporated polymerosomes, more specifically based on custom designed carboxylic PCL vesicles.

## 2.2. Experimental methods

**2.2.1. Materials:** 1,4-Cyclohexane diol, t-butyl acrylate, potassium t-butoxide, pyridinium chlorochromate (PCC), metachloroperbenzoic acid (MCPBA), Tin(II) 2-ethylhexanoate ( $\text{Sn}(\text{Oct})_2$ ), triethylene glycol monomethyl ether (TEG), polyethylene glycol monomethyl ether (MW = 2000, here after referred as PEG), caprolactone, Rhodamine B (Rh B), Ibuprofen (IBU) and camptothecin (CPT) were purchased from Aldrich chemicals. TEG and PEG were dried under vacuum oven prior to use. Catalyst  $\text{Sn}(\text{Oct})_2$  and caprolactone were distilled under vacuum and stored in glove box. All other solvents like tetrahydrofuran (THF) and trifluoroacetic acid (TFA) are purchased locally and distilled and kept under inert atmosphere prior to use.

**2.2.2. Measurements:** NMR was recorded using 400-MHz JEOL NMR Spectrophotometer. All NMR spectra were recorded in  $\text{CDCl}_3$  containing TMS as internal Standard. MALDI-TOF of the polymers was determined by using Applied Bio systems 4800 PLUS MALDI TOF/TOF analyzer. Polymer samples were dissolved in Tetrahydrofuran (THF) at 1mg/mL. Dihydroxy benzoic acid (DHB) was used as matrix. The matrix solution was prepared by dissolving 10 mg in 1 ml MeOH (or 30% ACN). To aid sample ionization, the MALDI target was pre spotted with 2mg/ml NaI in methanol and allowed to air-dry. Mass of the small intermediate precursors was determined using a HRMS-ESI-Q-Time of Flight LC-MS (SynaptG2, Waters). Gel permeation chromatographic (GPC) analysis which was performed using Viscotek VE 1122 pump, Viscotek VE 3580 RI detector and Viscotek VE 3210 UV/Vis detector in tetrahydrofuran (THF) using polystyrene as standards. Thermal analysis of all polymers was done using TA Q20 Differential Scanning Calorimeter. The instrument was calibrated with indium standards. All the polymers were heated to melt before recording their thermo grams to remove their previous thermal history. Polymers were heated and cooled at 10 °C/min under nitrogen atmosphere and their thermo grams were recorded. Thermal stability of the polymers was determined using Perkin Elmer thermal analyzer STA 6000 model at a heating rate of 10°C/min in nitrogen atmosphere. Water contact angle measurements were performed on a GBX model (DIGIDROP contact angle instrument) using Windrop software. Extreme care has been taken in carrying out sessile contact angle measurements to monitor contact angle values within 1 min to avoid the evaporation effects.

All contact angle measurements were carried out at room temperature (27 °C) and constant humidity (40–50%). The absorption and emission studies were done by a Perkin-Elmer Lambda 45 UV–visible spectrophotometer and SPEX Fluorolog HORIBA JOBIN VYON fluorescence spectrophotometer with a double-grating 0.22 m Spex1680 monochromator and a 450 W Xe lamp as the excitation source at room temperature. The excitation spectra were collected at 375 and 420 nm (Pyrene emission wavelength), and the emission spectra were recorded by exciting at the excitation maxima. The Pyrene samples were purged with N<sub>2</sub> gas for at least 15–20 min prior to photo physical experiments. Dynamic light scattering (DLS) was done using a Nano ZS-90 apparatus utilizing 633 nm red laser (at 90° angle) from Malvern Instruments. At 90° scattered fluctuations were detected to generate correlation function [ $g^2(t)$ ], from this function diffusion coefficient(D) calculated by using cumulant method. By applying stock-Einstein equation particle diameter was calculated. The reproducibility of the data was checked for at least three times using independent polymer solutions. The static light scattering experiment (SLS) was carried out using 3D-DLS spectrometer, from LS Instruments, Switzerland. The instrument consists of a He Ne laser having a wavelength of 632.8 nm attached to a computer using Lab view interface utilizing toluene as reference. The measurement was performed in autocorrelation mode from 20 to 130° by steps of 5°. FE-SEM images were recorded using Zeiss Ultra Plus scanning electron microscope. For FE-SEM analysis, the samples were prepared by drop casting on silicon wafers and coated with gold. TEM images were recorded using a Technai-300 instrument by drop casting the sample on Formvar-coated copper grid. The fluorescent micrographs were collected using Carl Zeiss Axiovert 200 microscope.

**2.2.3. Encapsulation in carboxylic PCL vesicles:** The detail procedure is given for Rhodamine-B encapsulation. In a typical experiment, 10 mg of the polymer and 1 mg of Rhodamine-B was dissolved in DMSO (2 ml). Distilled water (8 ml) was added drop wise into the polymer solution and the mixture was stirred at 25° C for 12 hours. The solution was transferred to a dialysis bag (MWCO=1000) and dialyzed against large amount of distilled water for 3-5 days. Fresh distilled water replaced periodically to ensure the removal of un-encapsulated molecules from the dialysis tube.

The drug loading efficiency (DLE) and drug loading content (DLC) were determined by absorption spectroscopy using the following equation:<sup>34</sup>

$$\text{DLE (\%)} = \{ \text{Weight of drug in vesicles} / \text{Weight of drug in Feed} \} \times 100 \%$$

$$\text{DLC (\%)} = \{ \text{Weight of drug in vesicles} / \text{Weight of Drug loaded vesicles} \} \times 100 \%$$

A similar procedure was followed to encapsulate Ibuprofen (IBU) and camptothecin (CPT) using 2 mg of drugs in the feed. Dual loading of Rh-B and IBU was performed using 1 mg of each of these molecules.

#### 2.2.4. *In vitro* drug release studies

Rh-B, IBU and CPT loaded vesicles were taken in a dialysis bag in 3 mL of solution and they were immersed in 100 ml beaker and dialyzed at 37 °C with constant stirring. Various pH buffers of 2.0, 4.0, 7.4 and 9.2 are employed for the dialysis studies. Simulated gastric fluid (SGF, 5.47 g HCl, 3.72 g KCl, 1 L water, pH 2) and simulated intestinal fluid (SIF, 8 g NaCl, 0.2 g KCl, 1.44 g Na<sub>2</sub>HPO<sub>4</sub>, 0.24 g KH<sub>2</sub>PO<sub>4</sub>, 1 L water, pH 7.4) were also prepared following literature report<sup>22</sup> for the released studies. At specific time intervals, 3.0 ml of the dialysate was withdrawn and replaced with an equal volume of fresh buffer. The amount of molecules released in each aliquot was measured using absorption spectroscopy and quantified to determine their percentage of cumulative release. Each experiment was triplicated in order to calculate standard error. Cumulative release (%) =  $C_n \times V_o / m \times 100$  where  $C_n$  is amount of loaded cargo in n<sup>th</sup> sample,  $V_o$  is total volume and  $m$  is total amount loaded in vesicles.

#### 2.2.5. Synthesis of t-butyl 3-((4-hydroxycyclohexyl) oxy) propionates (1)

1, 4-Cyclohexanediol (20.0 g, 172.0 mmol) and potassium t-butoxide (200 mg, 1.78 mmol) were taken in dry THF (200 mL) and stirred for 10 minutes under nitrogen. t-Butyl acrylate (11.0 g, 86.1 mmol) in dry THF (50 mL) was added drop wise and the reaction mixture was refluxed under dry conditions for 24 h. The solvent was removed by rotavapor and the content was neutralised with 1N HCl (20 mL). It was extracted with ethyl acetate and the organic layer was dried over anhydrous Na<sub>2</sub>SO<sub>4</sub>. The solvent was removed to get the product as viscous liquid. It was further purified by passing through silica column chromatography using ethyl acetate and petroleum ether (1 : 10 v/v) as eluent. Yield: 16.7 g (78.4 %). <sup>1</sup>H NMR (400MHz, CDCl<sub>3</sub>) δ ppm: 3.64 (m, 3H, O-CH<sub>2</sub>-and O-CH), 3.29-3.39 (m, 1H, CH-OH), 2.4 (t, 2H, -CH<sub>2</sub>CO-), 1.96-1.81 (m, 4H, OCH(CH<sub>2</sub>)<sub>2</sub>), 1.64-1.32 (m, 4H, CO(CH<sub>2</sub>)<sub>2</sub>), 1.45 (s, 9H, -C(CH<sub>3</sub>)<sub>3</sub>). <sup>13</sup>C-NMR (100 MHz, CDCl<sub>3</sub>) δ ppm: 171.08, 80.43, 69.50, 63.94, 63.53, 32.54, 30.33, 29.17 and 27.44. FT-IR (cm<sup>-1</sup>): 3421, 2977, 2935, 2863, 1727, 1456, 1393, 1366, 1255, 1155, 1106 and 1034. HR-MS (ESI<sup>+</sup>): m/z [M+Na<sup>+</sup>] calcd. for C<sub>13</sub>H<sub>24</sub>O<sub>4</sub> [M<sup>+</sup>] : 267.1572; found: 267.1562.



**2.2.6. Synthesis of tert-butyl 3-((4-oxocyclohexyl)oxy)propanoate (2):** PCC (16.7g, 77.9 mmol) was added to compound **1** (9.5 g, 38.9 mmol) in dry DCM (100 mL) under nitrogen atmosphere and the reaction mixture stirred at 25 °C for 4 h. The reaction mixture was filtered through molecular sieves to remove PCC salts. The filtrate was condensed and the resultant liquid was purified by passing through silica gel column by eluting with petroleum ether/EtOAc (1:4 v/v). The product was obtained as colourless liquid. Yield: 8.5 g (90 %). <sup>1</sup>H-NMR(400 MHz, CDCl<sub>3</sub>) δ ppm : 3.56 (m, 3H, O-CH<sub>2</sub> and O-CH), 2.58 (t, 2H, -CH<sub>2</sub>-CO), 2.64 (m, 2H, -(C=O)CH<sub>2</sub>-), 2.26 (m, 2H, -(C=O)CH<sub>2</sub>- ) 2.09 (m, 2H, -(CO)CH<sub>2</sub>-) 1.90(m, 2H, -(CO)CH<sub>2</sub>-), 1.45 (s, 9H, -C(CH<sub>3</sub>)<sub>3</sub>). <sup>13</sup>C-NMR (100MHz, CDCl<sub>3</sub>) δ ppm: 211.40, 170.99, 80.56, 72.74, 64.02, 37.02, 36.56, 30.40 and 20.04. FT-IR (cm<sup>-1</sup>): 2974, 2874, 2360, 1716, 1456, 1419, 1393, 1366, 1306, 1249, 1210 and 1100. HRMS (ESI<sup>+</sup>): m/z [M+Na<sup>+</sup>] calcd. for C<sub>13</sub>H<sub>22</sub>O<sub>4</sub> [M<sup>+</sup>] : 265.1415 ; found : 265.1411.

**2.2.7. Synthesis of tert-butyl 3-((7-oxooxepan-4-yl) oxy) propanoate (3):** m-Chloroperbenzoic acid (3.5 g, 17.3 mmol) was added slowly to a stirred solution of **2** (3.5 g, 14.4 mmol) in dry DCM (40 mL) under nitrogen atmosphere. To above reaction mixture, anhydrous NaHCO<sub>3</sub> (3.63g, 43.3 mmol) was added and the reaction was continued at 25 °C for 12 h. The solvent was removed and the residue was quenched with saturated aqueous NaHCO<sub>3</sub> solution (20 mL) and saturated aqueous Na<sub>2</sub>S<sub>2</sub>O<sub>3</sub> solution (20 mL). It was extracted with ethyl acetate and the organic layer was dried over anhydrous Na<sub>2</sub>SO<sub>4</sub>. After solvent evaporation, the crude product was purified by passing through silica gel column using ethyl acetate and petroleum ether (4:6 v/v). Yield= 3.2 g (92 %). The product **3** was obtained as colorless liquid <sup>1</sup>H-NMR (400 MHz, CDCl<sub>3</sub>) δ ppm : 4.40 (dd, 1H, COOCH), 4.06 (dd, 1H, COOCH) 3.60 (m, 4H, OCH<sub>2</sub>, OCH and COCH), 2.98 (dd, 1H, COCH), 2.48 (t, 2H, COCH<sub>2</sub>), 2.42-1.81 (m, 4H, OCH-(CH<sub>2</sub>)<sub>2</sub>), 1.46 (s, 9H, C(CH<sub>3</sub>)<sub>3</sub>) <sup>13</sup>C-NMR (100MHz, CDCl<sub>3</sub>) δ ppm: 176.55, 171.24, 80.99, 74.24, 64.24, 63.66, 36.77, 34.15, 28.40, 27.84 and 27.61. FT-IR (cm<sup>-1</sup>): 2925, 1725, 1456,1393, 1366, 1253, 1155, 1100 and 1058. HRMS (ESI<sup>+</sup>): m/z [M+K<sup>+</sup>] calcd. For C<sub>13</sub>H<sub>32</sub>O<sub>5</sub> [M<sup>+</sup>]: 299.3187; found: 299.3665.

**2.2.8. Ring opening polymerization of substituted Poly(caprolactone)s:** Typical procedure for ROP was described for the γ-substituted caprolactone monomer **3** with [M<sub>0</sub>]/[I<sub>0</sub>] = 100 and polyethylene glycol PEG-2000 monomethyl ether as initiator (for polymer PEG-*b*-BPCL<sub>100</sub>). MeO-PEG-2000 (31.0 mg, 0.0155 mmol) was taken in a flame dried schlenk tube and dry toluene (1.0 mL) was added under nitrogen atmosphere. To this mixture, Sn(Oct)<sub>2</sub> (3.1 mg, 0.0077 mmol) was added and the content was stirred at 25 °C 15 minutes under

nitrogen purge. The monomer **3** (0.4 g, 1.55 mmol) was added to the above mixture and the polymerization mixture was continued at 25 °C for 15 minutes under nitrogen purge. The polymerisation tube was immersed in preheated oil bath at 110 °C the polymerization was continued for 48 h with constant stirring. The polymerization mixture was precipitated in MeOH. The polymer was re-dissolved in THF and precipitated again in methanol. The purification was done at least twice to obtain highly pure polymer. Yield: 280 mg (70 %). <sup>1</sup>H-NMR (400MHz, CDCl<sub>3</sub>) δ ppm: 4.13 (s, 2H), 3.64 (s, 3.8 H), 3.45 (s, 1H), 3.38 (s, 1H), 2.44 (t, 2H), 2.35 (t, 2H), 1.93 – 1.81 (m, 2H), 1.81 – 1.67 (m, 4H), 1.44 (s, 9H, t-butyl). <sup>13</sup>C-NMR (400MHz, CDCl<sub>3</sub>): 173.63, 170.81, 80.72, 75.58, 70.68, 65.13, 61.47, 36.60, 33.04, 29.81, 28.86, and 28.22. FT-IR (cm<sup>-1</sup>): 2973, 2931, 1726 (C=O ester), 1457, 1364, 1251, 1156, 1099, 1062, 957, 898, 845 and 757. GPC molecular weights: M<sub>n</sub> = 18,400, M<sub>w</sub> = 24,900 and M<sub>w</sub>/M<sub>n</sub> = 1.35.

A similar procedure was followed for the synthesis of other compositions of PEG-*b*-BPCL<sub>x</sub> with x = 25, 50 and 75. Under the identical conditions caprolactone was also polymerized to produce a series of PEG-*b*-PCL<sub>x</sub> with x = 25, 50, 75, and 100. These details are provided below. Two homopolymers TEG-BPCL<sub>50</sub> and TEG-PCL<sub>50</sub> (these are not block copolymers) were also synthesized using triethyleneglycol monomethyl ether as initiator for [M<sub>0</sub>]/[I<sub>0</sub>] = 50 and these details are provided below.

**Synthesis of PEG initiated Amphiphilic Polycaprolactone (PEG-*b*-PCL<sub>25</sub>):** Caprolactone (0.5 g, 4.39 mmol), mPEG-2K (351.2 mg, 0.175 mmol) and Sn(Oct)<sub>2</sub> (35.5 mg, 0.0878 mmol) and <sup>1</sup>H NMR (400MHz, CDCl<sub>3</sub>) δ ppm: 4.05 (t, 2H), 3.64 (s, 6.2 H), 2.31 (t, 2H), 1.69 – 1.51 (m, 4H), 1.38 (t, 2H). FT-IR (cm<sup>-1</sup>): 3525, 2941, 2870, 1723, 1465, 1365, 1389, 1240, 1185, 1145, 1101, 1042, 956, 842 and 730. Yield: 300 mg (60%). M<sub>n</sub> (NMR) 5,306 g/mol; M<sub>n</sub> (SEC): 7,100 g/mol.

**Synthesis of PEG initiated Amphiphilic Polycaprolactone (PEG-*b*-PCL<sub>50</sub>):** Caprolactone (0.5 g, 4.39 mmol), mPEG-2K (175.6 mg, 0.0878 mmol) and Sn(Oct)<sub>2</sub> (17.7 mg, 0.0439 mmol) <sup>1</sup>H NMR (400MHz, CDCl<sub>3</sub>) δ ppm: 4.05 (t, 2H), 3.64 (s, 3.3 H), 2.31 (t, 2H), 1.69 – 1.51 (m, 4H), 1.38 (t, 2H). FT-IR (cm<sup>-1</sup>): 3525, 2942, 2867, 1722, 1767, 13665, 1293, 1239, 1179, 1100, 1040, 957 and 729. Yield: 400 mg (80%) M<sub>n</sub> (NMR) 8,156 g/mol; M<sub>n</sub> (SEC): 10,400 g/mol.

**Synthesis of PEG initiated Amphiphilic Polycaprolactone (PEG-*b*-PCL<sub>75</sub>):** Caprolactone (0.5 g, 4.39 mmol), mPEG-2K (117 mg, 0.0585 mmol) and Sn(Oct)<sub>2</sub> (11.8 mg, 0.029 mmol). <sup>1</sup>H NMR (400MHz, CDCl<sub>3</sub>) δ ppm: 4.05 (t, 2H), 3.64 (s, 2.36 H), 2.31 (t, 2H), 1.69 –

1.51 (m, 4H), 1.38 (t, 2H). FT-IR ( $\text{cm}^{-1}$ ): 2940, 2868, 2870, 1722, 1648, 1516, 1364, 1291, 1179, 1103, 1040, 956, 843 and 729. Yield: 390mg (78%).  $M_n$  (NMR) 10,660 g/mol;  $M_n$  (SEC): 11,500 g/mol.

**Synthesis of PEG initiated Amphiphilic Polycaprolactone (PEG-*b*-PCL<sub>100</sub>):** Caprolactone (0.5 g, 4.39 mmol), mPEG-2K (87.8 mg, 0.0439mmol) and Sn(Oct)<sub>2</sub> (8.8 mg, 0.0219 mmol). <sup>1</sup>H NMR (400MHz, CDCl<sub>3</sub>)  $\delta$  ppm: 4.06 (t, 2H), 3.64 (s, 1.78H), 2.31 (t, 2H), 1.69 – 1.51 (m, 4H), 1.38 (t, 2H). ). FT-IR ( $\text{cm}^{-1}$ ): 3648, 2943, 2867, 2361, 1722, 1648, 1516, 1464, 1365, 1292, 1239, 1174, 1102, 958, 839 and 728. Yield: 450mg (90%).  $M_n$  (NMR) 13,514 g/mol;  $M_n$  (SEC): 23,000 g/mol.

**Synthesis of  $\gamma$ - ter. Butyl substituted Amphiphilic polycaprolactone (PEG-*b*-BPCL<sub>25</sub>):**

Compound **3** (0.4 g, 1.55 mmol), mPEG (124 mg, 0.062 mmol) and Sn (Oct)<sub>2</sub> (12.5 mg, 0.031 mol). <sup>1</sup>H NMR (400MHz, CDCl<sub>3</sub>)  $\delta$  ppm: 4.05 (s, 2H), 3.64 (m, 10.6H), 3.45 (s, 1H), 3.38 (s, 1H), 2.44 (t, 2H), 2.35 (t, 2H), 1.93 – 1.81 (m, 2H), 1.81 – 1.67 (m, 4H), 1.44 (s, 9H). Yield: 300 mg (75%). FT-IR ( $\text{cm}^{-1}$ ): 2973, 2932, 1726, 1458, 1363, 1250, 1156, 1099, 1062, 959, 898, 846 and 757.  $M_n$  (NMR) 7,418 g/mol;  $M_n$  (SEC): 7,500 g/mol.

**Synthesis of  $\gamma$ - ter. Butyl substituted Amphiphilic polycaprolactone (PEG-*b*-BPCL<sub>50</sub>):**

Compound **3** (0.4 g, 1.55 mmol), mPEG (62 mg, 0.031 mmol), Sn(Oct)<sub>2</sub> (6.3 mg, 0.0155 mmol). <sup>1</sup>H NMR (400MHz, CDCl<sub>3</sub>)  $\delta$  ppm: 4.05 (s, 2H), 3.64 (m, 6.28 H), 3.45 (s, 1H), 3.38 (s, 1H), 2.44 (t, 2H), 2.35 (t, 2H), 1.93 – 1.81 (m, 2H), 1.81 – 1.67 (m, 4H), 1.44 (s, 9H). Yield: 370mg (92.5 %). FT-IR ( $\text{cm}^{-1}$ ): 2972, 2928, 2876, 1725, 1457, 1364, 1250, 1153, 1099, 956, 912, 846, 720 and 647.  $M_n$  (NMR) 12,836 g/mol;  $M_n$  (SEC): 9,200 g/mol.

**Synthesis of  $\gamma$ - ter. Butyl substituted Amphiphilic polycaprolactone. (PEG-*b*-BPCL<sub>75</sub>)**

Compound **3** (0.4 g, 1.55 mmol), mPEG (41.3 mg, 0.0206 mmol) and Sn(Oct)<sub>2</sub> (4.2 mg, 0.0103 mmol). <sup>1</sup>H NMR (400MHz, CDCl<sub>3</sub>)  $\delta$  ppm: 4.05 (s, 2H), 3.64 (s, 4.4 H), 3.45 (s, 1H), 3.38 (s, 1H), 2.44 (t, 2H), 2.35 (t, 2H), 1.93 – 1.81 (m, 2H), 1.81 – 1.67 (m, 4H), 1.44 (s, 9H). : FT-IR ( $\text{cm}^{-1}$ ): 2973, 2931, 1726, 1457, 1364, 1251, 1156, 1099, 957, 846, 720 and 647. Yield: 380mg (95%).  $M_n$  (NMR) 20,060 g/mol;  $M_n$  (SEC): 12,200 g/mol.

**Synthesis of TEG initiated Polycaprolactone (TEG - PCL<sub>50</sub>):** Caprolactone (0.5 g, 4.39

mmol), TEG (14.4 mg, 0.0878 mmol) and Sn(Oct)<sub>2</sub> (17.7 mg, 0.0439 mmol). <sup>1</sup>H NMR (400MHz, CDCl<sub>3</sub>)  $\delta$  ppm: 4.06 (t, 2H), 3.64 (s, 0.16 H), 2.31 (t, 2H), 1.69 – 1.51 (m, 4H), 1.38 (t, 2H). ). Yield: 300 mg (60%). FT-IR ( $\text{cm}^{-1}$ ): 3566, 2925, 2361, 1741, 1699, 1542, 1511, 1424, 1105, 822, and 619.  $M_n$  (NMR) 5,754 g/mol;  $M_n$  (SEC): 8,900 g/mol.

**Synthesis of  $\gamma$ - ter. Butyl substituted polycaprolactone (TEG - BPCL<sub>50</sub>):** Compound **3** (0.4 g, 1.55 mmol), TEG (5.1 mg, 0.031 mmol), Sn (Oct)<sub>2</sub> (6.3 mg, 0.0155 mmol). <sup>1</sup>H NMR (400MHz, CDCl<sub>3</sub>)  $\delta$  ppm: 4.13 (s, 2H), 3.64 (m, 2.17 H), 3.45 (s, 1H), 3.38 (s, 1H), 2.44 (t, 2H), 2.35 (t, 2H), 1.93 – 1.81 (m, 2H), 1.81 – 1.67 (m, 4H), 1.44 (s, 9H). FT-IR (cm<sup>-1</sup>): 3566, 2927, 2361, 1727, 1650, 1542, 1511, 1249, 1156, 1099, 956, 845, 756, 675 and 618. Yield: 370mg (85%). M<sub>n</sub> (NMR) 12,032 g/mol; M<sub>n</sub> (SEC): 11,000 g/mol.

**Synthesis of substituted carboxylic substituted Poly(caprolactone)s (PEG-*b*-CPCL<sub>x</sub>):** Trifluoroacetic acid (0.2 mL) was added slowly into PEG-*b*-BuCPCL<sub>100</sub> (200 mg) in dry DCM (5.0 mL) and the polymer solution was stirred at 25 °C for 30 minutes. The solvents were evaporated and the polymer was re-dissolved in THF and precipitated in cold methanol. The purification was repeated at least twice to get pure polymer. <sup>1</sup>H-NMR (400MHz, CDCl<sub>3</sub>)  $\delta$ : 4.14 (t, 2H, CH<sub>2</sub>OH), 3.84- 3.64 (m, 3.8 H, PEG and OCH<sub>2</sub>), 3.57 (m, 1H, OCH), 2.56 (t, 2H, CH<sub>2</sub>COOH), 2.38 (t, 2H, COCH<sub>2</sub>), 1.99 – 1.67 (m, 4H, -OCH (CH<sub>2</sub>)<sub>2</sub>). FT-IR (cm<sup>-1</sup>): 3447, 2932, 2450, 1711(C=O acid), 1355, 1257, 1175, 1096, 1059 and 955.

A similar procedure was followed for the hydrolysis of PEG-*b*-BPCL<sub>x</sub> to produce PEG-*b*-CPCL<sub>x</sub>, where x = 25, 50, 75 and also TEG-*b*-CPCL<sub>50</sub> from TEG-*b*-BPCL<sub>50</sub>.

**Synthesis of (PEG-*b*-CPCL<sub>25</sub>):**<sup>1</sup>HNMR (400MHz, CDCl<sub>3</sub>)  $\delta$ : 4.14 (t, 2H), 3.84- 3.64 (m 10.6H), 3.57 (m, 1H), 2.56 (t, 2H), 2.38 (t, 2H), 1.99 – 1.67 (m, 4H). FT-IR (cm<sup>-1</sup>): 3450, 2880, 1749, 1352, 1252, 1180, 1092, 948, 917, 841 and 730. M<sub>n</sub> (NMR) 6,242 g/mol; M<sub>n</sub> (SEC): 5,300 g/mol.

**Synthesis of (PEG-*b*-CPCL<sub>50</sub>):**<sup>1</sup>HNMR (400MHz, CDCl<sub>3</sub>)  $\delta$ : 4.14 (t, 2H), 3.84- 3.64 (m 6.3H), 3.57 (m, 1H), 2.56 (t, 2H), 2.38 (t, 2H), 1.99 – 1.67 (m, 4H). FT-IR (cm<sup>-1</sup>): 3447, 2923, 1717, 1454, 1352, 1252, 1179, 1091, 948 and 841. M<sub>n</sub> (NMR) 10,484 g/mol; M<sub>n</sub> (SEC): 7,200 g/mol.

**Synthesis of (PEG-*b*-CPCL<sub>75</sub>):**<sup>1</sup>HNMR (400MHz, CDCl<sub>3</sub>)  $\delta$ : 4.14 (t, 2H), 3.84- 3.64 (m, 4.4H), 3.57 (m, 1H), 2.56 (t, 2H), 2.38 (t, 2H), 1.99 – 1.67 (m, 4H). FT-IR (cm<sup>-1</sup>): 3503, 2932, 1720, 1355, 1255, 1173, 1096, 1062, 954 and 843. M<sub>n</sub> (NMR) 16,140 g/mol; M<sub>n</sub> (SEC): 10,500 g/mol.

**Synthesis of (TEG-*b*-CPCL<sub>50</sub>):**<sup>1</sup>HNMR (400MHz, CDCl<sub>3</sub>)  $\delta$ : 4.14 (t, 2H), 3.84- 3.64 (m, 2.12 H), 3.57 (m, 1H), 2.56 (t, 2H), 2.38 (t, 2H), 1.99 – 1.67 (m, 4H). FT-IR (cm<sup>-1</sup>): 3677, 2927, 2361, 1705, 1651, 1555, 1458, 1423, 1171, 1097 and 1055. M<sub>n</sub> (NMR) 9,456 g/mol; M<sub>n</sub> (SEC): 5,000 g/mol.

## 2.3. Results and Discussion

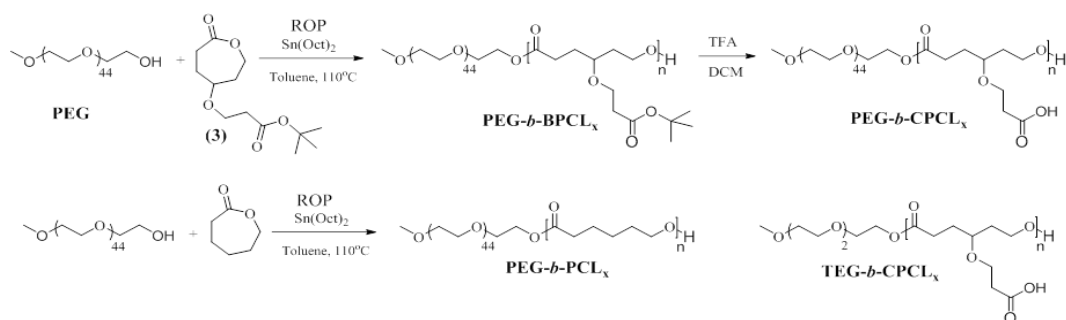
### 2.3.1 Synthesis and Characterization of Polymers

The synthesis of substituted caprolactone is shown in scheme 2.1. A new route is developed for producing these compounds from commercially available 1,4-cyclohexanediol through multi-step reactions. 1,4-cyclohexanediol was reacted with t-butyl acrylate in the presence of potassium t-OBu via Michael reaction to produce (1) in high yield. **1** was oxidized with PCC to convert the hydroxyl group into corresponding cyclohexanone derivative (**2**). The compound **2** was subjected to Baeyer villiger oxidation to produce  $\gamma$ -substituted ester caprolactone monomer **3** in good yield. All the above intermediates were completely characterized by NMR, FT-IR and HR-MS and their details are given below.



**Scheme 2.1.** Synthetic scheme of substituted CL monomer.

Polyethylene glycol monomethyl ether (MW = 2000, here after referred as PEG) was employed as hydrophilic initiator for the ROP using the  $\text{Sn}(\text{Oct})_2$  as transition metal catalyst. The ratio of the  $\text{Sn}(\text{Oct})_2$  catalyst to PEG was maintained as 1:2 in mole ratio so that the required concentration of active initiator  $\text{SnO-PEG}$  could be generated in-situ for the ROP initiation.<sup>65</sup> The monomer to initiator ratio was varied from  $[\text{M}_0]/[\text{I}_0] = 25, 50, 75$  and 100 to produce different amount of carboxylic functional groups in the Poly(caprolactone) chain in the diblock copolymers (see scheme 2.2). The ROP was first optimized for caprolactone monomer in laboratory conditions prior to the newly designed monomer **3**. Thus, the PEG-2000 initiated ROP produced two series of block copolymers  $\text{PEG-}b\text{-PCL}_x$  and  $\text{PEG-}b\text{-BPCL}_x$ , where  $x =$  represents the number of repeating units in the polymers. Further, triethylene glycol monomethyl ether (TEG) was employed as initiator to make two homopolymers  $\text{TEG-PCL}_{50}$  and  $\text{TEG-BPCL}_{50}$  (these are not block copolymers). For these homopolymers,  $[\text{M}_0]/[\text{I}_0]$  ratio was kept as 50 in the feed. The t-butyl ester group in the blocks of  $\text{PEG-}b\text{-BPCL}_x$  and homopolymer  $\text{TEG-BPCL}_{50}$  were hydrolysed to obtain their corresponding carboxylic acid derivatives  $\text{PEG-}b\text{-CPCL}_x$  and  $\text{TEG-CPCL}_{50}$ , respectively (B = t-butyl ester and C = carboxylic acid).



**Scheme 2.2.** Synthetic scheme of homo and block polymers from substituted CL monomer.

The  $^1\text{H-NMR}$  spectra of the PEG-*b*-BPCL<sub>*x*</sub> diblock copolymers are depicted in figure 2.5 where *x* is 25, 50, 75 and 100. The quantification of caprolactone units (repeating units-*X<sub>n</sub>*) in diblock polymers were done by comparing the -OCH<sub>2</sub>CH<sub>2</sub>O- in the PEG part appeared at 3.65 ppm for 180 protons (45 units x 4H) with the methylene protons of PCL at 4.05 (OCH<sub>2</sub>) as depicted in the figure 2.5 for both series of diblock copolymers (in detail explained for PEG-*b*-CPCL<sub>100</sub> below). From the figure 2.5 it is clearly evident in the above spectra that the intensity of the BPCL units increased (see the arrow mark in figure 2.5) with increase in the [M<sub>0</sub>]/[I] ratio in the feed. On the other hand PEG-*b*-PCL<sub>*x*</sub> block copolymers also characterized in similar way.

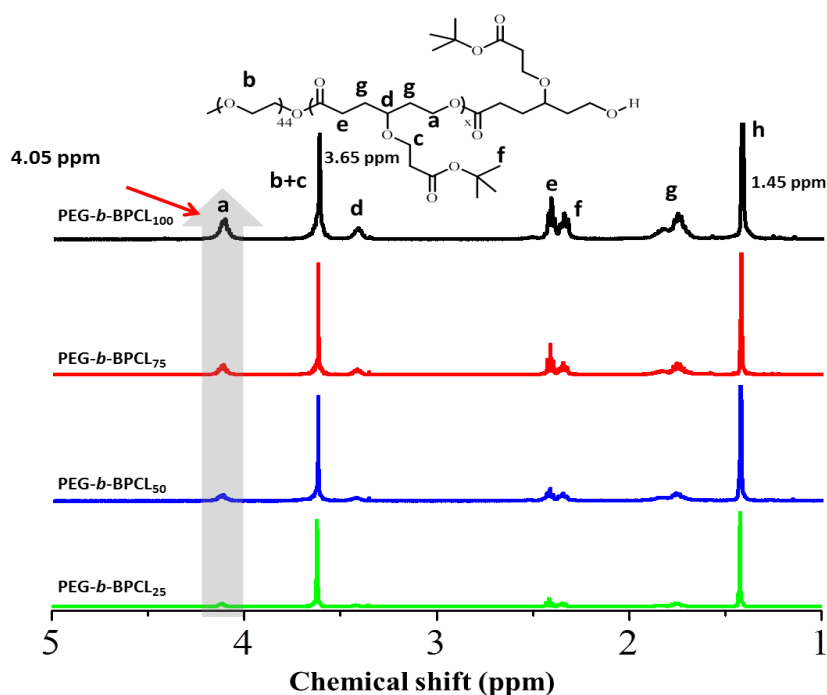


**Figure 2.5.** The stack plot of  $^1\text{H-NMR}$  spectra of PEG-*b*-BPCL<sub>*x*</sub> diblock copolymers.

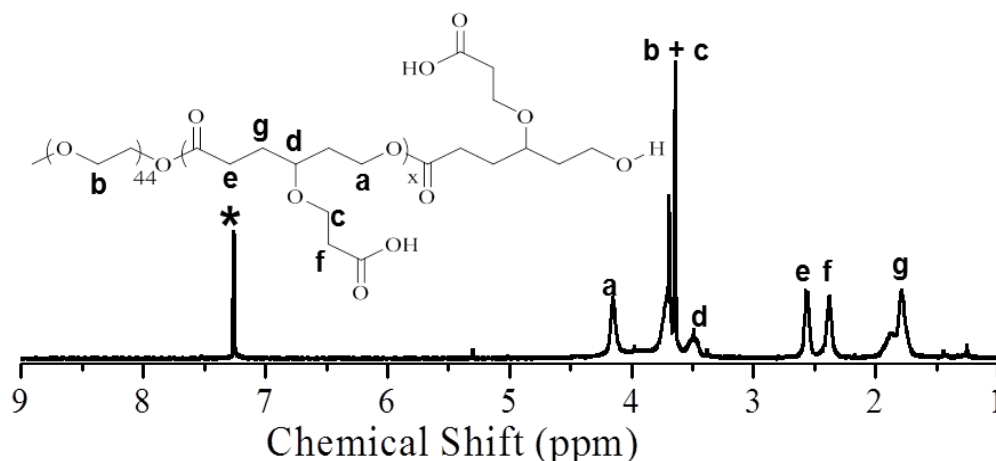


**Figure 2.6.**  $^1\text{H-NMR}$  spectrum of PEG-*b*-CPCL<sub>100</sub> block copolymer.

$^1\text{H-NMR}$  spectrum of PEG-*b*-CPCL<sub>100</sub> is shown in figure 2.6. The protons in the repeating units are assigned with alphabets in the structure and their corresponding peaks are indicated in the spectrum. In figure 2.6 -OCH<sub>2</sub>CH<sub>2</sub>O- in the PEG part (proton-b) appeared at 3.65 ppm and upon polymerization new ester peak appeared at 4.05 ppm (proton a) and all other CL repeating unit protons appeared with respect to expected structure. A similar NMR analysis was done for other samples to confirm their structure. The comparison of the peak intensities of the PEG part (proton-b at 3.65 ppm) and the CL repeating units (protons at 4.05 ppm) gave the number average degree of polymerization,  $n = 99$  in the present case. Similarly, the  $n$  values for PEG-*b*-PCL <sub>$x$</sub>  and PEG-*b*-CPCL <sub>$x$</sub>  were determined and these values are summarized in table 2.1. The  $n$ , number of repeating units in the copolymers were increased with the  $[\text{M}_0]/[\text{I}_0]$  in the feed showed a linear trend for both PEG-*b*-PCL <sub>$x$</sub>  and PEG-*b*-BPCL <sub>$x$</sub>  series (see figure 2.5).

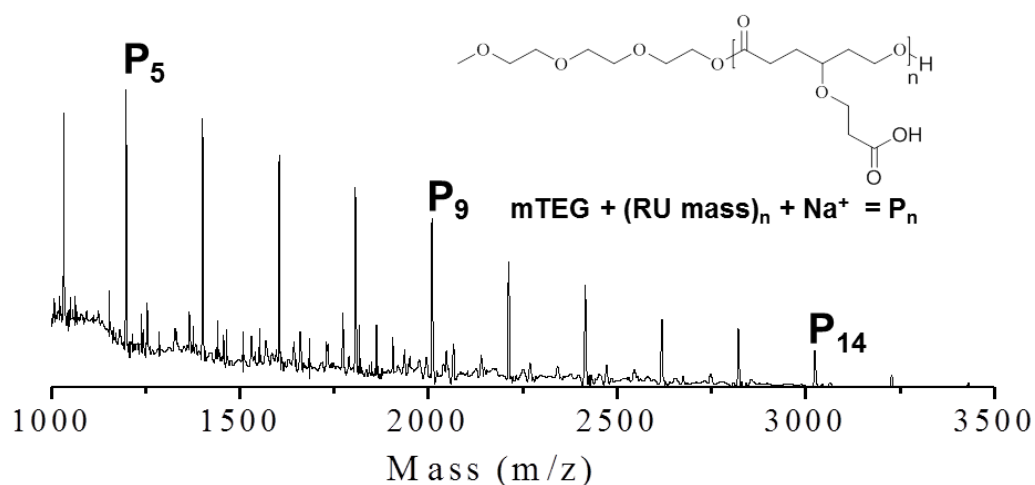


**Figure 2.7.** MALDI-TOF-MS spectrum of TEG-CPCL<sub>50</sub>.

MALDI-TOF is a powerful tool for the end group analysis of new polymers. For this purpose, the TEG initiated homopolymers TEG-CPCL<sub>50</sub> was subjected for the MALDI-TOF analysis. MALDI-TOF MS spectra of the TEG-CPCL<sub>50</sub> is shown in figure 2.7. Wherein, the peaks were well separated by 202 amu with respect to carboxylic caprolactone repeating unit mass. The peaks followed the sequence  $P_n = \text{MeO-TEG} + (202)_n + \text{Na}^+$  which confirmed the formation of expected polymer structure by ROP. Further, the MALDI-TOF mass spectra did not show peaks with respect to the presence of catalyst or other impurities<sup>66</sup> at the chain ends indicating the formation of highly pure polymer.

**Table 2.1.** Molecular weights and  $[M_0]/[I_0]$  ratio of PCL and substituted PCL

Polymer	Monomer	Feed [M <sub>0</sub> ]/[I <sub>0</sub> ]	M <sub>n</sub> <sup>b</sup>	N <sup>c</sup> (NMR)	M <sub>n</sub> <sup>d</sup> (NMR)	M <sub>n</sub> <sup>e</sup> (GPC)	M <sub>w</sub> <sup>e</sup> (GPC)	M <sub>w</sub> /M <sub>n</sub> <sup>e</sup> (GPC)
PEG- <i>b</i> -PCL <sub>25</sub>	CL	25	4,900	29	5,300	7,100	8,700	1.21
PEG- <i>b</i> -PCL <sub>50</sub>	CL	50	7,700	54	8,100	10,400	11,500	1.11
PEG- <i>b</i> -PCL <sub>75</sub>	CL	75	10,600	76	10,600	11,500	13,600	1.18
PEG- <i>b</i> -PCL <sub>100</sub>	CL	100	13,400	101	13,500	23,000	30,000	1.31
PEG- <i>b</i> -BPCL <sub>25</sub>	3	25	8,500	21	7,400	7,500	9,100	1.39
PEG- <i>b</i> -BPCL <sub>50</sub>	3	50	14,900	42	12,800	9,200	12,900	1.22
PEG- <i>b</i> -BPCL <sub>75</sub>	3	75	21,400	70	20,000	12,200	15,600	1.27
PEG- <i>b</i> -BPCL <sub>100</sub>	3	100	27,800	99	27,500	18,400	24,900	1.35
BPCL <sub>50</sub> <sup>a</sup>	3	50	13,100	46	12,000	11,000	14,700	1.34

<sup>a)</sup> Polymers are synthesized using MeO-TEG as initiator. <sup>b)</sup> Theoretical M<sub>n</sub> was calculated based on  $M_n = (\text{repeating unit mass}) \times n$ . <sup>c)</sup> number of repeating units are determined by <sup>1</sup>H-NMR. <sup>d)</sup> M<sub>n</sub> was calculated based on repeating units obtained from NMR i.e.  $M_n = (\text{repeating unit mass}) \times n$ . <sup>e)</sup> Molecular weights are determined by GPC using polystyrene as standard in THF

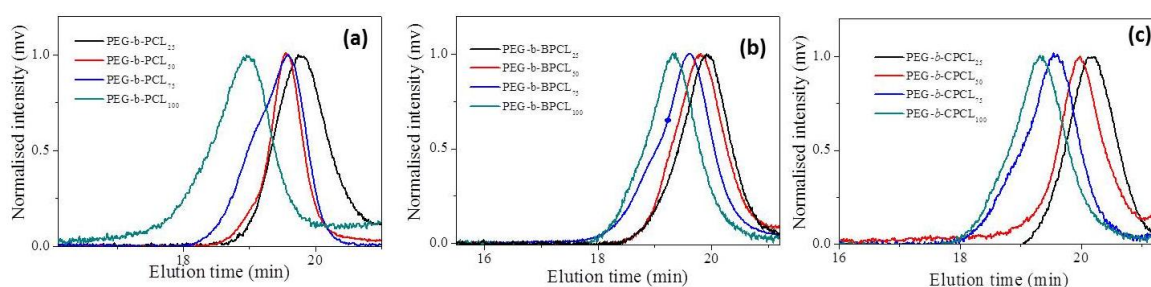


**Figure 2.8.** GPC chromatograms of PEG-*b*-PCL<sub>x</sub> (a), PEG-*b*-BPCL<sub>x</sub> (b), and PEG-*b*-CPCL<sub>x</sub> diblock copolymers.

The molecular weights of the polymers were determined by gel permeation chromatography using polystyrene standards. All the polymers showed mono modal (see figure 2.8) distribution and the M<sub>n</sub>, M<sub>w</sub> and polydispersities (M<sub>w</sub>/M<sub>n</sub>) are summarized in table 2.1. The M<sub>n</sub> of the polymers increased with increase in the  $[M_0]/[I_0]$  ratio in the feed in both



PEG-*b*-PCL<sub>x</sub> and PEG-*b*-BPCL<sub>x</sub> series. Further, the polydispersities of the polymers were also relatively low < 1.4 confirming the formation of well-defined homogeneous polymer in the ROP process.

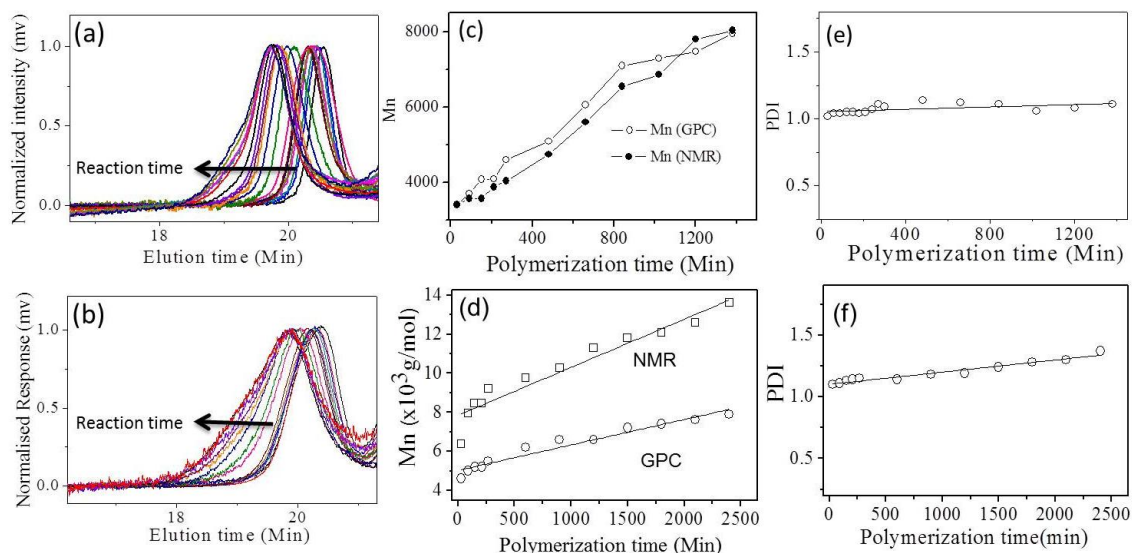


**Figure 2.9.** GPC chromatograms of aliquots of ROP kinetics for caprolactone (a) and monomer 3 (b), Plot of molecular weights (c) and PDI (d) of aliquots collected during the ROP reaction kinetics of caprolactone. Plot of molecular weights (e) and PDI (f) of aliquots collected during the ROP reaction kinetics of monomer 3.

To further understand the ROP capability of newly synthesized monomer; a detailed ROP kinetics was carried out for both CL and the new monomer **3**. For this purpose MeO-PEG-2000 was used as initiator and  $[M_0]/[I_0]$  ratio was fixed as 50. These kinetic reactions were performed for 48 h and samples were retrieved at various time intervals. The polymer samples were precipitated in methanol and the samples were subjected to both GPC and <sup>1</sup>H-NMR to determine their molecular weights and the degree of polymerization (*n*). The GPC chromatograms for reaction kinetics of CL and monomer **3** were presented in figure 2.9a and figure 2.9b respectively. In both cases, the GPC plots showed mono modal distribution and also showed gradual increase in molecular weights with reaction time. The  $M_n$  (GPC and NMR) of these samples were plotted against the polymerization reaction time for CL and as well as for new monomer **3** and are showed in figure 2.9c and 2.9d, respectively. The  $M_n$  observed from GPC and <sup>1</sup>H-NMR are similar to each other and is found to be linearly increase with polymerization time. On the other hand, in the case of monomer **3**, the  $M_n$  obtained from NMR was found to be slightly higher compared to GPC data indicating a slight under estimation of molecular weights by GPC. The polydispersities of these kinetic samples were plotted against the polymerization reaction time for CL and as well as for new monomer

**3** and showed in figure 2.9e and 2.9f, respectively.  $M_n$  linearly increased with the reaction time and the polydispersities of the samples were obtained below 1.2 (CL) and 1.4 (monomer **3**) indicating their narrow molecule weight distributions. Hence, it may be concluded that newly designed carboxylic functionalized caprolactone monomer **3** is very good for producing controlled molecular weights under control ROP kinetics, similar to that of caprolactone monomer.<sup>67, 68</sup> The TGA profiles of these newly synthesized diblock copolymers are shown decomposition at 240 °C as depicted in figure 2.10 a. In figure 2.10b DSC thermograms of these polymers are showed, which shows the thermal glass transition temperature ( $T_g$ ) around -10 °C, proves the amorphous nature of the block copolymer.

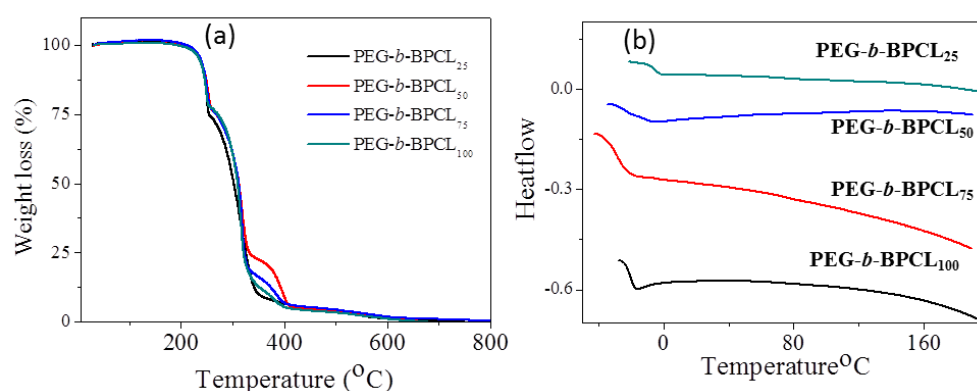


**Figure 2.10.** TGA profiles (a) and DSC thermograms (b) of the block polymers at 10 °C/min heating/cooling rate.

### 2.3.2. Self-assemblies of Substituted PCL

The newly designed PEG-*b*-CPCL<sub>x</sub> polymers have unique features of amphiphilic A-B diblocks with hydrophilic PEG and hydrophobic carboxylic substituted PCL chains. To determine the self-assembled structures in water, they were subjected to dynamic light scattering (DLS) measurement. The DLS histogram of two di-blocks PEG-*b*-BPCL<sub>100</sub> and its carboxylic derivative PEG-*b*-CPCL<sub>100</sub> are shown in figure 2.11a and 2.11b respectively. PEG-*b*-BPCL<sub>100</sub> was found to be partially soluble in water and produced turbid solution whereas the carboxylic functionalized block PEG-*b*-CPCL<sub>x</sub> was freely soluble in water (see vials figure 2.11a and 2.11b). DLS histogram of PEG-*b*-BPCL<sub>100</sub> showed bimodal distribution with an average size of 530 ± 10nm whereas PEG-*b*-CPCL<sub>100</sub> showed uniform mono modal distributions with average sizes of 100 ± 10nm.

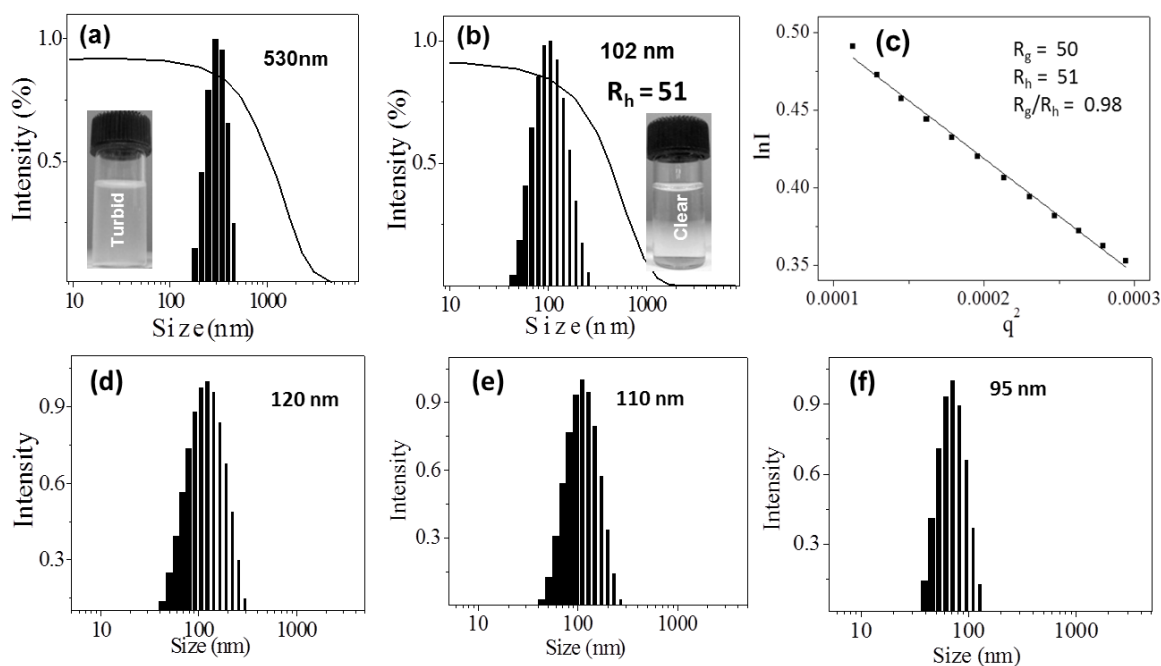


**Figure 2.11.** DLS histograms of *PEG-b-BPCL*<sub>100</sub> (a) and *PEG-b-CPCL*<sub>100</sub> (b) at 0.5 mg/mL at 25 °C. Static light scattering data of *PEG-b-CPCL*<sub>100</sub> (c). DLS histograms of *PEG-b-BPCL*<sub>25</sub> (d), *PEG-b-CPCL*<sub>50</sub> (e) and *PEG-b-CPCL*<sub>50</sub> (f) at 0.5 mg/mL at 25 °C.

The hydrodynamic radius of the vesicle ( $R_h$ ) was calculated as 51 nm (half-of the vesicular diameter, see figure 2.11b). Static light scattering analysis of the vesicles (see figure 2.11c) provided the radiation of gyration of vesicular assemblies ( $R_g$ ) from the slope of Guinier plot as 50 nm. The ratio of  $R_g/R_h$  was obtained as 0.98 which confirmed the existence of vesicular geometry of *PEG-b-CPCL*<sub>100</sub> diblock copolymer.<sup>69, 70</sup> Similar results were observed in other diblock copolymers including *PEG-b-CPCL*<sub>25</sub>, *PEG-b-CPCL*<sub>50</sub> and *PEG-b-CPCL*<sub>75</sub> as shown in figure 2.11d, e and f respectively. The size of the aggregates was decreased with increase in the carboxylic groups in the back bone of the diblock copolymer.

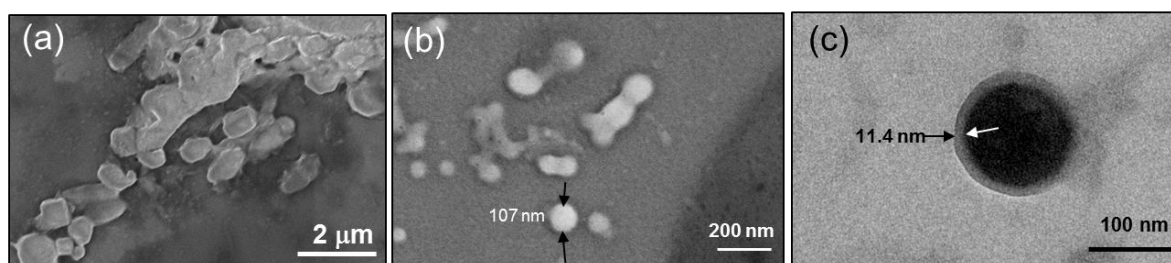


**Figure 2.12.** FE-SEM images of *PEG-b-BPCL*<sub>100</sub> (a) and *PEG-b-CPCL*<sub>100</sub> (b). HR-TEM image of *PEG-b-CPCL*<sub>100</sub> (c) at 0.5 mg/mL at 25 °C.

The morphologies of the PEG-*b*-PCL<sub>100</sub> and PEG-*b*-CPCL<sub>100</sub> nano-aggregates were analysed by electron microscopes. Field emission scanning electron microscopy (FE-SEM) images of these diblock aggregates are shown in figure 2.12a and 2.11b. PEG-*b*-CPCL<sub>100</sub> appeared as  $107 \pm 5$  nm soft spherical objects and resembles morphology of polymer vesicles whereas PEG-*b*-BPCL<sub>100</sub> showed the formation of larger particles of 0.5  $\mu\text{m}$  in size. The sizes of self-assembled aggregates in DLS (see figure 2.10) are in very good agreement with the sizes of the FE-SEM images. To further confirm the existence of the vesicle in PEG-*b*-CPCL<sub>100</sub> sample, it was subjected to high resolution transmission electron microscope (HR-TEM). In order to visualize more clearly the vesicle formation in the block copolymers, the samples were stained using uranyl acetate following reported procedure.<sup>74-76</sup> The vesicles obtained using the staining methods clearly showed the existence of vesicles in figure 2.12c. The vesicles were appeared as hydrophilic layer of 11.4 nm thickness with distinct inner cavity. Thus the, HR-TEM confirmed the formation of vesicular structures in PEG-*b*-CPCL<sub>100</sub>. Thus, the carboxylic acid PCL di blocks are very unique and capable of self-assembling into nano-vesicular scaffolds in water. Thus, the newly designed carboxylic PCL block copolymers are very unique to produce small and stable nano-aggregates in water.

No of CL Unit (n)	Image	Angle ( $\theta$ )	Image	Angle ( $\theta$ )	Image	Angle ( $\theta$ )
25		28.5		40.5		34.3
50		66.7		46.4		26.5
75		72.4		54.5		20.2
100		72.6		60.1		16.6

**Figure 2.13.** High definition images of water contact angle of polymers with their respective angles.

Water contact angle (WCA) measurements provide direct information on the hydrophilic or hydrophobic nature of amphiphilic polymers.<sup>71-73</sup> WCA for the newly synthesized block polymers including PEG<sub>x</sub>-*b*-PCL<sub>100</sub>, PEG<sub>x</sub>-*b*-BPCL<sub>100</sub> and PEG-*b*-CPCL<sub>100</sub> were determined by the sessile drop method. The photographs of water droplets on the

polymer film (on glass substrate) are shown in figure 2.13 along with their contact angles. PEG-*b*-BPCL<sub>x</sub> series showed increase in the WCA with increase in the number of caprolactone unit in the diblocks. The WCA for PEG-*b*-BPCL<sub>x</sub> series were found to be 40 to 60° with respect to hydrophobic in nature. A similar trend was also observed in the PEG-*b*-PCL<sub>x</sub> (see SF-17). This indicated that the hydrophobicity of the block copolymers increased with increases in the butyl-substituted units (or normal caprolactone unit). On the other hand, the carboxylic acid functionalized di-block PEG-*b*-CPCL<sub>x</sub> series showed excellent hydrophilicity with WCA less than 30°. <sup>73</sup> The increase in the hydrophilicity in PEG-*b*-CPCL<sub>x</sub> enhanced their water solubility as well as the formation of stable nano-aggregates.

### 2.3.3. Encapsulation Capabilities of PCL Vesicles

Vesicles are unique self-assembled structures for dual loading of hydrophobic and hydrophilic molecules in the layer and core, respectively. To study the loading capabilities of carboxylic PCL vesicles, water soluble Rhodamine-B (Rh-B) and water insoluble drugs Ibuprofen (IBU, anti-inflammatory drug) and camptothecin (CPT, anti-cancer drug) were chosen. In the present studies three types of loaded vesicles are produced from PEG-*b*-CPCL<sub>100</sub> diblock: (i) hydrophilic molecule Rh-B loaded vesicle ( $V_{\text{Rh-B}}$ ); (ii) hydrophobic drugs loaded vesicles  $V_{\text{IBU}}$  and  $V_{\text{CPT}}$  and (iii) hydrophilic + hydrophobic dual loaded vesicle  $V_{\text{RhB+IBU}}$ . Rh-B encapsulation is one of the most important control experiment to prove the existence of vesicular scaffolds in polymer assemblies. For example, micelles or nanoparticles cannot encapsulate the water soluble Rh-B since their internal part is hydrophobic.

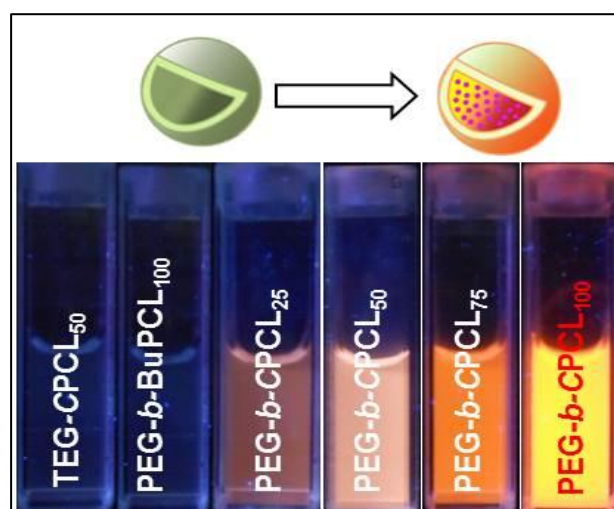


**Figure 2.14:** Photographs of vials containing the polymers after Rh-B encapsulation under UV light.



PEG-*b*-BPCL<sub>100</sub>, PEG-*b*-CPCL<sub>100</sub> and TEG-CPCL<sub>50</sub> were subjected to Rh-B encapsulation in water. The photographs of the Rh-B encapsulated samples in vials after dialysis are shown in figure 2.14 (photographs captured under hand held UV-light exposure). As it can be clearly evident that the carboxylic PCL block copolymer showed the stable encapsulation of Rh-B whereas its butyl ester and homopolymer TEG-CPCL<sub>50</sub> did not stabilize Rh-B. This observation confirmed that the diblock nature as well as the presence of carboxylic functional groups is essential to produce stable PCL vesicles in water.

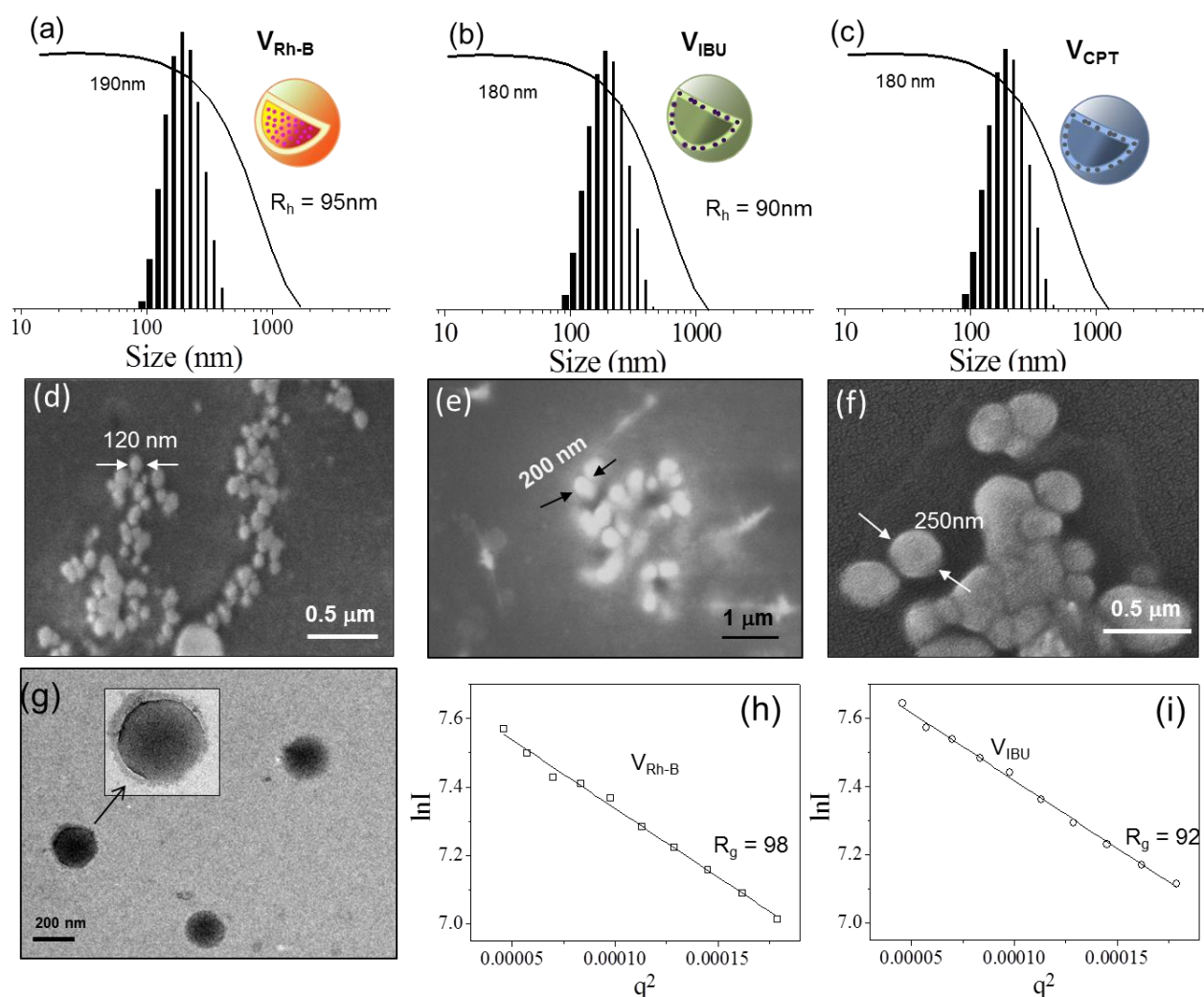


**Figure 2.15.** DLS histograms of  $V_{Rh-B}$ (a),  $V_{IBU}$ (b), and  $V_{CPT}$ (c). FESEM images of  $V_{Rh-B}$ (d),  $V_{IBU}$  (e), and  $V_{CPT}$ (f). HRTEM image of  $V_{Rh-B}$ (g). SLS plot for  $V_{Rh-B}$ (h) and  $V_{IBU}$  (i).

The carboxylic PCL loaded vesicles were further characterized by light scattering (dynamic and static) methods and electron microscopy their data are shown in figure 2.15. The DLS histograms for  $V_{Rh-B}$ ,  $V_{IBU}$  and  $V_{CPT}$  are provided in figure 2.15 a, b and c

respectively. The hydrodynamic diameter of the Rh-B, IBU and CPT loaded vesicle ranging between  $180 \pm 5$  nm to  $190 \pm 5$  nm (see figure 2.15a, b and c). In figure 2.15 d, e and f depicted the feSEM images of the  $V_{Rh-B}$ ,  $V_{IBU}$  and  $V_{CPT}$  assemblies respectively. These images showed the existence of soft spherical objects with  $200 \pm 5$  nm resembles with formation of vesicular assemblies in all the cases. The slight increase in size in the cargo loaded vesicles is attributed to the occupation of the guest molecules in the vesicular assemblies. The HR-TEM images of Rh-B loaded vesicles are shown in figure 2.15g, confirmed the existence of the vesicular assemblies. The hydrodynamic radius of the Rh-B loaded vesicle ( $R_h$ ) was calculated as 95 nm (see figure 2.15a). Static light scattering provided the radius of gyration of vesicular assemblies ( $R_g$ ) as 98 nm (see figure 2.15h). The ratio of  $R_g/R_h$  was obtained as 1.03 which confirmed the existence of vesicular geometry in Rh-B loaded samples.<sup>66</sup> In a similar way IBU loaded vesicles were also analysed. The hydrodynamic diameter of the IBU encapsulated vesicles was determined as  $180 \pm 5$  nm from DLS (see figure 2.13b). The ratio of  $R_g/R_h$  was obtained as 1.02 for IBU loaded vesicles (see figure 2.15i).

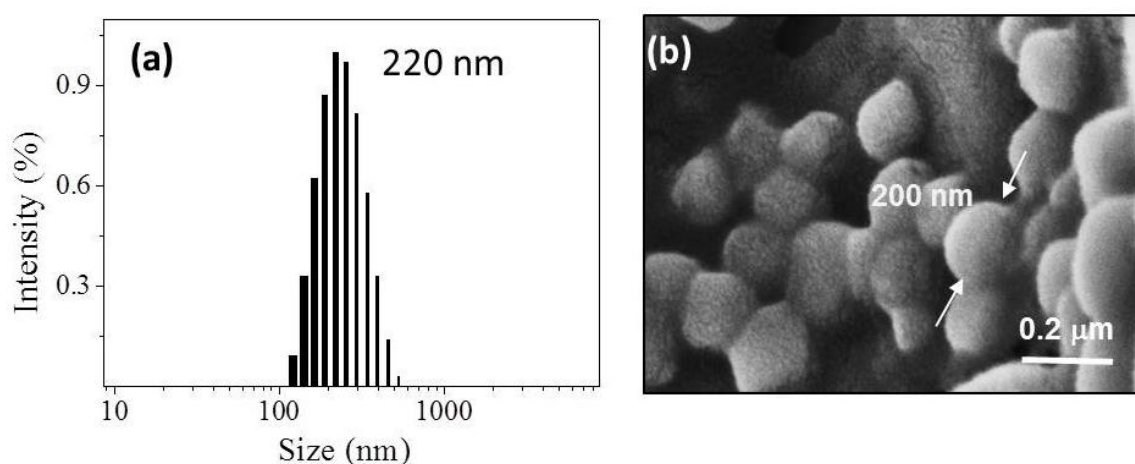


**Figure 2.16.** DLS histogram (a) and FESEM image (b) of  $V_{Rh-B+IBU}$  dual loaded vesicles.

Similarly, the self-assemblies of dual loaded  $V_{Rh-B+IBU}$  dual loaded vesicles were also confirmed and their details are given in figure 2.16a and b. The DLS histogram and feSEM images were provided in the figure, shows the formation  $200 \pm 10$  nm size nano-assemblies. Drug loading contents (DLC) of the vesicles were determined by absorbance spectroscopy. Absorbance spectra of drug loaded scaffolds were shown in figure 2.17a. The unloaded vesicular scaffold showed absorbance maxima at 190 nm which does not interfere with the drug molecules absorbance in the visible region. The  $V_{RhB}$  showed absorbance maxima at 555

nm and IBU  $V_{IBU}$  showed absorbance maxima at 265 nm. In case of dual loaded vesicles ( $V_{Rh-B+IBU}$ ), peaks for Rh-B and IBU are clearly visible. The camptothecin (CPT) loaded vesicles ( $V_{CPT}$ ) absorbance maxima for  $V_{CPT}$  was found at 365 nm. Based on the molar extinction coefficient of Rh-B, IBU and CPT, the drug loading content of individual vesicles were determined as 1.1 %, 9.5% and 1.2% for  $V_{RhB}$ ,  $V_{IBU}$  and  $V_{CPT}$ , respectively. The loading contents of Rh-B and IBU were determined as 1.7 % and 13% in the dual loaded  $V_{RhB+IBU}$  vesicle, respectively.

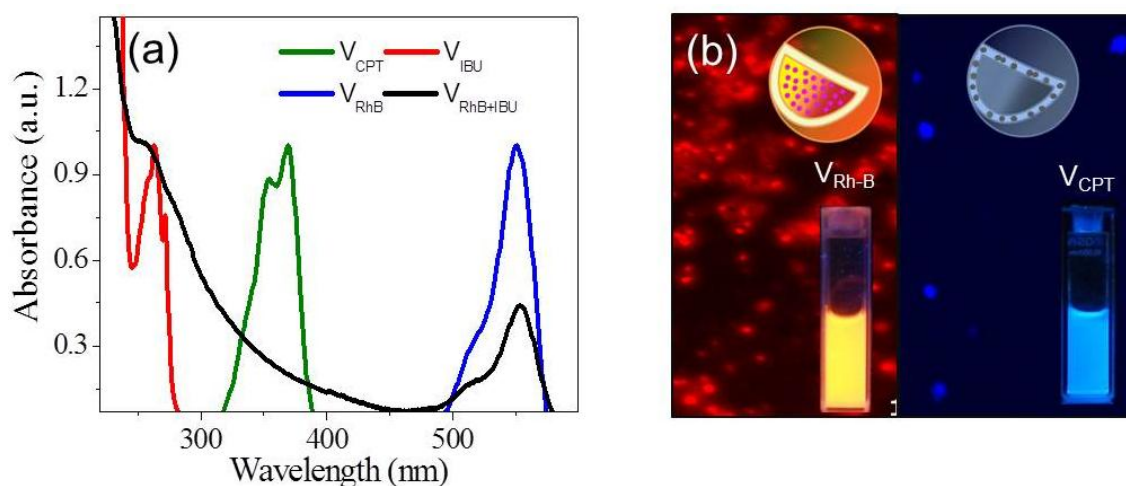


**Figure 2.17.** Absorbance spectra of loaded vesicles. (a) FL microscope images of  $V_{Rh-B}$  and  $V_{CPT}$ (b).

In similar way drug loading efficiencies were calculated for individual vesicles as 11%, 32%, and 12% for  $V_{RhB}$ ,  $V_{IBU}$  and  $V_{CPT}$ , respectively. The loading efficiency of Rh-B and IBU were determined as 17 % and 51% in the dual loaded  $V_{RhB+IBU}$  vesicle, respectively. Among all the loaded molecules, IBU showed higher loading ability and this was attributed to its smaller molecular size. The Rh-B and CPT are fluorescent molecules as a result their vesicles  $V_{RhB}$  and  $V_{CPT}$  were also found to be highly fluorescent. Fluorescent microscope images of these vesicles are shown in figure 2.17b. The  $V_{RhB}$  showed red fluorescent whereas  $V_{CPT}$  was found to be blue luminescent. The fluorescent maxima of loaded vesicles clearly matched with the appearance of red and blue luminescent in  $V_{RhB}$  and  $V_{CPT}$  respectively.



### 2.3.4. pH Response and Zeta potential of the PCL vesicles

Zeta potential measurement is very important tool for understanding the solution dynamic of charged aggregates or more likely self-assemblies of anionic (or cationic) polymeric nano-structures. In solution electrically charged species (nano- assemblies) tend to move under the effect of electrical field; thereby the Zeta potential of the spherical aggregates was expected to show significant change with pH of media. The custom designed PEG-*b*-CPCL<sub>x</sub> vesicles have carboxylic acid functional group anchored on the PCL backbone; as a result they were expected to show significant change in the self-assemblies with respect to the pH of the solution.

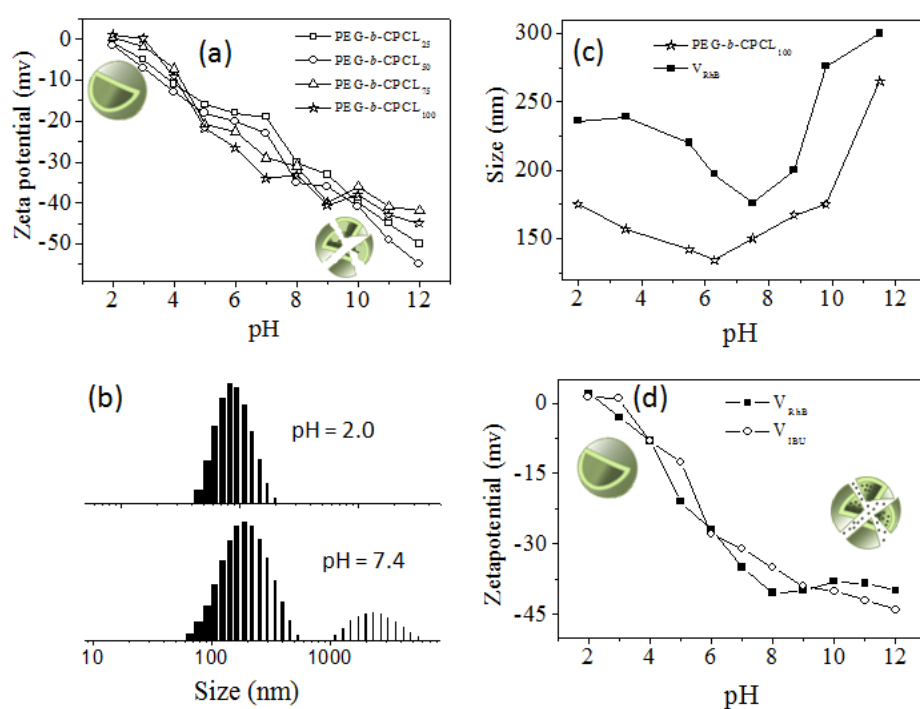


**Figure 2.18.** Zeta potential of PEG-*b*-CPCL<sub>x</sub> in various pH (0.5mg/mL) at 25 °C (a). DLS histograms of PEG-*b*-CPCL<sub>100</sub> at pH= 2.0 and 7.4 (b). Size of the PEG-*b*-CPCL<sub>100</sub> and V<sub>Rh-B</sub> in various pH (0.5mg/mL) at 25 °C (c). Zeta potential of V<sub>Rh-B</sub> and V<sub>IBU</sub> in various pH (0.5mg/mL) at 25 °C (d).

Zeta potential of the PEG-*b*-CPCL<sub>x</sub> vesicles were plotted against various pH and presented in figure 2.18a. The zeta potential of the vesicles increased (more negative potential) with increase in the pH as the carboxylic acid group became carboxylate anion at higher pH. The plots showed fast increase up to pH~ 7.0 (0 to -30 mV) and thereafter the increase was not so significant (-30 to -40 mV). This suggested that vesicular assemblies underwent structural changes from acidic to neutral pH whereas the structural change was less significant from neutral to basic pH. In order to trace these structural changes in the

vesicular assemblies, the size of the aggregates were also measured by DLS at various pH. DLS histograms of PEG-*b*-CPCL<sub>100</sub> at pH=2.0 and 7.4 are shown in figure 2.18b. The vesicles showed a mono-model distribution at pH=2.0 whereas a broad bi-model distribution was obtained with higher sizes at basic pH = 7.4. In figure 2.18c the plot of size of aggregates at various pH. The size of the aggregates did not change up to pH=6 which suggest that the vesicles are stable in the region pH < 6.0, further increase in pH produced larger size particles with respect to the breakage of the vesicular scaffold. This trend was matched with the zeta potential in figure 2.18a and the increases in the size of the polymer aggregates was attributed to the disassembly of PCL vesicles at higher pH due to the repulsion between the carboxylate anions in the hydrophobic layer. A similar trend was recently observed by Do et al. in PEG-polyacrylic acid self-assembly.<sup>77</sup> V<sub>RhB</sub> and V<sub>IBU</sub> loaded vesicles were also subjected for zeta potential and DLS measurements and their data are shown in figure 2.18d. These cargo loaded vesicles were also showed similar trend in their zeta potential as similar to that of unloaded vesicles (see figure 2.18a). The size of the V<sub>RhB</sub> also increased at higher pH with respect to the breakage of the vesicular structure. This confirmed that the pH responsive nature of the PCL vesicles not disturbed by the loaded drug in their layer or inside the vesicle. Thus, this custom designed PCL blocks are unique pH responsive vesicles and they are able to stabilize the hydrophilic as well as hydrophobic molecules (or drugs) in the strong acidic media (below pH < 2.0) and capable of selectively rupture to deliver them at neutral or higher pH.

### 2.3.5. *In vitro* delivery under Simulated GI tract

Oral drug delivery capability of PCL vesicular assemblies were tested under in-vitro conditions. The release characteristics of V<sub>Rh-B</sub> at 37 °C at various pH = 2.0, 4.0, 7.4 and 9.2 are shown in figure 2.19. The cumulative releases of the Rh-B releases were estimated by absorbance spectroscopy and there are plotted and shown in figure 2.19a. It can be evident that the vesicles were stable in strong acidic conditions (pH= 2.0) and only less than 15 ± 3 % of the loaded Rh-B content was released up on 24h was observed. At pH = 4.0, the releasing ability slightly increase to reach 30 ± 6 %. At neutral pH = 7.4, the vesicles underwent burst release in a short period of 4 h and thereafter continued controlled release to reach of 70 ± 7 % till 24 h. At basic pH = 9.2, the release profile increased further and almost 89 ± 9 % Rh-B released. This variable pH release kinetics clearly demonstrates the ability of the newly designed carboxylic functionalized PCL vesicles under controlled manner with respect to the

change of pH. In order to study the release kinetics of these PCL vesicles under GI tract, they were subjected to freshly prepared simulated gastric fluid (SGF, pH = 2.0) and simulated interstitial fluid (SIF, pH = 7.4) as per the literature reports.<sup>7</sup> Figure 2.19b showed the release kinetics of the  $V_{RhB}$  loaded vesicles under SGF and SIF. The vesicles were very stable in SGF whereas they completely broke to release the  $90 \pm 8\%$  of the Rh-B in SIF. In figure 2.19c, the hydrophobic drug loaded vesicles  $V_{IBU}$  and  $V_{CPT}$  were also showed similar burst release of the loaded drugs selectively in SIF. In figure 2.19d, the hydrophilic and hydrophobic dual loaded vesicle  $V_{IBU+RhB}$  was also found to show selective release in SIF as similar to their individual counterparts. The above in-vitro studies summarized that loaded PCL vesicles were stabilized in the gastric conditions and selectively collapse to release at interstitial pH.

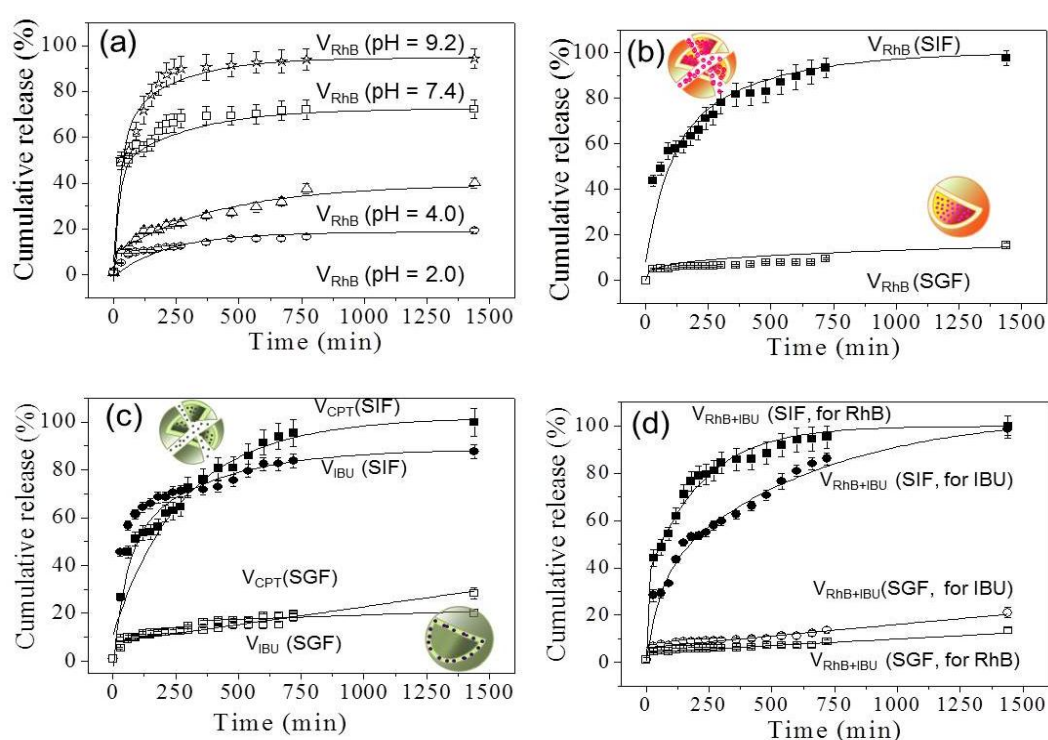


**Figure 2.19.** Cumulative release of  $V_{Rh-B}$  in various pH buffers at 37 °C (a). Cumulative release of  $V_{Rh-B}$  (b) and  $V_{IBU}$  and  $V_{CPT}$  (c) in SIF and SGF at 37 °C. The dual loaded vesicle  $V_{Rh-B+IBU}$  (d) in SIF and SGF at 37 °C.

The release kinetics of loaded molecules (or drugs) in the polymer matrix is a complex problem and not clearly understood till date. Peppas and coworkers<sup>78-80</sup> proposed the following semi-empirical model for the polymer drug releases either by diffusion, erosion or combination of both processes:

$$M_t / M_\infty = kt_n \text{ (or) } \log (M_t / M_\infty) = n \log t + \log k$$

Where  $M_t$  and  $M_\infty$  are cumulative release of loaded cargoes (or drugs) at time  $t$  and infinite,  $n$  is a release exponent and  $k$  is the rate constant. The value  $n$ -value provide direct information on the release kinetics either by Fickian diffusion ( $n = 0.43$ ) or non-Fickian mechanism ( $n < 0.43$ ) in which both diffusion and erosion occurred together.<sup>70</sup> This kinetic methodology was recently employed by Sanson et al.<sup>42</sup> and Yang et al.<sup>22</sup> independently in the release studies of hydrophilic or hydrophobic drugs. Since the present investigation provides unique opportunity to load both hydrophilic and hydrophobic in a single PCL vesicles, it would be important to understand their release pattern under SIF conditions. The release profiles of  $V_{IBU}$ ;  $V_{RhB}$ ;  $V_{CPT}$ ; and  $V_{IBU+RhB}$  under SIF at 7.4 were subjected to the above kinetics. The plots of the  $\log (M_t/M_\infty)$  versus  $\log t$  for the deliveries of Rh-B, IBU, CPT or IBU+Rh-B are shown in figure 2.20. The individual loaded vesicles  $V_{IBU}$ ;  $V_{RhB}$  and  $V_{CPT}$  showed release in two stages. These data were fitted with linear plot to obtain their  $n$  and their  $k$ -values from the slope and intercepts, respectively. These values are summarized in table 2.2.

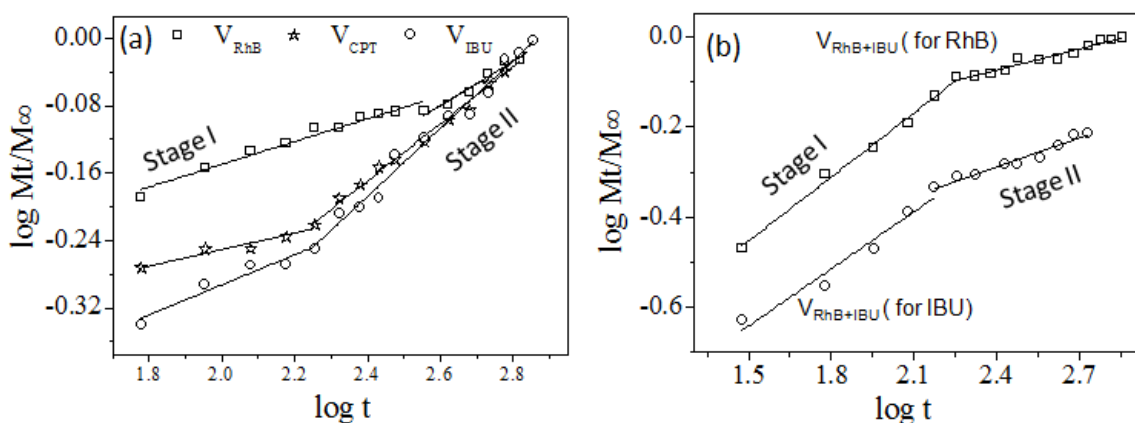


**Figure 2.20.** The plots of the  $\log (M_t/M_\infty)$  versus  $\log t$  for individual loaded vesicles (a) and dual loaded vesicle (b).

**Table 2.2.** Release kinetic parameters of vesicles

Sample	Stage-I			Stage-II		
	$n$	$k$	$R^2$	$n$	$k$	$R^2$
$V_{Rh-B}$	0.134	0.381	0.962	0.262	0.173	0.946
$V_{IBU}$	0.178	0.224	0.921	0.402	0.071	0.980
$V_{CPT}$	0.097	0.363	0.909	0.338	0.104	0.990
$d_{ual}$ (for Rh-B)	0.473	0.078	0.991	0.156	0.356	0.945
$d_{ual}$ (for IBU)	0.422	0.053	0.945	0.215	0.156	0.960

The individual loaded vesicles showed relatively low  $n$  values ( $n < 0.2$ ) in stage –I with respect to the 60 % drug release. This was attributed to both diffusion and erosion mechanism. The increase in the  $n$ -values ( $0.2 < n < 0.4$ ) in stage-II indicated that the remaining 40 % of the drugs are released may be through diffusion process. It is very important to note that the release kinetics of individual vesicles showed identical release patterns for both hydrophilic and hydrophobic cargoes. Thus, the vesicles are potential drug loading vectors for releasing both water soluble and water insoluble drugs under the identical rate in a single scaffold. On the other hand, the release kinetics of the drugs (or Rh-B) from the dual loaded vesicles were followed just opposite compared to their individual counterparts. Both IBU and Rh-B were released with large  $n$ -values ( $n \leq 4.3$ ) in the stage-I compared to stage-II ( $n < 0.21$ ). This revealed that the dual loaded vesicles first release its 60 % of the drugs predominately by diffusion controlled process rather than diffusion+ erosion. Though both individual and dual loaded vesicles followed a similar two stage kinetics; the ‘ $n$ ’ values revealed that the process in which the cargoes release seems to be different. The dual loaded vesicles released 60 % of the drug by diffusion process whereas the vesicles with individual drugs predominantly followed the combination of diffusion plus erosion. It suggested that the dual loading provide more stability in the vesicular assemblies which is less influenced by the erosion process. The present investigation provide first time insight into the concept of the dual drug delivery based on PCL vesicles for drugs (like CPT and IBU) and water soluble Rh-B molecules under GI tract. Though, the approach demonstrated here tested only few examples, it is not restricted to few cases, and in general, it is applicable to wide range of drugs which are yet to be explored in oral drug delivery.

#### **2.4. Conclusion**

In conclusion, the present investigation has successfully demonstrated the creation of pH responsive PCL vesicles, their loading and releasing capabilities of hydrophobic and hydrophilic molecules under simulated GI tract. A new carboxylic functionalized caprolactone monomer was designed and synthesized for the above purpose readily from commercial starting materials and polymerized using ROP. The carboxylic substituted PCL block copolymers PEG-b-CPCLx were very unique in producing water soluble nano-sized 80-250 nm vesicles. The existence of the PCL vesicle was confirmed by various techniques such as DLS, SLS, FESEM, HR-TEM, WCA and so on. These zeta potential and DLS studies revealed that pH responsive PCL vesicles were found to be stable up to  $\text{pH} < 6.0$  and they

ruptured to release the loaded drug molecules at neutral or basic pH > 7.0. The loading and delivering capabilities were investigated for water soluble molecules such as Rh-B and hydrophobic drugs like IBU or CPT. The *in vitro* release characteristics revealed that the PCL vesicles exclusively release the drugs only under SIF which is identical to our physiological conditions of small intestine. Further, the custom designed PEG-b-CPCLx block copolymers provide new opportunity to tag either drug molecules or antibody for site directed delivery in PCL systems while retaining the pH as stimuli for release. Further, the carboxylic acid group either may be partially or fully substituted with suitable chemical functional groups for application as scaffolds for stabilizing metal nano-particles. The nano-particles along with drug conjugates may provide new opportunity for real time imaging or delivery to specific tumor site and so on. Currently efforts are taken to employ these pH responsive PCL vesicles for delivery of anticancer drugs in collaboration with biology research groups which will be published elsewhere.

## 2.5. References

1. Al-Hilal, T. A.; Alam, F.; Byun, Y. *Adv. Drug Deliv. Rev.* **2013**, *65*, 845-864.
2. Ensign, L. M.; Cone, R.; Hanes, J. *Adv. Drug Deliv. Rev.* **2012**, *64*, 557-570.
3. Martindale, S. S. *Pharmaceutical Press, London, UK.* **2009**.
4. Jiang, B.; Hu, L.; Gao, C.; Shen, J. *Intl. J. Pharm.* **2005**, *304*, 220-230.
5. Potthast, H.; Dressman, J.B.; Junginger, H.E.; Midha, K.K.; Oeser, H. *J Pharm Sci* **2005**, *94*, 2121-2131.
6. Saltiel, A.R.; Khan, C.R. *Nature* **2001**, *414*, 799-806.
7. Gao, W.; Chan, J. M.; Farokhzad, O. C. *Mol. Pharmaceutics* **2010**, *7*, 1913-1920.
8. Huang, Y.; Tang, Z.; Zhang, X.; Yu, H.; Sun, H.; Pang, X.; Chen, X., *Biomacromolecules* **2013**, *14*, 2023-2032.
9. Mandracchia, D.; Pitarresi, G.; Palumbo, F. S.; Carlisi, B.; Giammona, G. *Biomacromolecules* **2004**, *5*, 1973-1982.
10. Paliwal, R.; Paliwal, S. R.; Agrawal, G. P.; Vyas, S. P. *Mol. Pharmaceutics* **2011**, *8*, 1314-1321.
11. Casadei, M. A.; Pitarresi, G.; Calabrese, R.; Paolicelli, P.; Giammona, G. *Biomacromolecules* **2008**, *9*, 43-49.
12. Kim, H.; Kang, Y. J.; Kang, S.; Kim, K. T., *J. Am. Chem. Soc.*, **2012**, *134*, 4030-4033.
13. Rodríguez-Hernández, J.; Lecommandoux, S. *J. Am. Chem. Soc* **2005**, *127* (7), 2026-2027.
14. Klaikherd, A.; Nagamani, C.; Thayumanavan, S. *J. Am. Chem. Soc* **2009**, *131*, 4830-4838.
15. Kim, K. T.; Cornelissen, J. J. L. M.; Nolte, R. J. M.; Hest, J. C. M. v. *J. Am. Chem. Soc* **2009**, *131*, 13908-13909.
16. Krannig, K.-S.; Schlaad, H. *J. Am. Chem. Soc* **2012**, *134*, 18542-18545.
17. Su, J.; Chen, F.; Cryns, V. L.; Messersmith, P. B., *J. Am. Chem. Soc* **2011**, *133*, 11850-11853.
18. Griset, A. P.; Walpole, J.; Liu, R.; Gaffey, A.; Colson, Y. L.; Grinstaff, M. W. *J. Am. Chem. Soc* **2009**, *131*, 2469-2471.
19. Lee, S.-M.; Chen, H.; Dettmer, C. M.; O'Halloran, T. V.; Nguyen, S. T., *J. Am. Chem. Soc* **2007**, *129*, 15096-15097.

20. Fuhrmann, G.; Grotzky, A.; Lucic, R.; Matoori, S.; Yu, H.; Zhang, B.; Walde, P.; Schluter, A.D.; Gauthier, M.A.; Leroux, J.-C., *Nature Chem.* **2013**, *5*, 582-589.
21. Gillies, E.R.; Frechet, J.M.J., *Bioconjugate chem.* **2005**, *16*, 361-368.
22. Yang, Y. Q.; Guo, X. D.; Lin, W. J.; Zhang, L. J.; Zhang, C. Y.; Qian, Y., *Soft Matter* **2012**, *8*, 454-464.
23. Yang, Y. Q.; Lin, W. J.; Zhao, B.; Wen, X. F.; Guo, X. D.; Zhang, L. J. *Langmuir* **2012**, *28*, 8251-8259.
24. Du, Y.; Chen, W.; Meng, F.; Zhong, Z., *Biomaterials*, **2012**, *33*, 7291-7299.
25. Roger, E.; Kalscheuer, S.; Kirtane, A.; Guru, B. R.; Grill, A. E.; Whittum-Hudson, J. *Mol. Pharmaceutics* **2012**, *9*, 2103-2110.
26. Felber, A. E.; Dufresne, M.-H.; Leroux, J.-C., *Adv. Drug Deliv. Rev.* **2012**, *64*, 979-992.
27. Du, J.; Tang, Y.; Lewis, A.L.; Armes, S.P., *J. Am. Chem. Soc.* **2005**, *127*, 17982-17983.
28. Du, J.; Armes, S.P., *J. Am. Chem. Soc.* **2005**, *127*, 12800-112801.
29. Zhu, L.; Zhao, L.; Yang, Z., *Langmuir*, **2012**, *28*, 11988-11996.
30. Zhang, J.; Wu, L.; Wang, Z.; Deng, C.; Liu, H.; Zhong, Z., *Langmuir*, **2012**, *28*, 2056-2065.
31. Du, J.; Fan, L.; Liu, Q., *Macromolecules*, **2012**, *45*, 8275-8283.
32. Blanazs, A.; Massignni, M.; Armes, S.P., *Adv. Funct. Mater.* **2009**, *19*, 2906-2914.
33. Sanson, C.; Diou, O.; Thévenot, J.; Ibarboure, E.; Soum, A.; Brûlet, A.; Miraux, S.; Thiaudière, E.; Tan, S.; Brisson, A.; Dupuis, V.; Sandre, O.; Lecommandoux, S., *ACS Nano* **2011**, *5* (2), 1122-1140.
34. Sanson, C.; Schatz, C.; Le Meins, J.-F. o.; Brûlet, A.; Soum, A.; Lecommandoux, S. *Langmuir* **2009**, *26* (4), 2751-2760.
35. Gaitzsch, J.; Appelhans, D.; Wang, L.; Battaglia, G.; Voit, B., *Angew. Chem. Int. Ed.* **2012**, *51*, 4448-4451.
36. Versluis, F.; Tomatsu, I.; Fregunese, C.; Tepper, A.W.J.W.; Staurt, M.C.A.; Kros, A., *J Am. Chem. Soc* **2009**, *131*, 13186-13187.
37. Pramod, P. S.; Takamura, K.; Chaphekar, S.; Balasubramanian, N.; Jayakannan, M., *Biomacromolecules* **2012**, *13*, 3627-3640.
38. Loamas, H.; Canton, I.; MacNiel, S.; Du, j.; Armes, S.P.; Ryan, A.J.; Lewis, A.L.; Battaglia, G., *Adv. Mater.* **2007**, *19*, 4238-4243.
39. Popescu, M.-T.; Tsitsilianis, C., *ACS Macro letter.*, **2013**, *2*, 222-225.



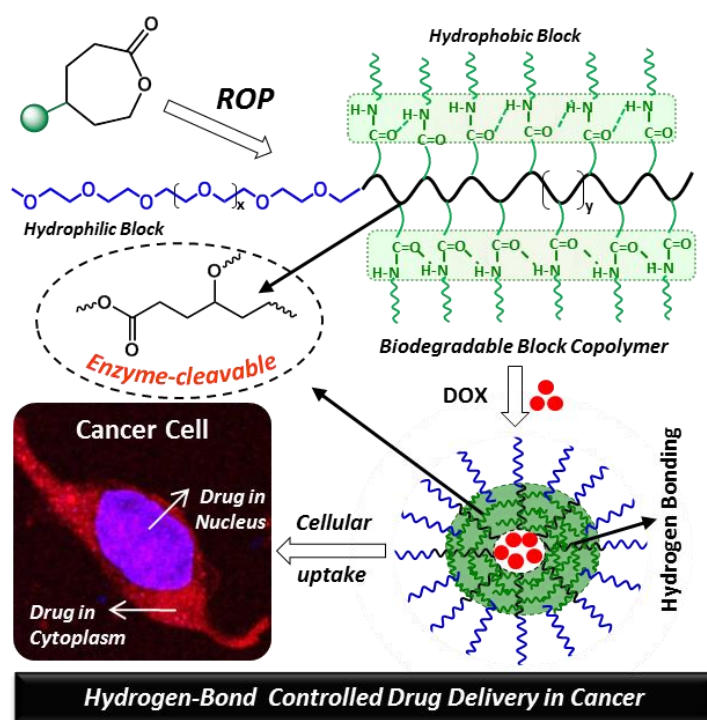
40. Yang, X.; Grailer, J.J.; Rowland, I.J.; Javedi, A.; Hurley, S.A.; Matson, V.Z.; Gong, S., *ACS Nano* **2010**, *4*, 6805-6817.
41. Sanson, C.; Diou, O.; Thévenot, J.; Ibarboure, E.; Soum, A.; Brûlet, A.; Miraux, S.; Thiaudière, E.; Tan, S.; Brisson, A.; Dupuis, V.; Sandre, O.; Lecommandoux, S., *ACS Nano* **2011**, *5*, 1122-1140.
42. Sanson, C.; Schatz, C.; Le Meins, J.-F.; Soum, A.; Thévenot, J.; Garanger, E.; Lecommandoux, S., *J. Controlled. Release* **2010**, *147*, 428-435
43. Jerome, C.; Lacomte, P., *Adv. Drug Deli. Rev.* **2008**, *60*, 1056-1076
44. Zupancich, J. A.; Bates, F. S.; Hillmyer, M. A. *Macromolecules* **2006**, *39*, 4286-4288
45. Geng, Y.; Discher, D. E. *J. Am. Chem. Soc* **2005**, *127*, 12780-12781.
46. Gou, M.; Men, K.; Shi, H.; Xiang, M.; Zhang, J.; Song, J.; Long, J.; Wan, Y.; Luo, F.; Zhao, X.; Qian, Z. *Nanoscale* **2011**, *3*, 1558-1567.
47. Schuetz, P.; Greenall, M. J.; Bent, J.; Furzeland, S.; Atkins, D.; Butler, M. F.; McLeish, T. C. B.; Buzza, D. M. A., *Soft Matter* **2011**, *7*, 749-759.
48. Šachl, R.; Uchman, M.; Matějček, P.; Procházka, K.; Štěpánek, M.; Špírková, M., *Langmuir* **2007**, *23* (6), 3395-3400.
49. Ghoroghchian, P. P.; Li, G.; Levine, D. H.; Davis, K. P.; Bates, F. S.; Hammer, D. A.; Therien, M. J. *Macromolecules* **2006**, *39* (5), 1673-1675.
50. Katz, J. S.; Eisenbrown, K. A.; Johnston, E. D.; Kamat, N. P.; Rawson, J.; Therien, M. J.; Burdick, J. A.; Hammer, D. A., *Soft Matter* **2012**, *8* (42), 10853-10862.
51. Chang, L.; Deng, L.; Wang, W.; Lv, Z.; Hu, F.; Dong, A.; Zhang, J. *Biomacromolecules* **2012**, *13*, 3301-3310.
52. Cheng, Y.; Hao, J.; Lee, L. A.; Biewer, M. C.; Wang, Q.; Stefan, M. C. *Biomacromolecules* **2012**, *13*, 2163-2173.
53. Rieger, J.; Bernaerts, K. V.; Du Prez, F. E.; Jérôme, R.; Jérôme, C. *Macromolecules* **2004**, *37*, 9738-9745.
54. Hao, J.; Servello, J.; Sista, P.; Biewer, M. C.; Stefan, M. C. *J. Mater. Chem.* **2011**, *21*, 10623-10628.
55. Tian, D.; Dubois, P.; Jérôme, R. *Macromolecules* **1997**, *30*, 1947-1954.
56. Yao, K.; Wang, J.; Zhang, W.; Lee, J. S.; Wang, C.; Chu, F.; He, X.; Tang, C., *Biomacromolecules* **2011**, *12*, 2171-2177.

57. Mahmud, A.; Xiong, X.-B.; Lavasanifar, A. *Macromolecules* **2006**, *39*, 9419-9428.
58. Patel, S. K.; Lavasanifar, A.; Choi, P. *Biomaterials* **2010**, *31*, 345-357.
59. Mahmud, A.; Patel, S.; Molavi, O.; Choi, P.; Samuel, J.; Lavasanifar, A., *Biomacromolecules* **2009**, *10*, 471-478.
60. Riva, R.; Schmeits, S.; Jérôme, C.; Jérôme, R.; Lecomte, P. *Macromolecules* **2007**, *40* (4), 796-803.
61. Li, H.; Riva, R.; Jérôme, R.; Lecomte, P. *Macromolecules* **2007**, *40* (4), 824-831.
62. Tian, D.; Halleux, O.; Dubois, P.; Jérôme, R.; Sobry, R.; Van den Bossche, G., *Macromolecules* **1998**, *31* (3), 924-927.
63. Trollsas, M.; Lee, V. Y.; Mecerreyes, D.; Lowenhielm, P.; Moller, M.; Miller, R. D.; Hedrick, J. L. *Macromolecules* **2000**, *33*, 4619-4627.
64. Trollsas, M.; Lowenhielm, P.; Lee, V. Y.; Moller, M.; Miller, R. D.; Hedrick, J. L., *Macromolecules* **1999**, *32*, 9062-9066.
65. Odian, G.; *Principles of polymerization, 4<sup>th</sup> edition, John –Wiley and sons* **2004**, pp 581-585.
66. Li, Y.; Hoskins, J.N.; Sreerama, S.G.; Grayson, S.M.; *Macomolecules* **2010**, *43*, 6225-6228.
67. Mishra, A. K.; Patel, V. K.; Vishwakarma, N. K.; Biswas, C. S.; Raula, M.; Misra, A.; Mandal, T. K.; Ray, B. *Macromolecules* **2011**, *44*, 2465-2473.
68. Kamber, N. E.; Jeong, W.; Gonzalez, S.; Hedrick, J. L.; Waymouth, R. M. *Macromolecules* **2009**, *42*, 1634-1639.
69. Houga, C. m.; Giermanska, J.; Lecommandoux, S. b.; Borsali, R.; Taton, D.; Gnanou, Y.; Le Meins, J-F. O. *Biomacromolecules* **2008**, *10*, 32-40.
70. Matsudo, T.; Ogawa, K.; Kokufuta, E. *Biomacromolecules* **2003**, *4*, 728-735.
71. Seyednejad, H.; Vermonden, T.; Fedorovich, N. E.; van Eijk, R.; van Steenberg, M. J.; Dhert, W. J. A.; van Nostrum, C. F.; Hennink, W. E. *Biomacromolecules* **2009**, *10*, 3048-3054.
72. Esteves, A. C. C.; Lyakhova, K.; van der Ven, L. G. J.; van Benthem, R. A. T. M.; de With, G. *Macromolecules* **2013**, *46*, 1993-2002.
73. Li, Y.; Peterson, J. J.; Jhaveri, S. B.; Carter, K. R. *Langmuir* **2013**, *29*, 4632-4639.
74. Sridhar, U.; Pramod, P. S.; Jayakannan, M.,. *RSC Advances*. ASAP, DOI:10.1039/c3ra43652g.
75. Moughton, A. O.; O'Reilly, R. K.. *Chem Commun* **2010**, *46* (7), 1091-1093.

76. Zhao, W.; Chen, D.; Hu, Y.; Grason, G. M.; Russell, T. P., *ACS Nano* **2010**,5 (1), 486-492.
77. Ren, T.; Liu, Q.; Lu, H.; Liu, H.; Zhang, X.; Du, J. *J. Mater. Chem.* **2012**, 22, 12329-12338.
78. Siepmann, J.; Peppas, N. A., *Adv. Drug Deliv. Rev.* **2001**, 48 , 139-157.
79. Young, C. R.; Dietzsch, C.; Cerea, M.; Farrell, T.; Fegely, K. A.; Rajabi-Siahboomi, A.; McGinity, J. W., *Int.J. Pharm.* **2005**, 301 , 112-120.
80. Li, Y.; Li, H.; Wei, M.; Lu, J.; Jin, L., *Chem. Eng. J.* **2009**,151 , 359-366.

## Chapter 3

### *Hydrogen-Bond Controlled Drug Delivery to Cancer Cells by Programming the Enzyme Degradation in Block Copolymer Nano-assemblies*



## ***Hydrogen-Bond Controlled Drug Delivery to Cancer Cells by Programming the Enzyme Degradation in Block Copolymer Nano-assemblies***

---

*Steady and control release of drugs from polymer scaffolds are urgently required to enhance the therapeutics in cancer treatment. To accomplish this goal, here new hydrogen-bond controlled drug delivery strategy is designed to programme the enzymatic degradation of block copolymer nano-assemblies at the intracellular compartments to deliver drugs to cancer cells. Hydrogen bonded polycaprolactone-block-polyethylene glycol copolymers were custom designed and self-assembled them as aqueous micellar aggregates of ~ 90-160 nm. These diblock polymer nanoparticles exhibited excellent capability for loading doxorubicin (DOX) and stabilized the drugs against leaching at extracellular circularly conditions (37 °C in PBS). At the intracellular level, lysosomal-esterase enzyme degraded the aliphatic polyester PCL backbone to release DOX in steady and controlled profiles. Cytotoxicity studies in cervical cancer (HeLa) and breast cancer (MCF-7) cell lines revealed that the newly engineered hydrogen bonded diblock copolymers are non-toxic to cells. In vitro cytotoxicity experiments pointed out that the steady DOX release from hydrogen bonded nanoparticles exhibited slow and steady cell killing compared to that of their non-hydrogen bonded analogues. In vivo mimicking cell line experiments were designed to study the action of drug on breast and cervical cancer cells by programmed incubation period. These cell-line experiments provided direct evidence for hydrogen-bond controlled lysosomal enzymatic cleavage of polymer-drug scaffolds at the intracellular level on their cell killing ability. Confocal microscopic images revealed that the hydrogen bonded nanoparticles were capable of transporting DOX across the cell membranes and accumulating the DOX predominantly in the cytoplasm and at peri-nuclear region. The present investigation described the structural engineering aspects in diblock copolymers and their hydrogen-bond controlled enzymatic-degradation for precise drug administration in cancer therapy.*

### 3.1. Introduction

Polymer-based drug delivery approaches are emerging as an important protocol for drug administration in cancer treatment.<sup>1-4</sup> High loading content, less cytotoxicity, accumulation of drugs at the cancer tissue via enhanced permeability and retention (EPR) effect and surface anchoring of target receptors are some of the added advantages in polymeric systems compared to other drug carriers.<sup>5-7</sup> Most of the drug molecules have a therapeutic window; in terms of drug concentration of above the it is toxic and below it is ineffective. In a conventional way drug dosage results in frequent cycles between the toxic and ineffective levels depending on the frequency with which the drug is administered.<sup>8</sup> To achieve the proper effective drug levels clinicians increase the dosage frequency. The alternative solution to resolve this issue is development of a controlled release system, where the drug molecules can release slowly over a period of time hence the concentration variations are insignificantly small and avoid the lessons the dosage frequency.<sup>8</sup> The additional advantage of these controlled release system involves patient compliance. It has now been realized that fast and burst release of drugs from the polymer nano-carrier is one of the major limitation in achieving controlled drug delivery which is desirable under *in vivo* conditions.<sup>9-10</sup>

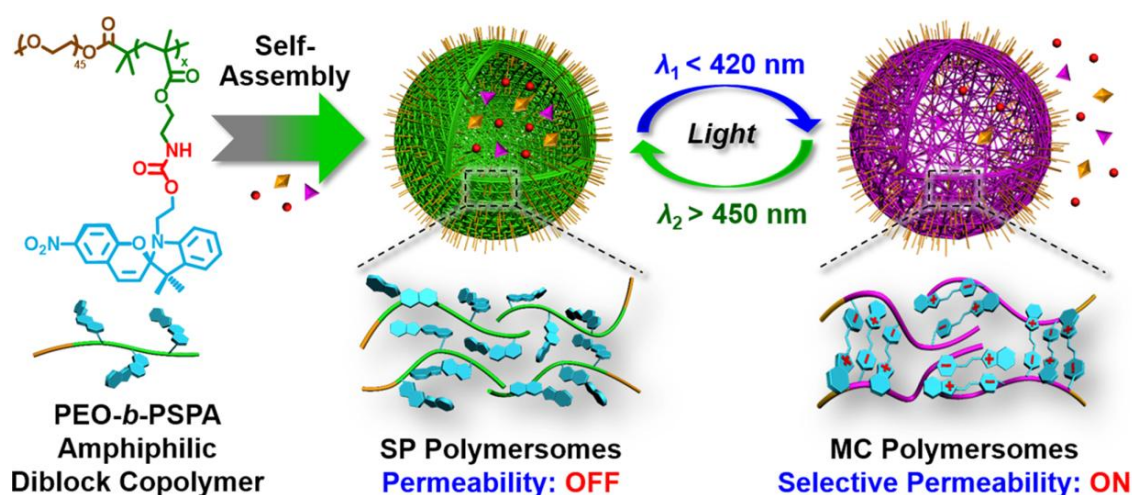


**Figure 3.1.** Schematic representations of photochromic polymersomes exhibiting photoswitchable and Reversible Bilayer Permeability (adapted from Wang et al. *J. Am. Chem. Soc.* **2015**, *137*, 15262-15275).

This problem can be approached either by the incorporation of multiple stimuli in single polymer nano-carrier or precisely programmed polymer degradation or disassembly at

the intracellular compartments. Multiple stimuli such as pH,<sup>11</sup> temperature,<sup>12-13</sup> light,<sup>14</sup> enzyme,<sup>15</sup> redox process,<sup>16</sup> and magnetic properties<sup>17</sup> have been widely explored for drug delivery. Non-covalent forces such as hydrogen bonding,  $\pi$ - $\pi$  stacking and electrostatic interactions were introduced to bring scaffold cleavage tunability towards the drug release process and at the same time provide additional stability to the drug molecules.<sup>17-18</sup> Wang et al. fabricated of photochromic polymerosomes, which shows photo switchable and reversible bilayer permeability from newly synthesised poly(ethylene oxide)-*b*-PSPA (PEO-*b*-PSPA) diblock copolymers. These polymerosomes, SP (spiropyran) moieties within bilayers undergo reversible photo triggered isomerization between hydrophobic to zwitterionic merocyanine states. In this study that have demonstrated photo switchable spatiotemporal release of 4',6-diamidino-2-phenylindole (DAPI, cell nuclei staining dye) within living HeLa cells (see

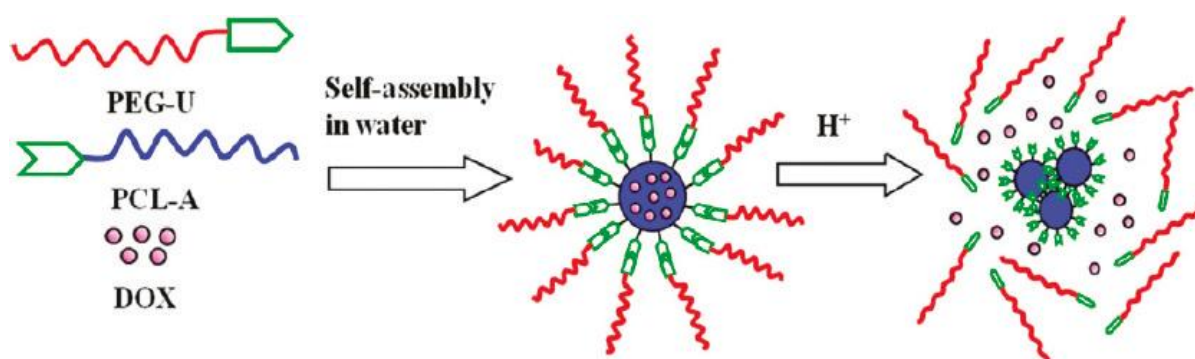
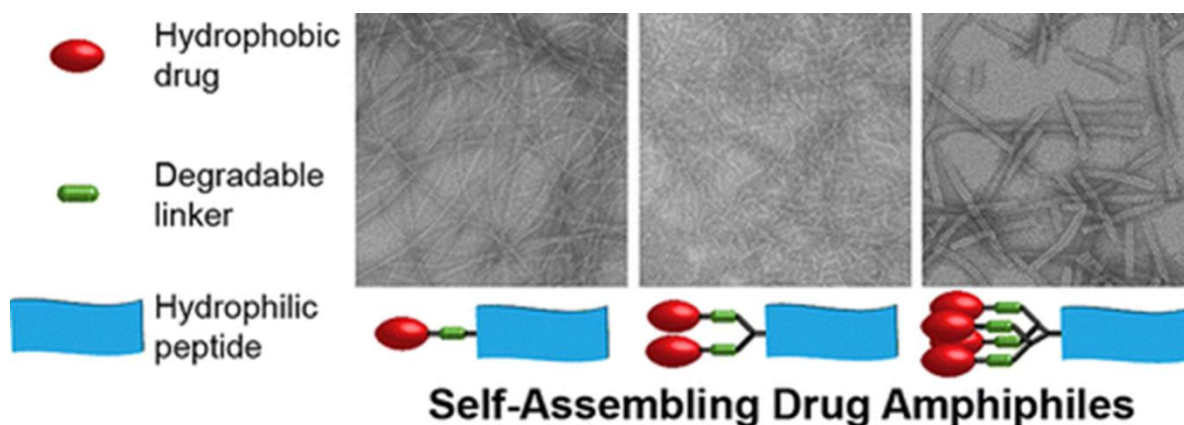


figure 3.1).<sup>19</sup>

**Figure 3.2.** Schematic representations synthesis of pH sensitive micelles from PCL-A and PEG-U polymers (adapted from Zhu and co-workers *Biomacromolecules* **2011**, *12*, 1370–1379).

Hydrogen bonded nucleic acid base pairs such as uracil-adenine and adenine-thymine were employed as reversible de-cross-linking agents to disassemble the block copolymer nanoparticles for doxorubicin and luciferase delivery, respectively.<sup>20-22</sup> Zhu and co-workers prepared Novel stimuli-responsive supramolecular copolymer micelles from adenine-terminated poly(caprolactone) (PCL-A) and uracil-terminated poly(ethylene glycol) (PEG-U) copolymers. Where, it is shown the formation of the stimuli responsive micelles due to the H-bonding between two polymer nucleobases (adenine and uracil). These micelles are loaded with DOX and delivered to HeLa, cervical cells (see figure 3.2).





**Figure 3.3.** Schematic representation of various CPT-Peptide amphiphiles and their aqueous self-assembly FESEM images. (adapted from Cheetam et al. *J. Am. Chem. Soc.*, **2013**, *135*, 2907–2910).

$\beta$ -Sheet hydrogen bonding were explored in amphiphilic oligopeptides to self-assemble them into micellar and vesicular nano-structures for drug delivery (see figure 3.3),<sup>23</sup> biomineralization<sup>24</sup> and tissue engineering,<sup>25</sup> etc. Coassemblies of the anionic polypeptide and cationic  $\beta$ -sheet peptide were reported for lonidamine delivery to the human osteosarcoma cell lines (see figure 3.4).<sup>26</sup> These recent reports emphasized the importance of non-covalent stabilization forces in biomedical research; however, the potential of hydrogen bonding interaction is still untapped to maximize the drug stability in polymer scaffold and also to programme the stimuli-responsive delivery at the intracellular compartments in cancer cells.

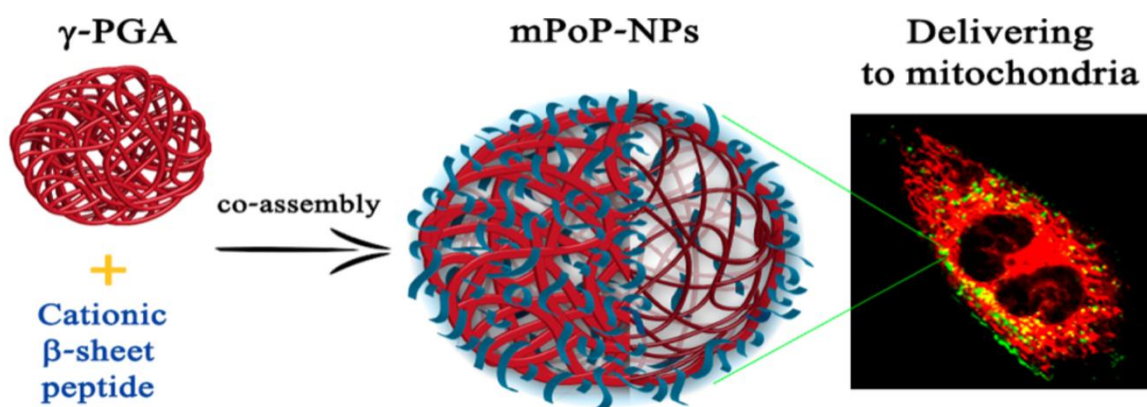


**Figure 3.4.** Schematic representations of the NPs' Hypothesized Structure, Showing  $\gamma$ -PGA, PoP-NPs and mPoP-NPs (Left, Center, and Right, Respectively) (adapted from Rapaport and co-workers *Biomacromolecules* **2015**, *16*, 3827-3835.).



In the present investigation, a new hydrogen-bond controlled drug delivery concept is developed based on enzyme-cleavable biodegradable polymer scaffold and the doxorubicin (DOX) delivery has been precisely programmed at the intracellular compartments of breast and cervical cancer cells. For this purpose, biodegradable substituted polycaprolactone (PCL) was chosen since it has excellent thermal and environmental stability, good enzymatic degradability, and capable of loading and delivering drugs.<sup>27,28</sup> Alkoxy and oligoethyleneoxy substituted PCL copolymers,<sup>29</sup> hydroxyl-functionalized<sup>30</sup> and imine functionalized<sup>31</sup> PCL block copolymers were employed as scaffolds for DOX, cucurbitacin, and siRNA delivery. From our group, we have reported carboxylic substituted PCL diblock copolymers for oral delivery of IBU and CPT.<sup>32</sup> Here, we propose a new hydrogen bonded block PCL copolymer design to study the role of non-covalent stabilized forces on the drug releasing profiles in cancer therapy. The new block copolymer design has following features: (i) hydrogen-bonded hydrophobic PCL core was carefully designed to program the lysosomal enzymatic cleavage of drug loaded nanoparticles at the intracellular compartments, (ii) the hydrophilic PEG shell at the nanoparticle periphery enhanced their aqueous dispersibility, (iii) non-hydrogen bonded block copolymer models were built to rationalize the “burst” versus “controlled” release, and (iv) appropriate *in vitro* and *in vivo* mimicking cell line experiments were designed to demonstrate the proof-of-concept of hydrogen-bond controlled drug release in cancer therapy, for the first time in the literature. This concept is schematically shown in figure 3.5.

The present investigation is emphasized to design and develop new classes of hydrogen bonded PCL diblock copolymers that are stable at extracellular circularity and degradable by lysosomal enzymes at the intracellular compartments to deliver cargoes to cancer cells. For this purpose, new substituted  $\epsilon$ -caprolactone monomers were custom designed with carboxylic ester and hydrogen bonded amide linkages (see figure 3.4) starting from a commercially available 1,4-cyclohexane diol. The ring opening polymerization of these monomers with PEG monomethyl ether produced amphiphilic PEG-*block*-substituted PCL block copolymers. These diblock copolymers self-assembled into 90-160 nm sized nanoparticles in water and anticancer drug doxorubicin (DOX) was loaded in their hydrophobic pocket. The aliphatic polyester PCL backbone ruptured in the presence of a lysosomal-esterase enzyme and released DOX at intracellular levels.

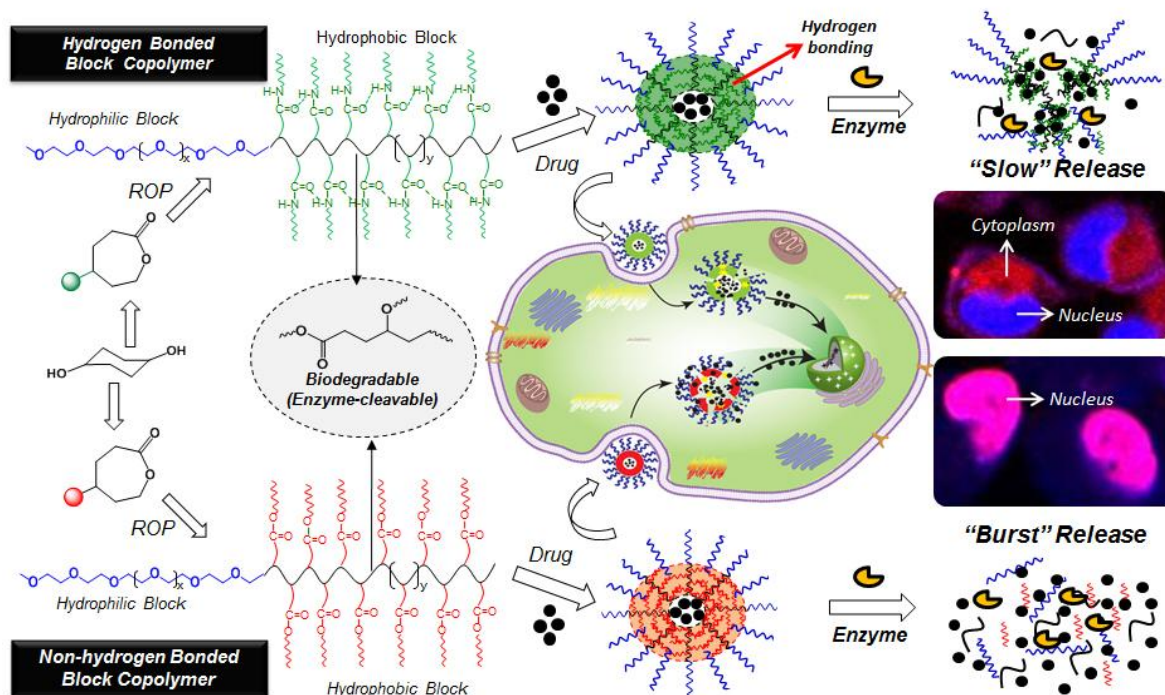


**Figure 3.5.** Hydrogen-bond controlled drug delivery in cancer cells from enzyme-responsive polycaprolactone diblock copolymer nano-assemblies.

The hydrogen bonded nanoparticle exhibited good drug stability and released the drugs in a “controlled” manner whereas un-controlled burst release was observed for non-hydrogen bonded nanoparticles. Cellular uptake and cytotoxicity were studied in cervical (HeLa) and breast cancer (MCF 7) cell lines. Time-dependent *in vitro* and *in vivo* mimicking cytotoxicity experiments were carefully designed to correlate the cell killing ability of hydrogen bonded nanoparticles over non-hydrogen bonded analogues. Confocal microscope analysis confirmed that the hydrogen bonded nanoparticles are very good drug carriers across the cell membranes in both cervical and breast cancer cells and predominately accumulated the drug in the cytoplasm and at peri-nuclear environment. The present investigation successfully demonstrated the concept of “hydrogen-bond controlled” drug delivery in cancer cells, more specifically based on biodegradable PCL diblock copolymer nano-assemblies.

## 3.2 Experimental methods

**3.2.1. Materials:** Cis, trans-1,4-cyclohexane diol, tertiary butyl acrylate, potassium tertiary butoxide, pyridinium chlorochromate (PCC), trifluoroacetic acid (TFA), 1-octanol, norbornane methanol, 1-octyl amine, L-phenylalanine, meta chloro per benzoic acid (mCPBA), doxorubicin hydrochloride (DOX.HCl), triethylamine (TEA), diethyl isopropyl ethylamine (DIPEA) were purchased from Aldrich. Cervical (Hela) and breast (MCF 7) cancer cells were maintained in DMEM (phenol red free medium: Gibco) containing 10% (v/v) fetal bovine serum (FBS) and 1% (v/v) penicillin–streptomycin at 37°C under a 5% CO<sub>2</sub> humidified atmosphere. Cells were washed with 40 % DPBS (Gibco), trypsinized using 0.05 % trypsin (Gibco) and seeded in 96 well or 6 well (as per experiment) flat bottomed plastic plates (Costar) for all assays. Tetrazolium salt, 3-(4,5-dimethylthiazolyl)-2,5-diphenyltetrazolium bromide (MTT), DMSO (dimethyl sulfoxide), Hoechst and 4% paraformaldehyde was obtained from Sigma. Fluoromount was obtained from Southern Biotech. Solvents like tetra hydro furan (THF), dichloromethane (DCM) and dimethylformamide (DMF) were locally purchased and dried prior to use.

**3.2.2. Methods:** NMR was recorded using 400-MHz JEOL NMR spectrophotometer. All NMR spectra were recorded in CDCl<sub>3</sub> containing TMS as an internal standard. The gel permeation chromatographic (GPC) analysis was performed using Viscotek VE 1122 pump, Viscotek VE 3580 RI detector, and Viscotek VE 3210 UV–Vis detector in tetrahydrofuran (THF) using polystyrene as standards. The thermal stability of the polymers was determined using Perkin-Elmer thermal analyser STA 6000 model at a heating rate of 10°C/min in a nitrogen atmosphere. The absorption spectra were recorded using Perkin-Elmer Lambda 45 UV–Vis spectrophotometer. Dynamic light scattering (DLS) was done using a Nano ZS-90 apparatus utilizing 633nm red laser (at 90° angle) from Malvern Instruments. At 90°, scattered fluctuations were detected to generate correlation function  $[g^2(t)]$ , from this function diffusion coefficient (D) was calculated by using the cumulant method. By applying the stock-Einstein equation, the particle diameter was calculated. The reproducibility of the data was checked at least three times using independent polymer solutions. FE-SEM images were recorded using a Zeiss Ultra Plus scanning electron microscope. For FE-SEM analysis, the samples were prepared by drop casting on silicon wafers. Atomic force microscope images were recorded for drop casted samples using Agilent instruments. The reproducibility of the data was checked for at least three independent amphiphilic solutions. TEM images were

recorded using a Technai-300 instrument by drop casting the sample on the Formvar-coated copper grid. The fluorescent micrographs were collected using Carl Zeiss Axiovert 200 microscope. The confocal micrographs were collected using LSM710 microscope.

**3.2.3. Synthesis of tert-butyl 3-((4-hydroxycyclohexyl) oxy)propionates (1):** t-Butyl acrylate (11.03 g, 86.09 mmol) in THF (50 mL) was added drop wise into a solution of 1,4-cyclohexane diol (20.00 g, 172 mmol) and potassium tert butoxide (200 mg) in THF (200 mL) at 25 °C under nitrogen atmosphere. The reaction was refluxed under nitrogen atmosphere for 24 h. The reaction mixture was neutralised with 1N HCl (20 mL) and the product was extracted into ethyl acetate. The organic layer was dried over anhy. Na<sub>2</sub>SO<sub>4</sub> and the solvent was evaporated to get the product as liquid. It was further purified by passing through silica gel column using ethyl acetate and hexane as eluent (1:10 v/v). Yield= 16.5 g (78 %). <sup>1</sup>H-NMR (400MHz, CDCl<sub>3</sub>) δ ppm: 3.64 (m, 3H, O-CH<sub>2</sub>- and O-CH), 3.29-3.39(m, 1H, HO-CH), 2.40 (t, 2H, -CH<sub>2</sub>CO-), 1.96-1.81(m, 4H, OCH(CH<sub>2</sub>)<sub>2</sub>) 1.64 and 1.32 (m, 4H, CO(CH<sub>2</sub>)<sub>2</sub>), 1.45 (s, 9H, -C(CH<sub>3</sub>)<sub>3</sub>). <sup>13</sup>C-NMR (100MHz, CDCl<sub>3</sub>) δ ppm: 171.08, 80.43, 69.50, 63.94, 63.53, 36.67, 32.54, 30.33, 29.17, 28.08, and 27.44. FT-IR (cm<sup>-1</sup>): 3421, 2977, 2935, 2863, 1727, 1456, 1393, 1366, 1255, 1155, 1106 and 1034. HRMS (ESI+): m/z [M+Na<sup>+</sup>] calcd. for C<sub>13</sub>H<sub>24</sub>O<sub>4</sub>[M<sup>+</sup>] = 267.1572; Found = 267.1564.

**3.2.4. Synthesis of tert-butyl 3-((4-oxocyclohexyl)oxy)propanoate (2):** PCC (39.01 g, 184.01 mmol) was added into the solution of compound **1** (15.00 g, 61.40 mmol) in dry DCM (200 mL). The reaction was allowed to stir at 37 °C for 5 h under nitrogen atmosphere. The reaction mixture was filtered and the filtrate was evaporated to get yellow liquid as product. It was further purified through silica gel column using hexane/ethyl acetate (15: 1 v/v) as eluent to obtain product as colourless liquid. Yield= 13.5 g (91 %). <sup>1</sup>H-NMR (400MHz, CDCl<sub>3</sub>) δ ppm : 2.96 (m, 3H, O-CH<sub>2</sub> and O-CH), 2.58 (t, 2H, -CH<sub>2</sub>-CO), 2.64 (m, 2H, -CH<sub>2</sub>-), 2.26 (m, 2H, -CH<sub>2</sub>-), 2.09 (m, 2H, -CH<sub>2</sub>), 1.90(m, 2H, -CH<sub>2</sub>) and 1.45 (s, 9H,-C(CH<sub>3</sub>)<sub>3</sub>). <sup>13</sup>C-NMR (100MHz, CDCl<sub>3</sub>) δ ppm: 211.40, 170.99, 80.56, 72.74, 64.02, 37.02, 36.56, 30.40 and 20.04. FT-IR (cm<sup>-1</sup>): 2974, 2874, 2360, 1716, 1456, 1419, 1393, 1366, 1306, 1249, 1210 and 1100. HRMS (ESI+): m/z [M+Na<sup>+</sup>] calcd. for C<sub>13</sub>H<sub>22</sub>O<sub>4</sub>[M<sup>+</sup>] = 265.1415 ; found = 265.1411.

**3.2.5. Synthesis of 3-((4-oxocyclohexyl)oxy)propanoic acid (3):** TFA (50 mL) was added into the solution of compound **2** (12.00 g, 49.5 mmol) in DCM (50 mL) and the reaction

mixture was stirred for 1 h at 25 °C. The TFA and DCM were evaporated under reduced pressure. The residue was dissolved in 200 mL of chloroform and washed with 1 M HCl (100 mL). The organic layer was dried over anhy. Na<sub>2</sub>SO<sub>4</sub> and concentrated using rotavapor to obtain yellow liquid as product. Yield = 8.0 g (86.7 %). <sup>1</sup>H-NMR (400MHz, CDCl<sub>3</sub>) δ ppm: 3.78 (m, 3H, -CH<sub>2</sub> and -O-CH), 2.67 (t, 2H, -CH<sub>2</sub>-CO-), 2.57 (m, 2H, -CH<sub>2</sub>), 2.27 (m, 2H, -CH<sub>2</sub>), 2.11 (m, 2H, -CH<sub>2</sub>) and 1.99 (m, 2H, -CH<sub>2</sub>). <sup>13</sup>C-NMR (100MHz, CDCl<sub>3</sub>) δ ppm: 212.26, 177.11, 72.82, 63.29, 36.87, 36.05 and 30.21. FT-IR (cm<sup>-1</sup>): 3446, 2929, 2360, 1700, 1418, 1346, 1306, 1245, 1187, 1105 and 1063. HRMS (ESI+): m/z [M+Na<sup>+</sup>] calcd. for C<sub>9</sub>H<sub>14</sub>O<sub>4</sub>[M<sup>+</sup>] = 209.0789; found = 209.0784.

**3.2.6. Synthesis of Alkyl 3-((4-oxocyclohexyl) oxy) propionate (4a):** Compound **3** (2.00 g, 10.7 mmol), 4-(dimethylamino) pyridine (DMAP, 131 mg, 1.07 mmol) and 1-octanol (1.54 g, 11.8 mmol) were taken in dry DCM (40 mL). The reaction vessel was cooled to 0 °C and 1-ethyl-3-((dimethylamino)propyl)carbodiimide hydrochloride (EDC.HCl, 2.47 g, 12.9 mmol) and diisopropylethylamine (DIPEA, 4.20 g, 32.3 mmol) were added. The reaction mixture was stirred at 0 °C for 2 h and then it was continued at 25 °C for 12 h. The solvent was evaporated under reduced pressure, and then crude product was extracted with ethyl acetate. The organic layer was washed with a saturated NH<sub>4</sub>Cl solution, dried over anhy. Na<sub>2</sub>SO<sub>4</sub> and then concentrated under reduced pressure. The crude product was further purified by passing through the silica gel column using hexane and ethyl acetate as eluent (1:10 V/V). Yield= 2.2 g (68.6 %). <sup>1</sup>H-NMR (400 MHz, CDCl<sub>3</sub>) δ ppm: 4.08 (t, 2H, COOCH<sub>2</sub>), 3.77-3.71 (m, 3H, OCH<sub>2</sub>and OCH), 2.59-2.54 (m, 4H, -OCH-(CH<sub>2</sub>)<sub>2</sub>), 2.24 (m, 2H, -COCH<sub>2</sub>), 2.08( m, 2H, -COCH<sub>2</sub>), 1.89 (m, 2H, -COCH<sub>2</sub>), 1.61 (m, 2H, -OCH<sub>2</sub>-CH<sub>2</sub>), 1.26 (m, 12H, octanol chain), 0.89 (t, 3H, -CH<sub>3</sub>). <sup>13</sup>C-NMR (100MHz, CDCl<sub>3</sub>) δ ppm: 211.8, 172.1, 73.0, 64.9, 63.9, 37.2, 35.6, 31.9, 30.6, 29.4, 28.7, 26.0, 22.7, and 14.2. FT-IR (cm<sup>-1</sup>): 2932, 2850, 1728, 1463, 1352, 1249, 1172, 1112, 1052, 950 and 727. HRMS (ESI+): m/z calculated. for C<sub>17</sub>H<sub>30</sub>O<sub>4</sub> [M<sup>+</sup>] = 298.2144; found = 298.2163.

**3.2.7. Synthesis of bicyclo [2.2.1](heptan-2-yl)methyl 3-((4-oxocyclohexyl)oxy) propanoate (4b):** Compound **3** (2.00 g, 10.7 mmol), 4-(dimethylamino) pyridine (DMAP, 131 mg, 1.07 mmol), norbornane methanol (1.41 g, 11.8 mmol), EDC.HCl (2.47 g, 12.9 mmol) and diisopropylethylamine (DIPEA, 4.20 g, 32.3 mmol) were used and the procedure described for compound **4a** was followed. Yield = 2.1 g (66 %). <sup>1</sup>H-NMR (400MHz, CDCl<sub>3</sub>) δ ppm : 4.1-3.82 (dd, 2H, -COOCH<sub>2</sub>) , 3.77 (t, 2H, OCH<sub>2</sub>), 3.73 (m, 3H, OCH and OCH<sub>2</sub>),

2.59 (m, 3H,  $-\text{CH}_2\text{CO}$  and  $\text{COOCH}_2\text{CH}-$ ), 2.2-1.9 (m, 8H,  $\text{CO}(\text{CH}_2\text{CH}_2)_2$ ), 1.7-1.3 (m, 6H,  $-\text{CHCH}_2\text{CH}-$ ), 1.09 (dd, 1H,  $-\text{CH}_2\text{CHCH}_2-$ ), 0.66 (dd, 1H,  $-\text{CH}_2\text{CHCH}_2-$ ).  $^{13}\text{C}$ -NMR (100MHz,  $\text{CDCl}_3$ )  $\delta$  ppm: 211.5, 171.7, 73.0, 65.0, 63.9, 37.2, 35.6, 31.8, 30.6, 29.8, 29.3, 28.7, 26.0, 22.7, and 14.3. FT-IR ( $\text{cm}^{-1}$ ): 2944, 2859, 1719, 1455, 1403, 1352, 1257, 1163, 1104, 1052, 1019, 949 and 761. HRMS (ESI+):  $m/z$  calcd. for  $\text{C}_{17}\text{H}_{26}\text{O}_4$  [ $\text{M}^+$ ] = 294.1831 ; found = 294.1901.

**3.2.8. Synthesis of octyl 3-((7-oxooxepan-4-yl)oxy)propanoate(5a):** *m*-Chloroperbenzoic acid (1.40 g, 8.1 mmol) was added slowly to a stirred solution of **4a** (2.00 g, 6.7 mmol) in dry DCM (60 mL) under nitrogen atmosphere. To above reaction mixture, anhydrous  $\text{NaHCO}_3$  (1.70 g, 20.2 mmol) was added and the reaction was continued at 25 °C for 12 h. The solvent was removed and the residue was neutralized with saturated aqueous  $\text{NaHCO}_3$  solution (10 mL) and saturated aqueous  $\text{Na}_2\text{S}_2\text{O}_3$  solution (10 mL). It was extracted with ethyl acetate and the organic layer was dried over anhydrous  $\text{Na}_2\text{SO}_4$ . After solvent evaporation, the crude product was purified by passing through silica gel column using ethyl acetate and petroleum ether (4:6 v/v). Yield= 1.5 g (71 %).  $^1\text{H}$ -NMR (400MHz,  $\text{CDCl}_3$ )  $\delta$  ppm : 4.45 (dd, 1H,  $\text{COOCH}$ ), 4.04-4.10 (dd, 1H,  $\text{COOCH}$  and  $\text{COOCH}_2$ ), 3.69 (m, 3H,  $\text{OCH}_2$  and  $\text{OCH}$ ), 2.95 (dd, 1H,  $\text{COCH}$ ), 2.55 (t, 2H,  $\text{COCH}_2$ ), 2.40 (dd, 1H,  $\text{COCH}$ ), 2.45-1.80 (m, 4H,  $\text{OCH}-(\text{CH}_2)_2$ ), 1.61 (m,  $\text{OCH}_2-\text{CH}_2-$ ) 1.26 (m, 10H of octanol chain) and 1.44 (s, 9H,  $\text{C}(\text{CH}_3)_3$ ).  $^{13}\text{C}$ -NMR: (100MHz,  $\text{CDCl}_3$ )  $\delta$  ppm: 176.2, 171.8, 77.2, 74.0, 64.9, 63.8, 63.4, 37.2, 35.4, 34.0, 31.8, 29.3, 28.7, 27.9, 27.4, 26.0, 22.7, and 14.2. FT-IR ( $\text{cm}^{-1}$ ): 2935, 2859, 1719, 1455, 1352, 1249, 1163, 1094, 1044, 975 and 660. HRMS (ESI+):  $m/z$  [ $\text{M}+\text{K}^+$ ] calcd. For  $\text{C}_{17}\text{H}_{30}\text{O}_5$  [ $\text{M}^+$ ] = 353.4220; found = 353.2103.

**3.2.9. Synthesis of bicyclo [2.2.1] (heptan-2-yl)methyl 3-((7-oxooxepan-4-yl)oxy)propanoate (5b):** Compound **4b** (2.00 g, 6.8 mmol),  $\text{NaHCO}_3$  (1.71 g, 20 mmol), *m*CPBA (1.40 g, 8.1 mmol) were used and the procedure described for compound **5a** was followed. Yield= 1.60 g (76 %).  $^1\text{H}$ -NMR (400MHz,  $\text{CDCl}_3$ )  $\delta$  ppm: 4.48 (dd, 1H,  $\text{COOCH}$ ), 4.14 (dd, 1H,  $\text{COOCH}$ ), 4.05-3.82 (dd, 2H,  $-\text{OCH}_2\text{CH}$ ), 3.71 (m, 3H,  $\text{OCH}$  and  $\text{OCH}_2$ ), 2.97 (dd, 1H,  $\text{COCH}$ ), 2.57 (m, 3H,  $\text{COCH}_2$  and  $\text{OCH}_2\text{CH}$ ), 2.42(dd, 1H,  $\text{COCH}$ ), 2.23-1.85 (m, 4H,  $\text{OCH}-(\text{CH}_2)_2$ ), 1.82-1.11 (m, 6H,  $-\text{CHCH}_2\text{CH}-$ ), 0.89 (dd, 1H,  $-\text{CH}_2\text{CHCH}_2-$ ), 0.66 (dd, 1H,  $-\text{CH}_2\text{CHCH}_2-$ ).  $^{13}\text{C}$ -NMR (100MHz,  $\text{CDCl}_3$ )  $\delta$  ppm: 176.2, 171.8, 74.1, 68.1, 66.7, 63.8, 63.4, 41.1, 39.8, 38.8, 38.5, 38.4, 36.7, 36.2, 35.4, 35.2, 34.1, 34.0, 33.9, 33.7, 29.9, 29.7,

28.9, 27.9, 27.4, and 22.7. FT-IR ( $\text{cm}^{-1}$ ): 2927, 2859, 1737, 1146, 1360, 1250, 1172, 1104, 1060, 957 and 718. HRMS (ESI+):  $m/z$  calcd. For  $\text{C}_{17}\text{H}_{26}\text{O}_5$  [ $\text{M}^+$ ] = 310.1780; found = 311.1810.

**3.2.10. Synthesis of N-octyl-3-((4-oxocyclohexyl)oxy)propanamide (6a):** Compound **3** (2.00 g, 10.7 mmol), 4-(dimethylamino) pyridine (DMAP, 131 mg, 1.07 mmol), 1-octylamine (1.53 g, 11.8 mmol) EDC.HCl (2.47 g, 12.9 mmol) and diisopropylethylamine (DIPEA, 4.20 g, 32.3 mmol) in DCM (40 mL) were used and the procedure described for compound **4a** was followed. Yield = 2.40 g, (75 %).  $^1\text{H-NMR}$  (400MHz,  $\text{CDCl}_3$ )  $\delta$  ppm : $\delta$  3.78 (t, 2H, - $\text{OCH}_2$ ), 3.75 (m, 1H, - $\text{OCH}$ ), 3.70 (t, 2H, - $\text{NCH}_2$ ), 2.60 (t, 2H,  $\text{COCH}_2$ ), 2.56 (t, 2H, - $\text{COCH}_2$ ), 2.26 – 2.07 (m, 4H, - $\text{CH}(\text{CH}_2)_2$ ), 1.99 – 1.52 (m, 16H, octylamine chain).  $^{13}\text{CNMR}$  (100MHz,  $\text{CDCl}_3$ )  $\delta$  ppm:  $\delta$  211.4, 171.9, 73.0, 64.9, 63.9, 37.2, 35.6, 31.9, 30.6, 29.8, 29.3, 28.7, 26.0, 22.7 and 14.2. FT-IR ( $\text{cm}^{-1}$ ): 3295, 3089, 2918, 2841, 1711, 1634, 1566, 1455, 1446, 1352, 1241, 1197, 1112, 1069, 967 and 727. HRMS (ESI+):  $m/z$  [ $\text{M}+\text{K}^+$ ] calcd. For  $\text{C}_{17}\text{H}_{31}\text{NO}_3$  [ $\text{M}^+$ ] = 336.4390; found = 336.2304.

**3.2.11. Methyl 2-(3-((4-oxocyclohexyl)oxy)propanamido)-3-phenylpropanoate (6b):** Compound **4** (2.00 g, 10.7 mmol), 4-(dimethylamino) pyridine (DMAP, 131 mg, 1.07 mmol), phenyl alanine hydrochloride (2.55 g, 11.8 mmol), EDC.HCl (2.47 g, 12.9 mmol) and diisopropylethylamine (DIPEA, 6.90 g, 53.7 mmol) in DCM (40 mL) were used and the procedure described for compound **4a** was followed. Yield = 2.60 g (70%).  $^1\text{H-NMR}$  (400MHz,  $\text{CDCl}_3$ )  $\delta$  ppm : 7.26 (m, 3H, = $\text{CH}$ ), 7.09 (m, 2H, = $\text{CH}$ ), 6.86 (d, 1H,  $\text{NH}$ ), 4.93 (m, 1H,  $\text{NHCH}$ ), 3.75 (s, 3H,  $\text{OCH}_3$ ), 3.73 (m, 2H,  $\text{OCH}_2$ ), 3.65 (m, 1H,  $\text{OCH}$ ), 3.16 (m, 2H, - $\text{CH}_2$ -Ar), 2.53 (t, 2H,  $\text{COCH}_2$ ), 2.40 (m, 1H,  $\text{NHCH}$ ), 2.18-1.81 ( $\text{O}(\text{CH}_2\text{CH}_2)_2\text{CO}$ ).  $^{13}\text{C-NMR}$  (100MHz,  $\text{CDCl}_3$ )  $\delta$  ppm: 210.80, 171.52, 171.32, 136.34, 128.43, 126.32, 125.92, 83.23, 65.43, 56.23, 51.92, 48.72, 37.23 and 35.32. FT-IR ( $\text{cm}^{-1}$ ): 3309, 2955, 2922, 2853, 1742, 1651, 1539, 1496, 1456, 1436 and 1209. HRMS (ESI+):  $m/z$  [ $\text{M}+\text{Na}^+$ ] calcd. For  $\text{C}_{19}\text{H}_{25}\text{NO}_5$  [ $\text{M}^+$ ] = 370.1733; found = 370.1003.

**3.2.12. Synthesis of N-octyl-3-((7-oxooxepan-4-yl)oxy)propanamide (7a):** Compound **6a** (2.00 g, 6.72 mmol),  $\text{NaHCO}_3$  (1.70 g, 20.1 mmol), mCPBA (1.40 g, 8.0 mmol) were used and the procedure described for compound **5a** was followed. Yield = 1.60 g (77 %).  $^1\text{H-NMR}$  (400MHz,  $\text{CDCl}_3$ )  $\delta$  ppm: 5.94 (s, 1H,  $\text{CONH}$ ), 4.43 (dd, 1H,  $\text{COOCH}$ ), 4.04 (dd, 1H,  $\text{COOCH}$ ), 3.79 – 3.63 (m, 3H,  $\text{CH-O-}$  and  $\text{O-CH}_2$ ), 3.23 (m, 2H,  $\text{NHCH}_2$ ), 2.90 (dd, 1H,

COCH), 2.48 – 2.31 (m, 3H, COCH and  $-\text{CH}_2\text{-CO}$ ), 2.07 – 1.91 (m, 4H,  $-\text{CH}(\text{CH}_2)_2$ ), 1.55 (m, 2H,  $-\text{NHCH}_2\text{-CH}_2-$ ), 1.37 – 1.16 (m, 10H, octylamine chain), 0.86 (t, 3H,  $\text{CH}_3$ ).  $^{13}\text{C-NMR}$  (100MHz,  $\text{CDCl}_3$ )  $\delta$  ppm: 176.1, 170.9, 74.6, 64.4, 63.6, 39.7, 37.3, 33.8, 31.5, 29.7, 29.3, 28.0, 27.5, 27.0, 22.7 and 14.1. FT-IR ( $\text{cm}^{-1}$ ): 3312, 3107, 2927, 2849, 1728, 1634, 1548, 1455, 1352, 1266, 1189, 1094 and 718. HRMS (ESI+):  $m/z$   $[\text{M}+\text{Na}^+]$  calcd. for  $\text{C}_{17}\text{H}_{31}\text{NO}_4$   $[\text{M}^+] = 336.2253$ ; found = 336.3710.

### 3.2.13. Methyl 2-(3-((7-oxooxepan-4-yl)oxy)propanamido)-3-phenylpropanoate (7b):

Compound **6b** (2.00 g, 6.76 mmol),  $\text{NaHCO}_3$  (1.45 g, 7.3 mmol), mCPBA (1.20 g, 6.9 mmol) were used and the procedure described for compound **5a** was followed. Yield = 1.70 g (81 %).  $^1\text{H-NMR}$  (400MHz,  $\text{CDCl}_3$ )  $\delta$  ppm: 7.24-7.06 (m, 5H, aromatic protons), 6.74(s, 1H, NH), 4.90(m, 1H, NCH), 4.26(dd, 1H, OCH), 3.89 (dd, 1H, OCH), 3.73 (s, 3H,  $\text{OCH}_3$ ), 3.65 (m, 3H,  $\text{OCH}_2$  and OCH), 3.59 (m, 2H,  $\text{CH}_2\text{CON}$ ), 2.76 and 2.46 (dd, 2H,  $\text{COCH}_2$ ), 2.29 (s,  $\text{CH}_2$ , Ar $\text{CH}_2$ ), 1.82 (m, 4H,  $\text{OCH}(\text{CH}_2)_2$ ).  $^{13}\text{C-NMR}$  (100MHz,  $\text{CDCl}_3$ )  $\delta$  ppm: 172.36, 171.87, 129.21, 128.41, 127.07, 64.63, 64.07, 63.13, 59.07, 52.80, 52.32, 37.62, 37.50, 35.80, 33.47, 29.61, 28.51, 27.58, 26.92, and 26.80. FT-IR ( $\text{cm}^{-1}$ ): 3355, 3081, 2952, 2859, 2593, 1719, 1660, 1523, 1429, 1343, 1189, 1089, 735, 705, 701 and 633. HRMS (ESI+):  $m/z$   $[\text{M}+\text{Na}^+]$  calcd. for  $\text{C}_5\text{H}_9\text{NO}_4$   $[\text{M}^+] = 386.1682$ ; found = 386.3710.

**3.2.14. Synthesis of PEG-*b*-SPCL diblock polymers:** The typical synthetic procedure was elucidated for PEG-*b*-PCLEC<sub>8</sub>; where,  $[\text{M}_0]/[\text{I}_0]$  is kept as 100. The initiator PEG<sub>2000</sub> (40.1 mg, 0.02 mmol), catalyst  $\text{Sn}(\text{Oct})_2$  (4.0 mg, 0.01 mmol) and the monomer **4a** (630 mg, 2.0 mmol) were taken in a flame-dried Schlenk tube under nitrogen atmosphere. The high vacuum was applied to this reaction mixture for 30-40 min with stirring at room temperature. The tube was immersed in preheated oil bath at 130 °C, after creating an inert environment inside. The polymerization was continued for 6 h with constant stirring. The crude polymer mixture was cooled to room temperature, dissolved in 1 mL dry THF and precipitated in cold MeOH. Re-precipitation performed at least twice to achieve pure polymer. Yield: 337 mg (53.5 %).  $^1\text{H-NMR}$  (400 MHz,  $\text{CDCl}_3$ )  $\delta$  ppm: 4.13 (m, 2H), 4.07 (m, 2H), 3.69-3.63 (m, 5.27 H), 3.45 (m, 1H), 2.52 (m, 2H), 3.38 (m, 2H), 1.86-1.78 (m, 4H), 1.26 (m, 10H) and 0.86 (m, 3H).  $^{13}\text{C-NMR}$  (100 MHz,  $\text{CDCl}_3$ ): 173.85, 172.02, 760.99, 65.20, 61.67, 35.73, 33.36, 32.22, 29.65, 29.04, 26.34, 23.06 and 14.51. FT-IR ( $\text{cm}^{-1}$ ): 2935, 2867, 1328, 1463, 1343, 1257, 1172, 1094, 1064, 941 and 727. GPC molecular weights:  $M_n = 12,300$ ,  $M_w = 15,100$  and  $M_w/M_n = 1.23$ .



A similar procedure was followed for the synthesis of other diblock copolymers and their NMR and molecular weight details are provided in below.

**3.2.15. Synthesis of PEG-*b*-PCLNB diblock polymer:** Monomer **5b** (1.28 g, 4.13 mmol), initiator PEG<sub>2000</sub> (82.6 mg, 0.041 mmol) and catalyst Sn(Oct)<sub>2</sub> (8.36 mg, 0.02 mmol). Yield = 900 mg (70.3 %). <sup>1</sup>H-NMR (400 MHz, CDCl<sub>3</sub>) δ ppm: 4.14 (m, 2.6 H), 3.91-3.81 (two t, 1.13 H), 3.69-3.63 (m, 4.50 H), 3.43 (m, 1 H), 2.52 (m, 2.12 H), 2.36 (m, 2.16 H), 2.22 (m, 2.83 H), 1.78 (m, 5.4 H), 1.49-1.09 (m, 7.4 H) and 0.68 (dd, 0.85 H). <sup>13</sup>C-NMR (100 MHz, CDCl<sub>3</sub>): 173.6, 171.8, 75.7, 70.6, 67.8, 66.7, 64.7, 61.3, 40.6, 39.6, 38.6, 36.8, 36.1, 35.4, 33.6, 32.6, 29.7, 29.0 and 22.5. FT-IR (cm<sup>-1</sup>): 3495, 2945, 2849, 1463, 1343, 1257, 1163, 1104, 1064, 975 and 795. GPC molecular weights: M<sub>n</sub> = 13,700, M<sub>w</sub> = 16,600 and M<sub>w</sub>/M<sub>n</sub> = 1.21.

**3.2.16. Synthesis of PEG-*b*-PCLAC<sub>8</sub> diblock polymer:** Monomer **7a** (760 mg, 2.43 mmol), initiator PEG<sub>2000</sub> (48.5 mg, 0.0242 mmol) and catalyst Sn(Oct)<sub>2</sub> (4.9 mg, 0.0121 mmol). Yield = 570 mg (75 %). <sup>1</sup>H NMR (400 MHz, CDCl<sub>3</sub>) δ ppm: 6.36 (br, -NH), 4.13 (m, 2 H), 3.68-3.63 (m, 5.32 H), 3.43 (m, 1 H), 3.21 (m, 2 H), 2.39 (m, 2 H), 1.9-1.71 (m, 4 H), 1.48 (m, 2 H), 1.26 (m, 10 H), 0.86 (t, 3 H). <sup>13</sup>C-NMR (100 MHz, CDCl<sub>3</sub>): 173.7, 171.4, 76.1, 70.2, 65.5, 61.1, 59.2, 39.6, 37.2, 32.7, 31.6, 29.0, 26.8, 22.7 and 14.1. FT-IR (cm<sup>-1</sup>): 3320, 3089, 3089, 2918, 2947, 1642, 1531, 1480, 1353, 1249, 1172, 1104, 957, 735, and 641. GPC molecular weights: M<sub>n</sub> = 10,000, M<sub>w</sub> = 14,100 and M<sub>w</sub>/M<sub>n</sub> = 1.41.

**3.2.17. Synthesis of PEG-*b*-PCLPhA diblock polymer:** Monomer **7b** (440 g, 1.21 mmol), initiator PEG<sub>2000</sub> (24.24 mg, 0.0121mmol) and catalyst Sn(Oct)<sub>2</sub> (2.45 mg, 0.006 mmol). Yield = 400 mg (90 %). <sup>1</sup>H NMR (400 MHz, CDCl<sub>3</sub>) δ ppm: 7.26-7.11 (m, 5 H), 6.78 (br, 1 H), 4.88 (br, 1 H), 4.08 (m, 2 H), 3.68-3.63 (m, 8.8 H), 3.40 (s, 1 H), 3.10 (m, 3 H), 2.41 (br, 3 H), 2.31 (br, 2 H), 1.71 (m, 5.5 H). <sup>13</sup>C-NMR (100 MHz, CDCl<sub>3</sub>): 173.5, 172.2, 171.4, 129.4, 128.6, 127.2, 75.9, 70.4, 65.1, 61.5, 53.3, 52.4, 37.7, 37.1, 32.7, 29.8 and 28.7. FT-IR (cm<sup>-1</sup>): 3346, 3072, 2961, 2875, 1737, 1634, 1531, 1437, 1368, 1257, 1181, 1094, 907, 727, 693 and 624. GPC molecular weights: M<sub>n</sub> = 11,100, M<sub>w</sub> = 15,100 and M<sub>w</sub>/M<sub>n</sub> = 1.36.

**3.2.18. Drug Encapsulation in Diblock Copolymer Scaffolds:** The detailed procedure is given for DOX (obtained from DOX.HCl treating with triethylamine) encapsulation. In a typical experiment, 10 mg of the polymer and 1 mg of DOX was dissolved in DMSO (2 mL). Distilled water (8 mL) was added dropwiseto the polymer solution, and the mixture was stirred at 25°C for 4 h. The solution was transferred to a dialysis bag (MWCO = 1000) and

dialyzed against a large amount of distilled water for 48 h. Fresh distilled water replaced periodically to ensure the removal of unencapsulated molecules from the dialysis tube.

The drug loading efficiency (DLE) and drug loading content (DLC) were determined by absorption spectroscopy using the following equations:<sup>32, 33</sup>

$$\text{DLE (\%)} = \{ \text{weight of drug in vesicles} / \text{weight of drug in feed} \} \times 100\%$$

$$\text{DLC (\%)} = \{ \text{weight of drug in vesicles} / \text{weight of drug-loaded nanoparticles} \} \times 100\%$$

**3.2.19. *In Vitro* Drug Release Studies:** Various drug loaded micellar self-assemblies were taken in a dialysis bag (in 3 mL), and they were immersed in a 100 mL beaker and dialyzed at 37°C with constant stirring. These micelles were exposed to PBS and esterase to study the stability and release kinetics. At specific time intervals, 3.0 mL of the dialysate was withdrawn and replaced with an equal volume of fresh buffer (or FBS). The amount of molecule (or drug) released in each aliquot was measured using absorption spectroscopy to quantify their percentage of cumulative release. For esterase aided release studies 10 units of enzyme were used, following the above-mentioned procedure.

Cumulative release (%) =  $C_n \times V_o / m \times 100$ , where  $C_n$  is the amount of loaded cargo in the  $n^{\text{th}}$  sample,  $V_o$  is total volume, and  $m$  is the total amount loaded in nanoparticles.

**3.2.20. Cell Viability Assay (MTT Assay):** To observe the effect of polymers alone, free drug and drug-loaded nanoparticles cell viability assay was performed in HeLa cell line using the tetrazolium salt, 3-(4, 5-dimethylthiazol-2,5-diphenyl tetrazolium bromide (MTT).  $10^3$  cells were seeded per well in a 96-well plate (Corning, U.S.A.) in 100 $\mu$ L of DMEM with 10% FBS (fetal bovine serum) and allowed to adhere for 16 h. Prior to drug treatment, media from cells was aspirated and various concentrations of drugs and drug-loaded nanoparticles were fed. A blank control, DMEM with FBS in the absence of compound was used in each experiment. All control and treated experiment wells were in triplicate. Cells were incubated for various time intervals without a change in medium. After incubation drug containing medium was aspirated. Freshly prepared stock of MTT in sterile PBS (5 mg/mL) was diluted to 50 $\mu$ g/mL in DMEM. 100  $\mu$ L of this solution was added to each well. Cells were then incubated with MTT for 4 h at 37°C. Medium with MTT was then aspirated from wells and the purple formazan crystals formed as a result of the reduction of MTT by mitochondrial dehydrogenase enzyme from cells were dissolved in 100 $\mu$ L of 100% DMSO (added per well). The absorbance from formazan crystals was immediately measured using microplate

reader at 570 nm (Varioskan Flash) and was representative of the number of viable cells per well. Values from the triplicates for each control and treated set were noted and their mean was used for calculations. The values thus obtained for the untreated control samples were equated to 100 % and relative percentage values for the drug, scaffold alone and drug-loaded nanoparticles were calculated accordingly.

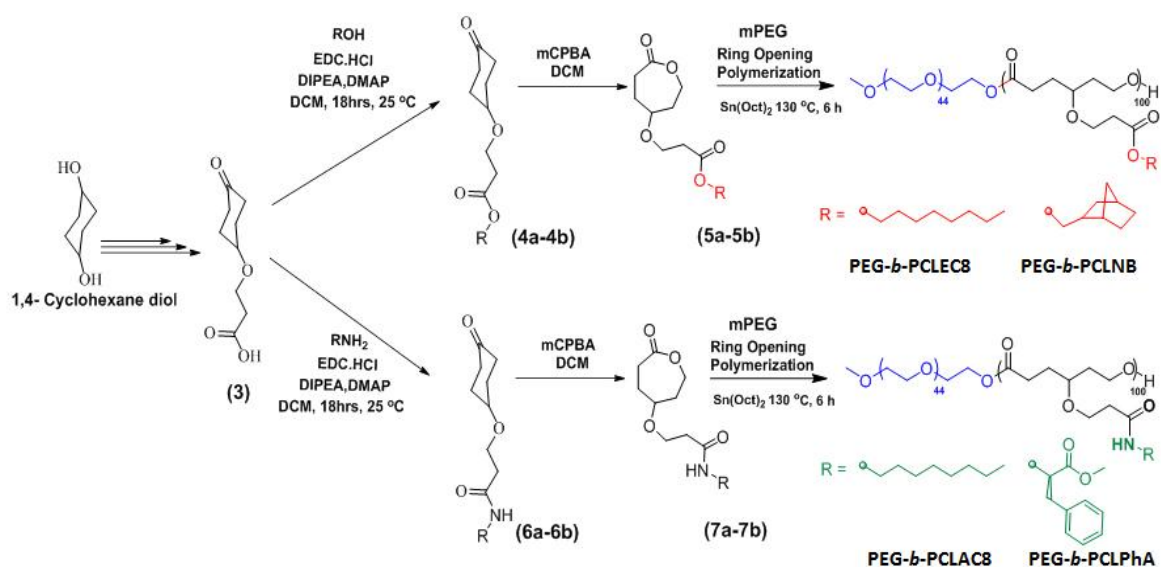
**3.2.21. *In vivo* mimicking assay:** To mimic *in vivo* conditions short time-MTT assay was studied. Wherein HeLa cells were seeded in 96 well plates with  $1 \times 10^3$  cells per well for 16 h. Later the media was removed and treated with various concentrations of drug and drug loaded nanoparticles. The compounds were incubated with cells for, 3 h, after incubation, the media was aspirated and fresh media was added. These cells were then incubated for various time intervals like 3, 6, 12 and 24h. After termination of the experiment, cell viability was determined using MTT assay.

**3.2.22. Cellular Uptake of DOX-loaded diblock nanoparticles by Confocal microscopy:** HeLa cells were seeded at a density of  $1 \times 10^5$  cells on flame-dried coverslips placed in 6 well plates containing DMEM medium with 10 % FBS and incubated at 37 °C for 16 h. The cells were then exposed to require concentrations of DOX loaded nanoparticles for 4 h in a CO<sub>2</sub> incubator at 37°C. After incubation, the drug-containing medium was aspirated from each well, and cells were washed twice with PBS ( $2 \times 1$  mL) and fixed with 4% paraformaldehyde solution in PBS for 10 min at room temperature. The cells were washed twice with PBS ( $2 \times 1$  mL) and stained with Hoechst solution in PBS. After 2 min incubation, at room temperature, in the dark, the excess dye was washed from the plate and cells were again gently rinsed with PBS for 1 min. The coverslips were mounted on slides using the fluoromount mounting medium (Southern Biotech) and dried overnight at room temperature in the dark. The cells were imaged using a confocal microscope using the  $\lambda$  420 nm (blue channel),  $\lambda$  440 nm (green channel) and  $\lambda$  560 nm (red channel) lasers. Images thus obtained were opened in the Image J analysis software and the image for each channel was separated.

### 3.3. Results and Discussion

#### 3.3.1. Synthesis and Characterization of Di-blocks

The amphiphilic diblock copolymers (PEG-*b*-SPCL) were synthesized by ring opening polymerization (ROP) of substituted caprolactone monomers prepared from 1, 4-cyclohexane diol through multi-step synthesis as shown in scheme 3.1. Michael addition reaction of 1, 4-cyclohexanediol with t-butyl acrylate produced compound (**1**) which was further oxidized to give the ketone derivative (**2**). The compound (**2**) was deprotected into its carboxylic acid (**3**). The compound (**3**) was reacted with 1-octanol and norbornane methanol to yield corresponding esters **4a** and **4b**, respectively. The Baeyer villager oxidation of **4a** and **4b** produced octyloxy and norbornane methoxy substituted caprolactone monomers **5a** and **5b**, respectively. The compound (**3**) was reacted with 1-octylamine and L-phenylalanine methyl ester to yield corresponding amides **6a** and **6b**, respectively. The Baeyer villager oxidation of **6a** and **6b** produced octylamide and L-phenylalanine amide substituted caprolactone monomers **7a** and **7b**, respectively. The structures of all these monomers and intermediates were characterized by <sup>1</sup>H-NMR, <sup>13</sup>C-NMR, FT-IR, and HR-MS.



**Scheme 3.1.** Synthesis of substituted caprolactone monomers and their di-block copolymers.

These newly synthesized monomers were subjected to ring opening polymerization (ROP) to produce substituted PCL diblock copolymers. For this purpose, polyethylene glycol monomethyl ether of molecular weight MW=2000 was used as an initiator and Sn(Oct)<sub>2</sub> was employed as catalyst (see scheme 3.1). The ratio between catalyst to initiator was maintained

as 1:2 for the in-situ generation of one-mole equivalents of ROP initiator MeO-PEG-O-Sn-O-PEG-OMe (bidentate catalyst).<sup>34</sup> The substituted caprolactone monomer to initiator concentration was maintained as  $[M]/[I] = 100$  and the polymerization was carried out for 6 h at 130 °C in melt (or neat) conditions. The polymers were purified by dissolving in tetrahydrofuran and precipitating in methanol. These diblocks were abbreviated as PEG-*b*-PCL<sub>X</sub> where X represents 1-octyloxy (PEG-*b*-PCLEC<sub>8</sub>), norbornane methoxy (PEG-*b*-PCLNB), octylamide (PEG-*b*-PCLAC<sub>8</sub>) and phenylalanine amide (PEG-*b*-PCLPhA).

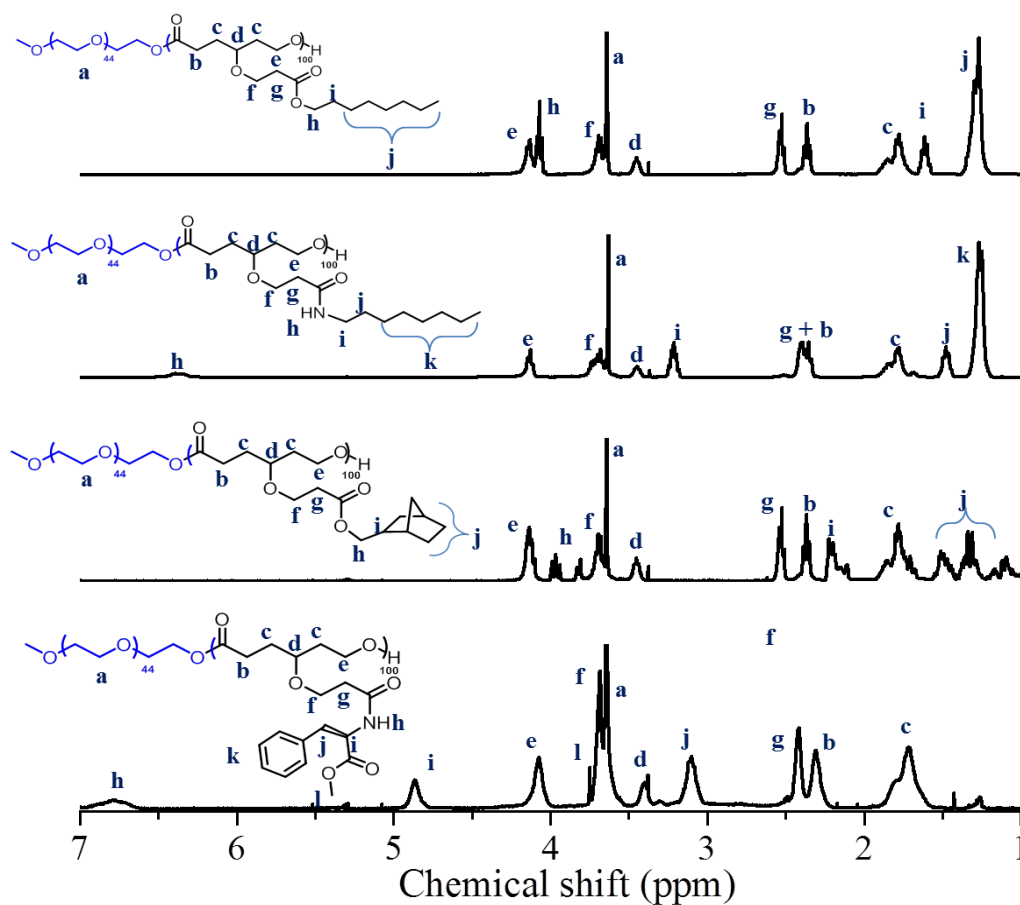


**Figure 3.6.** Stack plot of <sup>1</sup>H-NMRs of diblock copolymers.

The structures and molecular weight of these diblock copolymers were characterized by <sup>1</sup>H-NMR and GPC. The stack plot of <sup>1</sup>H-NMRs of polymers are provided in figure 3.6. The chemical structure of respective diblock copolymer is given and the different protons are assigned by alphabets. The determination of the n (number of repeating units) carried out as similar to described in chapter 2. In brief, explained for PEG-*b*-PCLEC<sub>8</sub> diblock copolymer and followed similar for rest. The protons ‘f’ in the

diblocks appeared a long with protons 'd' of PEG. The intensities of protons 'e' in the ester  $\text{OCH}_2$ - appeared at 4.13 ppm. Thus, the subtraction of peak intensities [(e+f) – a] provided the actual number of protons 'e'. The comparison of peak integrals of a (protons at 3.63 ppm) with protons e (at 4.13 ppm) provided the number average degree of polymerization (n) for the PCL backbone in the diblock structure. The number average molecular weights ( $M_n$ ) were calculated ( $M_n = n \times \text{repeating unit mass}$ ) and showed in table 3.1.

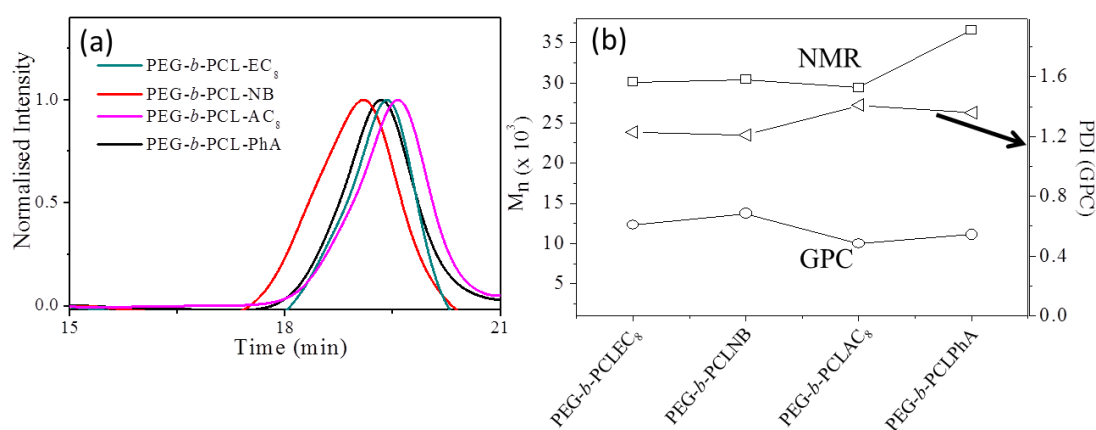


**Figure 3.7.** GPC chromatograms (a) and plot of molecular weights and polydispersity index (b) of diblock copolymers.

Further these diblock copolymers subjected to GPC in order to determine molecular weights and the polydispersity indexes. As seen figure 3.7a the GPC chromatograms of diblock copolymers exhibited monomodal distribution, which confirms the formation of pure and high molecular weights polymers (see table 3.1.). The molecular weights from NMR and GPC and PDI from GPC have been plotted and shown in figure 3.7b. The GPC underestimated the molecular weights over NMR, this might be attributed to the hydrodynamic radius of diblocks in THF. The polydispersity ( $M_w/M_n$ ) of the diblocks was obtained as 1.3 to 1.4 indicating the formation of narrow molecular weight polymers irrespective of the nature of the substitution in the  $\epsilon$ -caprolactone monomers.

### 3.3.2. Self-assembly of Amphiphilic Di-blocks

The newly designed substituted PEG-*b*-PCL<sub>X</sub> amphiphilic diblock copolymers have hydrophilic PEG and hydrophobic substituted PCL segments to self-assemble in water. The diblock copolymer (10.0 mg) was dissolved in DMSO and water mixture (2+8 mL) and

transferred to semi-permeable dialysis bag having MWCO=1000. The samples were dialyzed against a large amount of water for 48 h (fresh water was replenished at regular interval). At the end of the dialysis, clear polymer solutions were obtained.

**Table 3.1.** Molecular weights (NMR and GPC) of substituted diblock copolymers

Polymer	n (NMR)	$M_n$ (g/mol, NMR)	$M_n$ (g/mol, GPC)	$M_w$ (g/mol, GPC)	$M_w/M_n$ (GPC)
PEG- <i>b</i> -PCLEC <sub>8</sub>	96	30,100	12,300	15,100	1.23
PEG- <i>b</i> -PCLNB	98	30,400	13,700	16,600	1.21
PEG- <i>b</i> -PCLAC <sub>8</sub>	94	29,400	10,000	14,100	1.41
PEG- <i>b</i> -PCLPhA	101	36,600	11,100	15,100	1.36

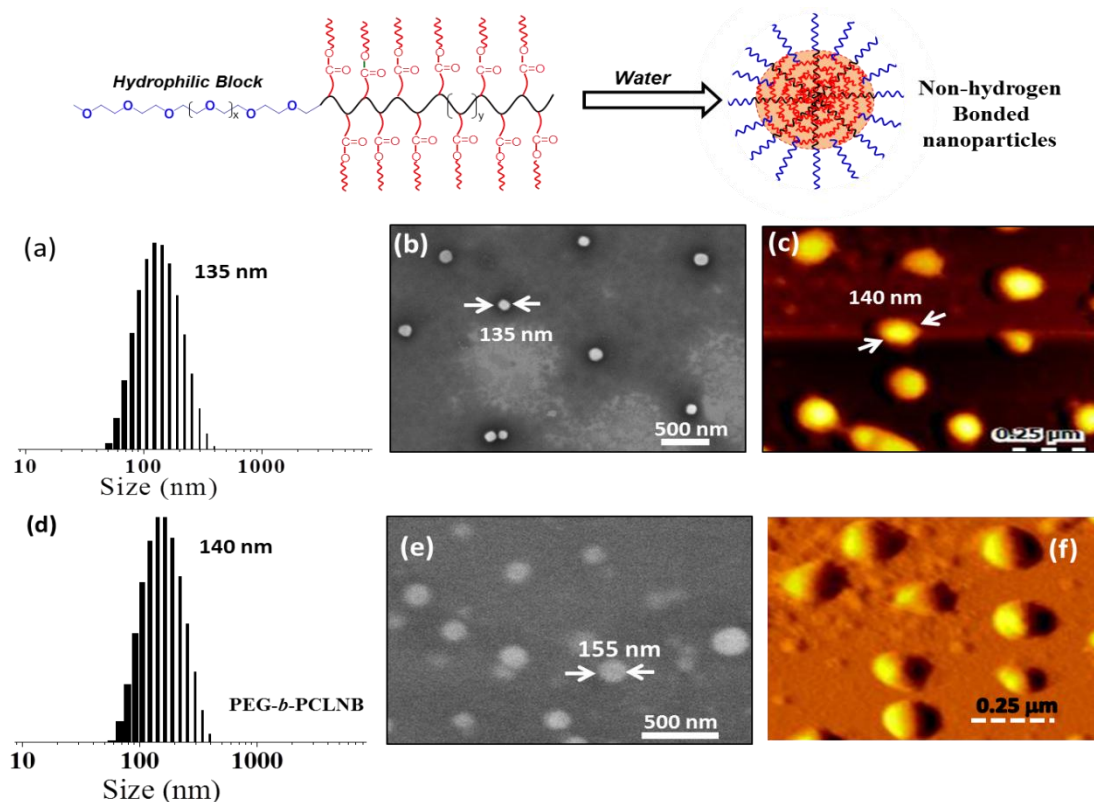


**Figure 3.8.** DLS histogram (a), FE-SEM image (b) and AFM image (c) of diblock copolymer PEG-*b*-PCLEC<sub>8</sub>. DLS histogram (d), FE-SEM image (e) and AFM image (f) of diblock copolymer PEG-*b*-PCLNB at concentration of 0.2 mg/mL.

The characterisation of these self-assembled of dialyzed solution was carried out using dynamic light scattering (DLS) and microscopic techniques depicted in figure 3.8. The

DLS histogram for PEG-*b*-PCLEC8 is shown in Figure 3.8a, exhibited mono-modal distribution with respect to the formation of 135 homogeneous polymer aggregates. Further to visualize the shape of the aggregates; the samples were subjected to field emission scanning electron microscopy (FESEM) and atomic force microscope (AFM). Further FESEM and AFM images of PEG-*b*-PCLAC<sub>8</sub> diblock aggregate are shown in figure 3.8b and c. The FESEM image exhibited the formation of spherical nanoparticles of 135 nm in size. AFM image in figure 3.8c further confirmed the formation of spherical micellar aggregates. The DLS histogram for PEG-*b*-PCLNB is shown in Figure 3.8d, exhibited mono-modal distribution with respect to the formation of 140 nm homogeneous polymer aggregates. FESEM and AFM images of PEG-*b*-PCLEC<sub>8</sub> diblock aggregate are shown in figure 3.8e and f. The FESEM image exhibited the formation of spherical nanoparticles of 155 nm in size. AFM image in figure 3.8f further confirmed the formation of spherical micellar aggregates. The nanoparticle size in FESEM and AFM images are in coherence with the sizes of their self-assembled aggregates (DLS data) in water.

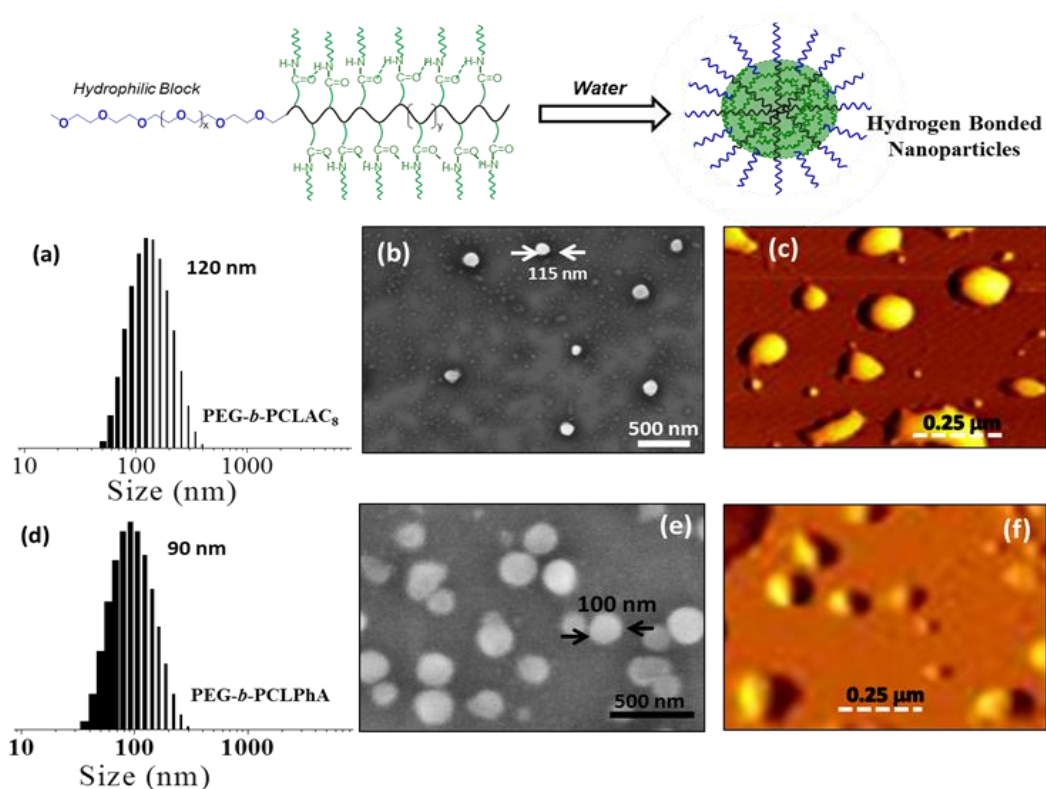


**Figure 3.9.** DLS histogram (a), FE-SEM image (b) and AFM image (c) of diblock copolymer PEG-*b*-PCLAC<sub>8</sub>. DLS histogram (d), FE-SEM image (e) and AFM image (f) of diblock copolymer PEG-*b*-PCLPhA at concentration of 0.2 mg/mL.

Similar techniques and protocols were used to characterise other two amide diblock copolymers (PEG-*b*-PCLAC<sub>8</sub> and PEG-*b*-PCLPhA). DLS histograms, FESEM and AFM



images of these diblock copolymers are provided in figure 3.9. These techniques confirm the formation of 120 and 100 nm size nanoparticles for PEG-*b*-PCLAC<sub>8</sub> and PEG-*b*-PCLPhA diblocks respectively. Overall the sizes of aggregates were obtained in the range of 90 to 160 nm for all four block copolymers. Based on the above analysis, it can be concluded that the newly designed substituted PCL block copolymers have good amphiphilic properties to self-assemble as stable nanoparticles in water.

### 3.3.3. Variable temperature <sup>1</sup>H-NMR analysis

Variable temperature <sup>1</sup>H-NMR analysis was employed to study the hydrogen bonding interactions between the -NH (donor) and -C=O (acceptor) in the amide diblock polymer scaffold. This experiment was performed for the PEG-*b*-PCLAC<sub>8</sub> diblock copolymer in DMSO-*d*<sub>6</sub> (see figures 3.10a and 3.10b). <sup>1</sup>H-NMR, spectra were recorded in the heating cycle from 25 to 75 °C (see figure 3.10a). The chemical shift of the amide peak (NH-CO) plotted against the temperature and shown in figure 3.10c. The N-H protons shifted from 7.76 ppm to 7.48 ppm with respect to the breakage of hydrogen bonding in the heating cycle. In the cooling cycle, the N-H protons shifted towards downfield region as hydrogen bonding was favoured at the low temperatures via inter-chain interactions. The plots in figure 3.10c confirmed the complete reversibility of the hydrogen bonding interactions in the amide diblock copolymers.

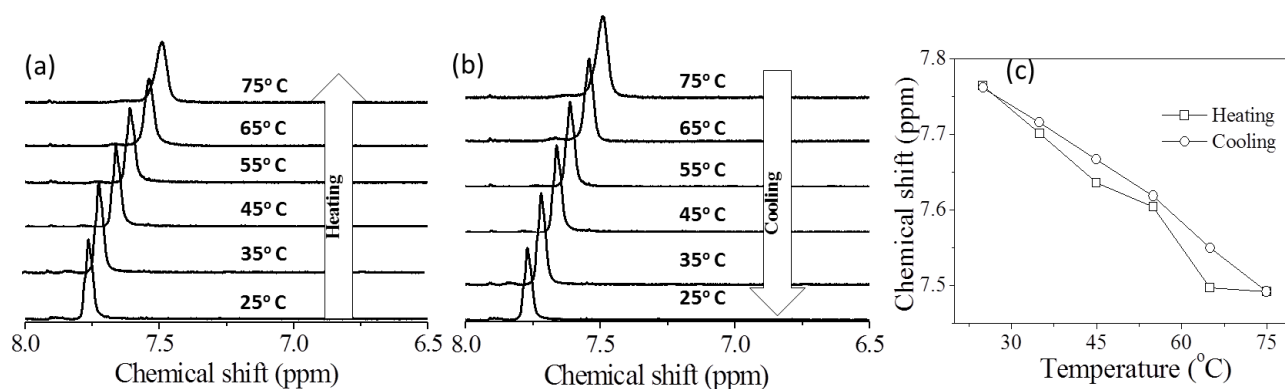


**Figure 3.10.** Variable temperature <sup>1</sup>H-NMR of PEG-*b*-PCLAC<sub>8</sub> in DMSO-*d*<sub>6</sub> at heating (a) and cooling (b) cycles. The plot of the chemical shift of N-H bond Vs. temperature (c).

### 3.3.4. DOX Encapsulation in Diblocks

To study the loading capabilities of the diblock amphiphilic nanoparticles; they were subjected to doxorubicin (DOX) encapsulation in water. For this purpose, the block copolymer (10 mg) and DOX (0.5 mg) were taken in DMSO + water mixture (2 mL + 8 mL) in a dialysis bag and dialyzed for more than 48 h in water. The unencapsulated drug was removed from the reservoir and continuously replenished with fresh water. The photograph of the vials containing the DOX-loaded diblock copolymers is shown in figure 3.11 a. The drug loading content (DLC) in the DOX-loaded diblock nanoparticles were determined by absorbance spectroscopy. The DLC was plotted against the respective substituent in PCL blocks and they are shown in figure 3.11b.

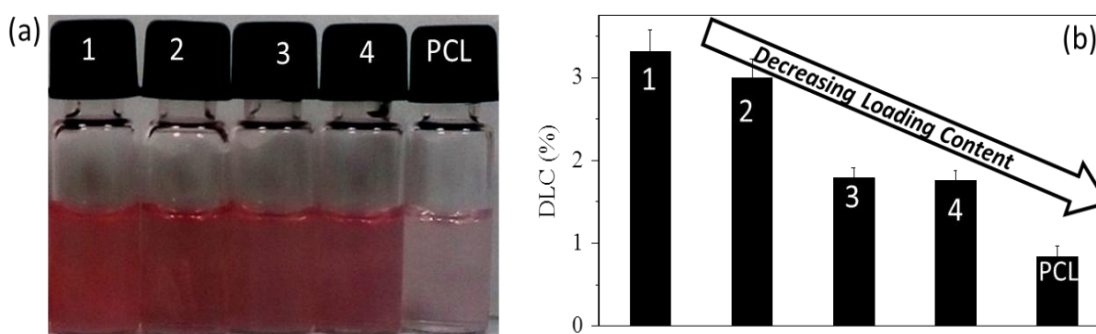


**Figure 3.11.** Photographs of the vials containing the diblock copolymers encapsulated with DOX (a). Drug loading content of the diblock copolymer nanoparticles determined by UV-Vis absorbance spectroscopy (b).

The DLC of the amphiphilic diblock copolymers decreased in the following order in PEG-*b*-PCL<sub>X</sub> where X = EC<sub>8</sub> > AC<sub>8</sub> > NB > PhA >> without substitution with the respective DLC values of 3.3 % > 3.1 % > 1.9 % > 1.8 % >> 0.9 %. This trend suggests that the octyl substituted (both with ester and amide linker) PCL segments are good candidates in the amphiphilic diblocks for maximum encapsulation of anticancer drugs. The amphiphilic unsubstituted PEG-*b*-PCL block showed low DLC indicating that the substitution in the PCL block is essential for the enhanced DOX-encapsulation capabilities. Both octyl amide and octyl ester substitution showed almost similar DLC whereas the bulkier substitutions such as norbornane and phenylalanine relatively reduced their DLC.

DOX-loaded diblock nanoparticles characterization was carried out as similar as of nascent polymers. The DLS histogram of DOX-loaded diblock (octyl ester) is shown in figures 3.12 a. which shows the similar size as nascent diblock copolymer. FESEM image of the DOX-loaded PEG-*b*-PCLEC<sub>8</sub> sample showed spherical morphology (See figures 3.12b).

AFM image of DOX-loaded PEG-*b*-PCLAC<sub>8</sub> (see in figure 3.12c) confirmed the spherical nanoparticles morphology.

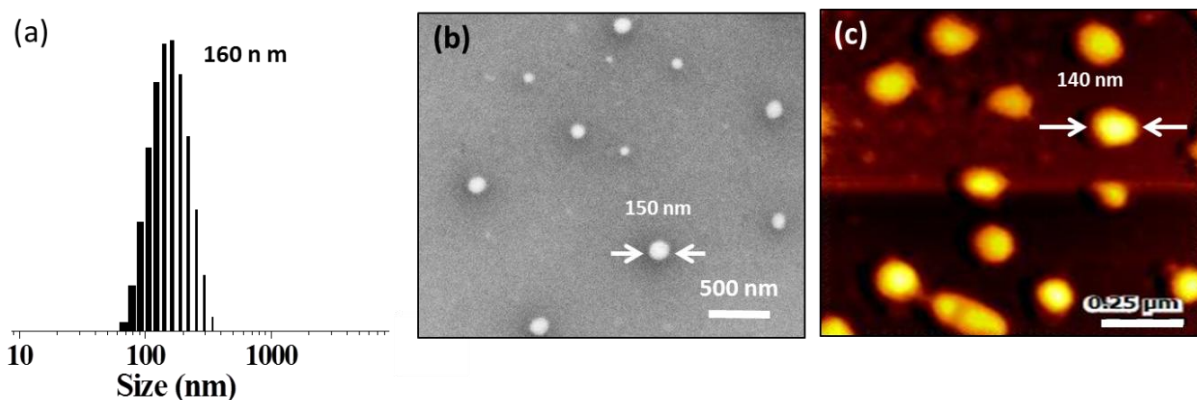


**Figure 3.12.** DLS histogram (a), FE-SEM (e) and AFM (f) images of the DOX-loaded PEG-*b*-PCLEC<sub>8</sub>.

DLS histograms and FESEM images of other DOX loaded diblock nanoparticle are represented in figure 3.13. The sizes of the nanoparticles ranging from 130 to 140 nm, which has slight increase in the sizes compare to the nascent polymer aggregates. These results suggested that the nanoparticles were stable with DOX encapsulation in water without changing their size and geometry in the self-assembly.

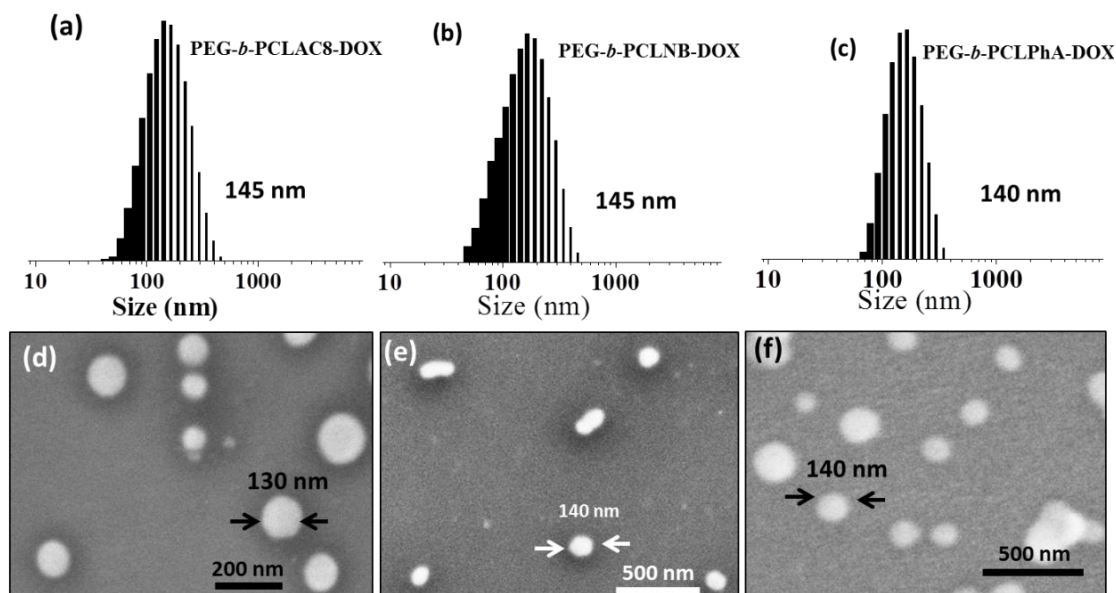


**Figure 3.13.** DLS histograms of PEG-*b*-PCLAC<sub>8</sub>-DOX (a), PEG-*b*-PCLNB-DOX (b) and PEG-*b*-PCLPhA-DOX(c). FESEM images of PEG-*b*-PCLAC<sub>8</sub>-DOX (d), PEG-*b*-PCLNB-DOX(e) and PEG-*b*-PCLPhA-DOX(f).

### 3.3.5. In Vitro DOX Release Studies

*In vitro* drug release studies of DOX-loaded polymeric nanoparticles were carried out in PBS (pH = 7.4 at 37 °C) and in the presence of esterase enzyme (in PBS at 37 °C) to investigate the effect of the hydrogen-bond interaction on the drug releasing capabilities. For this purpose, the DOX-loaded nanoparticles were taken in dialysis bag (MWCO = 1000) and incubated at 37 °C in PBS. The amount of DOX released was quantified by absorbance spectroscopy. The cumulative DOX release from the hydrogen bonded (amide block) and non-hydrogen bonded (ester block) nanoparticles were plotted and shown in figures 3.14a and 3.14b. All these nanoparticles were found to be stable in PBS and only small amount of drug was leached (< 15 %) at 37 °C under normal circular conditions. This indicates that the diblock nanoparticles exhibited very good stability in PBS irrespective of the difference in the types of the amide and ester substitution in the PCL backbone. The drug release profiles of DOX-loaded nanoparticles treated with 10 units of esterase enzyme in PBS at 37 °C are shown in figures 3.14a and 3.14b. This *in vitro* experiment resembles the cleavage of the drug loaded nanoparticles at the intracellular level by lysosomal enzymes (see Figure 3.1).

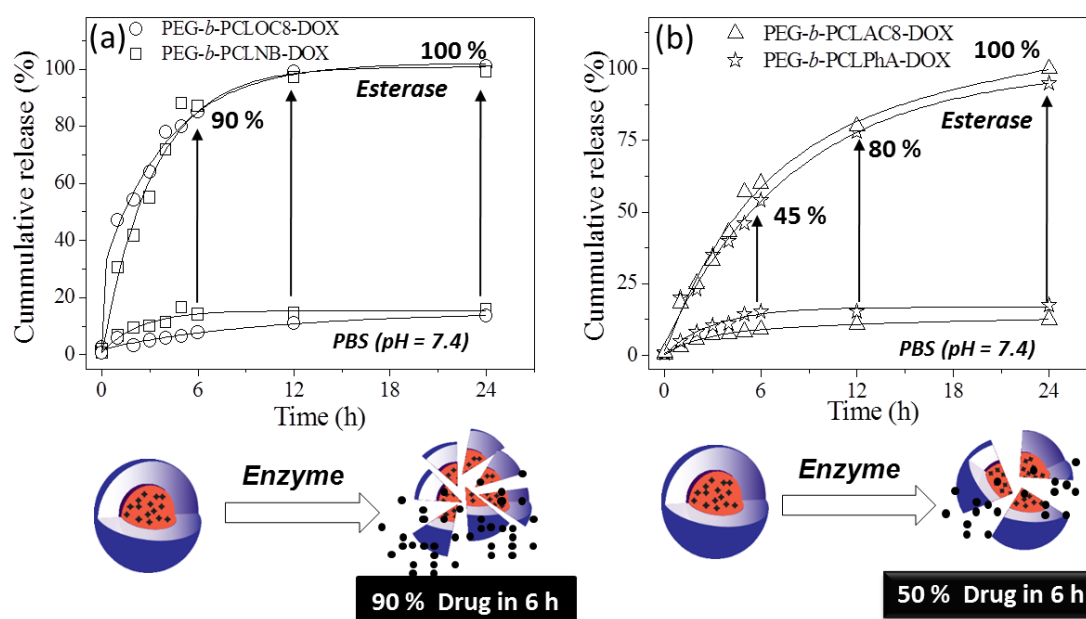


**Figure 3.14.** Cumulative drug release profiles of DOX-loaded non-hydrogen bonded (a) and hydrogen bonded (b) nanoparticles in PBS with and without esterase at 37 °C.

The PCL backbone is constituted by aliphatic ester linkages; thus, the attack of esterase enzyme abundant in the lysosomes is expected to rupture the nanoparticles to release the loaded cargoes at the intracellular compartments. Interestingly, the non-hydrogen bonded nanoparticles (octyloxy and nabornylmethyleneoxy) were found to exhibit much faster drug release compared to that of the hydrogen bonded (octylamide and phenylalanine amide) blocks. For example, the comparison of PEG-*b*-PCLEC<sub>8</sub> and PEG-*b*-PCLAC<sub>8</sub> drug release profiles at 6 h data (see figures 3.14a and 3.14b) clearly revealed that the non-hydrogen bonded ester block released ~ 90 % of drug whereas the latter showed only < 45 % release. It is important to mention that both these diblocks have almost identical DLC (see figure 3.11b); however, they largely vary by the drug release mechanism. The slow cleavage of the amide diblocks was attributed to the strong hydrogen bonding interactions among the amide linkage in the PCL backbone at the hydrophobic pocket that renders slow enzymatic cleavage

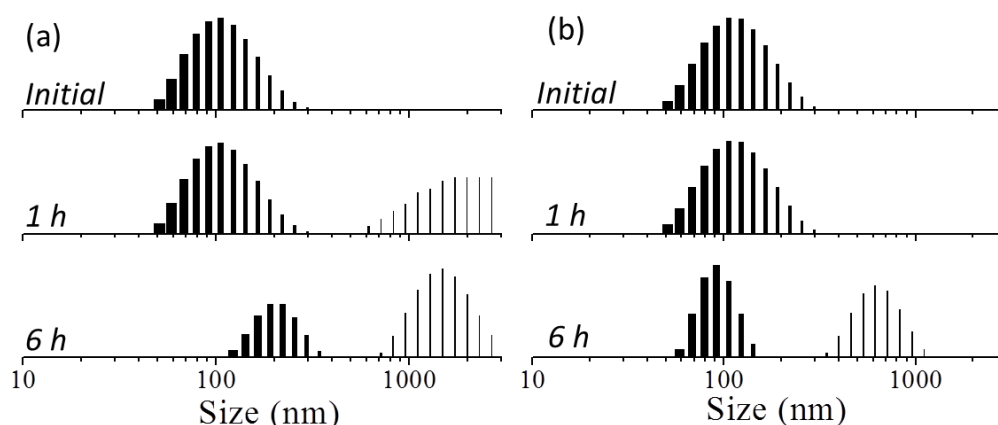


**Figure 3.15.** Time-dependent DLS histograms of PEG-*b*-PCLEC<sub>8</sub> (a) and PEG-*b*-PCLAC<sub>8</sub> (b) in the presence of 10 U esterase enzyme in PBS at 37 °C.

To support this claim, time-dependent DLS experiments were carried out in the presence of esterase enzyme (see figures 3.15a and 3.15b). DLS histograms of non-hydrogen bonded ester diblock PEG-*b*-PCLEC<sub>8</sub> (see figure 3.15a) signify the transformation of mono to multi-modal distributions within 1h of esterase enzyme addition. The formation of higher size aggregates is attributed to the cleavage of the tightly self-assembled nanoparticles into disassembled polymer chains. On the other hand, the amide diblock PEG-*b*-PCLAC<sub>8</sub> did not show a much abrupt change in the size of the aggregates initially and large size aggregates seem to be occurring only after 6h (see figure 3.15b). This clearly suggests that both the ester and amide diblock

nanoparticles are susceptible to enzymatic cleavage; however, the enzyme action on the PCL backbone at the hydrophobic chain was found to be slow down by hydrogen bonded amide linkages. A similar trend was observed in other diblocks i.e., the norbornyl diblock exhibited much faster enzymatic cleavage compared to phenylalanine amide diblock. Based on the *in vitro* drug release studies; it may be concluded that the amide side chain substitution in the PCL diblock enhances the stability of the loaded drugs and releases the drugs in a much more “controlled” manner compared to that of the ester diblocks which exhibited “burst” release

### 3.3.6. Cytotoxicity of DOX-loaded Nanoparticles

The cytotoxicity of the nascent and DOX-loaded diblock copolymer nanoparticles was investigated in cervical cancer (HeLa) and breast cancer (MCF 7) cell lines. The cytotoxicity of the diblock copolymers was studied in both cell lines by varying their concentration up to 40  $\mu\text{g/mL}$  (see figure 3.16a and 3.16b).

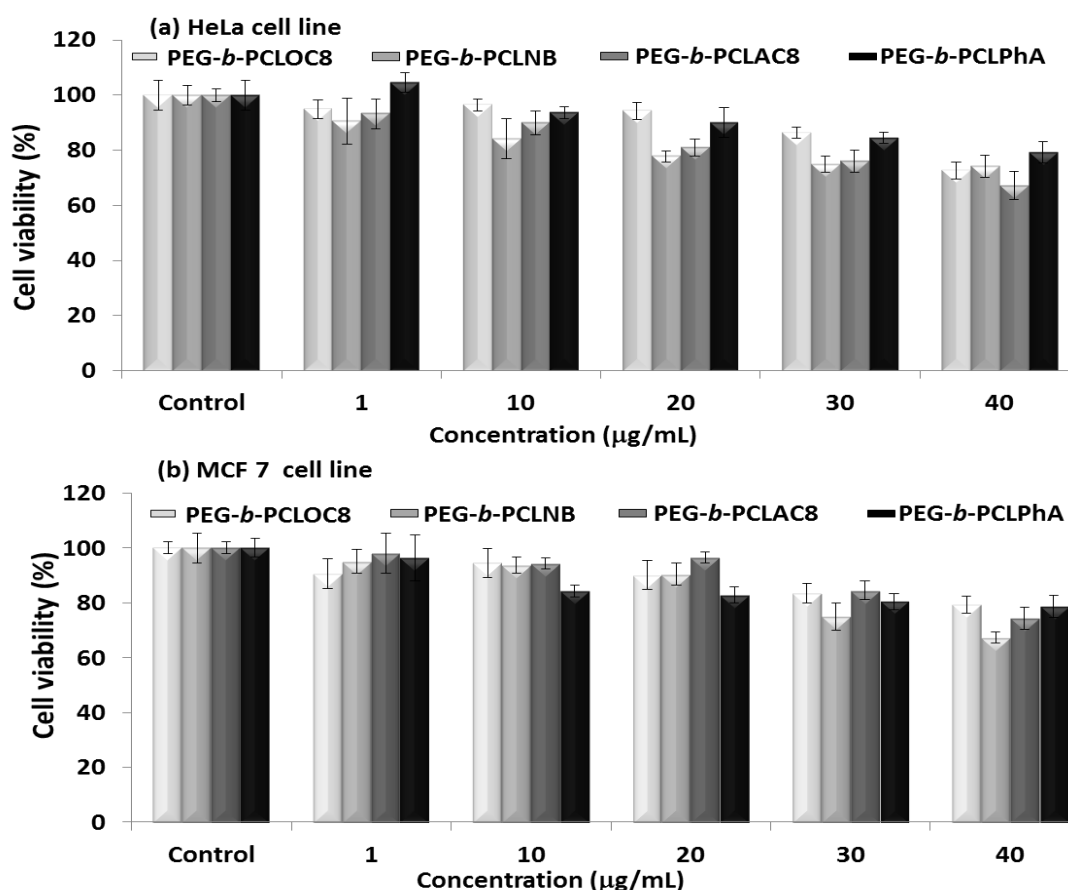


**Figure 3.16.** Histograms depicting the cytotoxicity of nascent diblock nanoparticles in HeLa (a) and in MCF 7(b) cell lines at various concentrations. The cytotoxicity histograms of DOX-loaded diblock nanoparticles in HeLa (c) and MCF 7(d) cell lines at various concentrations.

All the diblock copolymers were found to be non-toxic to cells irrespective of their structural variation in the PCL block up to 40 $\mu\text{g/mL}$  in both HeLa and MCF 7 cell line.

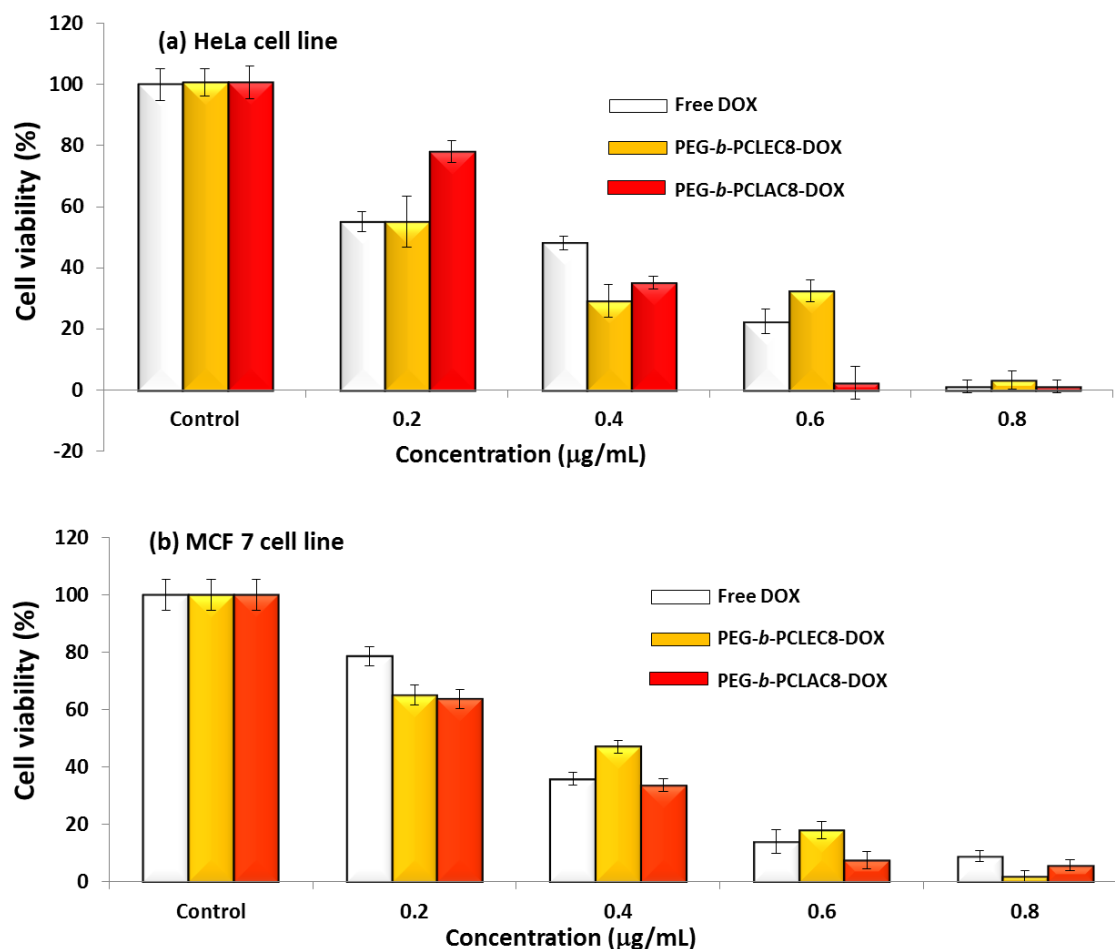


**Figure 3.17.** Histograms depicting the cytotoxicity of DOX-loaded diblock nanoparticles in HeLa (a) and MCF 7(b) cell lines at various concentrations.

DOX and DOX-loaded diblocks were fed to HeLa and MCF 7 cells with various concentrations in order to scrutinize their cytotoxicity. The concentration of DOX varied from 0.2  $\mu\text{g/mL}$  to 0.8  $\mu\text{g/mL}$  in both cells and the resulted histograms were depicted in figure 3.17a (HeLa) and in figure 3.17b (MCF 7) for PEG-*b*-PCLEC<sub>8</sub> and PEG-*b*-PCLAC<sub>8</sub> diblock copolymers. In HeLa, both free DOX and drug loaded polymer scaffolds showed IC<sub>50</sub> at 0.5 $\mu\text{g/mL}$  concentrations which are in accordance with earlier studies.<sup>35</sup> At a higher drug concentration (> 0.8  $\mu\text{g/mL}$ ), the DOX-loaded diblock copolymer scaffolds were found to be killing more than 95 % of the cells. In MCF 7, both free DOX and drug loaded polymer scaffolds showed IC<sub>50</sub> at 0.4  $\mu\text{g/mL}$



concentrations which are in agreement with earlier reports.<sup>36</sup> At a higher drug concentration ( $> 0.8 \mu\text{g/mL}$ ), the DOX-loaded diblock copolymer scaffolds were found to be killing more than 90 % of the cells.

These results explain that the DOX-loaded amide and ester diblocks showed excellent cell killing in both HeLa and MCF 7 cell lines. The *in vitro* drug release profiles in figure 3.14 clearly demonstrated that the non-hydrogen bonded ester diblocks showed “burst” release compared to “controlled” drug release profiles of hydrogen bonded amide blocks. This implies that at the initial stage of the drug administration, the non-hydrogen bonded ester diblock nanoparticles would rupture at much faster rate to release the drugs to accomplish faster cell death. In order to study the effect of the hydrogen bonding driven drug releasing pattern in the cell killing; two different *in vitro* experiments were designed in HeLa cell lines. In the first experiment, time-dependent *in vitro* cytotoxicity assay was done for free DOX and DOX-loaded nanoparticles at various incubation time of 6h, 12h, 24h, 48h and 72 h. Based on the cytotoxicity data in figure 3.17, the DOX concentration of  $0.8 \mu\text{g/mL}$  was chosen for this experiment. The histograms of cytotoxicity for free DOX and DOX-loaded amide and ester block nanoparticles are shown in figure 3.18.

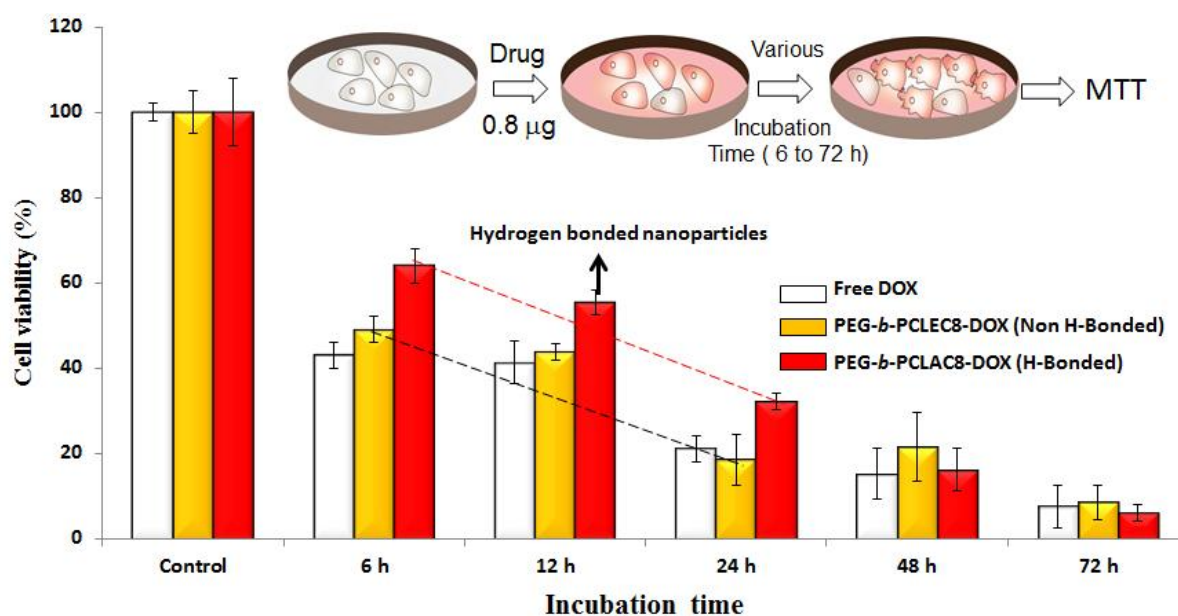


**Figure 3.18.** Cytotoxicity of DOX-loaded diblock nanoparticles at various time intervals in HeLa cells at  $0.8 \mu\text{g/mL}$ . The experiment is schematically shown in petri-dish model.



This data revealed that the non-hydrogen bonded DOX-loaded nanoparticles showed similar cell killing as free drug from 6 to 72 h incubation (see figure 3.18). This suggested that the DOX could be easily released by the esterase enzyme (as evident from figure 3.12a) from non-hydrogen bonded nanoparticles for faster cell killing as similar to that of free drug. On the other hand, the DOX-loaded hydrogen bonded nanoparticles showed relatively slow killing (20% less cytotoxicity) for the incubation of 6 to 24 hrs. At longer incubation time (48 and 72 h), complete cell death was accomplished by the amide ester blocks; however, the rate at which they kill the cancer cells significantly vary with respect to their chemical structures. The comparison of the *in vitro* drug release profiles in figure 3.14 and the cytotoxicity data in 3.18 suggested that the slow enzymatic cleavage and drug release from hydrogen bonded nanoparticles from 6 h to 24 h (see figure 3.14b) directly reflected on the rate of their cell killing.

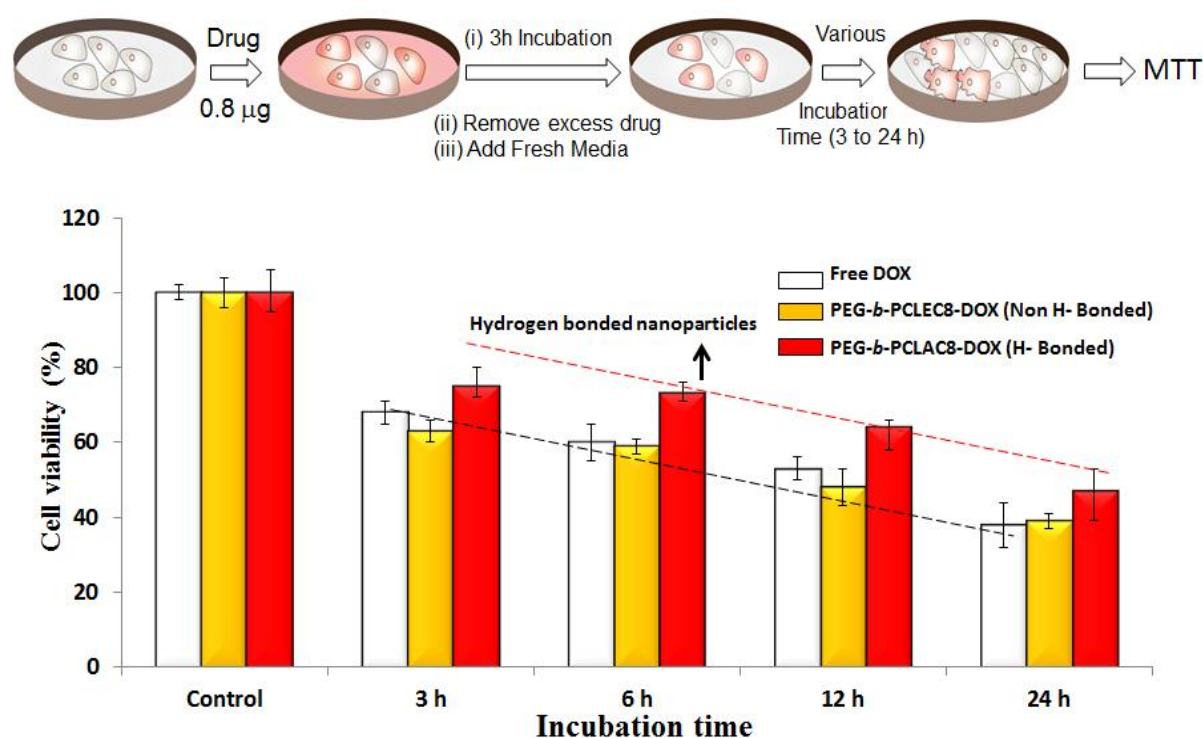


**Figure 3.19.** *In vivo* mimicking assay of DOX-loaded diblock nanoparticles at various time intervals in HeLa cells at 0.8 μg/mL. The experiment is schematically shown in petri-dish model.

To further confirm this process, a second control cell experiment was carried out in which the DOX-loaded nanoparticles (also free DOX) were administered initially for 3h. Subsequently, the excess drug was removed and fresh media was added. These cells were incubated for various time 3, 6, 12 and 24 h and then MTT was performed to determine their cytotoxicity (see figure 3.19). In this process, the drugs that were initially taken up by the cells actually inhibit the subsequent cell proliferation and mimic the *in vivo* type cell killing under *in vitro* conditions. Similar experiments were recently reported by Peer and co-workers in glycosaminoglycan particle nanoclusters.<sup>37-38</sup> For this experiment, the DOX concentration was chosen as 0.8  $\mu\text{g}/\text{mL}$  and their cytotoxicity data are summarized in figure 3.19. At 3h incubation, the cytotoxicity data were found to be similar in free as well as drug loaded nanoparticles (3h is not sufficient). For 6 h to 24 h incubation, the hydrogen bonded nanoparticles exhibited slower cell killing compared to the non-hydrogen bonded ester diblocks (see figure 3.19). The trend in the *in vivo* mimicking cell data were identical to that of the *in vitro* data in figure 3.18 suggesting that the hydrogen bonded nanoparticles are less susceptible to esterase enzyme cleavage at the intracellular compartments. Hence, it can be concluded that the nanoparticles based on amide diblocks are very useful for controlled release of drugs and the non-hydrogen bonded nanoparticles are good for faster drug release. Thus, these amide and ester block nanoparticles can be employed depending upon the need to deliver the drugs in controlled or burst manner for cancer treatment.

### 3.3.7. Confocal Imaging and Cellular Uptake

To track down the fate of the free DOX and DOX-loaded nanoparticles in the cytoplasm, their cellular uptake was scrutinized using confocal laser scanning microscopy (CLSM) in HeLa and MCF 7 cell lines. DOX-loaded nanoparticles and DAPI stained nuclei were visualized under CLSM at red ( $\lambda= 560$  nm) and blue ( $\lambda= 461$  nm) channels, respectively. The images corresponding to PEG-*b*-PCLEC<sub>8</sub>-DOX, PEG-*b*-PCLAC<sub>8</sub>-DOX and DAPI stained nuclei in HeLa cells along with the merged images are shown in figure 3.20. In HeLa cells, (see figure 3.20 first panel), strong red fluorescence was observed predominantly at the nucleus for DOX-loaded non-hydrogen bonded block nanoparticles (ester block).

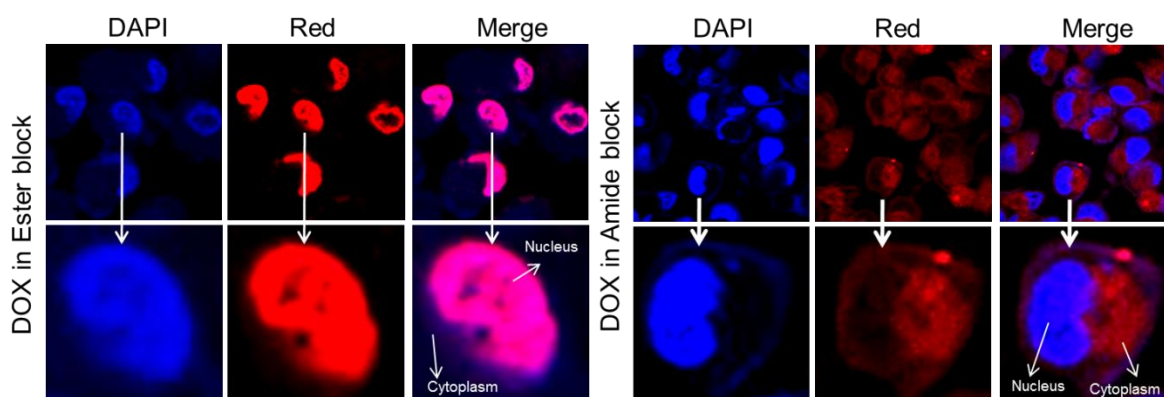


**Figure 3.20.** CLSM images of HeLa cells incubated with ester block ( $PEG-b-PCLEC_8-DOX$ ) and amide block ( $PEG-b-PCLAC_8-DOX$ ) nanoparticles. The nucleus was counterstained with DAPI (blue). The cells were observed through the red channel to locate DOX fluorescence (red).

The expanded cell images (see the second-row panel) distinctly showed magenta color with respect to the accumulation of DOX at the nucleus (dapi stained) and only trace amount of free drugs visible in the cytoplasm. On the other hand, the hydrogen bonded amide block copolymer nanoparticles predominately showed the DOX accumulation in the cytoplasm rather than at nuclei (see figure 3.20, last two row panels). In this case, the nuclei were visible as blue rather than magenta color as an indication of lack of DOX accumulation at the nucleus. This trend was attributed to the slow cleavage of the hydrogen bonded nanoparticles in the cytoplasm and the reduction in the drug accumulation at the nucleus. In the case of non-hydrogen bonded ester block nanoparticles, the fast degradation of the polymer chains by an enzyme in the cytoplasm induced burst release of DOX and this, in turn, enhances the DOX accumulation at the nuclei.

The cellular uptake images of DOX-loaded diblock copolymer nanoparticles in MCF 7 cell are shown in figure 3.21. The hydrogen bonded amide diblock nanoparticles exhibited the drug accumulation in the cytoplasm rather than at nucleus. This trend was again attributed to the slow cleavage of the amide hydrogen bonded blocks in the MCF 7 cells compared to that of the ester diblock copolymers. The DOX accumulation in the cytoplasm while released from hydrogen bonded nanoparticles and nuclear site while delivered from non-hydrogen bonded diblock copolymer nanoparticles seems to be identical for both cervical and breast cancer cells lines.

Despite significant difference among the features in these two cells lines; the control and burst release trends of the nanoparticles reflected on the degree of cell killing.

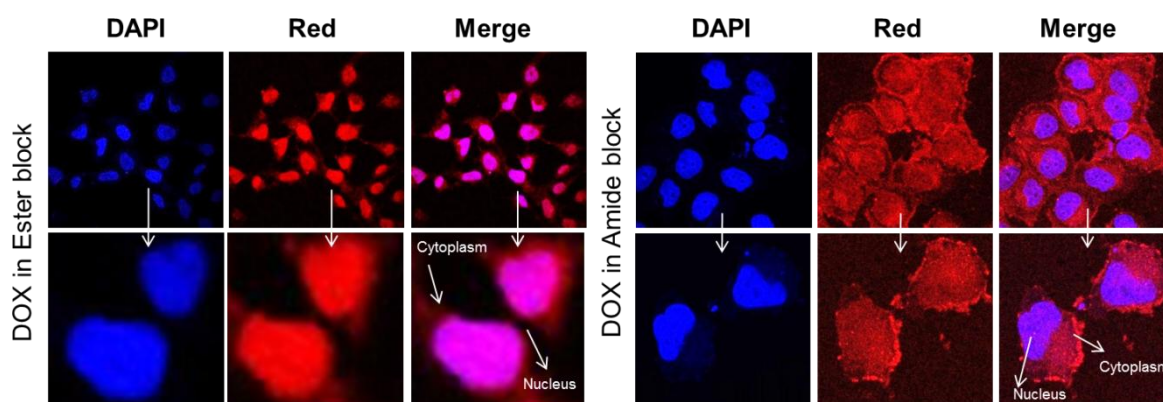


**Figure 3.21.** CLSM images of MCF 7 cells incubated with ester block ( $PEG\text{-}b\text{-}PCLEC_8\text{-}DOX$ ) and amide block ( $PEG\text{-}b\text{-}PCLAC_8\text{-}DOX$ ) nanoparticles. The nucleus was counterstained with DAPI (blue). The cells were observed through the red channel to locate DOX fluorescence (red).

Hence, it can be concluded that the hydrogen bonding interaction predominately regulates the enzymatic cleavage at the intracellular compartments for control DOX release from the block copolymer nanoparticle scaffolds. This concept was very well proven in the present investigation by carefully designing the biodegradable diblock copolymers, studying their enzymatic *in vitro* drug release kinetics, carrying out appropriate *in vitro* and *in vivo* mimicking cytotoxicity assays and tracing the DOX accumulation in the cytoplasm and nuclear environment by confocal microscopy. This present investigation established the proof-of-concept and provides more insight into the role of the hydrogen-bond controlled drug release in cancer therapy.

### 3.4. Conclusion

In summary, a new class of hydrogen bonded and enzyme-responsive (biodegradable) PCL diblock copolymer nanoparticles were designed and developed for loading and delivering anticancer drugs by “burst” and “controlled” release at the intracellular compartments in cervical (HeLa) and breast (MCF 7) cancer cells. Commercially available 1,4-cyclohexanol was employed as starting materials and new amide and ester substituted  $\omega$ -caprolactone monomers were tailor-made through multi-step synthesis. These monomers

were polymerized using PEG 2000 mono methyl ether as an initiator to make amide hydrogen bonded and non-hydrogen bonded (ester) PEG-*b*-PCL diblock copolymers. These new polymers were self-assembled in water as nanoparticles in which DOX was successfully loaded. The drug loading content of the diblock copolymer nanoparticles was found to be highly directed by the nature of the linear or bulky substituent. The hydrogen bonding interaction in the amide diblock was investigated in detail by variable temperature <sup>1</sup>H-NMR analysis. *In vitro* drug release studies revealed that the aliphatic polyester PCL chain was readily degradable by lysosomal esterase enzyme in PBS at 37 °C to release the loaded drugs. The hydrogen bonded copolymer nanoparticles were found to be very stable and underwent slow enzymatic degradation to release drugs in a controlled manner for prolonged period. The non-hydrogen bonded ester copolymers experienced burst release of drugs in un-controlled manner. This difference in the enzymatic degradation among the amide diblock copolymers (hydrogen bonded) and ester diblocks (non-hydrogen bonded) was tested for their cell killing ability in HeLa and MCF 7 cell lines. *In vitro* cytotoxicity tests revealed that the nascent polymer scaffolds were non-toxic to cells up to 40µg/mL. The DOX loaded nanoparticles accomplished more than 90 % cell killing in both HeLa and MCF 7 cells. Time-dependent *in vitro* cell studies further evident that the DOX loaded amide diblocks exhibited slower killing (20 % less) compared to the non-hydrogen bonded ester blocks. Both *in vitro* drug release profiles and *in vitro* cell line studies directly proved that the hydrogen-bond controlled drug delivery in the diblock copolymer design. The hydrogen bonding interaction was proven to be an important tool to control the drug release profiles of the anticancer drugs to cancer cells. The cellular uptake of the DOX loaded polymer nanoparticles and their cleavage in the cytoplasm was further supported by the confocal microscope imaging. The present investigation studied the role of the hydrogen binding interaction in PCL based diblock copolymers; however, this approach is not restricted only to the PCL design and in principle, it may be applicable to wide range of other polymeric nano-scaffolds. The present investigation clearly demonstrated that the introduction of secondary non-covalent forces such as hydrogen bonding interaction is very good tool for programming the drug release profiles from polymer scaffold for cancer therapy.

### 3.5. References

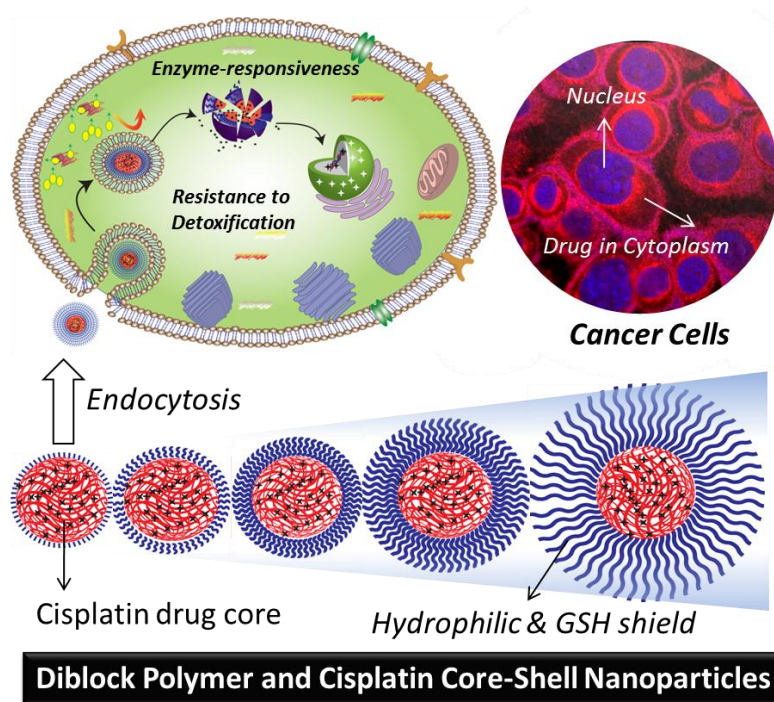
1. Duncan, R. *Nat. Rev. Cancer* **2006**, *6*, 688–701.
2. Haag, R.; Kratz, F. *Angew. Chem., Int. Ed.* **2006**, *45*, 1198-1215.
3. Chang, T. M. S. *Nat. Rev. Drug Discovery* **2005**, *4*, 221-235.
4. Moses, M. A.; Brem, H.; Langer R. *Cancer Cell.* **2003**; *4*, 337–341.
5. Davis, M. E.; Chen, Z.; Shin, M. D. *Nat. Rev. Drug Discovery* **2008**, *7*, 771–782.
6. Xiong, M.; Bao, Y.; Yang, X.; Wang, Y.; Sun, B.; Wang, J. *J. Am. Chem. Soc.* **2012**, *134*, 4355–4362.
7. Ryu, J.; Chacko, R.; Jiwapanich, S.; Bickerton, S.; Prakash Babu, R.; Thayumanavan, S. *J. Am. Chem. Soc.* **2010**, *132*, 17227-17235.
8. Uhrich, K. E. *Chem. Rev.* **1999**, *99*, 3181-3198.
9. Ambade, A. V.; Savariar, E. N.; Thayumanavan, S. *Mol. Pharm.* **2005**, *2*, 264–272.
10. Gao, W.; Chan J. M.; Farokhzad, O. C. *Mol. Pharm.* **2010**, *7*, 1913–1920.
11. Kashyap, S.; Jayakannan, M. *J. Mater. Chem. B*, **2014**, *2*, 4142–4152.
12. Hamner, K. L.; Alexander, C. M.; Coopersmith, K.; Reishofer, D.; Provenza, C.; Maye, M. M. *ACS Nano*, **2013**, *7*, 7011–7020.
13. Pasparakisa, G.; Vamvakaki, M. *Polym. Chem.*, **2011**, *2*, 1234-1248.
14. Place, E.S.; George, J.H.; Williams, C.K.; Stevens, M.M. Synthetic polymer scaffolds for tissue engineering. *Chem. Soc. Rev.* **2009**, *38*, 1139-1151.
15. Harnoy, A. J.; Rosenbaum, I.; Tirosh, E.; Ebenstein, Y.; Shaharabani, R.; Beck R.; Amir, R. *J. Am. Chem. Soc.* **2014**, *136*, 7531–7534.
16. Lee, J.-H.; Chen, K.-J.; Noh, S.-H.; Garcia, M. A.; Wang, H.; Lin, W.-Y.; Jeong, H.; Kong, B. J.; Stout, D. B.; Cheon, J.; Tseng, H.-R. *Angew. Chem., Int. Ed.*, **2013**, *52*, 4384–4388.
17. Shi, Y.; Steenbergen, M.J. V.; Teunissen, E. A.; Novo, L.; Gradmann, S.; Baldus, M.; Nostrum, C. F. V.; Hennink, W. E. *Biomacromolecules* **2013**, *14*, 1826–1837.
18. Klok, H-A.; Lecommandoux, S. *Adv. Mater.* **2001**, *13*, 1217-1229.
19. Wang, X.; Hu, J.; Liu, G.; Tian, J.; Wang, H.; Gong, M.; Liu, S. *J. Am. Chem. Soc.* **2015**, *137*, 15262-15275.
20. Wang, D.; Su, Y.; Jin, C.; Zhu, B.; Pang, Y.; Zhu, L.; Liu, J.; Tu, C.; Yan, D.; Zhu, X. *Biomacromolecules* **2011**, *12*, 1370-1379.
21. Fan, J.; Zeng, F.; Wu, S.; Wang, X. *Biomacromolecules* **2012**, *13*, 4126-4137.

22. Cao, Z.; Liu, W.; Liang, D.; Guo, G.; Zhang, J. *Adv. Funct. Mater.* **2007**, *17*, 246-252.
23. Cheetham, A. G.; Zhang, P.; Lin, Y-A.; Lock, L. L.; Cui, H. *J. Am. Chem. Soc.* **2013**, *135*, 2907-2910.
24. Xu, A-W.; Ma, Y.; Colfen, H. *J. Mater. Chem.* **2007**, *17*, 415-449.
25. Shah, R. N.; Shah, N. A.; Lim, M. M. D. R.; Hseih, C.; Nuber, G.; Stupp, S. I. *PNAS* **2010**, *107*, 3293-3298.
26. Cohen-Erez, I.; Rapaport, H. *Biomacromolecules* **2015**, *16*, 3827-3835.
27. Sisson, A L.; Ekinici, D.; Lenlein, A. *Polymer* **2013**, 4333-4350.
28. Jerome, C.; Lacomte, P. *Adv. Drug Delivery Rev.* 2008, *60*, 1056-1076.
29. Cheng, Y.; Hao, J.; Lee, L. A.; Biewer, M. C.; Wang, Q.; Stefan, M. C. *Biomacromolecules* **2012**, *13*, 2163-2173.
30. Mahmud, A.; Patel, S.; Molavi, O.; Choi, P.; Samuel, J.; Lavasanifar, A. *Biomacromolecules* **2009**, *10*, 471-478.
31. Ramgopal, Y.; Mondal, D.; Venkatraman, S.S.; Godbey, W. T.; Yuen, G. Y. *J BIOMED MATER RES B*, **2009**, *89*, 439-447.
32. Surnar, B.; Jayakannan, M. *Biomacromolecules* **2013**, *14*, 4377-4387.
33. Pramod, P. S.; Takamura, K.; Chaphekar, S.; Balasubramanian, N.; Jayakannan, M. *Biomacromolecules* **2012**, *13*, 3627-3640.
34. Odian, G. *Principles of Polymerization*, 4th ed.; John Wiley and Sons: New York, **2004**, 581-585.
35. Xia, X. X.; Wang, M.; Lin, Y.; Xu, Q.; Kaplan D. L. *Biomacromolecules* **2014**, *15*, 908-914.
36. Pramod, P. S.; Shaw, R.; Jayakannan, M. *Nanoscale* **2015**, *7*, 6636-6652.
37. Kohen, K.; Emmanuel, R.; Kishin-Finfer, E.; Shabath D.; Peer, D. *ACS Nano* **2014**, *8*, 2183-2195.
38. Bachar, G.; Kohen, K.; Hod, R.; Feinmesser, R.; Mizrachi, A.; Shpitzer, T.; Katz, O.; Peer, D. *Biomaterials*, **2011**, *32*, 4840-4848.



# Chapter 4

## *Core-Shell Polymer Nanoparticles for Prevention of GSH Drug Detoxification and Cisplatin Delivery*





---

## ***Core-Shell Polymer Nanoparticles for Prevention of GSH Drug Detoxification and Cisplatin Delivery***

---

*Platinum drug delivery against the detoxification of cytoplasmic thiols is urgently required for achieving efficacy in breast cancer treatment that has over expression of glutathione (GSH, thiol-oligopeptide). GSH resistant polymer-cisplatin core shell nanoparticles were custom designed based on biodegradable carboxylic functional polycaprolactone (PCL)-block- polyethylene glycol diblock copolymers. The core of the nanoparticle was fixed as 100 carboxylic units and shell part was varied using various molecular weight polyethylene glycol monomethyl ethers (MW of PEGs =100 to 5000 g/mol) as initiator in the ring opening polymerization. The complexation of cisplatin aquo species with the diblocks produced core-shell nanoparticles of 75 nm core with precise size control of the particles from 1 to 190 nm. The core-shell nanoparticles were found to be stable in saline and PBS and they exhibited enhanced stability with increase in the PEG shell at the periphery. The hydrophobic PCL layer on the periphery of the cisplatin core has behaved as protecting layer against the cytoplasmic thiol residues (GSH and cysteine) and exhibited < 5 % of drug detoxification. In vitro drug release studies revealed that the core-shell nanoparticles were ruptured upon exposure to lysosomal enzymes like esterase at the intracellular compartments. Cytotoxicity studies were performed both in normal wild type mouse embryonic fibroblasts (Wt-MEFs) cells, breast cancer (MCF 7) and cervical cancer (HeLa) cell lines. Free cisplatin and polymer drug core-shell nanoparticles showed similar cytotoxicity effect in the HeLa cells. In MCF 7 cells, the free cisplatin drug exhibited 50 % cell death whereas complete cell death (100 %) was accomplished by the polymer cisplatin core-shell nanoparticles. Confocal microscopic images confirmed that the core-shell nanoparticles were taken up by the MCF 7 and HeLa cells and they were accumulated both at the cytoplasm as well at peri-nuclear environments. The present investigation lays a new foundation for polymer based core-shell nanoparticles approach to overcome the detoxification in platinum drugs for the treatment of GSH over-expressed breast cancer cells.*

#### 4.1. Introduction

After the serendipitous discovery of cis-diamminedichloridoplatinum(II) (CDDP, Cisplatin) biological properties, cisplatin became one of the most widely employed anticancer drug as the first level chemotherapeutic agent in breast, testicular, ovarian, head and neck and lung cancers.<sup>1-2</sup> This prodigious anti-tumour activity of cisplatin occurred as it becomes activated intracellularly by the aquation of one of the two chloride ‘leaving’ groups, and subsequently forming DNA adducts by covalently binding to N-7 position of the guanine (see figure 4.1).<sup>3-</sup><sup>4</sup> This activates various signal-transduction pathways; for example, those involved in DNA-damage recognition and repair, cell-cycle arrest, and programmed cell death/apoptosis.<sup>5</sup> Unfortunately, the usage of cisplatin is hindered by its labile and non-specific activity, which leads to the side effects such as nausea, vomiting, fatigue, neurotoxicity, ototoxicity and nephrotoxicity.<sup>6</sup>

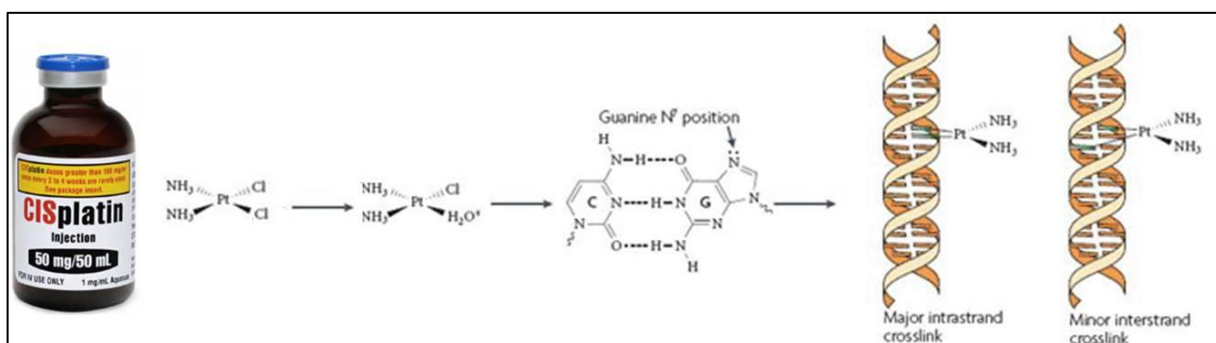


**Figure 4.1.** Cisplatin and its mechanism of action (adapted from Kelland’s *Nat. Rev. Cancer*, 2007, 7, 573-584).

To overcome the patient compliance, several other platinum derivatives such as oxaliplatin, picoplatin, carboplatin and satraplatin were also developed and approved by FDA for clinical trials.<sup>7-8</sup> One of the major obstacles in delivering the platinum drugs to cancer tissues was identified as the detoxification by cytoplasmic thiol species such as glutathione (GSH, an oligopeptide) at the intracellular compartments.<sup>9-14</sup> Recent *in vitro* cell line studies confirmed the over-expression of GSH in the breast cancer cells and their influence on the cisplatin detoxification during the drug administration in cancers.<sup>12-14</sup> Further, platinum drugs are also sensitive to ions (cations/anions) and proteins in blood plasma and they require additional stability for intravenous administration.<sup>15</sup> Polymer based drug delivery approaches are emerging as new trend to overcome the aforementioned limitation in the cisplatin drug administration.

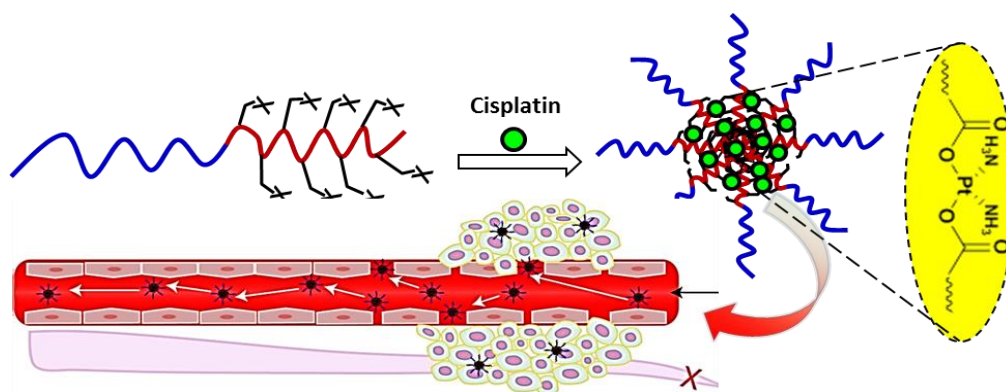


**Figure 4.2.** Schematic representation of polymer based cisplatin conjugated nanoparticles.

The polymer-cisplatin drug conjugates have also additional advantages of the passive selective accumulation at cancer tissues through enhanced permeability and retention (EPR) effect (see figure 4.2).<sup>16</sup> PEGylated cisplatin liposomal formulation, lipoplatin is currently tested for phase II level trials (see figure 4.3).<sup>17</sup> PEGylated block copolymers of poly(isobutylene-maleic acid)<sup>18</sup> and polyacrylates<sup>19-24</sup> are some of the important polymer systems that were explored for cisplatin conjugation. In these cases, the aquo cisplatin complex was conjugated with carboxylic acid functionality in the polymer backbone to preserve the drug in the active form prior to drug delivery.

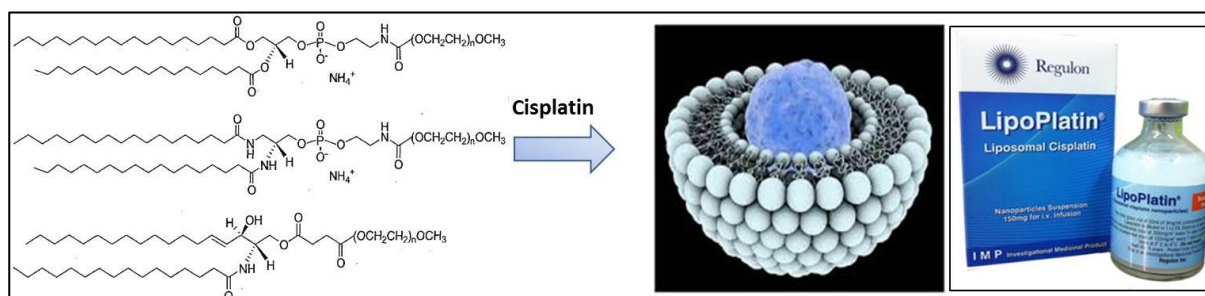


**Figure 4.3.** Schematic representation of lipoplatin formation from phospholipid molecules in water and clinically approved liposomal formulated lipoplatin (adapted from Boulikas and co-workers *J. of Drug Deliv.*doi:10.1155/2012/581363).

Kataoka and co-workers used PEGylated-poly(L-glutamic acid) copolymers for platinum conjugation and the resultant micellar drug conjugates were found to be effective in suppressing the growth of solid tumours (see figure 4.4).<sup>25-27</sup> As shown in figure 4.5 Ding et al. prepared PEG based conjugated polyelectrolyte (CPE) cisplatin nanoparticles (CPE-PEG-Pt) for simultaneous imaging and drug tracking in HepG2 cancer cells.<sup>28</sup>

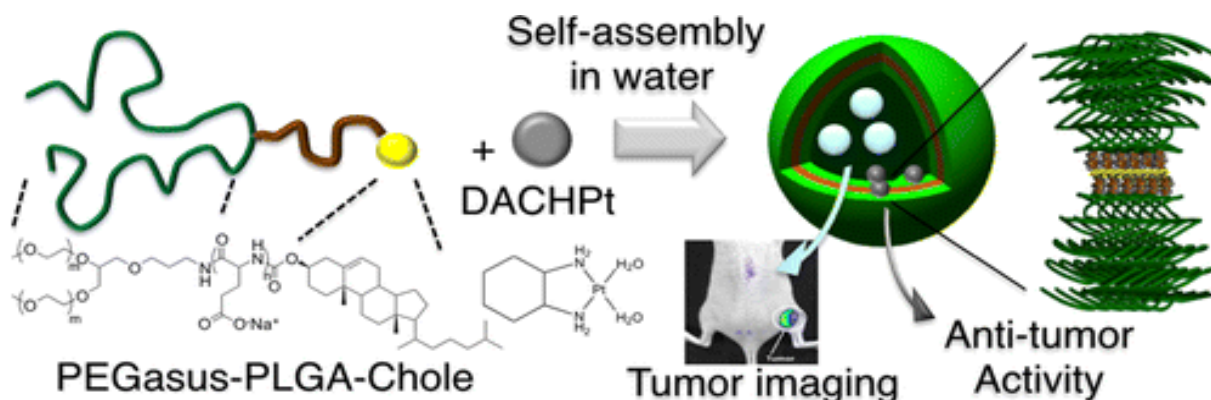


**Figure 4.4.** Schematic representation of formation of metallosomes from PEG-*b*-PLGA block copolymers and anti-tumor effect in mice model (adapted from Kataoka and co-workers. *J. Am. Chem. Soc.* **2012**, 134, 13172-13175).

Shell cross-linked Knedel-like nanoparticles were employed for cisplatin delivery and these nanoparticles were found to exhibit significant antitumor activity.<sup>29</sup> Folic acid-conjugated platinum nanoparticles,<sup>30</sup> PEGylated mesoporous silica nanoparticles,<sup>31</sup> PEGylated PLGA with targeted peptides (see figure 4.5)<sup>32</sup> and graphenes,<sup>33-34</sup> lipids<sup>35-36</sup> and amphiphilic oligomer based micelles,<sup>37</sup> cyclic tripeptides,<sup>38</sup> and gold nanoparticles<sup>39-40</sup> are some of the other approaches developed for cisplatin delivery. Despite the above examples investigated the importance of platinum drug delivery; the stability of the cisplatin drugs in the polymer scaffolds against the detoxification by cytoplasmic thiol species such as GSH was not addressed. Further, most of the above polymer scaffolds are non-biodegradable; thus, the polymer-drug cleavage mechanism at the intracellular compartments is not clearly understood. Hence, new efforts are required to develop polymer-cisplatin conjugates that are resistant to detoxification against cytoplasmic thiols (like GSH) to accomplish efficient treatment against breast cancers that are found to be overexpressed with GSH.

Enzyme cleavable polymer scaffolds are emerging as important approach for drug administration exclusively at intracellular compartments.<sup>41</sup> We and other research groups had earlier reported polysaccharide vesicles,<sup>42-44</sup> amphiphilic dendrons<sup>45-46</sup> and block copolymer assemblies<sup>47</sup> having enzyme-responsiveness for delivering anticancer drug molecules such as doxorubicin and camptothecin. Polycaprolactone (PCL) is important biodegradable aliphatic polyester that could be ruptured by lysosomal enzymes like esterase at the intracellular compartments for drug delivery.<sup>48</sup>

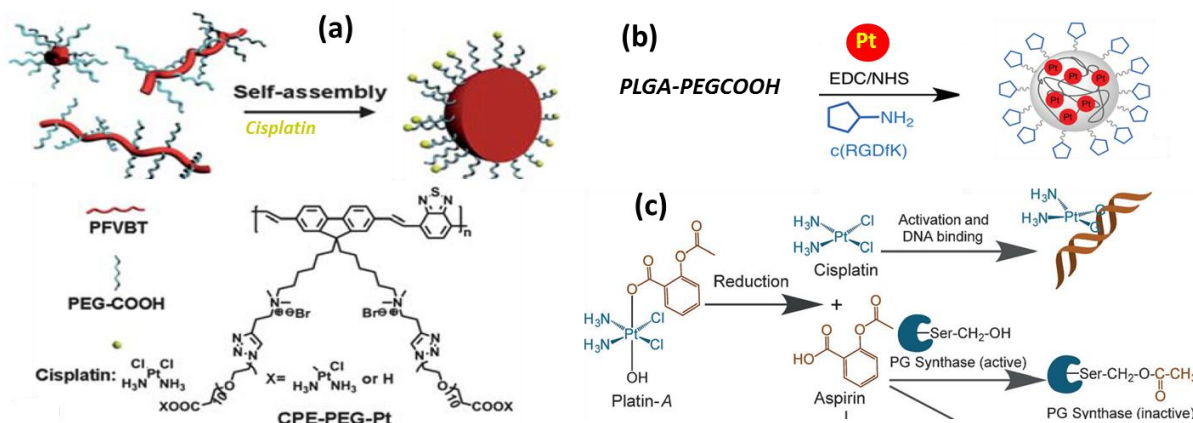


**Figure 4.5.** Schematic illustration of the synthesis of Pt nanoparticles with polyfluorene (a) (adapted from *Nanoscale* **2011**, 3, 1997-2002), PLGA-COOH (b) (adapted from *ACS NANO*, 6, **2012**, 4530–4539) and ibuprofen (adapted from *Angew. Chem. Int. Ed.* **2014**, 53, 1963 – 1967).

Recently, was reported new PEG-*b*-carboxylic polycaprolactone as pH responsive vesicular scaffolds for oral delivery of anticancer drugs under gastrointestinal tract.<sup>49</sup> Further, the preliminary attempts on this system revealed that these copolymers were capable for cisplatin drug chemical conjugation.<sup>50</sup> This has provided new opportunity for us to develop biodegradable diblock copolymer assemblies for cisplatin delivery to accomplish 100 % cell killing in breast cancer cells. The current design has three important components: (i) PEG chains for hydrophilic shell size-control and also for enhancing solubility of the nanoparticles in aqueous medium for drug administration, (ii) the carboxylic acid units anchored in the PCL backbone for conjugating cisplatin aquo complex which constitutes the drug core, and (iii) the hydrophobic PCL backbone act as protecting layer in between the shell and core against the platinum drug detoxification by cytoplasmic thiols such as GSH. Further, this design also has in-built enzyme-responsive PCL layer; thus, the drug-polymer conjugate could be cleaved by lysosomal enzymes at the intracellular compartments. This scaffold design for cisplatin delivery is shown in figure 4.6.

The present investigation is emphasised to develop new size-controllable and biodegradable diblock copolymer nanoparticle assemblies that are capable of achieving cisplatin complexation and also exhibited shielding towards the drug core against detoxification by cytoplasmic thiols (GSH) in breast cancer cells (see figure 4.6).



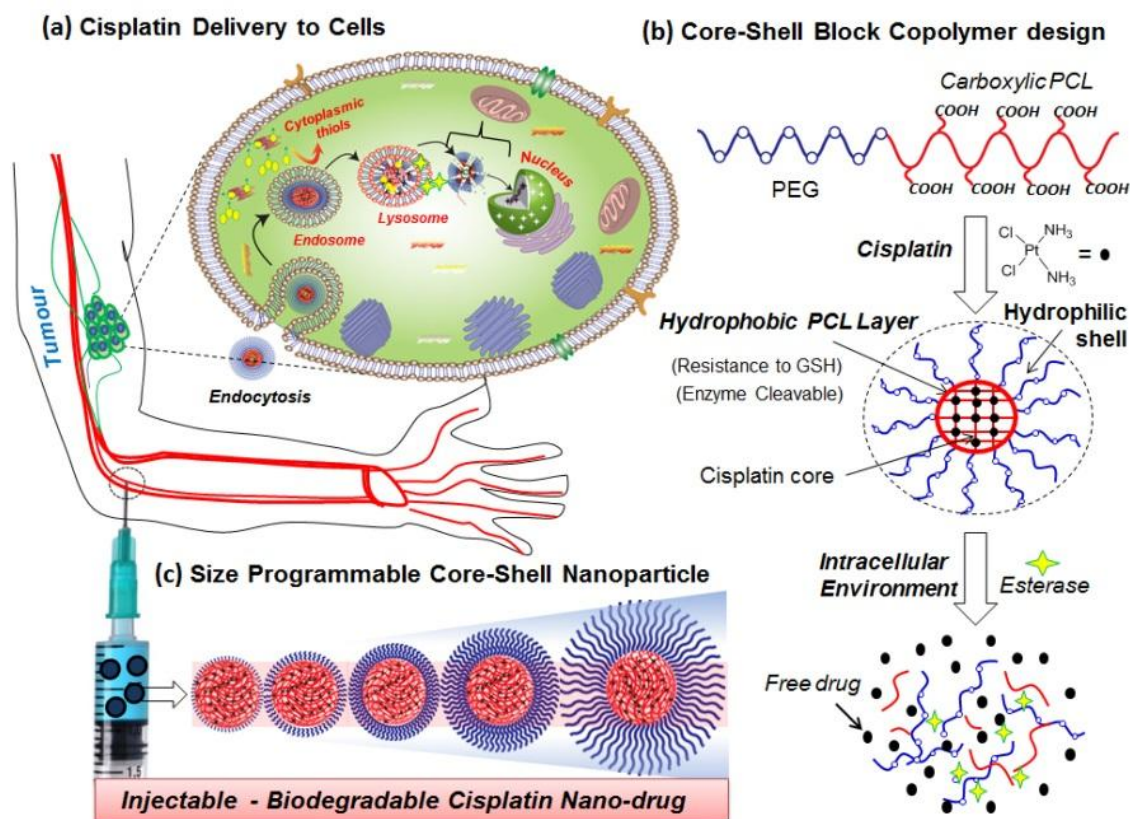


**Figure 4.6.** Core-shell polymer-cisplatin nanoparticle delivery to cancer cells (a). The delivery of the drugs at the intracellular compartments and their resistance to detoxification by cytoplasmic thiol species GSH (b). Diblock copolymer nano-drug design with variable shell size and fixed drug core (c).

The PEG<sub>x</sub>-*b*-CPCL diblocks were designed in such a way that the number of carboxylic functional units are maintained same as ~ 100 units in all the blocks and the PEG chains -(CH<sub>2</sub>CH<sub>2</sub>O)<sub>x</sub>- were systematically varied from x = 3, 7, 17, 45 and 113 to achieve size-controllable core-shell prodrug nanoparticles (see figure 4.6c). Cisplatin drug was chemically conjugated at the central core through Pt-OOR-PCL linkages which was protected at the periphery by the PEG-shells. This design enabled us to retain the central core as 75.0 ± 5 nm and vary the size of the shell precisely up to 190 nm. The role of the PEG-shell on the drug stability [in saline, PBS and fetal bovine serum (FBS)] and action against cytoplasmic thiol species like cysteine (amino acid residue) and glutathione (GSH) were investigated in detail. At the intracellular environment, the core-shell particle was cleaved by the esterase enzyme (present in the lysosome) to release the active Pt-drug for cell death. Thus, the new core-shell

polymer cisplatin nanoparticle design is both stable against detoxification for thiol-residues as well as cleavable at the intracellular compartments by esterase to deliver the cisplatin drugs. Cellular uptake and cytotoxicity of the core-shell nanoparticles were studied in normal (Wt-MEFs) and cancer (HeLa and MCF 7) cell lines. It was found that prodrugs showed selective and enhanced cytotoxicity exclusively in the breast cancer cells compared to other cell lines.

## 4.2. EXPERIMENTAL METHODS

**4.2.1 Materials:** Triethylene glycol monomethyl ether (TEG), polyethylene glycol monomethyl ether (here after referred as PEG) with molecular weight of 350, 750, 2000 and 5000, cisplatin, silver nitrate, ortho phenylene diammine (OPD), glutathione (GSH) and esterase were purchased from Aldrich chemicals. TEG and PEGs were dried under vacuum prior to use. Wild type mouse embryonic fibroblasts (Wt-MEFs), Cervical cancer (Hela cells) and Human breast cancer cells (MCF7) were maintained in DMEM (phenol red free medium: Gibco) containing 10% (v/v) fetal bovine serum (FBS) and 1% (v/v) penicillin–streptomycin at 37°C under a 5% CO<sub>2</sub> humidified atmosphere. Cells were washed with 40 % DPBS (Gibco), trypsinised using 0.05 % trypsin (Gibco) and seeded in 96 well or 6 well (as per experiment) flat bottomed plastic plates (Costar) for all assays. Tetrazolium salt, 3-(4, 5-dimethylthiazol-2,5-diphenyl)tetrazolium bromide (MTT), DMSO, Hoechst and 4% paraformaldehyde was obtained from Sigma. Fluoromount was obtained from Southern Biotech. All the solvents like tetrahydrofuran (THF), dichloromethane (DCM), trifluoroacetic acid (TFA) were purified and distilled prior to use. Monomer **3** was synthesised as described in chapter 1.

**4.2.2 Synthesis of PEG<sub>x</sub>-*b*-BPCL diblock polymers:** The typical synthetic procedure was elucidated for PEG<sub>5000</sub>-*b*-BPCL; where,  $[M_o]/[I_o]$  is kept as 100. The initiator PEG<sub>5000</sub> (193.8 mg, 0.0387 mmol), catalyst Sn(Oct)<sub>2</sub> (7.8 mg, 0.0193 mmol) and the substituted caprolactone monomer (1.0 g, 3.87 mmol) were taken in a flame-dried Schlenk tube under nitrogen atmosphere. High vacuum was applied to this reaction mixture for 45 min with stirring at room temperature. After achieving inert conditions inside the tube, it was immersed in preheated oil bath at 130 °C. The polymerization was continued for 6 h with constant stirring. The polymer mixture was cooled to room temperature and precipitated in cold MeOH. The polymer was redissolved in THF and

precipitated again in cold-methanol the process was repeated at least twice to obtain pure polymer. Yield: 700 mg (70 %).  $^1\text{H-NMR}$  (400 MHz,  $\text{CDCl}_3$ )  $\delta$  ppm: 4.13 (s, 2H), 3.63 (s, 6.51 H), 3.43 (s, 1H), 3.38 (s, 1H), 2.44 (t, 2H), 2.35 (t, 2H), 1.93–1.81 (m, 2H), 1.81–1.67 (m, 4H), 1.44 (s, 9H, t-butyl).  $^{13}\text{C-NMR}$  (100 MHz,  $\text{CDCl}_3$ ): 173.69, 170.81, 80.77, 75.62, 70.66, 65.13, 61.47, 36.60, 33.04, 29.81, 28.86, and 28.22. FT-IR ( $\text{cm}^{-1}$ ): 2973, 2931, 1727 (C=O ester), 1457, 1364, 1251, 1156, 1156, 1100, 1062, 959, 900, 845, and 757. GPC molecular weights:  $M_n = 18,400$ ,  $M_w = 24,900$ , and  $M_w/M_n = 1.35$ .

A similar procedure was followed for the synthesis of other block copolymers  $\text{PEG}_x\text{-}b\text{-BPCL}$  where  $x = 3, 7, 17$  and  $45$  which described below.

**Synthesis of BPCL:** CCL (1 g, 3.87 mmol), TEG (6.35 mg, 0.038 mmol) and  $\text{Sn}(\text{Oct})_2$  (7.7 mg, 0.019 mmol). **Yield:** 690 mg (69 %).  $^1\text{H NMR}$  (400MHz,  $\text{CDCl}_3$ )  $\delta$  ppm: 4.15 (s, 2H), 3.64 (m, 2.1 H), 3.44 (m, 1H), 2.44 (t, 2H), 2.34 (t, 2H), 1.94 – 1.84 (m, 4H), 1.45 (s, 9H). : **FT-IR ( $\text{cm}^{-1}$ ):** 2974, 2931, 1726, 1457, 1364, 1256, 1156, 1100, 957, 846, 726 and 647.  $M_n$  (NMR) 23,400 g/mol;  $M_n$  (GPC): 15,000 g/mol;  $M_w$  (GPC) =21,100 g/mol. PDI (GPC) = 1.40

**Synthesis of  $\text{PEG}_{350}\text{-}b\text{-BPCL}$ :** CCL (1 g, 3.87 mmol), m $\text{PEG}_{350}$  (13.5 mg, 0.038 mmol) and  $\text{Sn}(\text{Oct})_2$  (7.7 mg, 0.019 mmol). **Yield:** 760 mg (76 %).  $^1\text{H NMR}$  (400MHz,  $\text{CDCl}_3$ )  $\delta$  ppm: 4.14 (s, 2H), 3.64 (m, 2.3H), 3.45 (m, 1H), 2.44 (t, 2H), 2.34 (t, 2H), 1.93 – 1.81 (m, 4H), 1.45 (s, 9H). : **FT-IR ( $\text{cm}^{-1}$ ):** 2973, 2931, 1726, 1457, 1364, 1251, 1156, 1099, 957, 846, 720 and 647.  $M_n$  (NMR) 23,800 g/mol;  $M_n$  (GPC): 16,300 g/mol;  $M_w$  (GPC) =20,000 g/mol. PDI (GPC) = 1.22.

**Synthesis of  $\text{PEG}_{750}\text{-}b\text{-BPCL}$ :** CCL (1 g, 3.87 mmol), m $\text{PEG}_{750}$  (28.5 mg, 0.038 mmol) and  $\text{Sn}(\text{Oct})_2$  (7.7 mg, 0.019 mmol). **Yield:** 740 mg (74 %).  $^1\text{H NMR}$  (400MHz,  $\text{CDCl}_3$ )  $\delta$  ppm: 4.14 (s, 2H), 3.64 (m, 2.7 H), 3.45 (m, 1H), 2.44 (t, 2H), 2.34 (t, 2H), 1.93 – 1.81 (m, 4H), 1.45 (s, 9H): **FT-IR ( $\text{cm}^{-1}$ ):** 2973, 2931, 1726, 1457, 1364, 1251, 1156, 1099, 957, 846, 720 and 647.  $M_n$  (NMR) = 25,300 g/mol;  $M_n$  (GPC) = 16,700 g/mol;  $M_w$  (GPC) = 20,200 g/mol. PDI (GPC) = 1.20.

**Synthesis of  $\text{PEG}_{2000}\text{-}b\text{-BPCL}$ :** CCL (1 g, 3.87 mmol),  $\text{PEG}_{2000}$  (76 mg, 0.038 mmol) and  $\text{Sn}(\text{Oct})_2$  (7.7 mg, 0.019 mmol). **Yield:** 700 mg (70 %).  $^1\text{H NMR}$  (400MHz,  $\text{CDCl}_3$ )  $\delta$  ppm: 4.14 (s, 2H), 3.64 (m, 3.8 H), 3.46 (m, 1H), 2.44 (t, 2H), 2.34 (t, 2H), 1.93 – 1.84 (m, 4H), 1.45 (s, 9H). : **FT-IR ( $\text{cm}^{-1}$ ):** 2973, 2931, 1726, 1457, 1364, 1251, 1156, 1099, 957,



846, 720 and 647.  $M_n$  (NMR) 26,200 g/mol;  $M_n$  (GPC): 22,400 g/mol;  $M_w$  (GPC) = 22,400 g/mol. PDI (GPC) = 1.31.

**4.2.3 Synthesis of PEG<sub>x</sub>-*b*-CPCL diblock polymers:** Trifluoroacetic acid (0.2 mL) was added slowly into PEG<sub>5000</sub>-*b*-BPCL (200 mg) in dry DCM (5.0 mL), and the polymer solution was stirred at 25 °C for 30 min. The solvent was evaporated and the polymer was redissolved in THF and precipitated in cold methanol. The purification was repeated at least twice to get pure polymer. <sup>1</sup>H-NMR (400 MHz, CDCl<sub>3</sub>) δ: 4.14 (t, 2H, CH<sub>2</sub>OH), 3.84–3.64 (m, 3.7 H, PEG and OCH<sub>2</sub>), 3.57 (m, 1H, OCH), 2.56 (t, 2H, CH<sub>2</sub>COOH), 2.38 (t, 2H, COCH<sub>2</sub>), 1.99–1.67 (m, 4H, –OCH (CH<sub>2</sub>)<sub>2</sub>). <sup>13</sup>C-NMR (100 MHz, CDCl<sub>3</sub>): 173.68, 170.86, 80.72, 75.58, 70.72, 65.13, 61.50, 36.60, 33.14, 29.81, and 28.22. FT-IR (cm<sup>-1</sup>): 3447, 2932, 2450, 1711 (C=O), 1365, 1257, 1175, 1099, 1063, and 960.

**Synthesis of CPCL:** Trifluoroacetic acid (0.2 mL), BPCL (200 mg) and DCM (5.0 mL). <sup>1</sup>H NMR (400MHz, CDCl<sub>3</sub>) δ: 4.14 (t, 2H), 3.84- 3.64 (m 2.1 H), 3.57 (m, 1H), 2.54 (t, 2H), 2.36 (t, 2H), 1.99 – 1.67 (m, 4H). FT-IR (cm<sup>-1</sup>): 3450, 2880, 1720, 1352, 1252, 1180, 1092, 948, 917, 841 and 730.  $M_n$  (NMR) 18,300 g/mol;  $M_n$  (GPC): 9,000 g/mol; PDI (GPC) = 1.30.

**Synthesis of PEG<sub>350</sub>-*b*-CPCL:** Trifluoroacetic acid (0.2 mL), PEG<sub>350</sub>-*b*-BPCL (200 mg) and DCM (5.0 mL). <sup>1</sup>H-NMR (400MHz, CDCl<sub>3</sub>) δ: 4.14 (t, 2H), 3.64 (m 2.28H), 3.57 (m, 1H), 2.56 (t, 2H), 2.38 (t, 2H), 1.99 – 1.67 (m, 4H). FT-IR (cm<sup>-1</sup>): 3450, 2880, 1749, 1352, 1252, 1180, 1092, 948, 917, 841 and 730.  $M_n$  (NMR) 18,700 g/mol;  $M_n$  (GPC): 11,000 g/mol; PDI (GPC) = 1.24.

**Synthesis of PEG<sub>750</sub>-*b*-CPCL:** Trifluoroacetic acid (0.2 mL), PEG<sub>750</sub>-*b*-BPCL (200 mg) and DCM (5.0 mL). <sup>1</sup>H -NMR (400MHz, CDCl<sub>3</sub>) δ: 4.14 (t, 2H), 3.74- 3.64 (m 2.7 H), 3.57 (m, 1H), 2.56 (t, 2H), 2.38 (t, 2H), 1.99 – 1.67 (m, 4H). FT-IR (cm<sup>-1</sup>): 3450, 2880, 1749, 1352, 1252, 1180, 1092, 948, 917, 841 and 730.  $M_n$  (NMR) 19,900 g/mol;  $M_n$  (GPC): 12,200 g/mol; PDI (GPC) = 1.19.

**Synthesis of PEG<sub>2000</sub>-*b*-CPCL:** Trifluoroacetic acid (0.2 mL), PEG<sub>2000</sub>-*b*-BPCL (200 mg) and DCM (5.0 mL). <sup>1</sup>HNMR (400MHz, CDCl<sub>3</sub>) δ: 4.14 (t, 2H), 3.74- 3.64 (m 3.9 H), 3.57 (m, 1H), 2.56 (t, 2H), 2.38 (t, 2H), 1.99 – 1.67 (m, 4H). FT-IR (cm<sup>-1</sup>): 3450, 2880, 1749, 1352, 1252, 1180, 1092, 948, 917, 841 and 730.  $M_n$  (NMR) 21,000 g/mol;  $M_n$  (GPC): 12,700 g/mol; PDI (GPC) = 1.18.

**4.2.4 Preparation of Aquated Cisplatin  $[\text{Pt}(\text{NH}_3)_2(\text{OH}_2)_2]^{2+}$ :** Cisplatin (50 mg, 166 mmol, 1 equiv.) was dispersed in  $\text{H}_2\text{O}$  (50.0 mL) with constant stirring at  $37^\circ\text{C}$ . To this mixture, silver nitrate (56.4 mg, 332 mmol, 2 equiv.) was added and the resulting reaction mixture was stirred for 24 h in dark conditions. Formation of aquated cisplatin complex was confirmed by milky white silver chloride precipitation. Silver chloride was removed by centrifuging at 10,000 rpm for 1 h. Finally, the aquated cisplatin was obtained by filtration through  $0.2\ \mu\text{m}$  filter. The sample was lyophilized and stored at  $4^\circ\text{C}$ .

**4.2.5 Synthesis of the Polymer-cisplatin Conjugate:** A typical procedure for preparation of  $\text{PEG}_{5000}\text{-}b\text{-CPCL-CP}$  explained in detail.  $\text{PEG}_{5000}\text{-}b\text{-CPCL}$  diblock polymer (20.0 mg) was dissolved in NaOH (2 mL,  $1\ \text{mg}\cdot\text{mL}^{-1}$ ) and solution was stirred at  $37^\circ\text{C}$  for 30 min. Aquated cisplatin (16.4 mg, 55 mmol, the lyophilized sample) was added to the above polymer solution and the complex was stirred for 24 h at  $37^\circ\text{C}$ . The solution was transferred to a dialysis bag of molecular weight cut-off (MWCO = 1000) and dialyzed against large amount of distilled water for 2 days. Distilled water was replaced periodically to ensure the removal of un-encapsulated molecules from the dialysis tube. The solution recovered from dialysis tube was filtered through  $0.45\ \mu\text{m}$  filter, lyophilised and stored at  $4^\circ\text{C}$ . FT-IR ( $\text{cm}^{-1}$ ): 3300, 2920, 2880, 1660, 1560, 1395, 1360, 1090, 1050, 930, 830 and 548.

Similar procedure was used for making cisplatin complexes of copolymers and the details are given below.

**Synthesis of CPCL-CP:** CPCL (20 mg), NaOH (2 mL,  $1\ \text{mg}\cdot\text{mL}^{-1}$ ) and aquated cisplatin (16.4 mg, 55 mmol). **FTIR** ( $\text{cm}^{-1}$ ): 3290, 2929, 2880, 1660, 1560, 1395, 1360, 1090, 1050, 930, 830 and 545.

**Synthesis of  $\text{PEG}_{350}\text{-}b\text{-CPCL-CP}$ :**  $\text{PEG}_{350}\text{-}b\text{-CPCL}$  (20 mg), NaOH (2 mL,  $1\ \text{mg}\cdot\text{mL}^{-1}$ ) and aquated cisplatin (16.4 mg, 55 mmol). **FTIR** ( $\text{cm}^{-1}$ ): 3300, 2920, 2880, 1660, 1560, 1395, 1360, 1090, 1050, 930, 830 and 549.

**Synthesis of  $\text{PEG}_{750}\text{-}b\text{-CPCL-CP}$ :**  $\text{PEG}_{750}\text{-}b\text{-CPCL}$  (20 mg), NaOH (2 mL,  $1\ \text{mg}\cdot\text{mL}^{-1}$ ) and aquated cisplatin (16.4 mg, 55 mmol). **FTIR** ( $\text{cm}^{-1}$ ): 3300, 2950, 2880, 1660, 1565, 1395, 1350, 1090, 1050, 940, 830 and 548

**Synthesis of PEG<sub>2000</sub>-*b*-CPCL-CP:** PEG<sub>2000</sub>-*b*-CPCL (20 mg), NaOH (2 mL, 1 mg.mL<sup>-1</sup>) and aquated cisplatin (16.4 mg, 55 mmol). **FTIR** (cm<sup>-1</sup>): 3250, 2920, 2880, 1660, 1560, 1399, 1360, 1090, 1050, 935, 830 and 548.

**4.2.6 In Vitro Drug Release Studies:** Cisplatin loaded nanoparticles were taken in a dialysis bag (in 3 mL), and they were immersed in a 100 mL beaker and dialyzed at 37 °C with constant stirring. Various dialysis conditions like saline, PBS and FBS were employed for these studies. At specific time intervals, 3.0 mL of the dialysate was withdrawn and replaced with an equal volume of fresh buffer (or FBS). The amount of molecule (or drug) released in each aliquot was measured using absorption spectroscopy using ortho phenylene diammine (OPD) assay to quantify their percentage of cumulative release. For esterase aided release studies 10 units of enzyme was used, following the above mentioned procedure.

Cumulative release (%) =  $C_n \times V_o / m \times 100$ , where  $C_n$  is the amount of loaded cargo in the  $n^{\text{th}}$  sample,  $V_o$  is total volume, and  $m$  is the total amount loaded in nanoparticles.

**4.2.7 O-phenylenediamine (OPD) Colorimetric Assay:** Samples with unknown cisplatin (Pt) content were added to 0.5 mL of OPD solution in *N,N*-dimethylformamide (DMF) (1.2 mg.mL<sup>-1</sup>) and heated for 2 h at 100°C. The amount of Pt present in the sample was determined by measuring the absorbance at 706 nm (absorbance maxima of OPD-Pt complex). Molar extinction coefficient calculated for OPD-Pt as 24,310 L.mol<sup>-1</sup>.cm<sup>-1</sup>. The concentration of Pt released from the drug-conjugate was expressed as a ratio of the amount of platinum in the releasing solution from the polymer backbone.

The drug loading efficiency (DLE) and drug loading content (DLC) were determined by absorption spectroscopy using OPD colorimetric assay from the following equation:

$$\text{DLE (\%)} = \{ \text{weight of drug in NPs} / \text{weight of drug in feed} \} \times 100\%$$

$$\text{DLC (\%)} = \{ \text{weight of drug in NPs} / \text{weight of drug loaded NPs} \} \times 100\%.^{43-45}$$

**4.2.8 Preparation of Nile Red-encapsulated Pt-coordinated complex:** Nile Red was loaded (co-encapsulated) with cisplatin into diblock polymers, by adding an acetone solution of Nile Red (20 μL, 1 mM) and aquo solution of cisplatin (13 mM) to the polymer solution in water (5mL, 1 mg/mL), and then stirred for overnight. In order to

completely remove acetone, free Nile Red and free cisplatin the solution was dialyzed against water for 16 h at room temperature with a MWCO of 1000. After dialysis solution was filtered through 0.4  $\mu\text{m}$  filter, lyophilised and stored at 4°C.

**4.2.9 Cell Viability Assay (MTT Assay):** To perceive the effect of Cisplatin (CP), drug loaded scaffolds and polymers alone, a cell viability assay was performed in WT-MEF cell line, HeLa cell line and MCF 7 using the tetrazolium salt, 3-(4, 5-dimethylthiazol-2, 5-diphenyl tetrazolium bromide (MTT). 1000 cells were seeded per well in a 96-well plate (Corning, U.S.A.) in 100  $\mu\text{L}$  of DMEM with 10% FBS (fetal bovine serum) and allowed to adhere for 16 h. Prior to drug treatment, media from cells was aspirated and various concentrations of CP and scaffolds with encapsulated CP were added. A blank control, DMEM with FBS in the absence of cells was used in each experiment. All control and treated experiment wells were in triplicate. Cells were incubated for 72 h without a change in medium. After 72 h, drug containing medium was aspirated. Freshly prepared stock of MTT in sterile PBS (5 mg/mL) was diluted to 50  $\mu\text{g/mL}$  in DMEM. 100  $\mu\text{L}$  of this solution was added to each well. Cells were then incubated with MTT for 4 h at 37 °C. Medium with MTT was then aspirated from wells and the purple formazan crystals formed as a result of reduction of MTT by mitochondrial dehydrogenase enzyme from cells were dissolved in 100  $\mu\text{L}$  of 100 % DMSO (added per well). The absorbance from formazan crystals was immediately measured using micro plate reader at 570 nm (Varioskan Flash) and was representative of the number of viable cells per well. Values from the triplicates for each control and treated set were noted and their mean was used for calculations. The values thus obtained for the untreated control samples were equated to 100 % and relative percentage values for CP, scaffold alone and CP loaded nanoparticles were calculated accordingly. To mimic *in vivo* conditions short time MTT assay was studied. Wherein MCF 7 cells were seeded in 96 well plates with  $1 \times 10^3$  cells per well for 16 h. Later the media was removed and treated with various concentrations of cisplatin and polymer-cisplatin conjugates. The compounds were incubated with cells for different time intervals of 1, 2, 3 and 4 h separately. After incubation, the media was aspirated and fresh media was added. These cells were then incubated for additional 72 h. After termination of experiment, cell viability was determined using MTT assay.

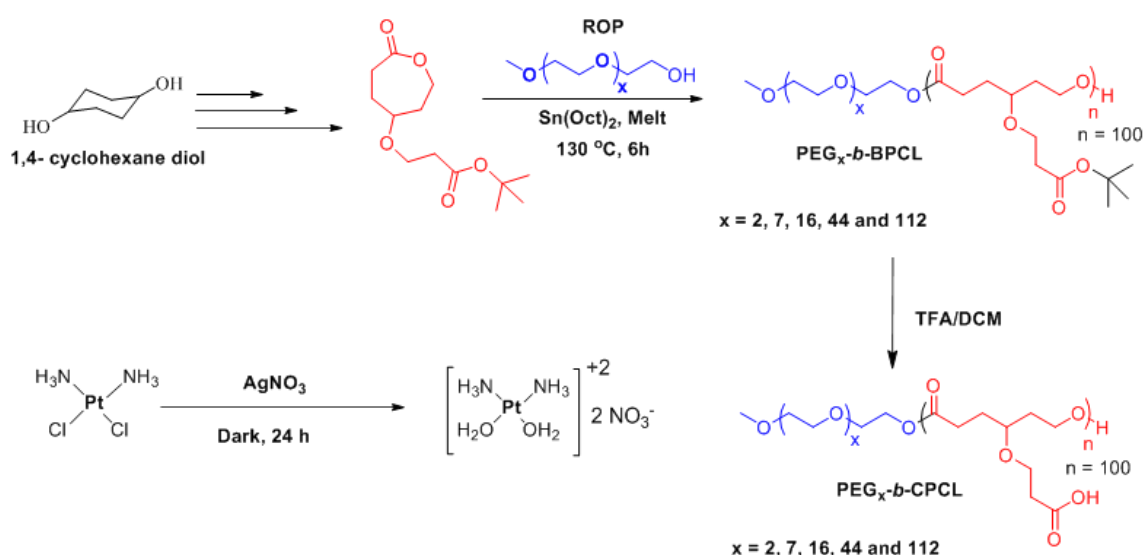
**4.2.10 Cellular Uptake of PEG-*b*-BPCL-CP-NR by Confocal microscopy:** HeLa cells were seeded at a density of  $1 \times 10^5$  cells on flame-dried cover slips placed in 6

well plates containing DMEM medium with 10 % FBS and incubated at 37 °C for 16 h. The cells were then exposed to required concentration of cisplatin alone, polymer scaffold alone, and NR loaded cisplatin-polymer nanoparticles for 4 h in a CO<sub>2</sub> incubator at 37°C. After incubation, drug-containing medium was aspirated from each well, and cells were washed twice with PBS (2 × 1mL) and fixed with 4% paraformaldehyde solution in PBS for 10 min at room temperature. The cells were washed twice with PBS (2 × 1mL) and stained with Hoechst solution in PBS. After 2 min incubation, at room temperature, in the dark, the excess dye was washed from the plate and cells were again gently rinsed with PBS for 1 min. The cover slips were mounted on slides using fluoromount mounting medium (SouthernBiotech) and dried overnight at room temperature in the dark. The cells were imaged using a confocal microscope using the  $\lambda$  420 nm (blue channel) and  $\lambda$  560 nm (red channel) lasers. Images thus obtained were opened in the Image J analysis software and the image for each channel was separated.

### 4.3. Results and Discussion

#### 4.3.1 Synthesis of Block Copolymer-Cisplatin Prodrug

The t-butyl carboxylic ester substituted caprolactone monomer (named **CCL**) was prepared from 1, 4-cyclohexanediol through multi-step reactions (detail procedure discussed in chapter 2). Diblock copolymers having variable polyethylene glycol chain length with fixed carboxylic polycaprolactone units were synthesized as shown in scheme 4.1. The PEG content in each block was varied using monomethyl ether end-capped oligo ethylene glycol  $\text{CH}_3(\text{OCH}_2\text{CH}_2)_x\text{OH}$  ( $x = 3, 8, 17, 45$  and  $113$ ) as initiator for the ring opening polymerization (ROP). For this purpose, monomethyl ethers of triethyleneglycol, PEG-350, PEG-750, PEG-2000 and PEG-5000 were employed as initiators along with  $\text{Sn}(\text{Oct})_2$  as a catalyst.



**Scheme 4.1.** Synthetic scheme for diblock polymers and their cisplatin aquo complex.

The monomer CCL to initiator ratio was maintained as  $[\text{M}]/[\text{I}] = 100$  and a solvent free bulk (or melt) ROP process was developed to produce these block copolymers in high purity for biomedical applications. The resultant diblock copolymers are named as  $\text{PEG}_x\text{-b-BPCL}$ , where  $x$  represents PEG chains (MW = 350, 750, 2000 and 5000), B-represents t-butyl ester. The triethyleneglycol monomethyl ether (TEG-OMe) initiated polymers referred as BPCL.

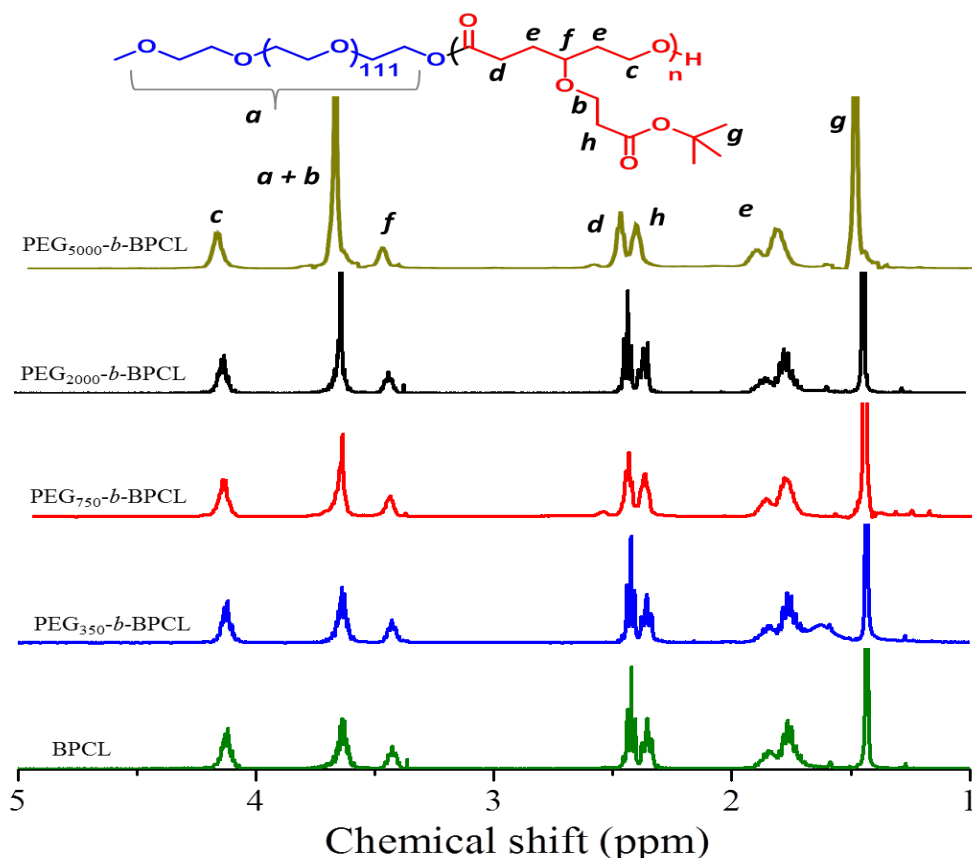


**Figure 4.7.**  $^1\text{H-NMR}$  spectra of  $\text{PEG}_{5000}\text{-}b\text{-BPCL}_{100}$  (a) and other block copolymers (b).

$^1\text{H-NMR}$  spectra of representative diblocks  $\text{PEG}_x\text{-}b\text{-BPCL}$  (B = Butyl protected) are shown in figure 4.7. The chemical structure of  $\text{PEG}_{5000}\text{-}b\text{-BPCL}$  diblock copolymer is given and the different proton are assigned by alphabets (see figure 4.7). The protons ‘b’ in the carboxylic CCL unit merged with protons ‘a’ in the PEG. The intensities of protons ‘c’ in the PCL backbone appeared at 4.15 ppm. Thus, the subtraction of peak intensities [(a+b) – c] provided the actual number of protons ‘a’. The comparison of peak integrals of a (protons at 3.65–3.68 ppm) with protons c (at 4.15 ppm) or t-butyl protons ‘g’ ( at 1.44 ppm) provided the number average degree of polymerization (n) for the PCL backbone in the diblock structure. A similar approach was adapted and the “n” values were determined for all the diblocks polymers. The number average molecular weights ( $M_n$ ) were estimated ( $M_n = n \times \text{repeating unit mass}$ ) and these values are summarized in table 4.1. As seen in figure 4.7 with increase in the PEG content in the diblocks, the peak at 3.64 ppm corresponding to  $(\text{OCH}_2\text{CH}_2)_x$  increased in the diblock copolymers.

The molecular weights of the polymers were determined by gel permeation chromatography in tetrahydrofuran. The GPC chromatograms of block copolymers before (PEG-*b*-BPCL) deprotection are provided in figure 4.8a. The chromatograms showed monomodal distribution and confirmed the formation of high molecular weight polymers. The  $M_n$ ,  $M_w$ , and polydispersity of polymers are given table 4.1. The molecular weights of the polymers increased with the PEG<sub>x</sub> chain length in the feed. The GPC technique underestimated the molecular weights of the diblocks compared to <sup>1</sup>H-NMR.

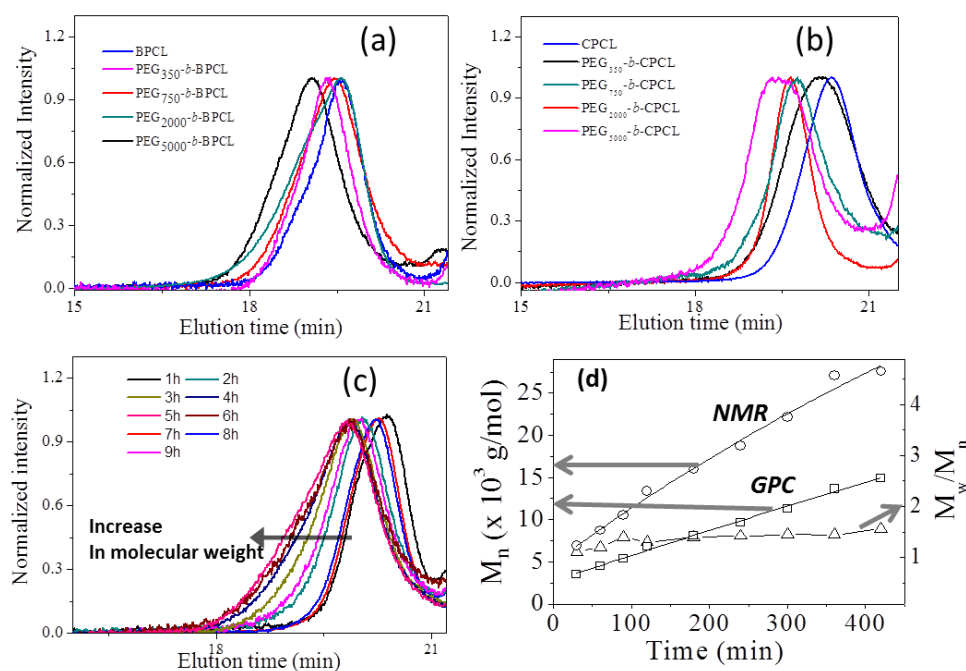


**Figure 4.8.** GPC chromatograms of PEG<sub>x</sub>-*b*-BPCL (a), PEG<sub>x</sub>-*b*-CPCL (b) The GPC chromatogram of polymerization kinetics of PEG<sub>2000</sub>-*b*-BPCL where the aliquots were taken at different time intervals (c) and the plots of  $M_n$  and PDI against polymerization time (d).

This trend was attributed to the usage of polystyrene standards for GPC calibration. To study the controlled (or livingness) ROP of CCL monomer; the kinetic polymerization was performed for PEG<sub>2000</sub>-*b*-BPCL diblock copolymer and aliquots were collected at regular interval. The molecular weights of these aliquots were determined by GPC and <sup>1</sup>H-NMR. The GPC chromatograms of these aliquots were plotted together and represented in figure 4.8c, which showed the gradual increase in molecular weight with time. The plots of  $M_n$  (from NMR and GPC) and polydispersity (PDI, from GPC) versus the reaction time are shown in see figure 4.8d. The plots for  $M_n$  followed linear trend over reaction time confirming the occurrence of the controlled process with respected to living ROP process. The polydispersity ( $M_w/M_n$ )



of the samples were obtained as  $\approx 1.4$  indicating the formation of narrow molecular weight diblock copolymers.

The t-butyl ester of carboxylic functional group was hydrolysed by trifluoroacetic acid to yield their corresponding carboxylic acid diblock copolymer PEG<sub>x</sub>-b-CPCL (see scheme 4.1, where C represents carboxylic acid). The hydrolysis of the t-butyl units was confirmed by <sup>1</sup>H-NMR and their spectra are similar to the figure 2.6 in chapter 2. The molecular weights of these de-protected diblocks were determined by GPC and their details are given in figure 4.8b and table 4.1. This data of PEG<sub>x</sub>-b-CPCL diblocks revealed that the molecular weights were not affected by the de-protection step. Based on the above analysis, we can conclude that the diblock copolymers with variable PEG chain the solvent free ROP process of new CCL monomer.

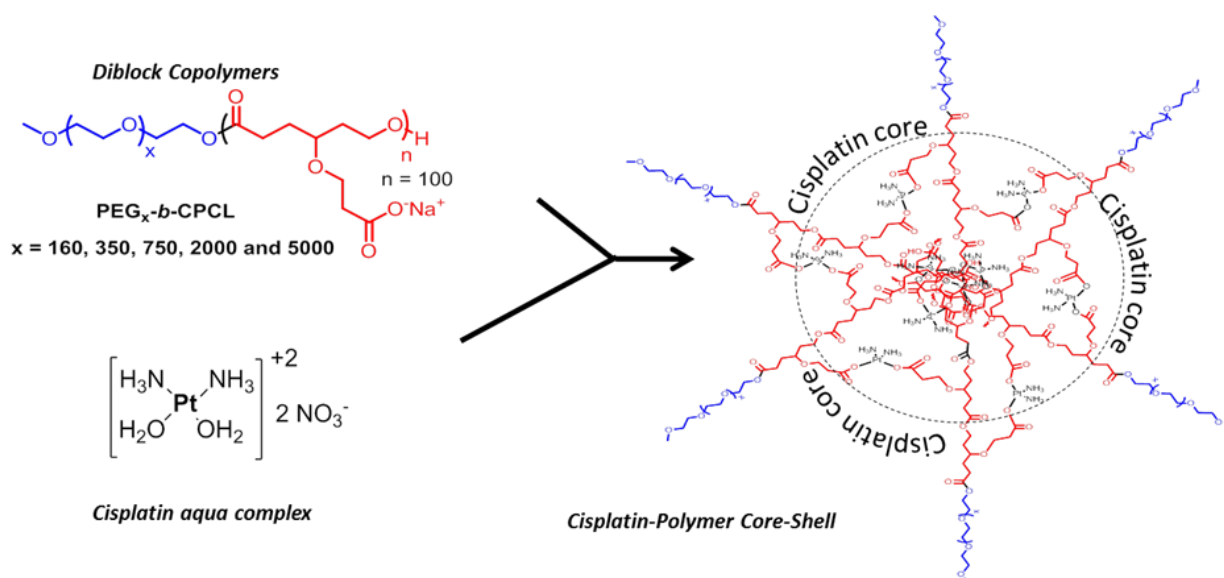
**Table 4.1.** Molecular weights and molecular weight distribution of PEG<sub>x</sub>-b-BPCL and PEG<sub>x</sub>-b-CPCL diblock polymers.

Polymer	n <sup>a</sup> (NMR)	M <sub>n</sub> <sup>b</sup> (g/mol, NMR)	M <sub>n</sub> <sup>c</sup> (g/mol, GPC)	M <sub>w</sub> <sup>c</sup> (g/mol, GPC)	M <sub>w</sub> /M <sub>n</sub> <sup>c</sup> (GPC)
BPCL	90	23,400	15,000	21,100	1.40
PEG <sub>350</sub> -b-BPCL	91	23,800	16,300	20,000	1.22
PEG <sub>750</sub> -b-BPCL	95	25,300	16,700	20,200	1.20
PEG <sub>2000</sub> -b-BPCL	94	26,200	17,000	22,400	1.31
PEG <sub>5000</sub> -b-BPCL	100	35,800	19,100	23,700	1.24
CPCL	90	18,300	9,000	11,700	1.30
PEG <sub>350</sub> -b-CPCL	91	18,700	11,000	13,700	1.24
PEG <sub>750</sub> -b-CPCL	95	19,900	12,200	14,600	1.19
PEG <sub>2000</sub> -b-CPCL	94	21,000	12,700	15,100	1.18
PEG <sub>5000</sub> -b-CPCL	89	23,000	13,100	22,200	1.69

<sup>a</sup> Number of repeating units are determined by <sup>1</sup>H-NMR. <sup>b</sup> M<sub>n</sub> was calculated based on M<sub>n</sub> = (repeating unit mass) x n. <sup>c</sup> Molecular weights and PDI determined by GPC using polystyrene as standard in THF

### 4.3.2. Cisplatin Chelation with Polymers

The *cis*-diamminediaqua platinum (II) complex was made by cisplatin and AgNO<sub>3</sub> in milli Q water and the resultant AgCl precipitate was removed by filtration.<sup>21</sup> The cisplatin aquo complex was reacted with sodium salts of PEG<sub>x</sub>-*b*-CPCL diblocks in deionised water for 24 h under dark (see scheme 4.2). The cisplatin aquo complex to diblock copolymer ratio was maintained as 1.0:1.1 (in mole ratio) to achieve complete chelation in the polymer. The resultant polymer-cisplatin complexes were filtered through 0.45 μm filters and dialyzed for 48 h to remove un-reacted cisplatin aquo complex. The dialyzed solutions were lyophilized to yield dark brown coloured polymer-cisplatin drug conjugates.



**Scheme 4.2.** Cisplatin complexation with sodiated diblock copolymers.

The formation of polymer cisplatin conjugate was confirmed by FT-IR technique (see figure 4.9). The carbonyl (–C=O) stretching frequency appeared as distinct band at 1720 cm<sup>-1</sup> in nascent polymer which disappeared upon complexation. A new band appeared at 1560 cm<sup>-1</sup> with respect to (Pt–O–C=O) stretching frequency of the metal carboxylate functional group.<sup>51-52</sup> Additionally, a distinct peak at 550 cm<sup>-1</sup> corresponding to Pt–O (metal alkoxide) bond stretching was clearly visible in the drug-polymer conjugate.<sup>51-52</sup>

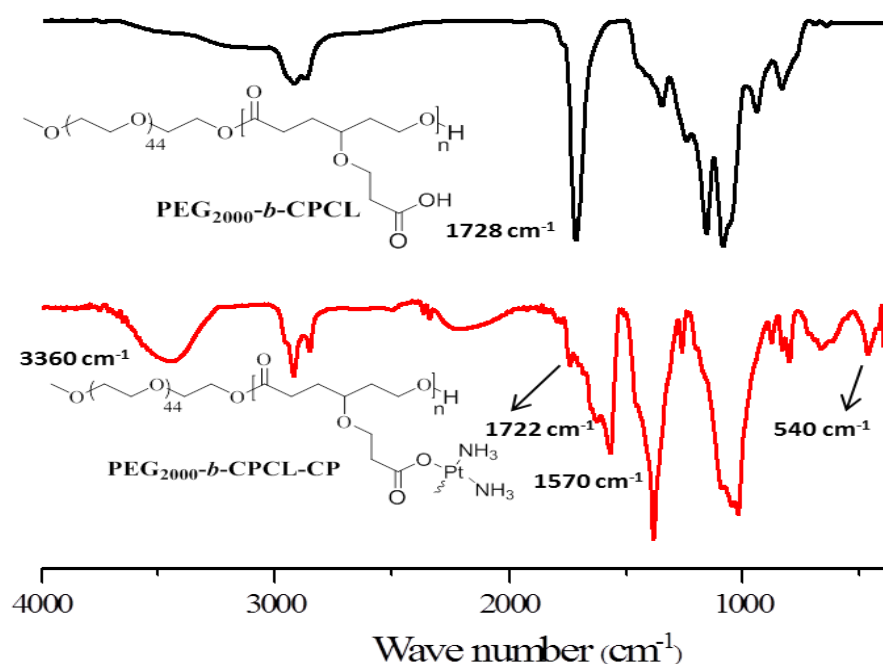


**Figure 4.9.** FT-IR spectra of PEG<sub>2000</sub>-b-CPCL and PEG<sub>2000</sub>-b-CPCL-CP.

Thermal gravimetric analysis (TGA) was used to estimate drug loading content of cisplatin in the polymer drug conjugates. The TGA plots for polymer-drug conjugates, diblock polymers and free cisplatin are shown in figure 4.10a. Briefly, these calculations were elucidated for PEG<sub>5000</sub>-b-CPCL-CP. The decomposition of the polymer started at 260 °C and it completely degraded at 500 °C. Cisplatin (alone) underwent stepwise decomposition and showed 60 % weight loss below 400 °C and platinum content remain unchanged up to 800°C. The diblock copolymers exhibited single-step decomposition at 300 °C. In contrast, the cisplatin-polymer conjugate showed different decomposition profiles: (i) below 380 °C with respect to the ligands attached to cisplatin (ii) from 380 to 580 °C with respect to the degradation of PEG-b-CPCL block and (iii) the residual platinum metal above at 600 °C.

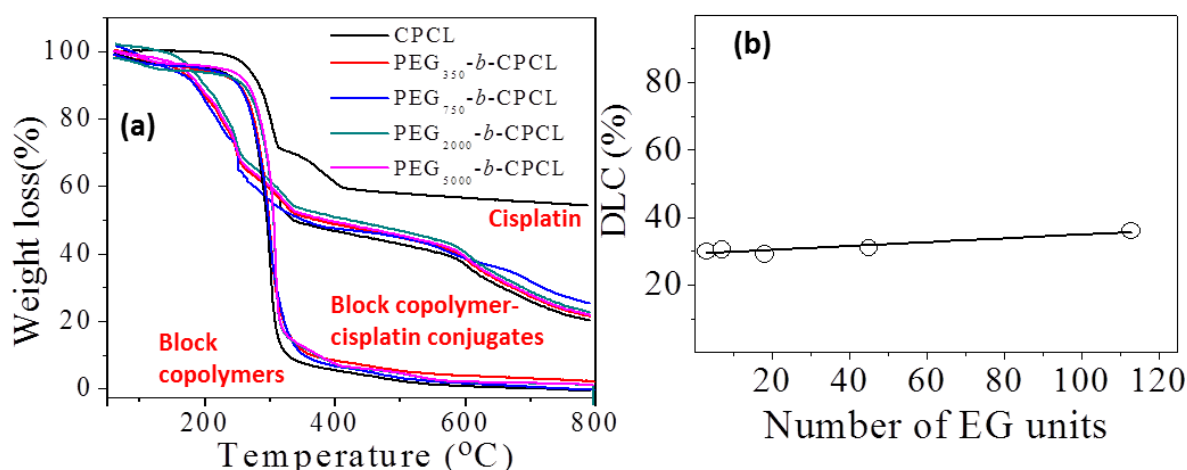


**Figure 4.10.** TGA plots of free cisplatin, diblock polymers and their cisplatin conjugates (a). The plot of DLC against number of EG units (b).

The drug conjugation efficiency (DCE) was estimated by following the procedure reported by Xu et al.<sup>53</sup>

$$\text{DCE} = m\text{Pt}_{\text{exp}}/m\text{Pt}_{\text{theo}} \times 100\% = (W_{\text{Pt}}/M_{\text{Pt}}) / (W_{\text{acid}}/2M_{\text{acid}}) \times 100\%$$

where,  $m\text{Pt}_{\text{theo}}$  is the theoretical molar amount of Pt;  $m\text{Pt}_{\text{exp}}$  is the experimental molar amount of Pt;  $W_{\text{Pt}}$  is the weight percent of Pt measured by TGA;  $M_{\text{Pt}}$  is the molecular weight of Pt;  $W_{\text{acid}}$  is the weight percent of acid repeating unit calculated by TGA data and  $M_{\text{acid}}$  is the molecular weight of acid repeating unit. Based on this equation, the DCE was obtained and the drug loading content (DLC) of drug-conjugates was calculated. The detailed calculations (see below) and DLC for all the polymer scaffolds are tabled in table 4.2. The plot of drug loading content for polymer-cisplatin conjugate for various PEG<sub>x</sub>-b-CPCL diblocks (see figure 4.10b) revealed that the DLC was retained as 35 % in all the samples. This further confirmed that all the carboxylic units in the diblock polymer were involved in complexation with cisplatin aquo complex irrespective of the PEGylated chain length. The DLC values from TGA are in good coherent with OPD assay UV values (explained later).

Calculation of Drug Loading Content(DLC) for PEG<sub>5000</sub>-*b*-CPCL-CP was described below following the report by Xu et al. (*Chem. Commun.* 2013, 49, 33–35):

$$f = \frac{m_{Pt-exp}}{m_{Pt-th}} \times 100\% = \frac{W_{Pt}/M_{Pt}}{W_{acid}/M_{acid} \times 2} \times 100\%$$

$$= \frac{20.2/195}{79.8 - \{[(20.2 \times 34.6)/65.4] \times (20200/25200)\}/404} \times 100\%$$

$$f = 75.7\%$$

**Calculation of Drug Loading Content (DLC):**

$$DLC = \frac{\text{initial feed} \times 75.7\%}{\text{polymer amount} + (\text{initial feed} \times 75.7\%)} \times 100\%$$

$$= \frac{15 \times 75.7\%}{20 + (15 \times 75.7\%)} \times 100$$

$$DLC = 36\%$$

For remaining polymer-drug conjugates DLC was calculated in similar way and tabled below.

**Table 4.2:** DLC determination using TGA and table shows the determined DLC using TGA and UV (using OPD assay) techniques.

S.No	Polymer drug conjugates	DLC (TGA)	DLC (UV)
1	CPCL-CP	28 %	25 %
2	PEG <sub>350</sub> - <i>b</i> -CPCL-CP	30 %	28 %
3	PEG <sub>750</sub> - <i>b</i> -CPCL-CP	31 %	34 %
4	PEG <sub>2000</sub> - <i>b</i> -CPCL-CP	31 %	27 %
5	PEG <sub>5000</sub> - <i>b</i> -CPCL-CP	36 %	39 %

### 4.3.3 Size and Shape of Polymer-Cisplatin Prodrug

To study the self-assembled structures of polymer-drug conjugates, the samples were dispersed in water and subjected to dynamic light scattering (DLS) analysis. The DLS histograms of polymer-drug conjugates for various PEG<sub>x</sub>-*b*-CPCL diblocks are shown in figures 4.11a to 4.11e. All histograms showed uniform monomodal distribution and the sizes of self-assembled objects were found to increase with PEG content in the diblocks. The smallest conjugate CPCL-CP (with triethylene glycol hydrophilic unit) showed the formation of  $70 \pm 5$  nm size assemblies. With increase in the EG unit, the size of the aggregates in DLS increased up to  $190 \pm 5$  nm (see figure 4.11k). Field emission scanning electron microscopy (FESEM) images of these polymer-cisplatin conjugates are shown in figures 4.11f to 4.11j. FESEM images exhibited the formation of the spherical nano-particular morphologies. The sizes of nanoparticles in FE-SEM images are in very good agreement with the DLS size of the samples in water (see figure 4.11k).

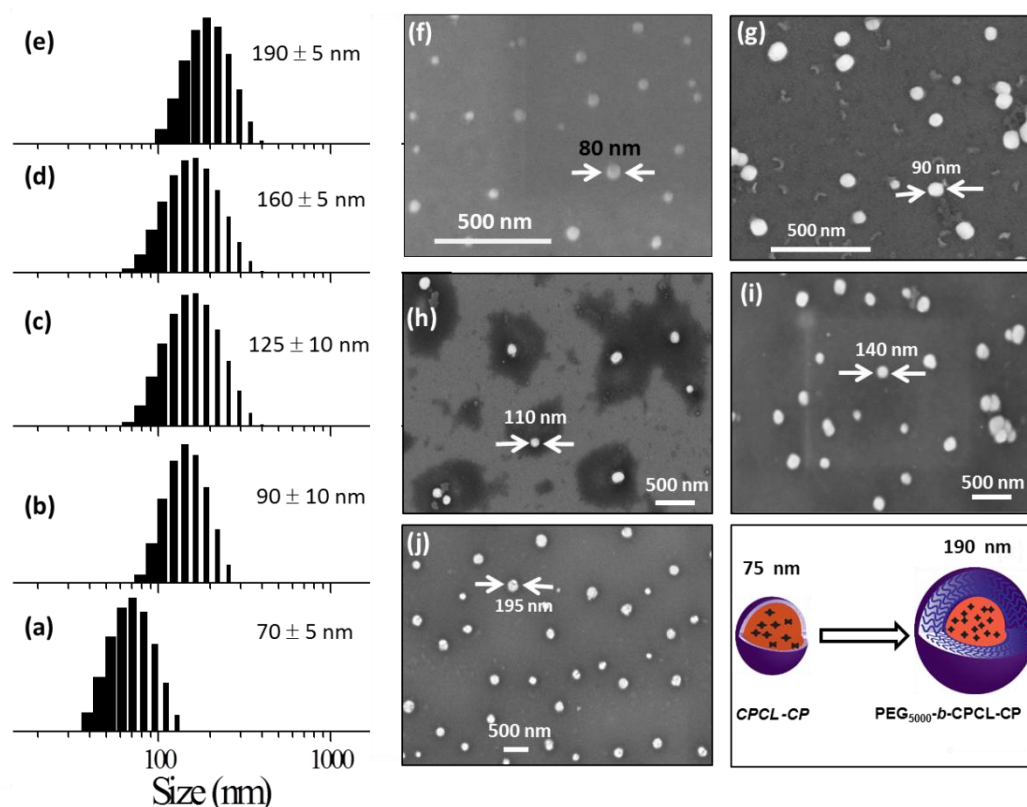


**Figure 4.11.** DLS histograms of CPCL-CP (a), PEG<sub>350</sub>-*b*-CPCL-CP (b), PEG<sub>750</sub>-*b*-CPCL-CP(c), PEG<sub>2000</sub>-*b*-CPCL-CP (d) and PEG<sub>5000</sub>-*b*-CPCL-CP (e). FESEM images of CPCL-CP(f), PEG<sub>350</sub>-*b*-CPCL-CP(g), PEG<sub>750</sub>-*b*-CPCL-CP(h), PEG<sub>2000</sub>-*b*-CPCL-CP(i) and PEG<sub>5000</sub>-*b*-CPCL-CP (j). Pictorial representation of core-shell nanoparticles (k).

A core-shell nanoparticle model is proposed for the increase in the polymer-drug conjugated nanoparticle size with number of ethylene glycol units in the diblocks as represented in figure 4.12a. The core of the nanoparticles are retained same and the hydrophilic shell varied by the increase in the PEG chains. This was accomplished since all the diblocks in PEG<sub>x</sub>-*b*-CPCL have same number of carboxylic units (100 units and they have identical DLC, see table 4.2 and figure 4.10b) for cisplatin conjugation. This model is further validated by plotting the size of the nanoparticles obtained from DLS and FESEM against the number of ethylene glycol units on the periphery (see figures 4.12b and 4.12c). These plots showed a linear trend with an intercept of 70 nm and slopes of 1.06 and 1.01, for DLS and FESEM images respectively. The intercept value of 70 nm is corresponding to the core of the nanoparticles in CPCL-CP.

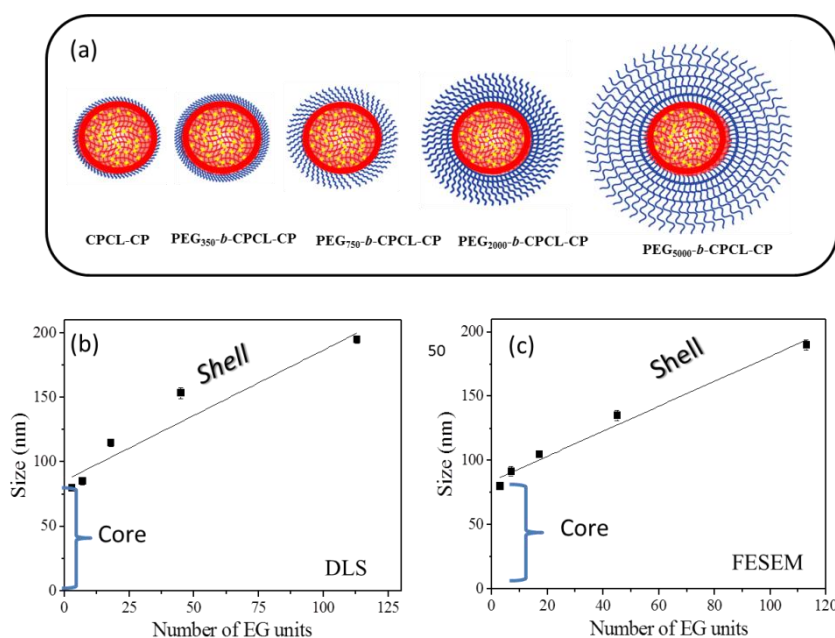


**Figure 4.12.** Schematic representation of nanoparticles (a). The plots of nanoparticle size from DLS (b) and FESEM (c) against number of ethylene glycol units in the diblocks.

Thus, 70 nm is assigned to the core of all the nanoparticles since they have same number of COOH units and cisplatin content (evident from figure 4.10b). The increase in the nanoparticle size more than 70 nm was attributed to the increase in the ethylene glycol units on the periphery of the nanoparticles. The slopes of the plots in figure 4.12b and 4.12c were obtained as  $\sim 1.0$ , which further supported the linear increase in core shell nanoparticle with increase in the (OCH<sub>2</sub>CH<sub>2</sub>) units at the periphery.



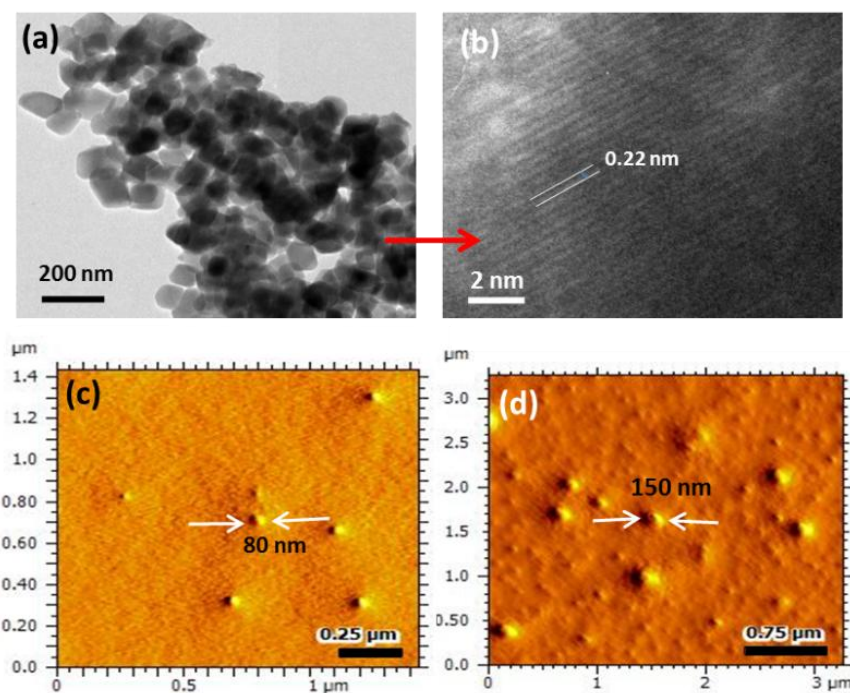


**Figure 4.13.** High resolution TEM image (a) and lattice fringes (b) of  $PEG_{2000}$ -*b*-CPCL-CP. AFM images of CPCL-CP (c) and  $PEG_{2000}$ -*b*-CPCL-CP (d) in the tapping mode.

The core shell nanoparticles were subjected to atomic force microscopy (AFM) and high-resolution transmission electron microscope (HR-TEM) analysis. The HR-TEM images of  $PEG$ -*b*-CPCL-CP are shown in figures 4.13a and 4.13b. The nanoparticles appeared as spherical objects having a dark contrast at the hydrophobic core filled with platinum metal. In fig 4.13b, the lattice fringes were observed and the space between two subsequent fringes was obtained as 0.23 nm as reported in literature.<sup>29</sup> AFM analysis was carried out for two conjugates (CPCL-CP and  $PEG_{2000}$ -*b*-CPCL-CP) and their images are shown in figures 4.13c and d respectively. The AFM image of CPCL-CP confirmed the existence of the nanoparticle of size  $75 \pm 10$  nm and  $PEG_{2000}$ -*b*-CPCL-CP showed the formation of  $150 \pm 10$  nm nanoparticles. Thus, both AFM and HR-TEM analysis support the observation of spherical core-shell nanoparticle morphology by FESEM (also DLS).



#### 4.3.4 Core-shell Nanoparticle stability in Saline, PBS and FBS

To study the effect of the PEG shell on stability of nanoparticle and cisplatin release from nanoparticle core; the release studies were carried out under various *in vitro* conditions. The stability of the core-shell nanoparticles were investigated in milli-Q water (pH=6.8), saline (pH = 7.2), PBS (pH = 7.4) and FBS (pH= 7.2) and the results are shown in figure 4.15. Earlier it had been reported that the cisplatin prodrugs were susceptible to cleave in the presence of chloride ions. To test the role of PEG-shell on the de-chelation, two polymer-cisplatin drug conjugates CPCL-CP and PEG<sub>5000</sub>-*b*-CPCL-CP were chosen and subjected to release studies in saline and water. For this purpose, typically, the polymer-cisplatin conjugates were dialyzed at 37°C in the respective media (saline or water) in a semi-permeable membrane having MWCO = 1000.

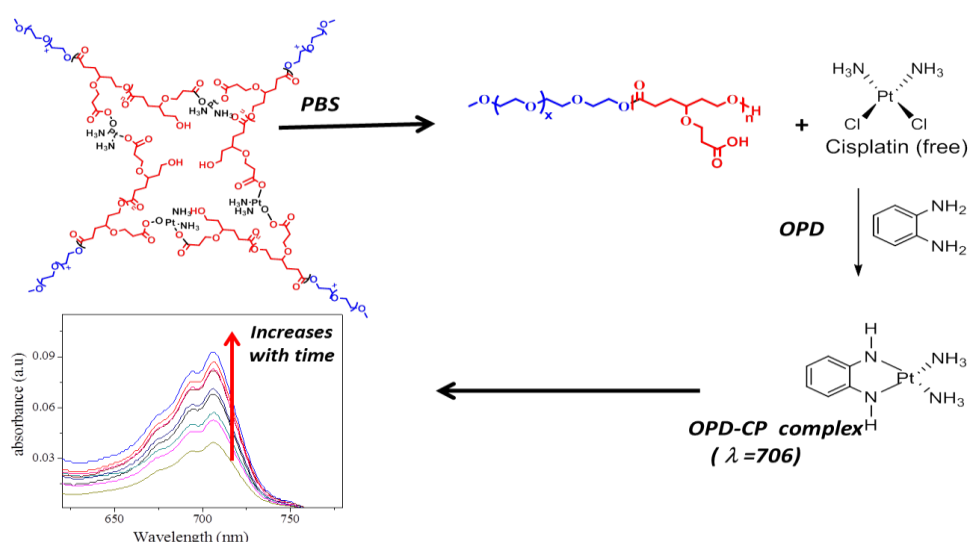


**Figure 4.14.** OPD assay for the determination of cisplatin content in dialysis method.

The amount of cisplatin released in the media was quantified using *o*-phenylenediamine (OPD) colorimetric assay and the details are given in figure 4.14. The cumulative release was calculated as follows:

Cumulative release (%) =  $C_n \cdot V_o / m \cdot 100\%$  where  $C_n$  is the amount of loaded cargo in the  $n^{\text{th}}$  sample,  $V_o$  is the total volume and  $m$  is total amount loaded in prodrug.

The cumulative cisplatin release patterns of CPCL-CP and PEG<sub>5000</sub>-*b*-CPCL-CP in milli Q water are shown in figure 4.15a. The nanoparticles showed < 10 % cisplatin release in milli Q water. This suggested that the polymer-cisplatin

nanoparticles were stable and they could be stored in milli Q water. The drug release in saline showed difference in the release profiles with respect to the size of the PEG shell. The CPCL-CP nanoparticle did not have PEG shell protection; as a result, the chloride ions present in the saline (0.9 %), cleaved the cisplatin core easily and released the entire drug. Interestingly, the PEG shell protection in PEG<sub>5000</sub>-*b*-CPCL-CP (see figure 4.15a) controlled the Cl<sup>-</sup> attack on the cisplatin core; thus, only 50 % of the drugs got released immediately. The remaining 50 % of the drugs were bound to the polymer and retained against leaching for a prolonged period > 48 h.

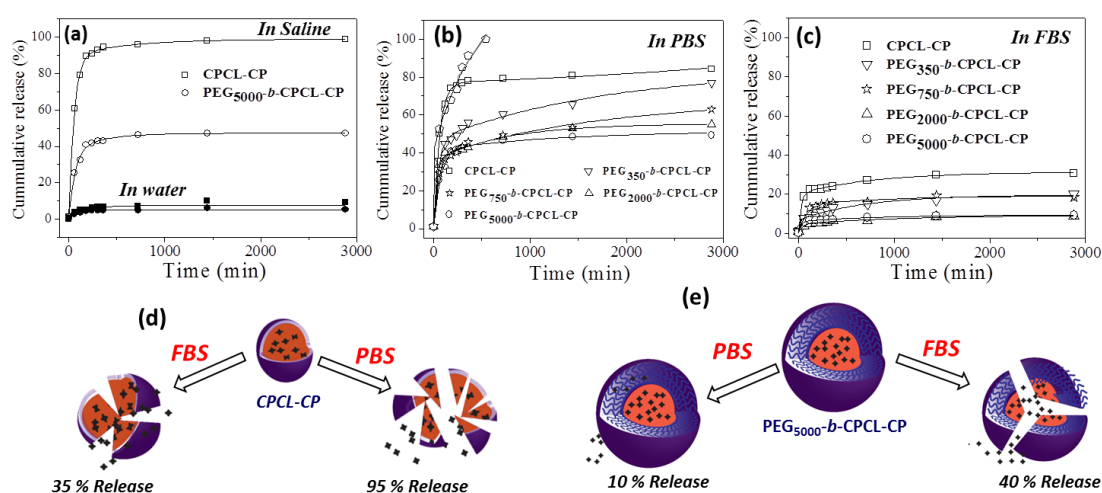


**Figure 4.15.** Cumulative release of cisplatin from nanoparticles in saline and water (a), in PBS (b) and in FBS (c) at 37 °C. The possible cleavage mechanism for the drug release from CPCL-CP (d) and PEG<sub>5000</sub>-*b*-CPCL-CP (e).

The stability of the polymer-cisplatin drug nanoparticle in phosphate saline buffers (PBS) is shown in figure 4.15b. The phosphate ions PO<sub>4</sub><sup>2-</sup> in PBS was capable of dechelating the polymer-cisplatin drug.<sup>54</sup> In CPCL-CP nanoparticle (without any PEG shell protection) showed > 85 % of cisplatin leaching. The PEG shell protection in PEG<sub>x</sub>-*b*-CPCL-CP nanoparticles avoided the leaching in saline (figure 4.15a). The drug release trend in PBS was found to almost similar to that of saline. Interestingly, in FBS (Fetal bovine serum, pH= 7.2) the polymer-cisplatin nanoparticles showed significant enhancement in stability compared to PBS (also in saline). The nanoparticle without PEG shell (CPCL-CP) showed < 20 % leaching. Whereas, the PEG shell protected nanoparticle (PEG<sub>5000</sub>-*b*-CPCL-CP) was found to be very stable (< 10 % leaching in FBS). The schematic representation of breakage of the polymer

core-shell nanoparticle in saline, PBS and FBS with respect to PEG shell protection are shown in figure 4.15d and 4.15e. The PEG shell protection was found to be very crucial factor for stabilizing the cisplatin drug conjugates for intravenous administration. The PEG shell enhanced the solubility of the core-shell nanoparticles against anions such as  $\text{Cl}^-$  and  $\text{PO}_4^{2-}$  etc. Further, the enhanced stability in FBS was an added advantage for the intravenous delivery of these nanoparticle systems. This results support that once the polymer-drug conjugate enter into the blood stream; they could be very stable against proteins and other biological species present in the serum (as shown in hand model figure 4.6a for intravenous administration). Thus, based on above results the polymer-cisplatin nanoparticles can be stored in milli Q water and can be used for direct administration into the blood stream for maximizing the efficacies in cancer treatment.

#### 4.3.5 GSH Resistance and Enzyme-responsive cleavage

Sulphur containing biological species such as cysteine (amino acid residues) and oligopeptides like glutathione (GSH) were reported to be detoxifying for cisplatin drugs in cancer therapy.<sup>10</sup> Reactions of the GSH and cysteine with cisplatin were known to produce S-Pt bond that could be monitored by absorption spectroscopy.<sup>36</sup> To study the stability of the core-shell nanoparticles against cytoplasmic thiol residues, several model release studies were performed. The reactions were carried out in dark at 37 °C in 0.1 mM Tris-HCl buffer containing 4.6 mM NaCl at pH 7.4. The UV-Vis absorbance spectra for reaction product of free cisplatin with GSH are shown in figure 4.16a. Cisplatin reaction with GSH produced new absorbance peak at 260 nm which was assigned to the formation of Pt-S bond (see figure 4.16a).<sup>40</sup> Interestingly, the reaction product of GSH with  $\text{PEG}_x\text{-}b\text{-CPCL-CP}$  core-shell nanoparticles did not show any new peak for Pt-S bond (see figure 4.16b). Similar results were also observed for the reaction with cysteine, the S-containing amino acid. The absorbance was plotted against time for GSH and cysteine action on free cisplatin and two polymer nanoparticles CPCL-CP and  $\text{PEG}_{2000}\text{-}b\text{-CPCL-CP}$ . From figures 4.16c, it was very clear that the free cisplatin reacted with these thiol species and produced Pt-S bond. This provided direct evidence that cisplatin underwent detoxification in cytoplasm due to S-rich biological species as pictorially represented in figure 4.16e. On the other hand, the polymer-cisplatin core-shell nanoparticles were found to be resistant to these cytoplasmic thiol species. There was no increase in the absorbance peak corresponding

to Pt-S bond formation (see figure 4.16d). This observation supported that the newly designed core-shell nanoparticles were able to stabilise the platinum drug against cytoplasmic thiol species for efficient delivery to cancer cells as shown schematically in figure 4.16f.

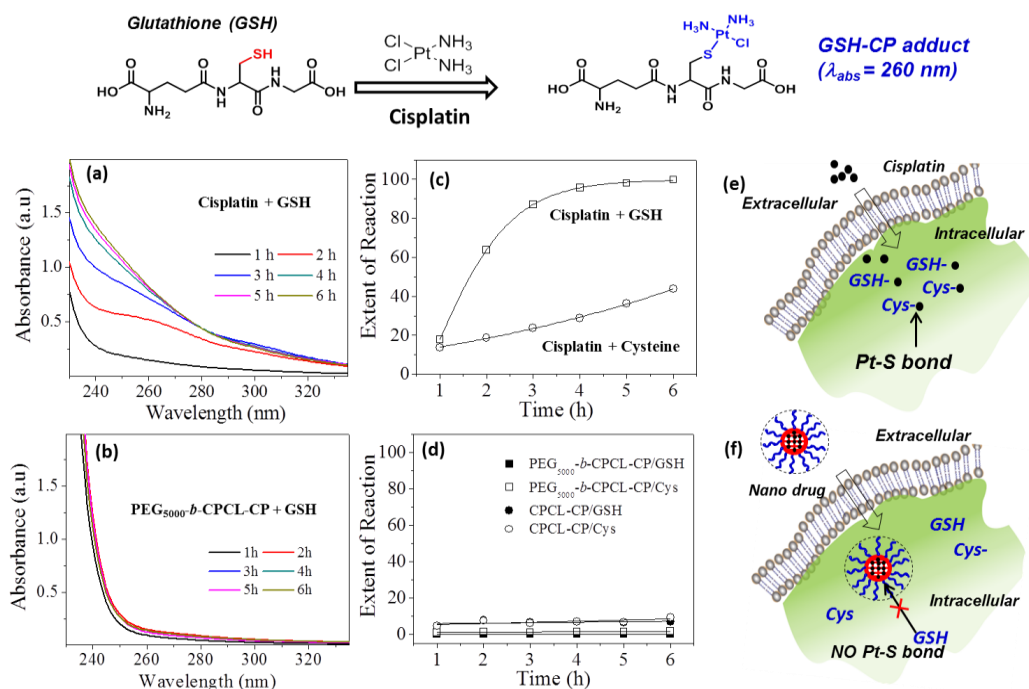


**Figure 4.16.** Reaction of GSH and cisplatin; Absorbance spectra of free cisplatin drug (a) and core shell nanoparticle (b) in reaction with GSH. The extent of the reaction (monitored at absorbance maxima at 260 nm) against time of the reaction for free cisplatin (c) and core shell cisplatin nanoparticles (d) upon exposure to Cysteine and GSH. Schematic representation of free cisplatin (e) and cisplatin polymer nanoparticles (f) entry into the cytoplasm and their possible interaction with GSH or cysteine in the Pt-S bond formation.

To track the intracellular fate of the nanoparticle in the presence of enzyme rich lysosomes and cytoplasmic thiols two different types of experiments were performed with PEG<sub>2000</sub>-b-CPCL-CP conjugate (see figure 4.17). In type 1 experiment, the samples were subjected to the lysosomal compartment conditions wherein esterase leads to the cleavage of this polymer cisplatin conjugate made up of biodegradable PCL units. To address this concept, the cumulative release profiles of the polymer-drug conjugates were studied in the presence of 10 U of esterase.<sup>43-45</sup> Amount of cisplatin released were monitored using OPD assay. This esterase enzyme was added in two ways: (i) at the initial stage at 37 °C and (ii) addition after the

incubation of nanoparticles for 24 h at 37 °C. The cumulative release profiles for addition of esterase at the initial stage (see figure 4.17a) revealed that the PCL backbone was cleaved by the enzyme and the cisplatin release occurred at fast rate. In the second experiment, the incubation of nanoparticle showed an initial 40 % leaching (as observed in figure 4.15b). The administration of esterase after 24h facilitated the instantaneous rupturing of the PCL core and release of the remaining drug (see figure 4.17a). Hence, it can be concluded that the core-shell nanoparticle preserved the drug and only ruptured in the presence of lysosomal enzymes to release the loaded cargoes at the intracellular compartments.

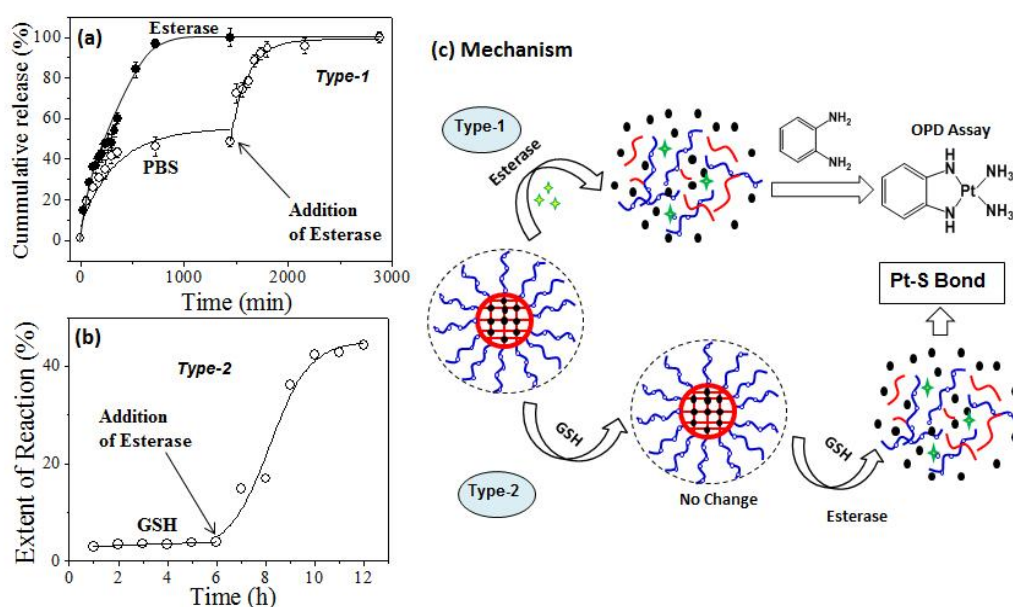


**Figure 4.17.** Cumulative drug release of cisplatin from  $PEG_{2000}$ -b-CPCL-CP with respect to the administration of esterase at initially or after incubating in PBS for 24 h (a). The extent of GSH attack (monitored at 260 nm absorbance) on  $PEG_{2000}$ -b-CPCL-CP for initial 6 h and after the administration of esterase enzyme in Tris-buffer (b). Schematic representation of nanoparticle dissociation by esterase enzyme alone (type -1) and its resistance to GSH and subsequent cleavage followed by the entry of esterase enzyme (type 2) (c).

The type 2 experiment was performed to understand the nature of interaction between the GSH and polymer cisplatin conjugate. In type 2, the GSH was administered first to mimic entry of the cisplatin conjugate and immediate exposure to GSH in the cytoplasm upon taken by cells. The data in figure 4.17b confirmed that the cisplatin polymer conjugate was stable against GSH for the period of more than 6 h. The subsequent administration of esterase (after 6 h of GSH exposure), the polymer backbone immediately disassociated to release the cisplatin drug. At this stage, the

drug has exposure to already present GSH in the medium to produce Pt-S bond. In the actual in vitro cellular administration, the drug would have equal chance to reach the nucleus to promote cell death. This control experiment attempts to mimic the intracellular environment from which it is clearly evident that the polymer cisplatin conjugate is stable against GSH and it could be cleaved by the esterase enzyme present in the lysosomal compartments. The cleavage of the polymer cisplatin nanoparticles in presence of esterase and GSH in type-1 and type-2 model experiments are schematically shown in figure 8c. The results clearly demonstrated that drug detoxification against the GSH and ensuring efficient cisplatin administration to nucleus of the cell to enhance the cell death.

#### 4.3.6 Cellular Uptake and Cytotoxicity

The cytotoxicity of the diblock copolymers and their Cisplatin conjugates were investigated in wild type mouse embryonic fibroblasts (WT-MEFs), breast cancer (MCF 7) and cervical cancer (HeLa) cell lines. Breast cancer cells (MCF 7) are inherently 10 times over-expressed with cytoplasmic thiol residues such as GSH (in mM) compared to other cancer cells (Hela).<sup>7</sup> The cytotoxicity of the nascent diblock copolymers were first tested in HeLa cell lines by varying their concentration. The data showed in figure 4.18a indicated more than 50 % cell viability for 10  $\mu\text{g}/\text{mL}$  concentration.<sup>23</sup>

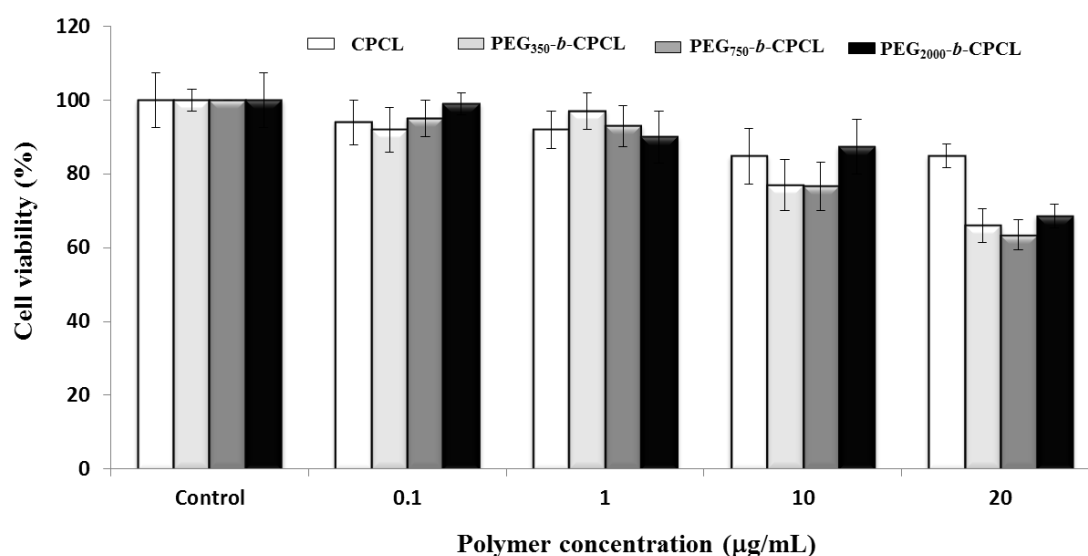


**Figure 4.18.** Histogram depicting cytotoxicity of diblock polymers in HeLa cells at various concentrations.

At higher concentration the cell viability gradually decreased with increase in the polymer content. These results confirmed that the custom designed diblock copolymers possessed high biocompatibility up to 10 $\mu$ g/mL which is typically employed concentration for synthetic polymers in drug delivery.<sup>21</sup>

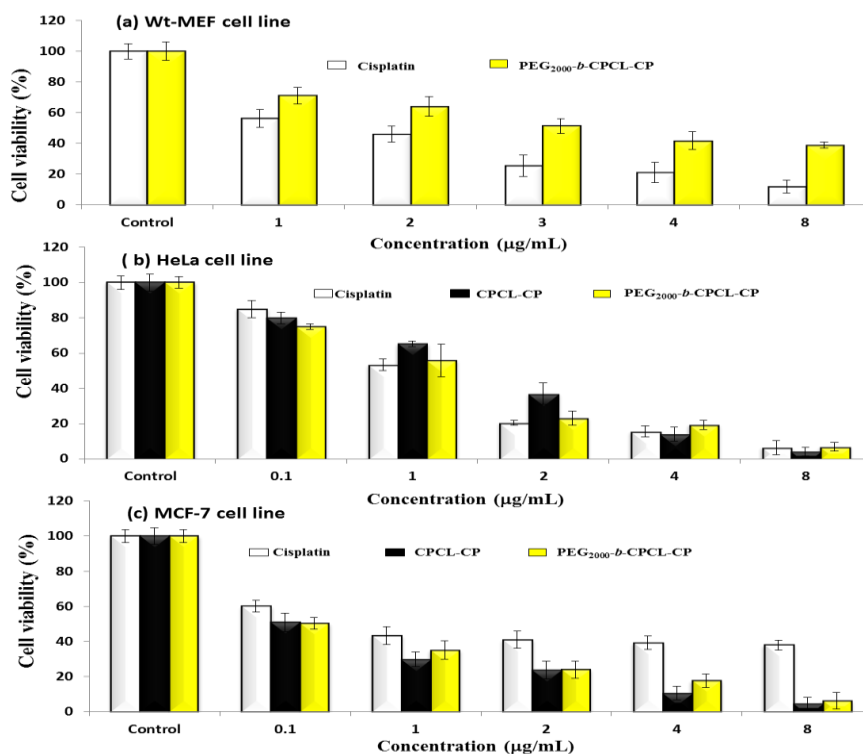


**Figure 4.19.** Histogram depicting Cytotoxicity of cisplatin and PEG<sub>2000</sub>-b-CPCL in WT-MEF (a) at various concentrations. Cytotoxicity of cisplatin, CPCL-CP and PEG<sub>2000</sub>-b-CPCL in HeLa (b) and MCF cells (c) at various concentrations.

Cytotoxicity of free cisplatin drug and polymer drug conjugates without protection (CPCL-CP) and with PEG shell protection (PEG<sub>2000</sub>-b-CPCL-CP) were tested in normal (WT-MEFs) and cancer (MCF 7 and HeLa) cell lines. The free cisplatin drug concentration was maintained as equivalent to drug conjugates in the polymer (DLC = 33 %). The concentration of cisplatin drug was varied from 0.1  $\mu$ g/mL to 8.0  $\mu$ g/mL and their cytotoxicity data are summarized for WT-MEFs, HeLa and MCF 7 cells in figures 4.19a, 4.19b and 4.19c, respectively. In figure 4.19a, the data supported that the free cisplatin was toxic to normal cells; however, the cisplatin polymer nanoparticles were non-toxic. In HeLa cell lines, both free cisplatin drug and polymer-drug conjugates showed 50 % killing in cells at 1.0  $\mu$ g/mL concentrations

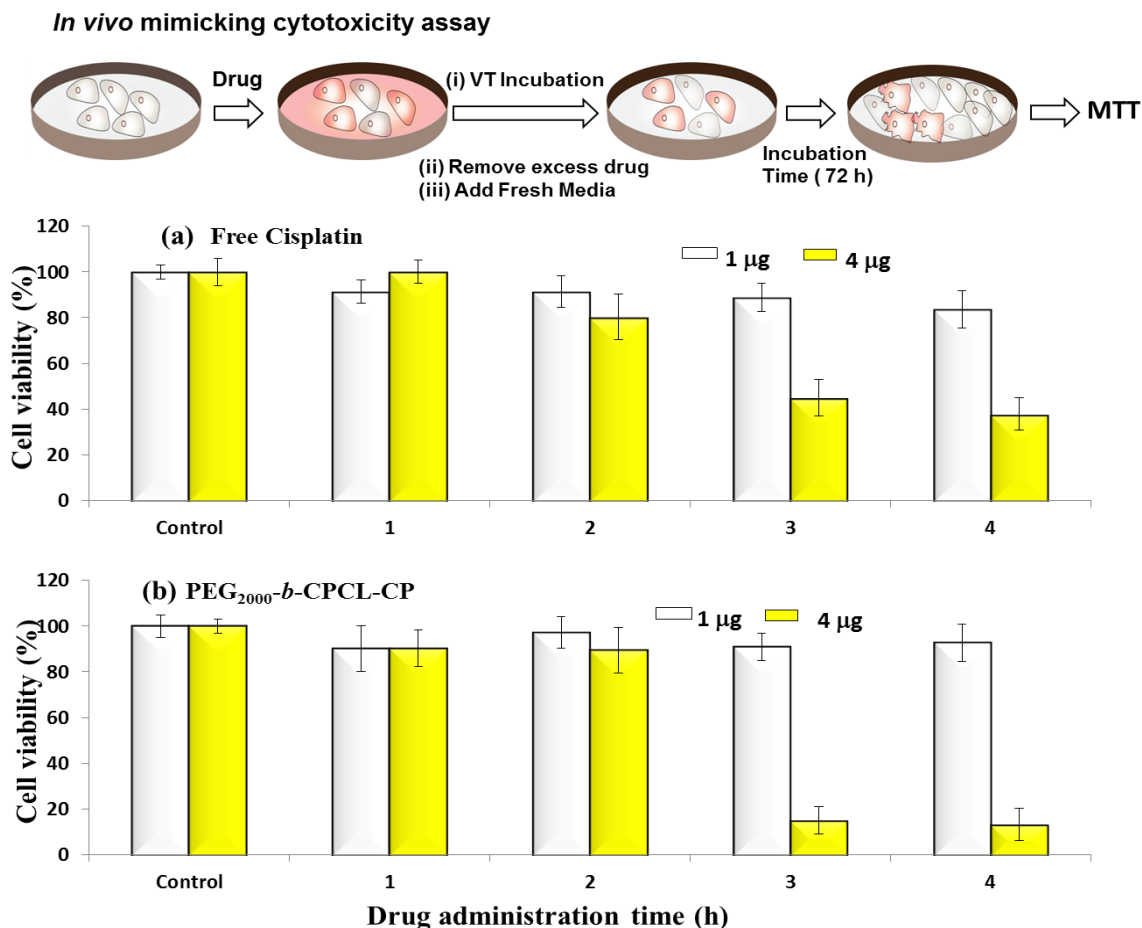
which is in accordance with earlier observations.<sup>55</sup> At higher drug concentration  $> 4.0$   $\mu\text{g/mL}$ ; less than 10 % cells were viable (see figure 4.19b). Interestingly, the breast cancer cells showed a dramatic difference for free cisplatin and polymer-conjugated drugs (see figure 4.19c). Free cisplatin drug showed 50 % killing in cells at 1.0 – 2.0  $\mu\text{g/mL}$  which is similar to that of earlier observation.<sup>56</sup> The cell viability for free cisplatin drug did not change much at higher concentrations and 40 % of cells were viable even at larger drug concentrations of 10  $\mu\text{g/mL}$ .

On the other hand, the polymer-cisplatin drug conjugate showed significant improvement in the cell killing. The % cell death increased significantly with increase in the concentration of polymer-cisplatin drug conjugates and only  $< 10$  % of the cells were viable at 4.0  $\mu\text{g/mL}$  (see figure 4.19c). The free cisplatin drug was ineffective to achieve complete cell killing in MCF 7 which was overcome upon conjugating the drug in the diblock structures. The ineffective cell death for the free drug can be attributed to the over expression of GSH in MCF 7 cells and the detoxification of free cisplatin drugs. On the other hand, the cisplatin in the core of the polymer assembly provided shielding against the detoxification (see figure 4.16) and enhanced the drug stability for increasing cell death. Further, the polymer cisplatin conjugates could also be cleaved in a controlled manner by the intracellular enzymes like esterase so that the drug is released in a controlled manner for a longer period of time to achieve complete cell killing (evident in figure 4.16a). Thus, the polymer drug conjugates carry these additional advantages to accomplish complete cell death which is not possible in free cisplatin drugs. The present *in vitro* studies provided direct evidence for the need to conjugate cisplatin drugs in the polymer scaffold to achieve complete cell death in the presence of GSH which is over expressed in breast cancer tissues.

Peer and co-workers developed *in vitro* cell line experiments that could mimic *in vivo* type conditions for nanoparticle treatment in cancer cells.<sup>(57, 58)</sup> As per this experimental protocol, free and polymer bound drugs were administered and incubated for short period (typically 1 to 4 hrs). The excess drug was washed and removed and they were further allowed for cell proliferation for longer time (up to 72 h). In this process, the drugs were initially taken up by the cells (prior to the washing) control the cell proliferation and their growth similar to that of *in vivo* conditions (see the illustration in figure 4.20). In the present investigation, a similar experiment was carried out for free drug and cisplatin polymer



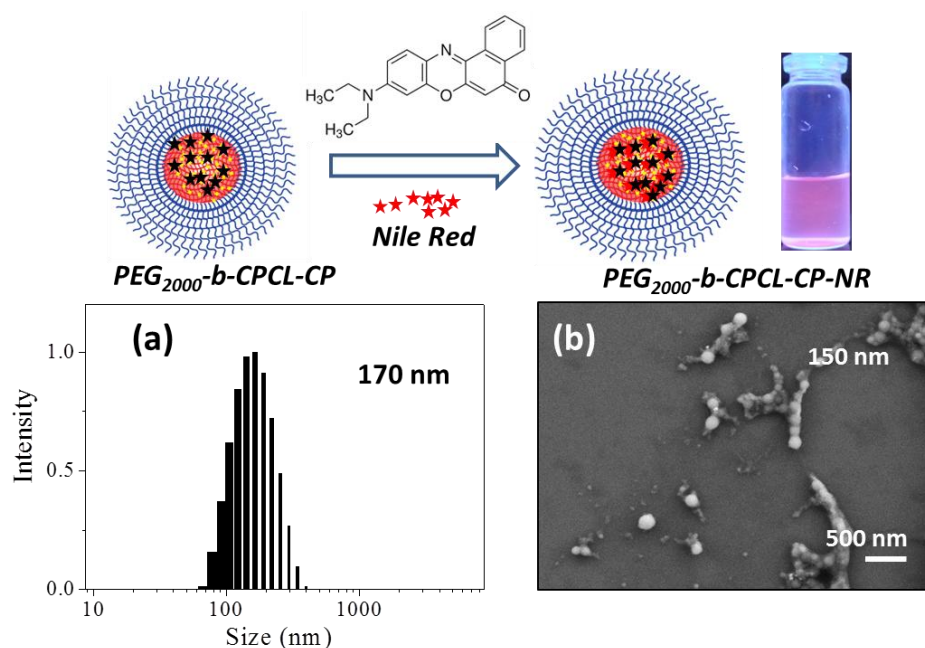
nanoparticle in MCF 7 cells and the details are given in figure 4.20. The cells were initially administered and incubated for 1, 2, 3 and 4 hrs with free cisplatin and in the polymer conjugated form.



**Figure 4.20.** Illustration of *in vivo* mimicking assay. Histogram showing the *in vivo* mimicking cytotoxicity experiment. Cisplatin and PEG<sub>2000</sub>-b-CPCL-CP in MCF 7 cells at various drug administration or incubation time period at different concentrations (1 and 4  $\mu\text{g}/\text{mL}$ ). The cells were washed after the said incubation time and allowed to proliferate for 72 h post washing.

The drug concentrations in the above experiment were varied as 1.0 and 4.0  $\mu\text{g}/\text{mL}$  (based on the MCF 7 data in figure 4.19c) and the cells were incubated for 72 h. According to figures 4.20a and 4.20b, it is clear that at lower drug concentration (1.0  $\mu\text{g}/\text{mL}$ ) both free and cisplatin polymer nanoparticle did not exhibit significant cell killing. Thus at lower drug concentration, the *in vitro* experiments in which the cells were allowed to proliferate continuously (see figure 4.19c) behave similar to that of *in vivo* mimicking experiment. Interestingly, at higher drug concentration (at 4.0  $\mu\text{g}/\text{mL}$ ), the free drug and cisplatin polymer

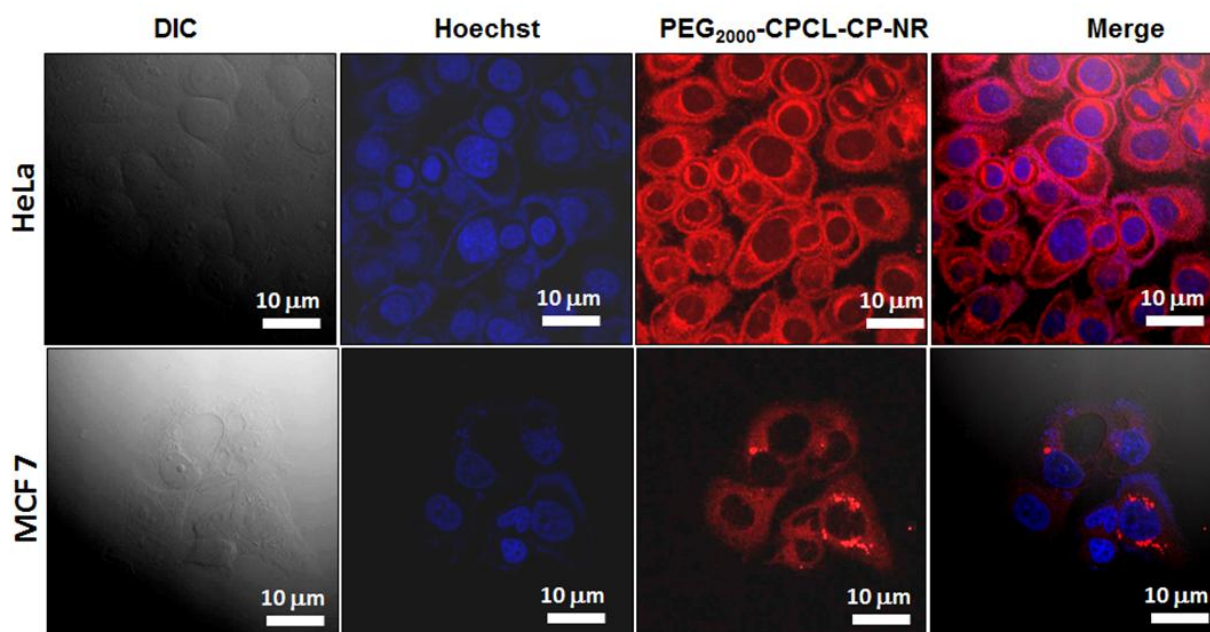
nanoparticle exhibited significant difference in the cell killing. For example, the free drug showed only 50 % cell death whereas the cisplatin polymer nanoparticle accomplished almost 90 % cell death. This *in vivo* mimicking experiment confirmed the efficient cell killing by the cisplatin polymer nanoparticle as similar to that of observed in the *in vitro* data (see figure 4.19c). Hence, it may be concluded that the custom designed cisplatin polymer nanoparticles are very efficient prodrugs for breast cancer treatment. Further, *in vivo* experiments in mice model would provide more insight into the drug action which will be done in the future studies.



**Figure 4.21.** The illustration of the  $PEG_{2000}$ -*b*-CPCL-CP-NR core-shell nanoparticle and its solution under UV light. DLS histogram (a) and FESEM image (b) of  $PEG_{2000}$ -*b*-CPCL-CP-NR.

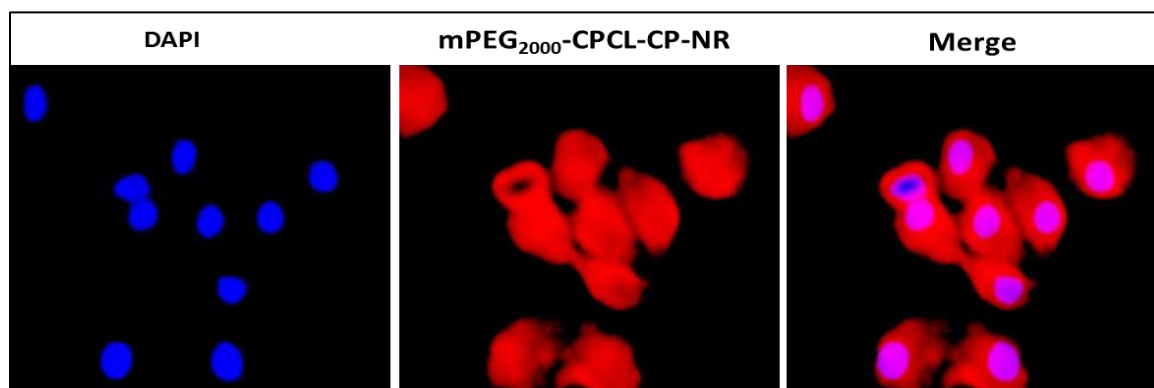
The cellular uptake of the polymer cisplatin nanoparticles in the cytoplasm was scrutinised in HeLa and MCF-7 cells using confocal laser scanning microscopy (CLSM) and fluorescence microscopy. Since, cisplatin is non-luminescent in nature, it needs to be co-encapsulated with a fluorescent molecule. Nile red (NR) was chosen as a probe which was encapsulated in the hydrophobic PCL core. Further cisplatin aquo complex and NR were stirred together with  $PEG_{2000}$ -*b*-CPCL<sub>100</sub>-CP at 37 °C for 24 h. The unencapsulated dyes were removed by dialysis (MWCO=1000). Structural characterization of this NR loaded polymer cisplatin nano-particle was done and the details are shown in figure 4.21. DLS histograms and FESEM image of  $PEG_{2000}$ -*b*-CPCL<sub>100</sub>-CP-NR exhibited 150-170 nm size particles (see figure 4.21a and b). The illustration and the image of the NR loaded nanoparticle solution under UV light depicted in

figure 4.21, shows the NR loading. These NR loaded nanoparticles (PEG<sub>2000</sub>-*b*-CPCL-CP-NR) were incubated to HeLa and MCF-7 cells for 4 h at 37 °C. The nanoparticle concentration used for treatment was 10 µg/mL with 3.3 µg of cisplatin and 0.17 µg of NR. The red fluorescence from NR at ~ 560 nm was monitored through the red channel (λ = 568 nm). The blue fluorescence produced by the cell nuclei after Hoechst staining was observed through the blue channel (λ = 461 nm).



**Figure 4.22.** CLSM images of HeLa cells and MCF 7 cells incubated with PEG<sub>2000</sub>-*b*-CPCL-NR nanoparticles. The nucleus was counter stained with Hoechst (blue). The cells were observed through red channel to locate NR fluorescence

The images corresponding to PEG<sub>2000</sub>-*b*-CPCL-CP and Hoechst fluorescence in HeLa and MCF-7 cell along with the merged image are shown in figure 4.22. As shown in the images, strong NR fluorescence was observed at the intracellular compartment in the cytoplasm and at the peri-nuclear region. At present, it is rather difficult to make any conclusion on the difference in the uptake of the nanoparticles based on the fluorescence intensity of the cell images. The cellular uptake of the nanoparticles was also studied by using fluorescent microscopy technique in HeLa cells and images are shown in figure 4.23. Fluorescence microscopy images also supported the peri-nuclear localization of cisplatin loaded nanoparticle inside the cells. The images revealed that the polymers were capable of delivering the cargoes both at the cytoplasm as well as the peri-nuclear environment.



**Figure 4.23.** Fluorescence microscopy images of  $PEG_{2000}$ -*b*-CPCL-CP-NR nanoparticles

Based on these studies, it may be concluded that these nanoparticles accumulate in the cytoplasm and also in the peri-nuclear region. Further, *in vivo* studies are required to check these nanoparticles administration in animal models. Nevertheless, the present investigation provided proof for the need to conjugate cisplatin drugs to achieve resistance to detoxification by GSH in breast cancer cells and for enhancing their efficacy. Though, the approach has been demonstrated only for cisplatin, in principle, it can be expanded to other platinum based drugs for resistance against cytoplasmic thiol residues. Further, the core-shell strategy is also, in principle, expanded to other metal nanoparticles for stabilizing them in aqueous medium. Currently, efforts are taken to proceed in these directions to expand the diblock polymer core-shell approach for various biomedical applications.

#### 4.4. Conclusion

In summary, new classes of biodegradable diblock copolymer core-shell nanoparticle assemblies were designed and developed for cisplatin delivery against detoxification of cytoplasmic thiol residues in breast cancer cells. The complexation of cisplatin aquo complex with the above said diblock copolymers produced core-shell nanoparticles. In this process, the core of the particles was fixed as 75 nm and the hydrophilic PEG shell was varied by varying the PEG chain length in the ROP process. The core-shell nanoparticles were found to be very stable in FBS and water. In PBS and saline, the drug stability increased with increase in the PEG shell protection layer. *In vitro* drug release studies revealed that the PEG shell protected cisplatin drug against the attack by the cytoplasmic thiol residues GSH and they were free from detoxification. Further, the biodegradable aliphatic PCL ester backbone was found to be shielding the GSH

action against cisplatin core and it ruptured only upon exposure to esterase enzyme at conditions identical to that of intracellular compartments. Cytotoxicity of the polymer and polymer-cisplatin conjugates was tested in MCF 7 and HeLa cell lines. The nascent polymers were found to be biocompatible and non-toxic to cells. In HeLa cell lines, both the free cisplatin drug and polymer-cisplatin core-shell nanoparticle showed almost identical cytotoxicity. Free cisplatin drug failed to kill all the cells in MCF 7 and the cells were viable more than 50 % even at very high drug concentration. Over-expression of GSH in MCF 7 was attributed to poor killing by free cisplatin drug. The polymer-cisplatin nanoparticles showed enhanced cell killing in MCF 7 and the cell viability is found to be < 10 % at 4  $\mu\text{g/mL}$  drug concentration. This selective and enhanced cell killing in MCF 7 cells by the polymer nanoparticle was attributed to their resistance to drug detoxification by GSH. Cellular uptake of the nanoparticles in the cytoplasm and peri-nuclear environment assemblies were confirmed by confocal and fluorescence microscopic analysis using Nile red as fluorophore. The present polymer-cisplatin core-shell approach provides new platform for delivery of platinum based drugs against cytoplasmic thiol detoxification which is very useful for achieving 100 % killing in breast cancer cells that have over expression of GSH.

## 4.5 References

1. Klein, A. V.; Hambley, T. W. *Chem. Rev.* **2009**, *109*, 4911-4920.
2. Foertes, M. A.; Alonso, A.; Perez, J. M. *Chem. Rev.* **2003**, *103*, 645-662.
3. Wang, D.; Lippard, S. J. *Nat. Rev. Drug Discovery* **2005**, *4*, 307.
4. Jamieson, E. R.; Lippard, S. J. *Chem. Rev.* **1999**, *99*, 2467.
5. Todd, R. C.; Lippard, S. J. *Metallomics* **2009**, *1*, 280.
6. Miller, R. P.; Tadagavadi, R. K.; Ramesh, G.; Reeves, W. B. *Toxins* **2010**, *2*, 2490
7. Wong, E.; Giandomenico, C. M. *Chem. Rev.* **1999**, *99*, 2451-2466.
8. Wheate, N. J.; Walker, S.; Craig, G. E.; Oun, R. *Dalton Trans*, **2010**, *39*, 8113-8127..
9. Siddik, Z. H. *Oncogene*, **2003**, *22*, 7265-7279.
10. Dabrowiak, J. C.; Goodisman, J.; Souid, A. K. *Drug Metab. Dispos.* **2002**, *30*, 1738-1744.
11. Balendiran, G. K.; Dabur, R.; Fraser, D.; *Cell Biochem. Funct.* **2004**, *22*, 343-352.
12. Perry, R. R.; Mazzeta, J.; Levin, M.; Barranco, S. C. *Cancer* **1993** *72*, 783-787.
13. Kasherman, Y.; Sturup, S.; Gibson, D.; *J. Med. Chem.* **2009**, *52*, 4319-438.
14. Syng-ai, C.; Kumari, A. L.; Khar, A. *Mol. Cancer Ther.* **2004**, *3*, 1101-1107.
15. Kelland, L.; *Nat. Rev. Cancer*, **2007**, *7*, 573-584.
16. Fang, J.; Nakamura, H.; and Maeda, H. *Adv. Drug Delivery Rev.*, **2011**, *63*, 136-151.
17. Nowotnik, D.; Cvitkovic, E. *Adv. Drug Delivery Rev.* **2009**, *61*, 1214-1219.
18. Rademaker-Lakhai, J. M.; Terret, C.; Howell, S. B.; Baud, C. B.; Boer, R. F. D. B.; Pluim, D.; Beijnen, J. H.; Schellens, J. H. M.; Droz, J-P. *Clin. Cancer. Res.* **2004**, *10*, 3386-3395.
19. Nuhn, L.; Hartmann, S.; Palitzsch, B.; Gerlitzki, B.; Schmitt, E.; Zentel, R.; Kunz, H. *Angew. Chem. Int. Ed.* **2013**, *52*, 10652-10656.
20. Doung, H. T. T.; Huynh, V. T.; De Souza, P.; Stenzel, M. H. *Biomacromolecules* **2010**, *11*, 2290-2299.
21. Huynh, V. T.; Chen, G.; De souza, P.; Stenzel, M. H. *Biomacromolecules* **2011**, *12*, 1738-1751.

22. Lee, S-M, O'Halloran, T. V.; Nguyen, S. B. T. *J. Am. Chem. Soc.* **2010**, *132*, 17130-17138.
23. Huynh, V. T.; De souza, P.; Stenzel, M. H. *Macromolecules* **2011**, *44*, 7888-7900.
24. Karim, K. J. A.; Binauld, S.; Scarano, W.; Stenzel, M. H. *Polym. Chem.* **2013**, *4*, 5542.
25. Kaida, S.; Cabral, H.; Kumagai, M.; Kishimura, A.; Tereda, Y.; Sekino, M.; Aoki, I.; Nishiyama, N.; Tani, T.; Kataoka, K. *Cancer Res.* **2010**, *70*, 7031-7041.
26. Nishiyama, N.; Okazaki S.; Cabral, H.; Miyamoto, M.; Sugiyama, Y.; Nishio, K.; Mastumura, Y.; Kataoka, K. *Cancer Res.* **2003**, *63*, 8977-8983.
27. Osada, K.; Cabral, H.; Mochida, Y.; Lee, S.; Nagata, K.; Matsuura, T.; Yamamoto, M.; Anraku, Y.; Kataoka, K. *J. Am. Chem. Soc.* **2012**, *134*, 13172-13175.
28. Ding, D.; Li, K.; Zhu, Z.; Pu, K-Y., Hu, Y.; Jiang, X.; Liu, B. *Nanoscale*, **2011**, *3*, 1997-2002.
29. Zhang, F.; Elsabahy, M.; Zhang, S.; Lin, L. Y.; Zou, J.; Wooley, K. L. *Nanoscale* **2013**, *5*, 3220-3225.
30. Teow, Y. Valiyaveetil, S. *Nanoscale* **2010**, *2*, 2607-2613.
31. Morelli, C.; Maris, P.; Sisci, D.; Perrotta, E.; Brunelli, E.; Perrotta, I.; Panno, M. L.; Tagarelli, A.; Versace, C.; Casula, M. F.; Testa, F.; Ando, S.; Nagy, J. B.; Pascqua, L. D.; *Nanoscale* **2011**, *3*, 3198-3207.
32. Graf, N.; Bielenberg, D.; Kolishetti, K.; Muus, C.; Banyard, J.; Farokhzad, O. C.; Lippard, S. J. *ACS NANO*, **2012**, *6*, 4530-4539.
33. Wang, F. Liu, J. *Nanoscale* **2014**, *6*, 7079-7084.
34. Maity, A. R.; Chakraborty, A.; Mondal, A.; Jana, N. R. *Nanoscale* **2014**, *6*, 2752-2758.
35. Khiati, S.; Luvino, D.; Oumzil, K.; Chauffert, B. Campio, M.; Barthelemy, P. *ACS NANO* **2011**, *5*, 8649-8655.
36. Guo, S.; Wang, Y.; Miao, L.; Xu, Z.; Lin, C.M.; Zhang, Y.; Huang, L. *ACS NANO* **2013**, *7*, 9896-9904.
37. Qi, X.; Li, N.; Gu, H.; Xu, Y.; Xu, Y.; Jiao, Y.; Xu, Q.; Li, H.; Lu, J. *Nanoscale* **2013**, *5*, 8925-8929.
38. Yuan, Y.; Kwok, R. T. K.; Tang, B. Z.; Liu, B. *J. Am. Chem. Soc.* **2014**, *136*, 2546-2254.

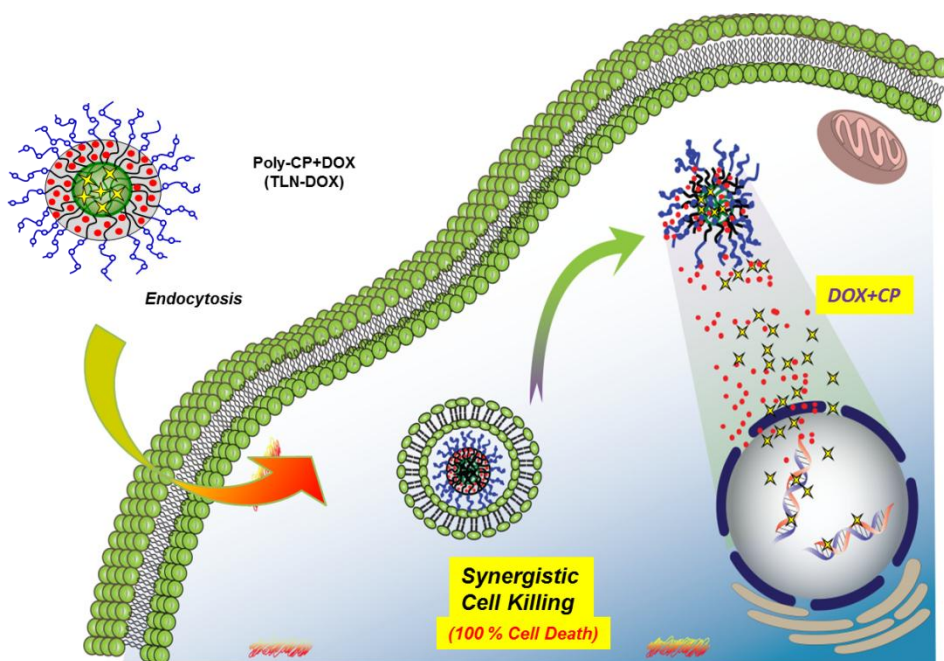
39. Setua, S.; Ouberai, M.; Piccirillo, S. G.; Watts, C.; Welland, M. *Nanoscale* **2014**, *6*, 10865-10873.
40. Min, Y.; Mao, C-Q.; Chen, S.; Ma, G.; Wang, J.; Liu, Y. *Angew. Chem. Int. Ed.* **2012**, *51*, 6742-6747.
41. Hu, Q.; Katti, P. S.; Gu, Z. *J. Am. Chem. Soc.* **2014**, *6*, 12273-12286.
42. Zhuang, J.; Gordon, M. R.; Venture, J.; Li L.; Thayumanavan S. *Chem. Soc. Rev.* **2013**, *42*, 7421-7435.
43. Pramod, P. S.; Takamura, K.; Chaphekar, S.; Balasubramanian, N.; Jayakannan, M. *Biomacromolecules* **2012**, *13*, 3627-3640.
44. Pramod, P. S.; Shaw R.; Jayakannan, M. *Nanoscale*, **2015**, *7*, 6636-6652.
45. Pramod, P. S.; Shaw R.; Chaphekar, S.; Balasubramanian, N.; Jayakannan, M. *Nanoscale*, **2014**, *6*, 11841-11855.
46. Harnoy, A. J.; Rosenbom, I.; Tirosh, E.; Ebenstein, Y.; Saharabani, R.; Beck, R.; Amir, R. J. *J. Am. Chem. Soc.* **2014**, *136*, 7531-7534.
47. Samarajeeva, S.; Shrestha, R.; Li, Y.; Wooley, K. L. *J. Am. Chem. Soc.* **2012**, *134*, 1235-1242.
48. Rainbolt, E. A.; Washington, K. E.; Biewer M.C.; Stefan, M.C. *Polym. Chem.*, **2015**, *6*, 2369-2381.
49. Surnar, B.; Jayakannan, M.; *Biomacromolecules* **2013**, *14*, 4377- 4387.
50. Surnar, B.; Pramod, P. S.; Jayakannan, M.; *Z. Anorg. Allg. Chem.* **2014**, *640*, 1119-1126.
51. Ski, R. W.; Kuduk-Jaworska, J.; Michalska, D. *J Mol Struc-Theochem.* **2006**, *758* 169-179.
52. Allen, A. D.; Theophanides, T. *Can. J. Chem.* **1964**, *42*, 1551-1554.
53. Xu, J.; Fu, Q.; Ren, J-M.; Bryant. G.; Qiao, G. G. *Chem. Commun.* **2013**, *49*, 33-35.
54. Todd, R. C.; Lovejoy, K. S.; Lippard, S. J. *J. Am. Chem. Soc.* **2007**, *129*, 6370-6371.
55. K. Osada, H. Cabral, Y. Mochida, S. Lee, K. Nagata, T. Matsuura, M. Yamamoto, Y. Anraku, K. Kataoka, *J. Am. Chem. Soc.* 2012, **134**, 13172-13175.
56. T. C. Johnstone, N. Kulak, E. C. Pridgen, O. C. Farokhzad, R. Langer, S.J. Lippard, *ACS NANO* **2013**, *7*, 5675-5683.
57. Kohen, K.; Emmanuel, R.; Kishin-Finifer, E.; Shabath, D.; Peer, D. *ACS Nano*, **2014**, *8*, 2183-2195.



58. Bachar, G.; Kohen, K.; Hod, R.; Feinmesser, R.; Mizrachi, A.; Shpitzer, T.; Katz, O.; Peer, D. *Biomaterials*, **2011**, *32*, 4840–4848.

## Chapter 5

### *Triple Layer Nanoparticle Approach for Cisplatin-Doxorubicin Combination Therapy*



---

## ***Triple Layer Nanoparticle Approach for Cisplatin-Doxorubicin Combination Therapy***

---

*Combination chemotherapy is quintessential to combat the cisplatin resistance in breast cancers by achieving synergistic cell killing. To accomplish this goal, drug GSH-detoxification and DNA repair need to be retarded as these are some of the reasons for resistance. In order to fix this new triple layer nanoparticles (TLNs) were custom designed based on biodegradable polycaprolactone i.e. polyethylene glycol (PEG)-block-(PCL)-block-carboxylic functional polycaprolactone (CPCL) triblock copolymers (TBs). The complexation of cisplatin aquo species with the triblock copolymers fabricated triple layer nanoparticles (TLNs) of  $150\pm 10$  nm size. The hydrophobic anticancer drug DOX was encapsulated in middle PCL layer of TLNs to achieve synergistic cell killing in breast cancer cells. These dual loaded nanoparticles were found to be stable in PBS; they exhibited ~ 90 % cisplatin stability due to subsumed PCL layer between PEG shell and CPCL core. The hydrophobic PCL layer also behaved as a protecting layer against the cytoplasmic GSH and completely inhibited the drug detoxification. In vitro drug release studies revealed that the dual loaded nanoparticles ruptured upon exposure to lysosomal enzymes and showed controlled release up to 2 days. Cytotoxicity studies were performed both in normal wild-type mouse embryonic fibroblasts (Wt-MEFs) cells, breast cancer (MCF 7) and cervical cancer (HeLa) cell lines. In MCF 7 cells, the free cisplatin drug exhibited 50 % cell death whereas complete cell death (100 %) with synergistic killing was accomplished by the TLNs. Confocal microscopic images confirmed that the core-shell nanoparticles were taken up by the MCF 7 cells and accumulated in the nuclear environment. The present investigation lays a new foundation for polymer based TLNs approach to overcome the GSH detoxification and DNA-Pt adduct repair in case of platinum drugs for the treatment of resistant breast cancer cells.*

## 5.1. Introduction

Cisplatin is one of the best first line chemotherapeutic agents for most of the cancers. Today it is used to medicate 32 to 78 treatments regimes as listed by Martindale.<sup>1-2</sup> However, it's usage in several tumours is hindered because of the various side effects and drug resistance.<sup>3</sup> Although cancer tissues could be intrinsically resistant to cisplatin or it could be acquired after initial treatment.<sup>4-5</sup> The anti-tumour effect of cisplatin completely depends on the formation of DNA-Pt adduct, because for cisplatin DNA is the final target in order to achieve cell killing.<sup>6-7</sup> The drug-resistance can occur in tumours because of reduction in the level of DNA platination, through several mechanisms, such as (1) through reduced drug uptake, (2) through drug detoxification by GSH in cells and (3) through DNA repair (see figure 5.1).<sup>8-11</sup>

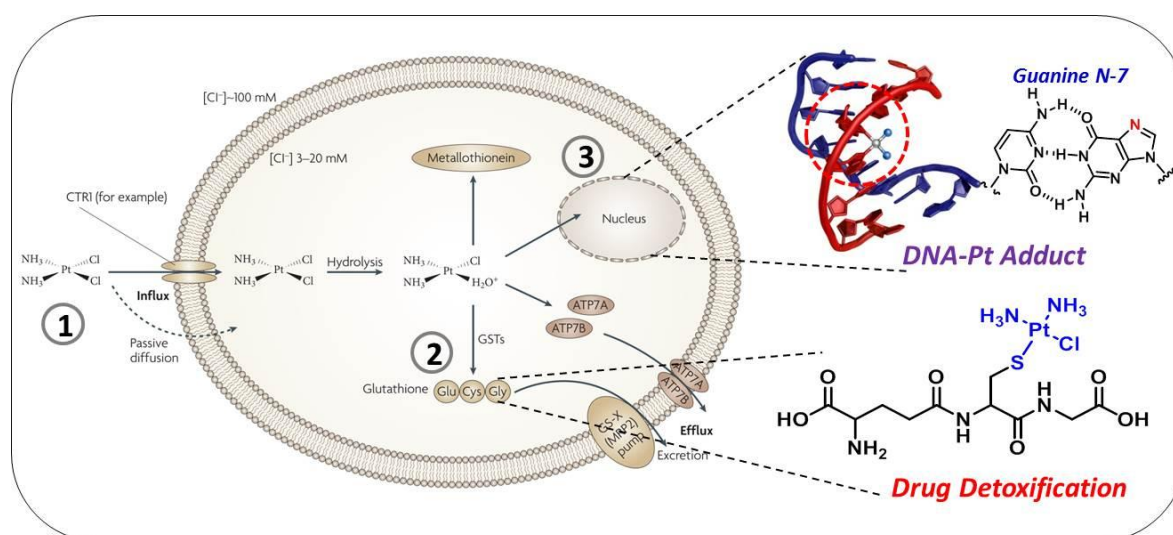
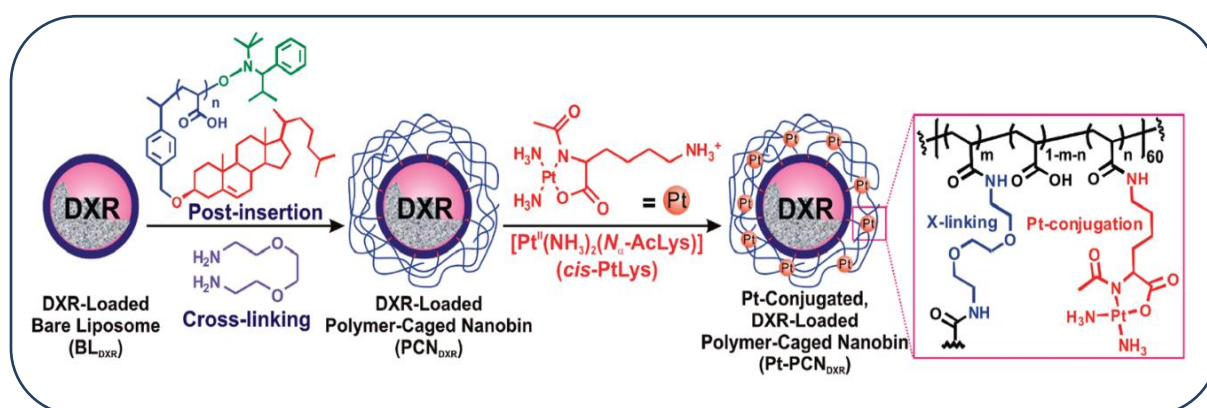


**Figure 5.1.** Schematic illustration of obstacles in cisplatin delivery such as (1) reduced cellular uptake, (2) GSH detoxification and (3) DNA-Pt adduct repair. (adapted from Kelland et al. *Nat. Rev. Cancer* **2007**, 7, 573–584).

In cisplatin resistant tumours such as breast and ovarian cancers combination chemotherapy is employed as an important tool to combat against resistance.<sup>12</sup> In contrast to single anti-tumour agent, the combination chemotherapy may show additive or synergistic or antagonistic effects.<sup>13-18</sup> In combination chemotherapy, cisplatin is mostly used in combination with doxorubicin, epirubicin and amrubicin, the anthracyclines identified as active agents.<sup>19</sup> Along with these combinations, cisplatin is also collectively given with mustards (cyclophosphamide and ifosfomide),<sup>20</sup> antimetabolites (gemcitabine, methotrexate and 5-flourouracil)<sup>21</sup> and taxols (paclitaxel).<sup>22</sup> On the other hand, the anthracyclines are comparatively cheaper and it is well known that these anthracyclines decrease the DNA-Pt

adduct repair and increase the toxicity.<sup>23</sup> Combining both agents with cisplatin has shown an increased response rate in phase III clinical trials.<sup>15-16</sup> The combination of epirubicin with cisplatin is an effective treatment for ovarian cancer which is also in clinical trials.<sup>18</sup> The clinicians came up with these magic drug combinations, but these cocktails also showed side effects due to nonspecific accumulation and interaction with ions (cations/anions) and proteins in blood plasma, which forced clinicians to use these drugs in lower doses.<sup>11</sup> To avoid these side effects nano-aggregate (polymer or metal based) based drug delivery approaches emerged as a new field to achieve efficient cisplatin + DOX co-administration.<sup>24-26</sup> These systems provide additional advantages of the passive selective accumulation at cancer tissues through enhanced permeability and retention (EPR) effect.<sup>27</sup> Therefore, the combined chemotherapy strongly demands an efficient delivery vehicle that can carry multiple cargos to the target site as well as can escape non-specific interaction with ions, protein and with GSH oligopeptide. The adoption of polymer based nano-carriers could easily decrease the side effects of cisplatin and increase their therapeutic efficacy.



**Scheme 5.1.** Preparation of cisplatin conjugated, DOX loaded polymer caged nanobins. (adapted from Nguyen et al. *J. Am. Chem. Soc.* **2010**, *132*, 17130–17138)

The co-delivery of cisplatin with DOX carried out using nano-carriers, some of them are described below. Shanmugam et al. synthesized oligonucleotide-Au nano-rods to deliver cisplatin and DOX to cervical cancer cells (HeLa).<sup>28</sup> The combination chemotherapy using polymer based nano-carrier delivery systems has been reported rarely. Chen et al. prepared nanoparticles from physical mixing of 10-hydroxy camptothecin (HCPT) and DOX without any surfactant or solubilizing agent. Wherein, they have shown the synergistic killing of breast cancer cells (MCF 7). Nguyen and co-workers used a polymer-lipid hybrid nano-carrier to co-deliver cisplatin and DOX (see scheme 5.1).<sup>29</sup> Wherein, DOX was physically

encapsulated into the liposome that was caged with cholesterol terminated poly acrylic acid conjugated with cisplatin.

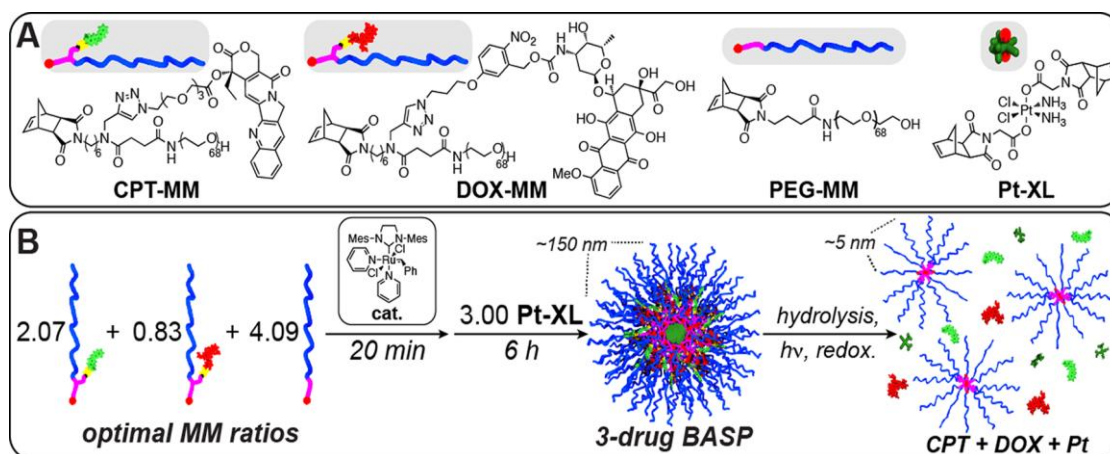
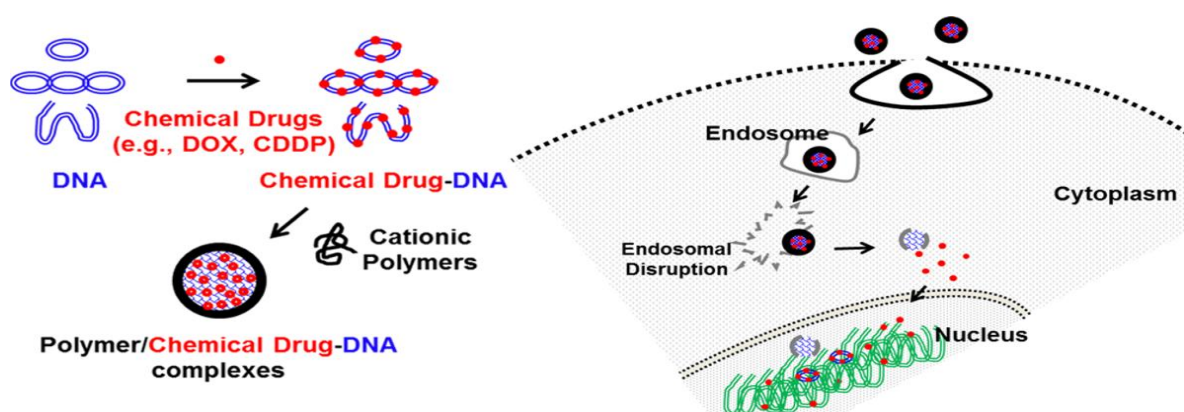


**Figure 5.2.** Structures of monomers used (A). Schematic for synthesis of three-drug-loaded brush arm star particles (BASP), (B). Drug release occurs in response to three distinct triggers adapted from Jonson *et al.* *J. Am. Chem. Soc.* **2014**, 136,5896–5899).

Jonson and co-workers prepared photo triggered poly(norbornene anhydride) based nanoparticles for combined delivery of cisplatin with doxorubicin and camptothecin to ovarian (OVCAR3) cells. They have prepared various monomers with drugs attached to it. In this work they have shown the release of the drugs due to three different stimuli's (see figure 5.2).<sup>30</sup> Kang *et. al* synthesised cisplatin and doxorubicin encapsulated DNA polyplexes for co-delivery to breast cancer cells (see scheme 5.2).<sup>31</sup> Wherein, luciferase pDNA was used as a delivery vehicle for DOX and cisplatin, and then these drug-loaded pDNA were complexed with poly ethylene imine (PEI) polycations to provide nano-aggregates. Although aforementioned polymeric combination therapy scaffolds discuss the significance of cisplatin co-drug delivery, the role of GSH detoxification has not been examined and more importantly most of these polymer scaffolds are non-biodegradable, so the fate of these scaffolds is not clear.

Henceforth, there is an urgent need for new efforts to fabricate biodegradable polymeric delivery vehicles which can chelate with cisplatin as well as encapsulate DOX, that can inhibit the GSH-detoxification and DNA-Pt adduct repair to accomplish efficient treatment against resistant breast cancer cells. Enzyme degradable polymer scaffolds are evolving as an important approach for drug administration at intracellular compartments of cancer cells. Polycaprolactone (PCL) is significant biodegradable aliphatic polyester that could be cleaved by lysosomal enzymes like esterase at the intracellular compartments for drug delivery.<sup>32</sup>





**Scheme 5.2.** Schematic preparation of polymer/chemical drug–nucleic acid complexes and the proposed concept of their intracellular delivery (adapted from Kang *et al. Mol. Pharmaceutics* **2015**, *12*, 2845–2857)

Recently, we have published a report on pH responsive carboxylic substituted PCL diblock copolymers based vesicles for oral delivery of camptothecin and ibuprofen under gastro intestinal (GI) tract.<sup>33</sup> These diblock copolymers were further employed for cisplatin delivery to the breast cancer cells against glutathione (GSH) detoxification.<sup>34-35</sup> This offered us a new opportunity to build novel triblocks which can chelate with cisplatin as well as load DOX; these biodegradable block assemblies have been employed for combination therapy to overcome the problem of resistance and achieve efficient cell death in resistant breast cancer cells.

In the present investigation we have fabricated carboxylic functionalised triblock copolymers (PEG-*b*-PCL-*b*-CPCL) which have three important components obtained from each block individually: (i) PEG chain for hydrophilic shell for improving solubility and stability of the nanoparticles in buffer medium for drug administration, (ii) the hydrophobic PCL provides the opportunity to encapsulate hydrophobic anticancer drugs such as DOX, and (iii) the carboxylic CPCL block for chelation with cisplatin aquo complex to constitute the drug-core. Also the PCL block acts as a protecting layer against the drug detoxification by cytoplasmic thiols such as GSH and also decreases the drug leaching from CPCL core. Further, this design has also provided us with an opportunity that it is made up of biodegradable PCL and CPCL layers; hence, these multi-drug loaded polymer scaffolds could be cleaved by lysosomal enzymes at the intracellular compartments. The scaffold design for combination therapy of cisplatin and DOX delivery is shown in figure 5.3

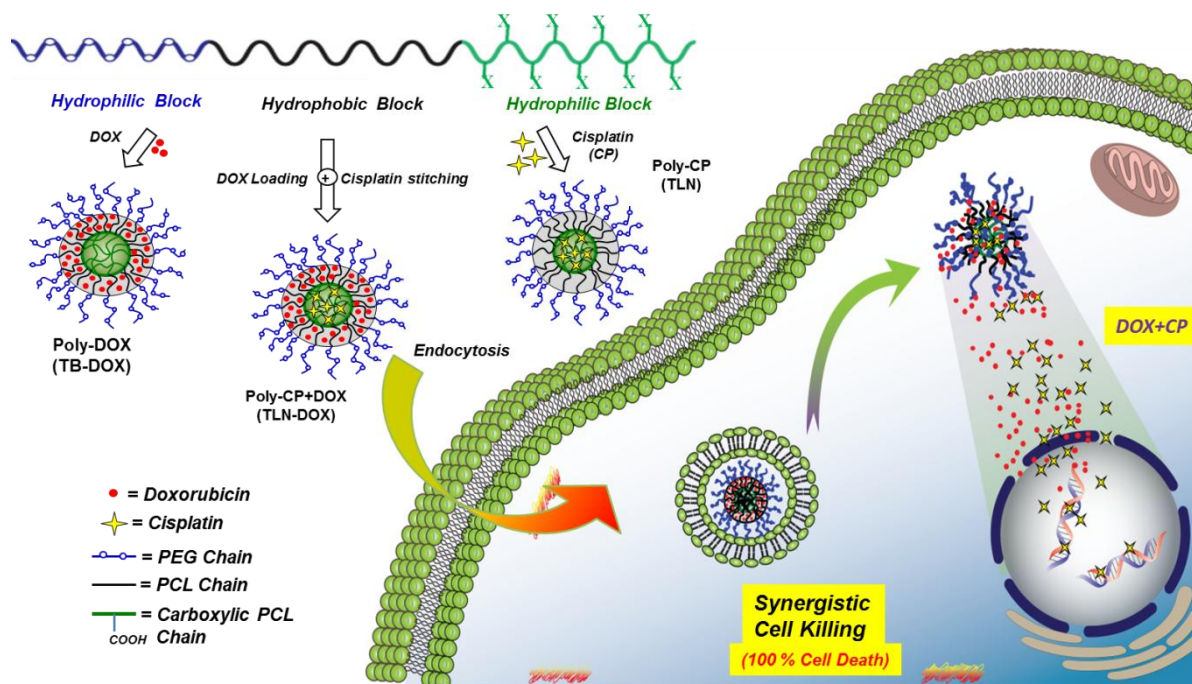


**Figure 5.3.** Combination therapy of dual drug loaded TLNs; cisplatin and DOX co-delivery to the intracellular compartments of cancer cells.

The present investigation aimed to build PEG-*b*-PCL-*b*-CPCL, new triblock copolymers (TBs) that have the privilege of cisplatin conjugation and DOX encapsulation to achieve reduced GSH-detoxification and DNA-Pt adduct repair in breast cancer cells (see figure 5.3) to accomplish synergistic killing. These triblocks were designed in such a way that the length of PEG and carboxylic PCL (CPCL) chains is kept constant in all the blocks and the middle PCL block is varied as 25, 50 and 100 caprolactone repeating units. Cisplatin drug was chemically conjugated at the central core CPCL block which was protected by the middle PCL and periphery PEG-blocks. This strategy enabled the ~150 nm size triple layer nano-particles (TLNs) with PEG shell, PCL middle block and inner CPCL-CP core; further the middle PCL blocks were encapsulated with DOX, a hydrophobic drug to demonstrate synergism. The effect of the PCL middle block on the drug stability, DOX encapsulation, GSH-detoxification and nanoparticles biodegradability was investigated in detail. At the intracellular compartment, cisplatin and DOX were co-delivered by TLNs which were cleaved by the esterase enzyme (present in the lysosome) to release the drugs to achieve synergistic cell killing. Thus, the multi-drug loaded new triple layer nanoparticles reduced the GSH-detoxification as well as inhibited the DNA-Pt adduct repair; these scaffolds are also cleavable at the intracellular compartments by esterase to deliver drugs. Cellular uptake and cytotoxicity of the multi-drug loaded TLNs were studied in normal (WT-MEFs) and cancer



(HeLa and MCF 7) cell lines. It can thus be accentuated that selective and enhanced cytotoxicity was achieved exclusively in the breast cancer cells compared to other cell lines for the tailor-made TLNs with highly efficient synergism.

## 5.2. EXPERIMENTAL METHODS

**5.2.1. Materials:** Tin(II) 2-ethylhexanoate ( $\text{Sn}(\text{Oct})_2$ ), polyethylene glycol monomethyl ether with molecular weight of 2000 ( $\text{PEG}_{2000}$ ),  $\epsilon$ -caprolactone, cisplatin, silver nitrate, orthophenylenediamine (OPD), glutathione (GSH), doxorubicin (DOX) and esterase were purchased from Aldrich chemicals. Wild-type mouse embryonic fibroblasts (Wt-MEFs), cervical cancer cells (HeLa) and human breast cancer cells (MCF7) were maintained in DMEM (phenol red medium: Gibco) containing 10 % (v/v) fetal bovine serum (FBS) and 1 % (v/v) penicillin–streptomycin at 37 °C under a 5 %  $\text{CO}_2$  humidified atmosphere. Cells were washed with 40 % DPBS (Gibco), trypsinized using 0.05 % trypsin (Gibco) and seeded in 96 well or 6 well (as per experiment) flat bottomed plastic plates (Costar) for all assays. Tetrazolium salt, 3-(4,5-Dimethylthiazol-2-yl)-2,5-Diphenyltetrazolium Bromide (MTT), DMSO, DAPI and 4 % paraformaldehyde were obtained from Sigma. Fluoromount was obtained from Southern Biotech. All the solvents like tetrahydrofuran (THF), dichloromethane (DCM), trifluoroacetic acid (TFA) were purified and distilled prior to use. Synthesis of *tert-butyl 3-((4-oxocycloheptyl)oxy)propanoate*, the substituted caprolactone monomer has been explained in chapter 2.

### 5.2.2. Synthetic Procedure for Block Copolymers

**5.2.3. Synthesis of PEG-*b*-PCL-*b*-BPCL triblock polymers** The typical synthetic procedure is elucidated for  $\text{PEG}_{2000}$ -*b*- $\text{PCL}_{50}$ -*b*- $\text{BPCL}_{100}$ , this triblock synthesized in two steps. In first step,  $[\text{M}_0]/[\text{I}_0]$  is kept as 50 i.e. monomer 1 (caprolactone,  $\text{M}_1$ ) to initiator PEG which provide diblock with 50 PCL units. To this block monomer 2 (substituted caprolactone,  $\text{M}_2$ ) was added considering the formed diblock as a macro-initiator  $[\text{M}_0]/[\text{I}_0]$  is kept as 100. The initiator  $\text{PEG}_{2000}$  (70.16 mg, 0.035 mmol), catalyst  $\text{Sn}(\text{Oct})_2$  (7.0 mg, 0.0175 mmol) and monomer 1 (200 mg, 1.75 mmol) were taken in a flame-dried Schlenk tube under nitrogen atmosphere. High vacuum was applied to this reaction mixture for 45 min with stirring at room temperature. After achieving inert conditions inside the tube, it was immersed in preheated oil bath at 110 °C. The polymerization was continued for 6 h with constant stirring. Substituted

caprolactone monomer 2 (900 mg, 3.508 mmol) was added to the schlenk tube under high inert conditions and temperature of oil bath was raised to 130 °C. Reaction was continued for additional 24 h to achieve triblock copolymer. The polymer mixture was cooled to room temperature, dissolved in THF (2 mL) and precipitated in cold MeOH. Yield = 800 mg (72 %). <sup>1</sup>H-NMR (400 MHz, CDCl<sub>3</sub>) δ ppm: 4.13 (m, 2 H), 4.04 (m, 1 H) 3.63 (m, 3.68 H), 3.43 (m, 1 H), 3.36 (s, 3 H), 2.44 (t, 2 H), 2.36 (t, 2 H), 2.29 (m, 1 H), 1.77 (m, 4 H), 1.67 (m, 2 H), 1.44 (s, 9 H, t-butyl), 1.36 (m, 1.5 H). <sup>13</sup>C-NMR (100 MHz, CDCl<sub>3</sub>): 173.5, 173.4, 170.8, 80.5, 75.5, 70.6, 64.8, 64.1, 61.2, 36.5, 34.1, 32.9, 29.7, 28.2, 25.8, 24.4. FT-IR (cm<sup>-1</sup>): 2978, 2862, 1790, 1704 (C=O ester), 1423, 1318, 1146, 1156, 1100, 949, 900, 845, and 721. GPC molecular weights: M<sub>n</sub> = 15,000, M<sub>w</sub> = 27,100 and M<sub>w</sub>/M<sub>n</sub> = 1.80. A similar procedure was followed for the synthesis of other block copolymers.

**5.2.4. Synthesis of PEG-*b*-PCL<sub>25</sub>-*b*-BPCL triblock polymer:** Monomer 1 (200 mg, 1.75 mmol), monomer 2 (1.8 g, 7.01 mmol), initiator PEG<sub>2000</sub> (140 mg, 0.07 mmol) and catalyst Sn(Oct)<sub>2</sub> (14 mg, 0.035 mmol). Yield = 1.4 g (70 %). <sup>1</sup>H-NMR (400 MHz, CDCl<sub>3</sub>) δ ppm: 4.13 (m, 2 H), 4.04 (m, 0.5 H) 3.63 (m, 3.8 H), 3.43 (m, 1 H), 3.36 (s, 3 H), 2.44 (t, 2 H), 2.36 (t, 2 H), 2.29 (m, 0.5 H), 1.77 (m, 4 H), 1.67 (m, 1 H), 1.44 (s, 9 H, t-butyl), 1.36(m, 0.5 H). <sup>13</sup>C-NMR (100 MHz, CDCl<sub>3</sub>): 173.5, 173.5, 170.8, 80.5, 75.4, 64.8, 64.1, 61.2, 36.5, 34.1, 32.9, 29.7, 28.9, 28.3, 28.1, 25.4 and 24.6. FT-IR (cm<sup>-1</sup>): 2979, 2862, 1790, 1704 (C=O ester), 1423, 1318, 1145, 1150, 1105, 940, 905, 846, and 720. GPC molecular weights: M<sub>n</sub> = 12,000, M<sub>w</sub> = 23,100 and M<sub>w</sub>/M<sub>n</sub> = 1.92.

**5.2.5. Synthesis of PEG-*b*-PCL<sub>100</sub>-*b*-BPCL triblock polymer:** Monomer 1 (300 mg, 2.63 mmol), monomer 2 (678 mg, 2.62 mmol), initiator PEG<sub>2000</sub> (52.6 mg, 0.026 mmol) and catalyst Sn(Oct)<sub>2</sub> (5.27 mg, 0.013 mmol). Yield = 700 mg (71 %). <sup>1</sup>H-NMR (400 MHz, CDCl<sub>3</sub>) δ ppm: 4.13 (m, 2 H), 4.04 (m, 2 H) 3.63 (m, 3.78 H), 3.43 (m, 1 H), 3.36 (s, 3 H), 2.44 (t, 2 H), 2.36 (t, 2 H), 2.29 (m, 2 H), 1.77 (m, 4 H), 1.67 (m, 4 H), 1.44 (s, 9 H, t-butyl), 1.36 (m, 2 H). <sup>13</sup>C-NMR (100 MHz, CDCl<sub>3</sub>): 173.5, 173.4, 170.8, 80.6, 75.5, 70.5, 64.8, 64.1, 61.2, 36.5, 34.1, 32.9, 29.7, 28.9, 28.3, 28.1, 25.5 and 24.6. FT-IR (cm<sup>-1</sup>): 2979, 2864, 1791, 1705 (C=O ester), 1424, 1319, 1144, 1154, 1104, 949, 906, 844, and 728. GPC molecular weights: M<sub>n</sub> = 16,000, M<sub>w</sub> = 27,500 and M<sub>w</sub>/M<sub>n</sub> = 1.71.

**5.2.6. Synthesis of PEG-*b*-PCL-*b*-CPCL triblock polymers (TBs):** Trifluoroacetic acid (0.5 mL) was added slowly into PEG-*b*-PCL<sub>50</sub>-*b*-BPCL (500 mg) in dry DCM

(10.0 mL) and the polymer solution was stirred at 25 °C for 30 min. The solvents were evaporated and the polymer was redissolved in THF and precipitated in cold methanol. Yield = 350 mg (88 %). <sup>1</sup>H-NMR (400 MHz, CDCl<sub>3</sub>) δ: 4.15 (m, 2 H), 4.03 (m, 1 H) 3.70-3.63 (m, 3.65 H), 3.43 (m, 1 H), 3.36 (s, 3 H), 2.58 (t, 2 H), 2.36 (t, 2 H), 2.29 (m, 1 H), 1.77 (m, 4 H), 1.67 (m, 2 H), 1.33 (m, 1.4 H). FT-IR (cm<sup>-1</sup>): 3447, 2975, 2861, 1795, 1711 (C=O ester and acid), 1423, 1312, 1144, 1156, 1140, 943, 902, 845, and 720. GPC molecular weights: M<sub>n</sub> = 12,100, M<sub>w</sub> = 22,700 and M<sub>w</sub>/M<sub>n</sub> = 1.87. A similar procedure was followed for the synthesis of other block copolymers PEG-*b*-PCL<sub>x</sub>-*b*-CPCL where x = 25 and 100

**5.2.7. Synthesis of PEG-*b*-PCL<sub>25</sub>-*b*-CPCL:** Trifluoroacetic acid (0.5 mL), PEG-*b*-PCL<sub>25</sub>-*b*-BPCL (500 mg) and DCM (5.0 mL). Yield = 300 mg (75 %). <sup>1</sup>H-NMR (400 MHz, CDCl<sub>3</sub>) δ: 4.15 (m, 2 H), 4.03 (m, 0.5 H) 3.70-3.63 (m, 3.66 H), 3.43 (m, 1 H), 3.36 (s, 3 H), 2.58 (t, 2 H), 2.36 (t, 2 H), 2.29 (m, 0.5 H), 1.77 (m, 4 H), 1.67 (m, 1 H), 1.33 (m, 0.5 H). FT-IR (cm<sup>-1</sup>): 3440, 2976, 2862, 1791, 1719 (C=O ester and acid), 1423, 1311, 1142, 1154, 1140, 943, 902, 842, and 725. GPC molecular weights: M<sub>n</sub> = 11,100, M<sub>w</sub> = 19,700 and M<sub>w</sub>/M<sub>n</sub> = 1.77.

**5.2.10. Synthesis of PEG-*b*-PCL<sub>100</sub>-*b*-CPCL:** Trifluoroacetic acid (0.5 mL), PEG-*b*-PCL<sub>100</sub>-*b*-BPCL (500 mg) and DCM (5.0 mL). Yield = 290 mg (72 %). <sup>1</sup>H-NMR (400 MHz, CDCl<sub>3</sub>) δ: 4.15 (m, 2 H), 4.03 (m, 2 H), 3.70-3.63 (m, 3.66 H), 3.43 (m, 1 H), 3.36 (s, 3 H), 2.58 (t, 2 H), 2.36 (t, 2 H), 2.29 (m, 2 H), 1.77 (m, 4 H), 1.67 (m, 4 H), 1.33 (m, 2 H). FT-IR (cm<sup>-1</sup>): 3440, 2976, 2862, 1791, 1719 (C=O ester and acid), 1423, 1311, 1142, 1153, 1140, 943, 902, 842, and 721. GPC molecular weights: M<sub>n</sub> = 14,100, M<sub>w</sub> = 24,700 and M<sub>w</sub>/M<sub>n</sub> = 1.75.

**5.2.11. Preparation of Aquated Cisplatin [Pt(NH<sub>3</sub>)<sub>2</sub>(OH)<sub>2</sub>]<sup>2+</sup>:** Cisplatin (50 mg, 99.6 μmol, 1 equiv.) was dispersed in H<sub>2</sub>O (30.0 mL) with constant stirring at 37 °C. To this mixture, silver nitrate (34 mg, 199 μmol, 2 equiv.) was added and the resulting reaction mixture was stirred for 24 h in dark conditions. Formation of aquated cisplatin complex was confirmed by milky white silver chloride precipitation. Silver chloride was removed by centrifuging at 10,000 rpm for 1 h. Finally, the aquated cisplatin was obtained by filtration through 0.22 μm filter. The sample was lyophilized and stored at 4 °C.

**5.2.12. Synthesis of the Polymer-cisplatin Conjugate (or Triple Layer Nanoparticle, TLN):** A typical procedure for preparation of PEG-*b*-PCL<sub>50</sub>-*b*-CPCL-

CP is explained in detail. PEG-*b*-PCL<sub>50</sub>-*b*-CPCL triblock polymer (20.0 mg) was dissolved in NaOH (2 mL, 1 mg.mL<sup>-1</sup>) and the solution was stirred at 37 °C for 30 min. Aquated cisplatin (7.92 mg, 0.03 mmol, the lyophilized sample) was added to the above polymer solution and the complex was stirred for 24 h at 37 °C. The solution was transferred to a dialysis bag of molecular weight cut-off (MWCO = 1000) and dialyzed against a large amount of distilled water for 2 days. Distilled water was replaced periodically to ensure the removal of unencapsulated molecules from the dialysis tube. The solution recovered from dialysis tube was filtered through 0.45 µm filter, lyophilised and stored at 4 °C. FT-IR (cm<sup>-1</sup>): 3350, 2920, 2880, 1669, 1566, 1393, 1360, 1091, 1050, 930, 830 and 544. A similar procedure was used for making cisplatin complexes of triblock copolymers.

**5.2.13. Synthesis of the PEG-*b*-PCL<sub>25</sub>-*b*-CPCL-CP:** PEG-*b*-PCL<sub>25</sub>-*b*-CPCL (20 mg), NaOH (2 mL, 1 mg.mL<sup>-1</sup>) and aquated cisplatin (8.7 mg, 0.033 mmol). FTIR (cm<sup>-1</sup>): 3291, 2929, 2882, 1660, 1563, 1395, 1360, 1095, 1050, 931, 832 and 549.

**5.2.14. Synthesis of the PEG-*b*-PCL<sub>100</sub>-*b*-CPCL-CP:** PEG-*b*-PCL<sub>100</sub>-*b*-CPCL (20 mg), NaOH (2 mL, 1 mg.mL<sup>-1</sup>) and aquated cisplatin (6.7 mg, 0.025 mmol). FTIR (cm<sup>-1</sup>): 3291, 2929, 2882, 1660, 1563, 1395, 1360, 1095, 1050, 931, 832 and 549.

**5.2.15. Preparation of DOX-encapsulated Pt-coordinated complex:**The detailed procedure is given for DOX (obtained from DOX.HCl treating with triethylamine) encapsulation of PEG-*b*-PCL<sub>50</sub>-*b*-CPCL-CP. In a typical experiment, 5 mg of the lyophilized drug conjugate and 0.5 mg of DOX was dissolved in DMSO (1 mL). Distilled water (4 mL) was added dropwiseto the polymer solution, and the mixture was stirred at 25 °C for 2 h. The solution was transferred to a dialysis bag (MWCO = 1000) and dialyzed against a large amount of distilled water for 24 h. Fresh distilled water replaced periodically to ensure the removal of unencapsulated molecules from the dialysis tube. After dialysis, solution was filtered through 0.4 µm filter, lyophilised and stored at 4 °C.

Using similar protocol DOX was loaded into the drug conjugate and triblock polymers, detailed information is provided in supporting information. The drug loading efficiency (DLE) and drug loading content (DLC) were determined by absorption spectroscopy using the following equations:

$$\text{DLE (\%)} = \{ \text{weight of drug in nanoparticle} / \text{weight of drug in feed} \} \times 100\%$$

$\text{DLC (\%)} = \{ \text{weight of drug in nanoparticles} / \text{weight of drug-loaded nanoparticles} \} \times 100\%$

**5.2.16. In Vitro Drug Release Studies:** Cisplatin conjugated nanoparticles (TLN), DOX loaded (TB-DOX) and dual drug loaded nanoparticles (TLN-DOX) were taken in a dialysis bag (3 mL), immersed in a 100 mL beaker and dialyzed against PBS and in presence of esterase against PBS at 37 °C with constant stirring. At specific time intervals, 3.0 mL of the dialysate was withdrawn and replaced with an equal volume of fresh buffer. The amount of cisplatin released in each aliquot was measured using absorption spectroscopy via the orthophenylenediamine (OPD) assay to quantify the percentage of cumulative release. In a similar way, DOX release from nanoparticles was observed by subjecting the aliquots directly to absorption spectroscopy to quantify the percentage of cumulative release. For esterase aided release studies 10 units of enzyme was used, following the above-mentioned procedure.

Cumulative release (%) =  $C_n \times V_o / m \times 100$ , where  $C_n$  is the amount of loaded cargo in the  $n^{\text{th}}$  sample,  $V_o$  is total volume, and  $m$  is the total amount loaded in nanoparticles.

**5.2.17. O-phenylenediamine (OPD) Colorimetric Assay:** Samples with unknown cisplatin (Pt) content were added to 0.5 mL of OPD solution in *N, N*-dimethylformamide (DMF) (1.2 mg.mL<sup>-1</sup>) and heated for 2 h at 100 °C. The amount of Pt present in the sample was determined by measuring the absorbance at 706 nm (absorbance maxima of OPD-Pt complex). Molar extinction coefficient calculated for OPD-Pt is 24,310 L.mol<sup>-1</sup>.cm<sup>-1</sup>. The concentration of Pt released from the drug-conjugate was expressed as a ratio of the amount of platinum in the buffer solution from the polymer nanoparticle.

The drug loading efficiency (DLE) and drug loading content (DLC) were determined by absorption spectroscopy using OPD colorimetric assay from the following equation:<sup>34</sup>

$\text{DLE (\%)} = \{ \text{weight of drug in NPs} / \text{weight of drug in feed} \} \times 100\%$

$\text{DLC (\%)} = \{ \text{weight of drug in NPs} / \text{weight of drug loaded NPs} \} \times 100\%$ .

**5.2.18. Cell Viability Assay (MTT Assay):** To study the toxicity of polymers alone, cisplatin (CP), doxorubicin (DOX), CP-conjugates TLN, DOX loaded polymer scaffolds (TB-DOX) and dual drug loaded scaffolds (TLN-DOX) a cell viability assay was performed in WT-MEF, HeLa and MCF 7 cell lines using the tetrazolium salt, 3-

(4,5-Dimethylthiazol-2-yl)-2,5-Diphenyltetrazolium Bromide (MTT). 1000 cells were seeded per well in a 96-well plate (Corning, U.S.A.) in 100  $\mu$ L of DMEM with 10 % FBS (fetal bovine serum) and allowed to adhere for 16 h. Prior to drug treatment, media from cells was aspirated and various concentrations of drugs and cargo loaded scaffolds were added. A blank control, DMEM with FBS in the absence of cells was used in each experiment. All control and treated experiment wells were in triplicate. Cells were incubated for 72 h without a change in media. After 72 h, drug containing media was aspirated. Freshly prepared stock of MTT in sterile PBS (5 mg/mL) was diluted to 50  $\mu$ g/mL in DMEM. 100  $\mu$ L of this solution was added to each well. Cells were then incubated with MTT for 4 h at 37  $^{\circ}$ C. Media with MTT was then aspirated from wells and the purple formazan crystals formed as a result of the reduction of MTT by mitochondrial dehydrogenase enzyme from cells were dissolved in 100  $\mu$ L of 100 % DMSO (added per well). The absorbance from formazan crystals was immediately measured using microplate reader at 570 nm (Varioskan Flash) and was representative of the number of viable cells per well. Values from the triplicates for each control and treated set were noted and their mean was used for calculations. The values thus obtained for the untreated control samples were equated to 100 % and relative percentage values for drugs, scaffold alone and drugs loaded nanoparticles were calculated accordingly.

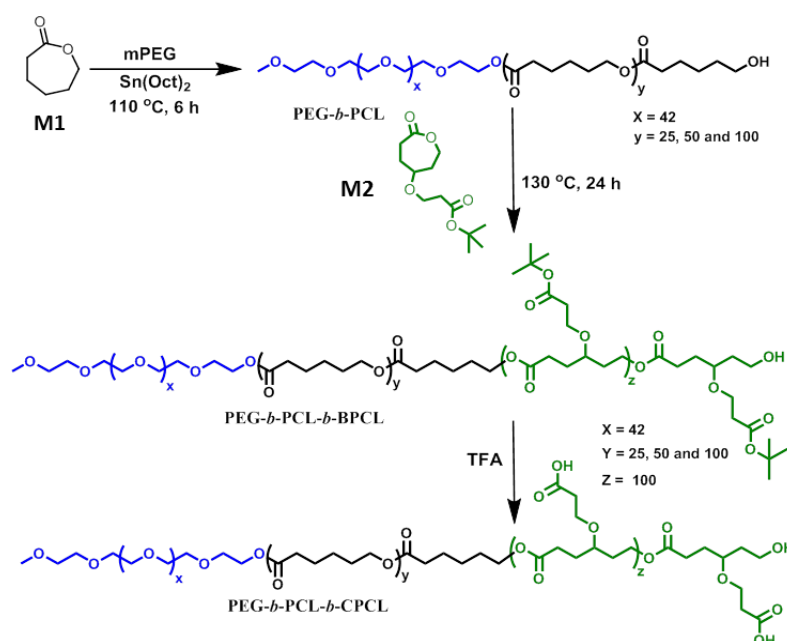
**5.2.19. Cellular Uptake of PEG-*b*-PCL-*b*-CPCL-CP-DOX by Confocal microscopy:** Cells were seeded at a density of  $1 \times 10^5$  cells on flame-dried coverslips placed in 6 well plates containing DMEM media with 10 % FBS and incubated at 37  $^{\circ}$ C for 16 h. The cells were then exposed to required concentration of DOX alone, TB-DOX, and TLN-DOX for 4 h in a CO<sub>2</sub> incubator at 37  $^{\circ}$ C. After incubation, the drug-containing media was aspirated from each well, and cells were washed twice with PBS (2  $\times$  1mL) and fixed with 4 % paraformaldehyde solution in PBS for 10 min at room temperature. The cells were washed twice with PBS (2  $\times$  1mL) and stained with DAPI solution in PBS. After 2 min incubation, at room temperature, in the dark, the excess dye was washed from the plate and cells were again gently rinsed with PBS for 1 min. The coverslips were mounted on slides using the fluoromount mounting medium (SouthernBiotech) and dried overnight at room temperature in the dark. The cells were imaged using a confocal microscope using the  $\lambda$  420 nm (blue channel) and  $\lambda$  560 nm

(red channel) lasers. Images thus obtained were opened in the Image J analysis software and the image for each channel was separated.

### 5.3. Results and Discussion

#### 5.3.1. Synthesis and Characterization of Triblocks

The TLNs were synthesized from carboxylic functionalized triblock copolymers, PEG-*b*-PCL-*b*-CPCLs as shown in scheme 5.3 and figure 5.7. These block copolymers consist of three dissimilar blocks wherein each block has a different purpose to accomplish. Here CPCL (carboxylic polycaprolactone) helps in conjugating cisplatin, PCL (polycaprolactone) block helps in physical encapsulation of hydrophobic drugs and PEG block protects the loaded drugs and stabilizes (or increases the half-life) in blood plasma. These triblocks were prepared by ring opening polymerization of caprolactone (monomer 1, M<sub>1</sub>) and t-butyl carboxylic ester substituted caprolactone (monomer 2, M<sub>2</sub>) in the presence of PEG as initiator along with Sn(Oct)<sub>2</sub> as the catalyst. M<sub>1</sub> is commercially available and M<sub>2</sub> was synthesized as shown in our earlier work. In these triblock copolymers, PEG and CPCL block length were fixed and PCL unit was varied from 25, 50 and 100 (PCL<sub>x</sub>, where x = 25, 50 and 100). For this the M<sub>2</sub> to initiator ratio was maintained as [M]/[I] = 100 and M<sub>1</sub> to initiator ratio was varied from 25, 50 and 100.



**Scheme 5.3.** Synthesis of triblock copolymers.

The ROP process was carried out via the solvent free bulk (or melt) route to produce these block copolymers with high purity for biomedical applications. The ROP of caprolactone monomer was carried out for 6 h at 110 °C in melt (or neat) conditions and after 6 h  $M_2$  was added to the reaction under highly inert conditions and stirred for additional 24 h at 130 °C in order to achieve triblock copolymer. The resultant triblock copolymers are named as PEG-*b*-PCL<sub>*x*</sub>-*b*-BPCL, where *x* represents 25, 50 and 100 and B represents t-butyl ester. In order to confirm the in situ formed diblock (PEG-*b*-PCL) before addition of the second monomer parallel reactions were performed with similar conditions at the same time. One of the reactions was stopped without addition of  $M_2$  and characterized using similar techniques as was used for triblocks.

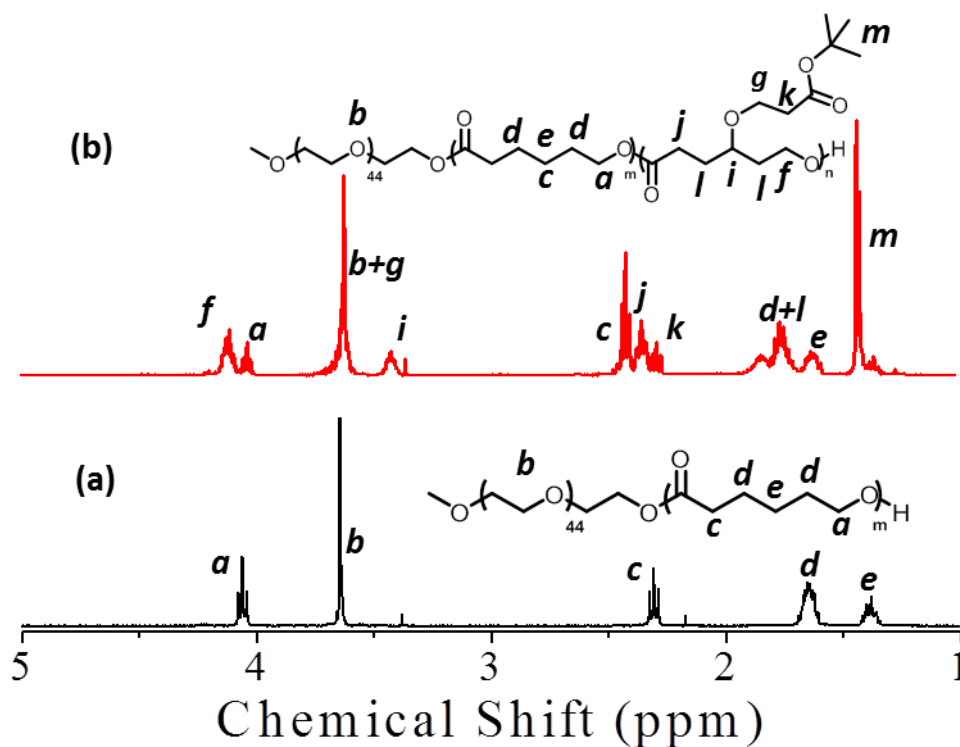


**Figure 5.4.**  $^1\text{H-NMR}$  of PEG-*b*-PCL (a) and PEG-*b*-PCL-*b*-BPCL (b) block copolymers.

$^1\text{H-NMR}$  spectra of diblock PEG-*b*-PCL<sub>50</sub> and triblock PEG-*b*-PCL<sub>50</sub>-*b*-BPCL (B = Butyl protected) is shown in figure 5.4. The chemical structure of these block copolymers is provided and the different protons are assigned by alphabets (see figure 5.4). The spectrum in figure 5.4a represents the PEG-*b*-PCL<sub>50</sub> diblock, where the -OCH<sub>2</sub>CH<sub>2</sub>O- protons of the PEG chain appeared at 3.63 ppm (proton-b) and a new ester peak corresponding to the CL part appeared at 4.03 ppm (proton a) and all other CL repeating unit



protons appeared as expected. The comparison of the peak intensities of the PEG part (proton-b at 3.63 ppm) and the CL protons (proton-a at 4.03 ppm) gave the degree of polymerization,  $n = 50$  in the present case.

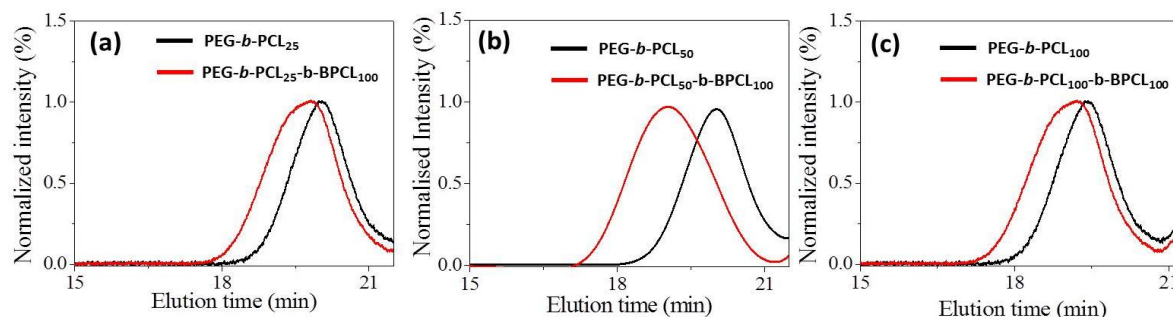


**Figure 5.5.** GPC chromatograms of PEG-*b*-PCL<sub>25</sub> and PEG-*b*-PCL<sub>25</sub>-*b*-BPCL (a), PEG-*b*-PCL<sub>50</sub> and PEG-*b*-PCL<sub>50</sub>-*b*-BPCL (b) and PEG-*b*-PCL<sub>100</sub> and PEG-*b*-PCL<sub>100</sub>-*b*-BPCL block copolymers.

The spectra in figure 5.4b represent the PEG-*b*-PCL<sub>50</sub>-*b*-BPCL triblock that clearly shows the presence of BPCL protons in addition to PEG-*b*-PCL diblock protons. Wherein, the protons ‘g’ in the carboxylic BPCL unit merged with protons ‘b’ belonging to the PEG part. The intensities of protons ‘f’ in the BPCL backbone appeared at 4.13 ppm. Thus, the subtraction of peak intensities [(g+b) – f] provides the actual number of protons ‘g’. The comparison of peak integrals of b (protons at 3.65-3.68 ppm) with protons f (at 4.13 ppm) or t-butyl protons ‘m’ (at 1.45 ppm) provides the degree of polymerization ( $n$ ) for the BPCL backbone in the triblock structure. This confirms the formation of perfect triblock copolymers. A similar approach was adapted and the “ $n$ ” values for PCL and BPCL blocks were determined for all the triblocks polymers. The number average molecular weights ( $M_n$ ) were estimated, as can be seen in table 1.

In addition to NMR, gel permeation chromatography (GPC) was carried out in tetrahydrofuran for further confirmation of triblock formation and molecular weight determination of the blocks. The GPC chromatograms of PEG-*b*-PCL<sub>25</sub> with PEG-*b*-PCL<sub>25</sub>-*b*-BPCL, PEG-*b*-PCL<sub>50</sub> with PEG-*b*-PCL<sub>50</sub>-*b*-BPCL and PEG-*b*-PCL<sub>100</sub> and PEG-*b*-PCL<sub>100</sub>-*b*-BPCL triblocks are plotted together and shown in figure 5.5a, b and c respectively. In all three cases the triblock copolymer chromatogram shifts to lower retention time after addition of another block. The molecular weights of the polymers increased after incorporation of the third block; this suggests the formation of higher molecular weight triblocks. The number average ( $M_n$ ) and weight average ( $M_w$ )

molecular weights and polydispersity (PDI) of polymers are given in supporting information (see table 1). The GPC technique underestimated the molecular weights of the blocks compared to  $^1\text{H-NMR}$ . This trend was attributed to the usage of polystyrene standards for GPC calibration.

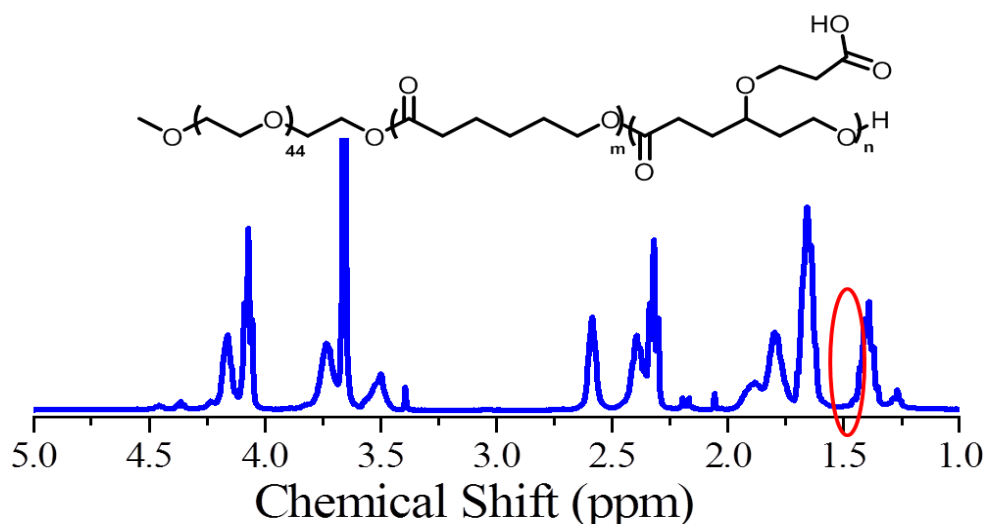


**Figure 5.6.**  $^1\text{H-NMR}$  of PEG-*b*-PCL<sub>50</sub>-*b*-CPCL triblock copolymer.

**Table 1:** Molecular weights of triblock copolymers determined by  $^1\text{H-NMR}$  and GPC.

Polymer	$M_n$ (g/mol, NMR)	$M_n$ (g/mol, GPC)	$M_w$ (g/mol, GPC)	$M_w/M_n$ (GPC)
PEG- <i>b</i> -PCL <sub>25</sub> - <i>b</i> -BPCL	30,100	12,000	23,100	1.92
PEG- <i>b</i> -PCL <sub>50</sub> - <i>b</i> -BPCL	33,200	15,000	27,100	1.81
PEG- <i>b</i> -PCL <sub>100</sub> - <i>b</i> -BPCL	39,200	16,000	27,500	1.71
PEG- <i>b</i> -PCL <sub>25</sub> - <i>b</i> -CPCL	24,500	11,100	19,700	1.77
PEG- <i>b</i> -PCL <sub>50</sub> - <i>b</i> -CPCL	27,600	12,100	22,700	1.87
PEG- <i>b</i> -PCL <sub>100</sub> - <i>b</i> -CPCL	33,500	14,100	24,700	1.75

GPC chromatograms for other blocks also show the clear difference between di and triblocks, which also clearly support the formation of triblocks. The *t*-butyl ester of the carboxylic functional group in triblock polymers was hydrolysed by trifluoroacetic acid to yield their corresponding carboxylic acid triblock copolymer PEG-*b*-PCL-*b*-CPCL (where C represents carboxylic acid). The hydrolysis of the *t*-butyl units was confirmed by  $^1\text{H-NMR}$  and their spectra are given in figure 5.6 for PEG-*b*-PCL<sub>50</sub>-*b*-CPCL-CP. Deprotection of the *t*-butyl group was confirmed by the

disappearance of the peak corresponding to t-butyl protons at 1.43 ppm as shown with red circle in figure 5.6. The molecular weights of these de-protected blocks were determined by  $^1\text{H-NMR}$  and GPC and are provided in table 1. The GPC chromatogram of PEG-*b*-PCL-*b*-CPCL triblocks revealed that the molecular weights were not altered by the de-protection step. Based on the above analysis, it can be concluded that the triblock copolymers with variable PCL middle block were synthesized with good yield using the solvent free ROP process.

### 5.3.2. Cisplatin chelation with Triblock Copolymer

After successful formation of carboxylic group bearing PEG-*b*-PCL-*b*-CPCL triblocks (TBs), they were chelated with cisplatin aquo complex (see figure 5.7). As depicted in figure 5.7, it formed spherical aggregates those were purified using dialysis method (detail explained in chapter 4). These nanoparticles used for physical encapsulation of DOX and these two single-loaded drug scaffolds were used as control for the dual drug loaded nanoparticles.

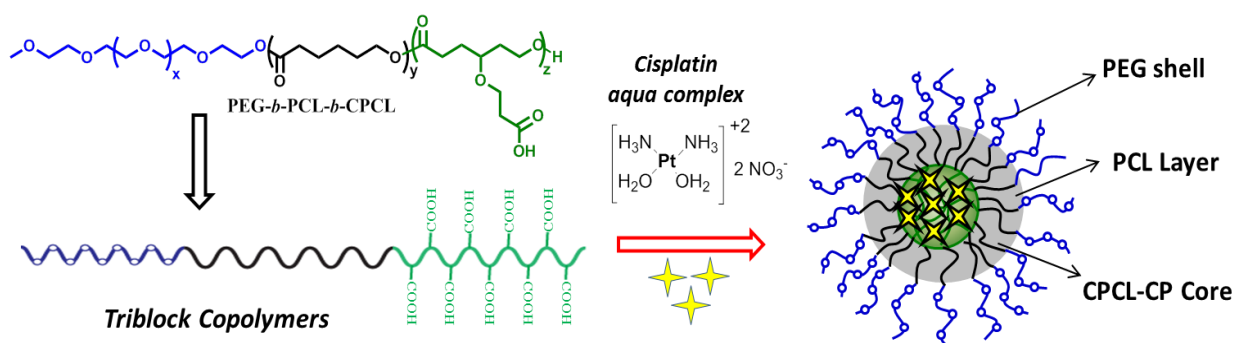


**Figure 5.7.** Chelation of cisplatin aquo complex with triblock copolymers.

The formation of triblock cisplatin conjugate was confirmed by FT-IR technique and spectra before and after cisplatin is shown in figure 5.8a and b. The shift in the nascent polymer carbonyl peak to  $1558 \text{ cm}^{-1}$  and appearance of a new peak at  $545 \text{ cm}^{-1}$  ( $\text{Pt-O-C=O}$ ) confirms the chelation.<sup>36-37</sup> Thermal gravimetric analysis (TGA) was used to estimate drug loading content of cisplatin in the polymer-drug conjugates. The TGA plots for TB<sub>50</sub> (PEG-*b*-PCL<sub>50</sub>-*b*-CPCL), free cisplatin and TLN<sub>50</sub> (PEG-*b*-PCL<sub>50</sub>-*b*-CPCL-CP) are shown in figure 5.8c. Briefly, the calculations are elucidated here for the same polymer and for rest of the polymers it is shown in chapter 4. The decomposition of the polymer started at  $260 \text{ }^\circ\text{C}$  and it completely degraded at  $500 \text{ }^\circ\text{C}$ .

Free cisplatin underwent stepwise decomposition and showed 60 % weight loss below 400 °C and the platinum content did not change up to 800 °C. On the other hand, drug-conjugated polymer exhibited single-step decomposition at 330 °C giving 28 % weight loss and remained unchanged up to 600 °C. These weight % values were feeded in below mentioned empirical formula to estimate the drug conjugation efficiency (DCE) as reported by Xu et al.<sup>38</sup>

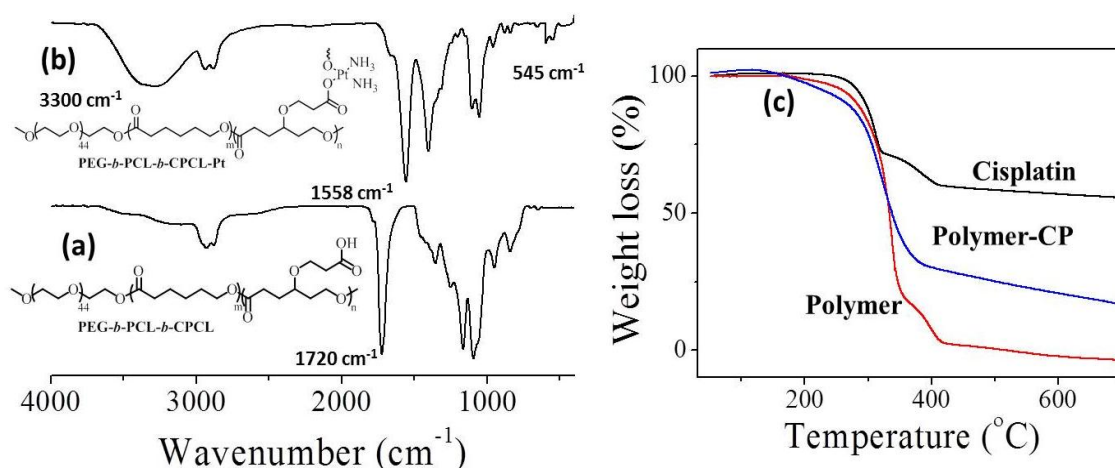


**Figure 5.8.** FT-IR spectra of triblock copolymer (a) and its cisplatin conjugate (b). TGA plots (c) of free cisplatin, TB and TLN.

$DCE = mPt_{exp}/mPt_{theo} \times 100\% = (W_{Pt}/M_{Pt})/(W_{acid}/2M_{acid}) \times 100\%$  where,  $mPt_{theo}$  is the theoretical molar amount of Pt;  $mPt_{exp}$  is the experimental molar amount of Pt;  $W_{Pt}$  is the weight percent of Pt measured by TGA;  $M_{Pt}$  is the molecular weight of Pt;  $W_{acid}$  is the weight percent of acid repeating unit calculated by TGA data and  $M_{acid}$  is the molecular weight of acid repeating unit. Based on this equation, the DCE was obtained and the drug loading content (DLC) of drug-conjugates was calculated. The detailed calculations and DLC for all the polymer scaffolds are provided in table 2.

**Table 2:** Drug loading content determined using TGA and absorbance

S.No	Polymer drug conjugates	DLC (TGA)	DLC (UV)
1	PEG- <i>b</i> -PCL <sub>25</sub> - <i>b</i> -CPCL-CP	29 %	26 %
2	PEG- <i>b</i> -PCL <sub>50</sub> - <i>b</i> -CPCL-CP	32 %	29 %
3	PEG- <i>b</i> -PCL <sub>100</sub> - <i>b</i> -CPCL-CP	31 %	33 %

### spectroscopy.5.3.3. Size and Shape of Polymer-Cisplatin Prodrug

The self-assembled nano-structures of triblock-drug conjugates were dispersed in water and subjected to dynamic light scattering (DLS), field emission scanning electronic microscopy (FESEM) and high resolution transmission electronic microscopic (HR-TEM) analysis. The detailed characterization of TLN<sub>50</sub> is depicted in figure 5.9. The DLS histogram of polymer-drug conjugate, TLN<sub>50</sub> in figure 5.9 a shows uniform monomodal distribution and the sizes of self-assembled nanoparticles is found to be  $150 \pm 5$  nm. FESEM image of this polymer-cisplatin conjugate, shown in figure 5.9 b, exhibits the creation of globular nano-particular morphologies. In the HR-TEM image of TLN<sub>50</sub>, nanoparticles appeared as spherical objects having a dark contrast at the CPCL core filled with platinum metal, as shown in figure 5.9c.

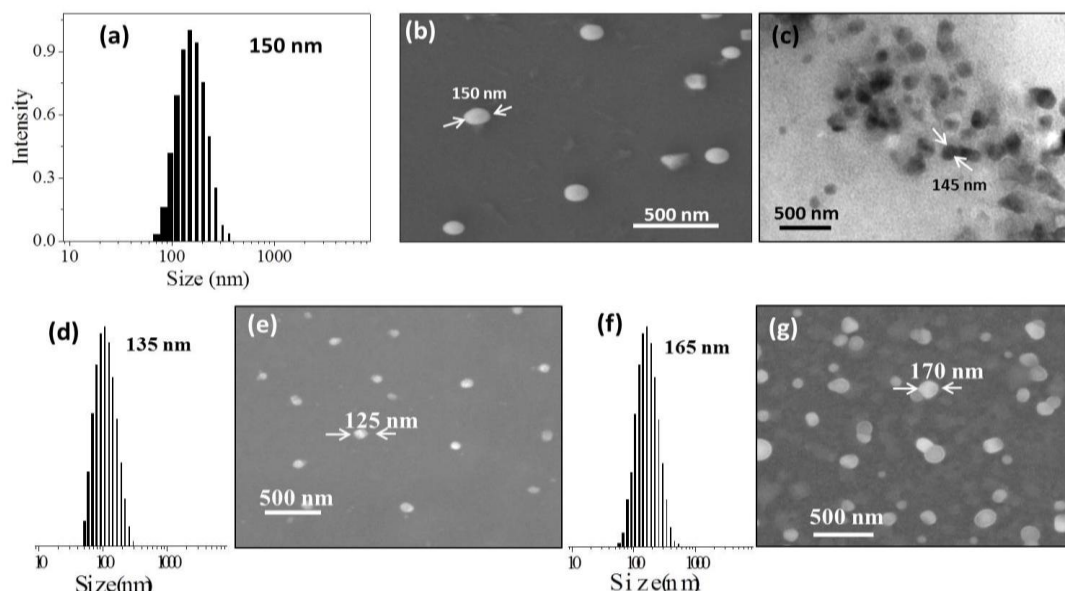


**Figure 5.9.** DLS histogram (a), FESEM (b), and HR-TEM (c) images of TLN<sub>50</sub> in milli Q water at 0.2 mg/mL concentration. DLS histogram and FESEM image of TLN<sub>25</sub> (d and e) and TLN<sub>100</sub>.

The sizes of nanoparticles in FESEM and HR-TEM images are in good coherence with the DLS size of the samples in water. The DLS histograms and FESEM images of other TLNs, i.e. PEG-*b*-PCL<sub>25</sub>-*b*-CPCL-CP (TLN<sub>25</sub>) and PEG-*b*-PCL<sub>100</sub>-*b*-CPCL-CP (TLN<sub>100</sub>) are depicted in figure 5.7. TLN<sub>25</sub> (figure 5.9d) showed monomodal histogram of 135 nm and in FESEM image (see figure 5.9e) showed formation of 125 nm spherical aggregates. TLN<sub>100</sub> (figure 5.9f) nanoparticles showed monomodal histogram of 165 nm size aggregates. Further these nanoparticles were subjected to FESEM and the image is shown in figure 5.9 g, wherein it showed the formation of spherical particles. The FESEM sizes were found to be in

good coherence with DLS sizes. After successful construction of TLNs with cisplatin-CPCL chelation, further, we aimed at loading doxorubicin (DOX) in PCL layer in order to attain synergistic killing from dual drug loaded TLNs.

#### 5.3.4. Stability of TLNs in PBS

The release studies were carried out to scrutinize the effect of the PEG shell and PCL middle layer on the stability of nanoparticle and cisplatin release from nanoparticle core, under various *in vitro* conditions. The stability of the core-shell nanoparticles (CPCL-CP, A; PEG<sub>2000</sub>-*b*-CPCL-CP, B) and TLNs (TLN<sub>25</sub>, C; TLN<sub>50</sub>, D) was investigated in milli-Q water (pH = 6.8), PBS (pH = 7.4) and in presence of esterase, the results of which are shown in figure 5.10. Earlier it had been reported that the cisplatin prodrugs are susceptible to cleave in the presence of chloride ions.<sup>39</sup> As it is already proven from chapter 3 that is the PEG shell could stabilize 50 % of the drug in PBS. In the present study, to investigate the role PCL layer in stabilizing cisplatin further in the core. In all the release studies the amount of cisplatin released was quantified using *o*-phenylenediamine (OPD) colorimetric assay and the details are given in the chapter 2. The cumulative release was calculated as follows: Cumulative release (%) =  $C_n * V_o / m * 100\%$  where  $C_n$  is the amount of loaded cargo in the  $n^{\text{th}}$  sample,  $V_o$  is the total volume and  $m$  is total amount loaded in prodrug.

The release studies were carried out for all the nanoparticles in milli-Q water and the data is shown in figure 5.10, where core-shell and TLNs exhibited < 10 % cisplatin release in milli-Q water. This suggests that polymer-cisplatin nanoparticles were stable and they could be stored in milli-Q water. To test the role of PCL-layer on the de-chelation of cisplatin from CPCL core, TLNs were subjected to release studies in PBS and data is presented in figure 5.10. In figure 5.10b to 5.10c the release plots in milli Q water and in PBS are shown for TLNs along with core-shell nanoparticles (same as our chapter 2) in order to study the role of additional PCL layer on the stability of the drug in PBS. The CPCL-CP nanoparticle (A) did not have PEG shell protection against Cl<sup>-</sup> ions; as a result, the cisplatin core easily released the entire drug (see figure 5.10 b). However, in PEG<sub>2000</sub>-*b*-CPCL-CP nanoparticle (B) as shown in figure 5.10 c PEG shell protects the cisplatin against Cl<sup>-</sup> attack and only 52 % of the drug got released in 12 h. The remaining 48 % of the drug was bound to the polymer and retained without leaching for a prolonged period of > 48 h. This data clearly



indicated that PEG-shell containing nanoparticles fail to prevent 52% cisplatin leaching in blood plasma conditions.

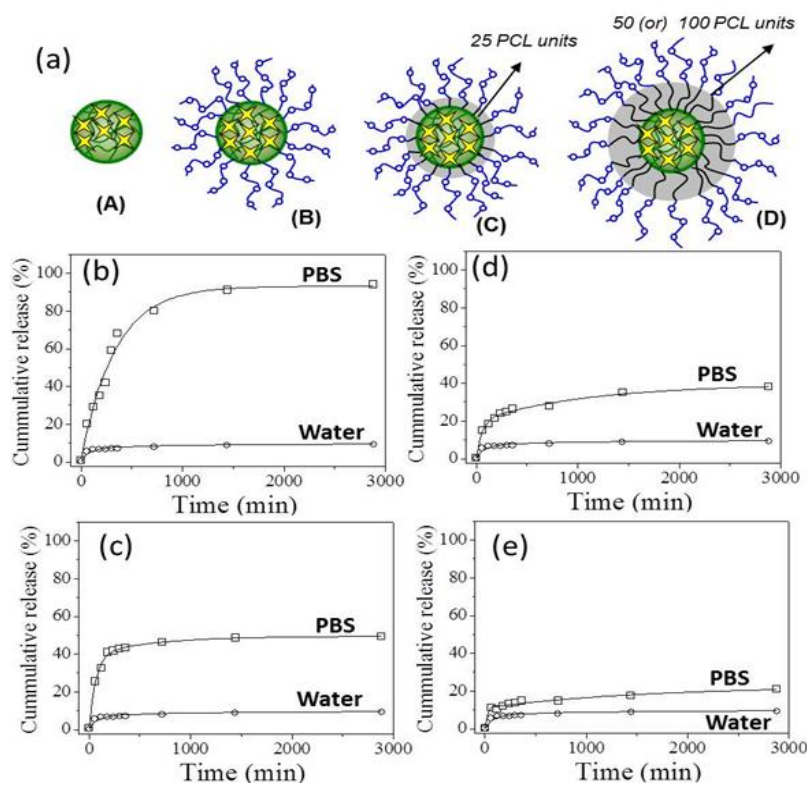


**Figure 5.10.** Schematic representation of nanoparticles (a). Cumulative release of cisplatin in milli Q water and in PBS for core shell nanoparticles CPCL-CP (b), PEG-b-CPCL-CP (c), TLN<sub>25</sub> (d) and TLN<sub>50</sub> (e) at 37 °C.

On the other hand, the added PCL layer between PEG shell and CPCL-CP core renders increased cisplatin protection in the core of the TLN. In the case of TLN<sub>25</sub> 45 % drug leaching (see figure 5.10 d) was observed, i.e. 55 % cisplatin protection was achieved. But in the case of TLN<sub>50</sub> we were able to accomplish greater than 85 % cisplatin protection respectively (see figure 5.8e). For TLN<sub>100</sub> data is not shown here which also showed similar (90 %) results as TLN<sub>50</sub>. These release profiles in PBS clearly show that embedding the hydrophobic PCL layer in between PEG-shell and CPCL-CP core helps in enhancing the stability of cisplatin multi-fold compared to the core shell nanoparticles (CPCL-CP and PEG-b-CPCL-CP) in blood plasma conditions. This phenomenon can be attributed to the hydrophobic PCL units inhibiting the penetration of ions ( $\text{Cl}^-$  and  $\text{PO}_4^-$ ) that leads to decreased de-chelation and release of cisplatin from the CPCL core. Hence, it can be concluded that highly stable TLNs were tailor-made to protect ~ 90 % cisplatin, which can increase the drug half-life in blood plasma.

### 5.3.5. Stability of TLNs in presence of Esterase in PBS

To investigate the cisplatin release from TLNs in the presence of enzyme rich lysosomes, they were subjected to the esterase enzyme which cleaves the polymer cisplatin conjugate made up of biodegradable PCL and CPCL units. This was scrutinized by the cumulative release of the TLNs in the presence of 10 U of esterase.<sup>40</sup> The amount of cisplatin released was monitored using OPD assay.

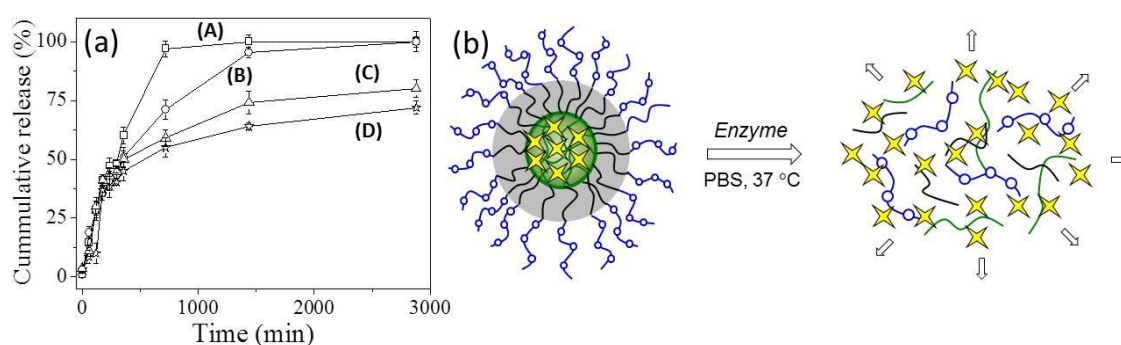


**Figure 5.11.** Cumulative release of cisplatin from nanoparticles in the presence of esterase in PBS at 37°C (a). Schematic representation of nanoparticles and their cleavage in the presence of esterase enzyme (b).

The cumulative release profiles for the addition of esterase to core-shell nanoparticles and TLNs are shown in figure 5.11a. The cumulative release profiles revealed that the CPCL backbone was cleaved by the esterase enzyme and cisplatin release occurred at a fast rate in the CPCL-CP and PEG-*b*-CPCL-CP core-shell nanoparticles (as seen in chapter 3). On the other hand, TLNs showed controlled cisplatin release in 48 h for TLN<sub>25</sub>, TLN<sub>50</sub> nanoparticles, i.e. 80 % and 72 % respectively. Schematic representation for esterase cleavage of TLN<sub>50</sub> to release cisplatin is shown in figure 5.11b. This might be due to the inclusion of hydrophobic PCL layer in between PEG shell and CPCL-CP core which was able to slowdown the penetrating capability of the enzyme to the CPCL core. The increase of the PCL layer led to more sluggish polymer degradation and subsequently decreased cisplatin release. Hence, it can be concluded that the novel TLNs have the potential to preserve the drug under blood plasma conditions and release the loaded cargoes in a controlled manner in the presence of lysosomal enzymes for a longer time at the intracellular compartments.



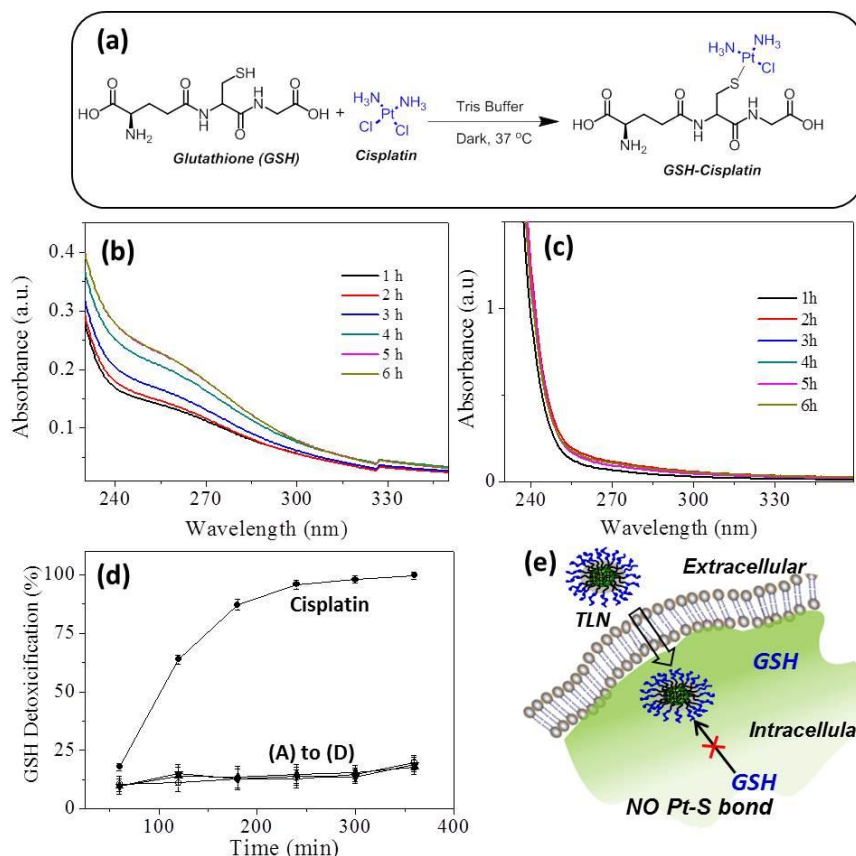


**Figure 5.12.** Reaction of cisplatin with GSH in Tris buffer at 37 °C (a). Absorbance spectra of free cisplatin drug (b) and TLNs (c) in reaction with GSH. Monitoring of the extent of reaction (at the absorbance maximum of 260 nm) against time of the reaction for free cisplatin and TLNs upon exposure to GSH (d). Schematic representation of TLNs (e) entry into the cytoplasm and their possible interaction with GSH in Pt-S bond formation.

### 5.3.6. GSH detoxification

As mentioned earlier glutathione (GSH), a sulfur containing oligopeptide present in cytoplasm, causes cisplatin detoxification which is one of the major reasons of drug resistance. To study the cisplatin detoxification caused by GSH, model reactions were performed (see figure 5.12a). The formation of S-Pt bond in the reaction of GSH and cisplatin was monitored using UV-Visible spectroscopy (peak at 260 nm).<sup>41</sup> The absorbance plots depicted in figure 5.12b and 5.12c correspond to GSH reaction with cisplatin and TLNs, respectively. These absorbance values were plotted against time for GSH action on free cisplatin and TLNs. The increase in the absorbance clearly shows that the free cisplatin reacted with this thiol species and produced Pt-S bond as seen in figure 5.12d. On the other hand TLN<sub>50</sub> did not show any new peak for Pt-S bond (see figure 5.12d) as was observed for CPCL-CP and PEG<sub>2000</sub>-*b*-CPCL-CP in our earlier work (in chapter 3). These observations clarify that TLNs were found to be

stable against cytoplasmic thiol species and may transport the drug to the nucleus as illustrated in figure 5.12 e.

### 5.3.7. Cytotoxicity TLNs

The cytotoxicity of the polymers alone, free cisplatin and TLN were investigated in wild-type mouse embryonic fibroblasts (WT-MEFs), breast cancer (MCF 7) and cervical cancer (HeLa) cell lines. Breast cancer cells (MCF 7) have 10 times over-expression of cytoplasmic thiol residues such as GSH (in mM) compared to other cancer cells (HeLa and MEF cells). The cytotoxicity of the nascent triblock copolymers was first tested in WT-MEF, HeLa and MCF 7 cell lines by varying their concentrations up to 40  $\mu\text{g/mL}$ . The data shown in figure 5.13a, b and c corresponds to block copolymers in WT-MEF, HeLa and MCF 7 cell lines respectively.

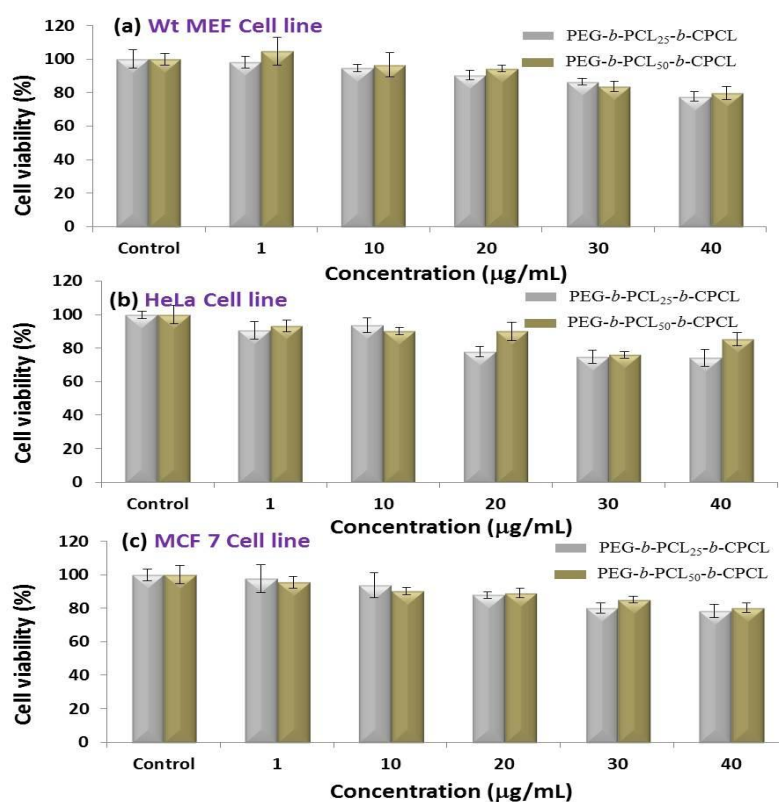


**Figure 5.13.** Histogram depicting cytotoxicity of triblock copolymers in WT-MEF (a), HeLa (b) and MCF 7 (c) cells at various concentrations.

This data indicates that more than 90 % cell viability was observed up to 30  $\mu\text{g/mL}$  concentration in all the cell lines. These results confirmed that the triblock copolymers possessed high biocompatibility at concentrations which is usually employed for synthetic polymers in drug delivery.

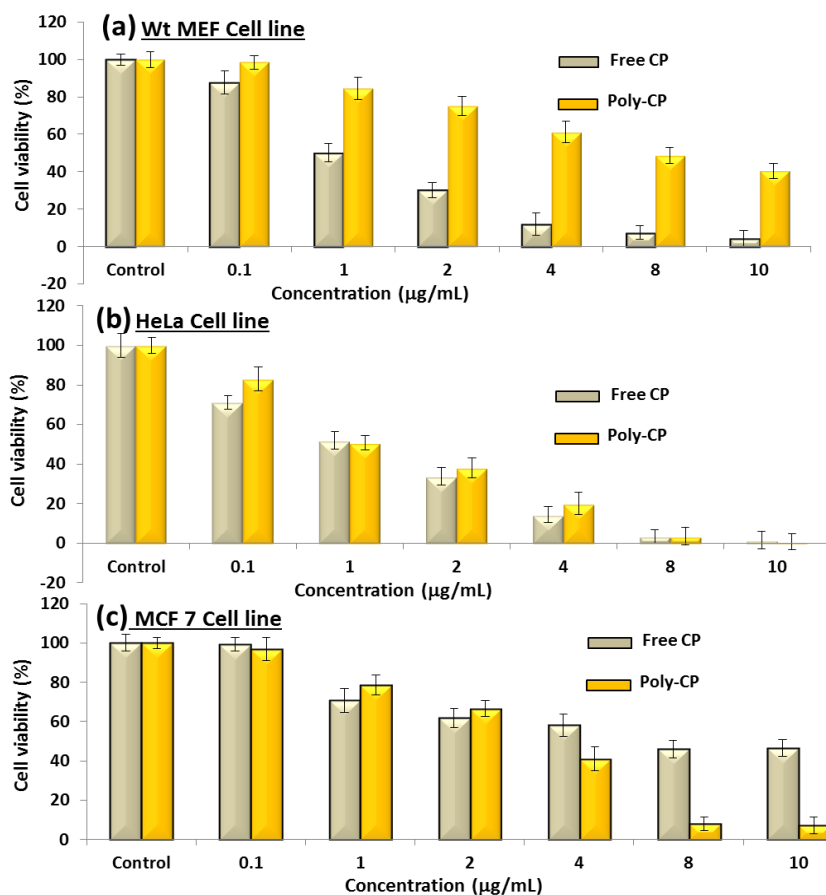


**Figure 5.14.** Histogram depicting cytotoxicity of free cisplatin and TLN (Poly-CP) in WT-MEF (a), in HeLa cells (b) and in MCF 7 cells (c) at various concentrations.

Cytotoxicity of free cisplatin and nano-carrier (TLN<sub>50</sub>) were tested in normal (WT-MEFs) and cancer (HeLa and MCF 7) cell lines. TLN<sub>50</sub> was chosen for cytotoxicity and rest of the studies as this scaffold showed prominent release and GSH detoxification studies. In this experiment concentration of cisplatin drug was varied from 0.1 µg/mL to 10.0 µg/mL and their cytotoxicity data is summarized for WT-MEFs, HeLa and MCF7 in figure 5.14. Histograms of TLN with respect to free drug are shown in figure 5.14a for WT-MEF cell line. This data shows that cisplatin is toxic to normal cells and the IC<sub>50</sub> value is 1.5 µg/mL. However, the polymer TLN<sub>50</sub> was comparatively non-toxic. The cytotoxicity of free cisplatin and TLN<sub>50</sub> in HeLa cells shown in figure 5.14b, free cisplatin and TLN showed 50 % killing in cells at 1.3 µg/mL concentration which is in accordance with earlier observations.<sup>42</sup> At higher concentrations nanoparticle and free drugs showed > 90 % cell killing. On the other hand, in breast cancer cell lines, as shown in figure 5.14c, cytotoxicity of free cisplatin

and TLN showed a vivid difference in MCF 7 cells. The free cisplatin drug showed 50 % killing in cells at  $> 4.0 \mu\text{g/mL}$  concentration which is similar to that of earlier observations.<sup>43</sup> The cytotoxicity of free cisplatin becomes stagnant after  $4.0 \mu\text{g/mL}$  concentration up to  $10.0 \mu\text{g/mL}$ . On the other hand, the TLN showed great enhancement in the cell killing. Cytotoxicity improved two fold in the case of TLN, wherein  $> 90\%$  cell killing was observed at  $8.0 \mu\text{g/mL}$ . The decreased cytotoxicity for free cisplatin can be attributed to the over expression of GSH in MCF 7 cells which leads to the detoxification of free cisplatin drugs. However, TLN provides shielding against GSH which increases the probability of DNA chelation and thus enhances the cell death. As was outlined in the Introduction, two major problems related to resistance in cancer cells are GSH detoxification and DNA-repair. Till here it has been able to tackle the first problem that is GSH detoxification; TLN was able to shield cisplatin against GSH and deliver it to the DNA to achieve toxicity. The present *in vitro* studies provide direct evidence for the need to conjugate cisplatin drugs in the polymer scaffold to achieve complete cell death in the presence of GSH which is over expressed in breast cancer tissues. Thus, the polymer drug conjugates carry these additional advantages to accomplish complete cell death which is not possible in free cisplatin drugs.

### 5.3.8. DOX encapsulation

As pointed out earlier, DNA repair is one of the major problems associated with cisplatin chemotherapy and is also a reason for cisplatin resistance. To overcome this problem, cisplatin has to be used in combination with other anticancer drugs such as DOX. As it is known that the anti-cancer drugs such as anthracyclines (mainly DOX) are known to inhibit the DNA repair mechanism after cisplatin chelation. This increases cytotoxicity by stabilizing the DNA-Pt adduct which may culminate into synergistic killing of cancer cells. This combination of drugs (or therapy) may help to combat cisplatin resistance in various types of cancers such as breast cancer. To accomplish this TLN<sub>50</sub> was chosen to encapsulate DOX along with TB<sub>50</sub> as a control in this experiment. DOX encapsulation was also carried out for CPCL-CP and PEG-*b*-CPCL-CP core-shell nanoparticles in order to understand the importance of PCL layer. These nanoparticles were subjected to DOX encapsulation in milli-Q water (pH = 6.8). In this investigation, the nanoparticles (5 mg) and DOX (0.5 mg) were taken in DMSO + water

mixture (1 mL + 4 mL) in a dialysis bag and dialyzed for more than 24 h against water. The unencapsulated drug was removed from the reservoir by continuously replacing with fresh water.

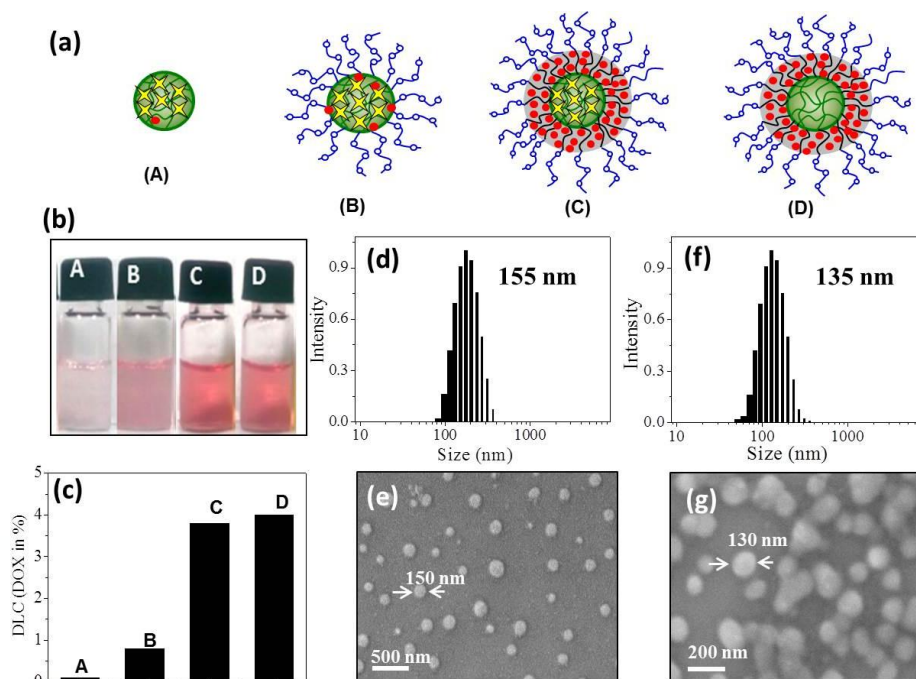


**Figure 5.15.** Schematic representation of DOX loaded nanoparticles (a) and its solution containing vials photograph (b) and drug loading content (c) of the block copolymer nanoparticles determined by UV-Vis absorbance spectroscopy. DLS histogram (d), FESEM image (e) of TLN<sub>50</sub>-DOX; DLS histogram (f), FESEM image (g) of TB<sub>50</sub>-DOX in milli-Q water at 0.2 mg/mL concentration.

The illustration of these DOX loaded nanoparticles and the photograph of the vials containing the solution is depicted in figure 5.15a and 5.15b, respectively. The color intensity of nanoparticle solution clearly suggested that CPCL-CP and PEG-*b*-CPCL-CP core-shell nanoparticles showed minimum loading, whereas TLN<sub>50</sub> and TB<sub>50</sub> showed a huge amount of DOX loading. These nanoparticle solutions were subjected to absorbance spectroscopy in order to determine drug loading content (DLC) in the DOX-loaded nanoparticles. The DLC was plotted against the respective nanoparticles and they are presented in figure 5.15c. The DLC of the core-shell nanoparticles was negligible (0.1-0.8 %) as they lack the PCL layer, whereas in the case of TLNs and triblocks DLC was observed as 3.8 and 3.9 % respectively, which can be attributed to the fact that they have a hydrophobic PCL layer which helps

encapsulate the hydrophobic drug DOX (see figure 5.15a). The nano-assemblies of DOX loaded nanoparticles were characterized using DLS, sizes of these DOX-loaded nanoparticles were found to be very similar to that of their nascent nanoparticles. The DLS histogram and FESEM images of TLN<sub>50</sub>-DOX and TB<sub>50</sub>-DOX are shown in figure 5.15d to 5.15g. TLN<sub>50</sub>-DOX (figure 5.15d) and TB<sub>50</sub>-DOX (figure 5.15f) nanoparticles showed monomodal histogram of 155 and 135 nm size aggregates respectively. Further these nanoparticles were subjected to FESEM and the images are shown in figure 5.15e and 5.15g for TLN<sub>50</sub>-DOX and TB<sub>50</sub>-DOX respectively; both showed the formation of spherical nano-particles. The FESEM sizes were found to be in correlation with DLS sizes. This observation indicates that the PCL block is very essential for enhanced DOX-encapsulation capabilities. This PCL layer subsumed between PEG shell and cisplatin anchored CPCL core opens up new opportunities where various hydrophobic anticancer drugs can be loaded to achieve combination therapy.

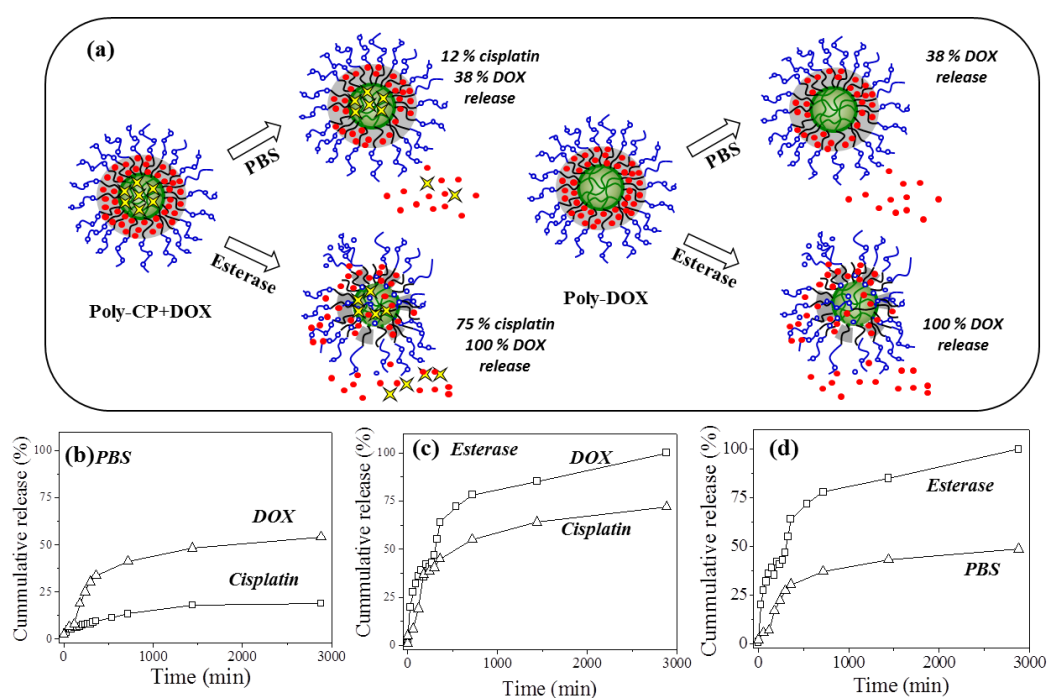


**Figure 5.16.** Schematic representation of drug release from nanoparticles (a), cumulative drug release profiles of dual drug loaded nanoparticles in PBS without (b) and with 10 U esterase (c) at 37 °C. Cumulative drug release profiles of DOX loaded triblock copolymer in PBS without and with 10 U esterase (d) at 37 °C.

These DOX-loaded polymeric nanoparticles (dual drug loaded TLN-DOX, and TB-DOX) were subjected to *in vitro* drug release studies in PBS (pH = 7.4 at 37 °C) and in the presence of esterase enzyme (in PBS at 37 °C). For this purpose, the DOX-loaded nanoparticles were taken in dialysis tube (MWCO = 1000) and immersed in

PBS at 37 °C. In this experiment absorbance spectroscopy was used to determine the released cisplatin (using OPD assay) and DOX amount in the reservoir. The cumulative release from nanoparticles was plotted and is shown in figures 5.16b and 5.16c. The dual drug loaded TLN-DOX nanoparticles release < 12 % of cisplatin and 38 % of DOX at 37 °C under blood plasma conditions as seen in figure 5.16b, also schematically illustrated in figure 5.16a. This indicates that the dual drug loaded nanoparticles TLN-DOX exhibit similar cisplatin stability as TLN (see figure 5.10e) at blood plasma conditions. However, DOX releases faster than cisplatin; this might be attributed to the fact that DOX is physically encapsulated and non-covalently bound to the outer PCL hydrophobic layer compared to the covalent interactions of cisplatin with CPCL core. Further, dual drug loaded TLN-DOX was treated with 10 units of esterase enzyme in PBS at 37 °C and their cisplatin and DOX release profiles are shown in figure 5.16b. As can be seen from the release profile, DOX undergoes burst release (100 %) in presence of esterase whereas cisplatin exhibited more controlled release of up to 75 % in 48 h (see figure 5.11a). The DOX release observed from TB-DOX in PBS with and without esterase was similar to what was observed in TLN-DOX (see figure 5.11 d); this is diagrammatically shown in figure 5.11a. This *in vitro* experiment models the cleavage of the drug loaded nanoparticles at the intracellular level under lysosomal conditions. These particles are made with biodegradable PCL middle layer and CPCL-CP core aliphatic ester linkages; thus, the esterase enzyme that is abundant in the lysosomes is expected to rupture the nanoparticles to release the loaded cargoes at the intracellular compartments. Interestingly, these particles showed slow and controlled release of cisplatin, while much faster release of DOX was observed. The slow release might be attributed to the hydrophobic PCL layer that retards the penetration of enzyme to the inner core and slows down the cleavage and release of cisplatin from TLN-DOX.

### 5.3.9. Cytotoxicity of TB-DOX nanoparticles

The cytotoxicity of the free DOX, and TB-DOX, and their combinations were investigated in wild-type mouse embryonic fibroblasts (WT-MEFs), breast cancer (MCF 7) and cervical cancer (HeLa) cell lines. In this experiment concentration of DOX concentration varied from 0.1 µg/mL to 1.0 µg/mL and their cytotoxicity data is summarized for WT-MEFs, HeLa and MCF7 in figure 5.17. Histograms of TB-DOX and free DOX are shown in figure 5.17a for WT-MEF cell line. This data demonstrates

that free DOX is toxic to normal cells and its IC<sub>50</sub> value is 0.5  $\mu\text{g/mL}$ ; however, the DOX loaded polymer nanoparticle (TB-DOX) was comparatively non-toxic to the cells.

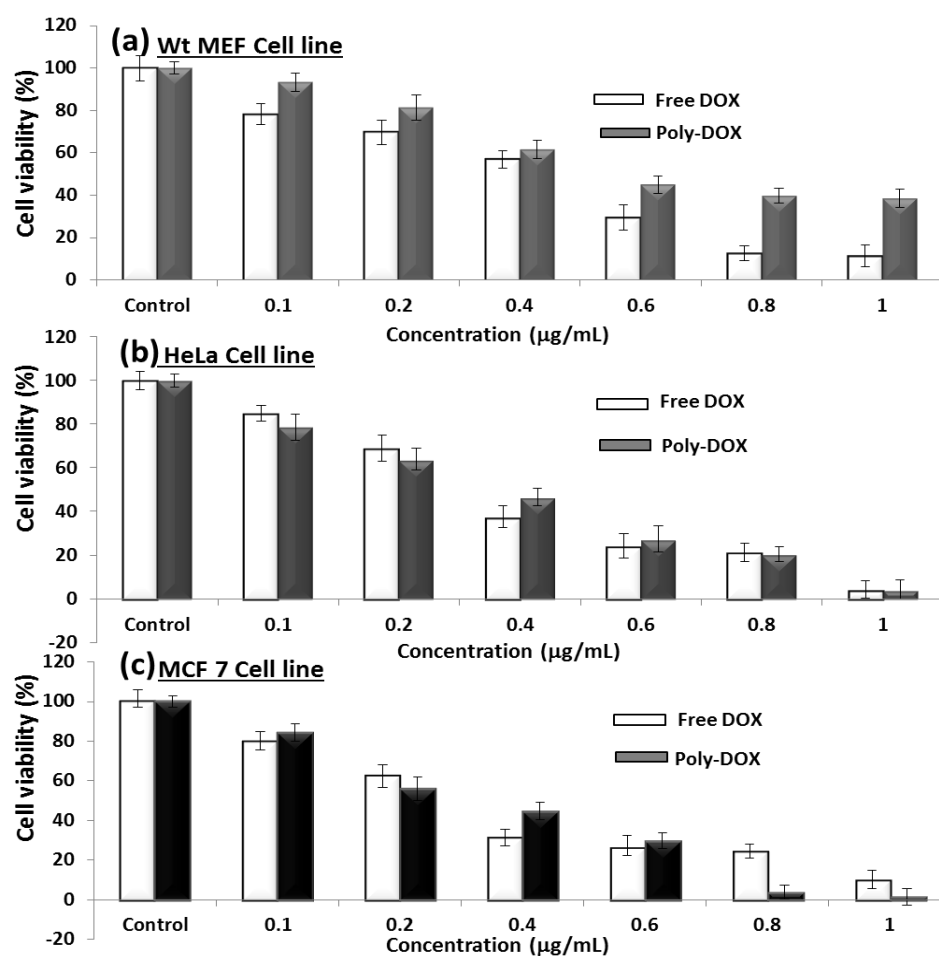


**Figure 5.17.** Histogram depicting cytotoxicity of free DOX and TB-DOX (Poly-DOX) in WT-MEF (a), in HeLa cells (b) and in MCF 7 cells (c) at various concentrations.

In figure 5.17b, the histograms are shown for free DOX and TB-DOX in HeLa cell line. Wherein, both free DOX and TB-DOX showed 50 % killing at 0.6  $\mu\text{g/mL}$  concentration which is similar to the earlier observations. On the other hand, in breast cancer cell line, as shown in figure 5.17c, free DOX and TB-DOX showed 50 % killing in cells at 0.6  $\mu\text{g/mL}$  concentration which is similar to the earlier observations.<sup>43</sup> The cytotoxicity data of free DOX in HeLa and MCF 7 cell line showed similar results as TB-DOX nanoparticles. But in non-cancerous cell line (Wt-MEF) TB-DOX proved as



comparatively non-toxic over free drugs. Thus, it can be concluded that selective targeting to the cancer cells over normal cell can be achieved using this triblock copolymer approach.

### 5.3.10. Cytotoxicity of Dual Loaded Nanoparticle (TLN-DOX)

The TLN accomplished anti-tumour effect by shielding against GSH which increases the cell death. However, there is still probability of cellular resistance as CP-DNA adduct can be repaired by proteins which may inhibit the toxicity of the drug. To deal with this obstacle we used combination therapy where cisplatin is combined with DOX, an anthracycline which inhibits the DNA repair.<sup>19</sup> The cisplatin chelated DOX encapsulated TLN-DOX was tested in cisplatin resistant MCF 7 cell line. In TLN-DOX, cisplatin and DOX ratio was maintained as 7.6, in accordance to their IC<sub>50</sub> values. The anti-tumor effect of DOX, CP, TB-DOX, TLN and TLN-DOX in combination and separately was initially evaluated in MCF 7 breast cancer cell line (see figure 5.14 and 5.17). In the case of free DOX and TB-DOX cytotoxicity was observed with IC<sub>50</sub> value of 0.5 µg/mL, as shown in figure 5.14c. However, cisplatin and TLN exhibited very different toxicity profiles, where cisplatin showed IC<sub>50</sub> of 8-9 µg/mL in accordance to the literature and TLN showed significant increase in cell killing at 10 µg/mL concentrations, that is > 90% cytotoxicity with IC<sub>50</sub> of 1.5 µg/mL, as can be seen in figure 5.17c. The physical mixture of both free drugs showed similar toxicity as free DOX (see figure 5.18a). When these two anticancer drugs were assimilated together in TLN-DOX, it exhibited robust enhancement of combination potency, with dose-effect profiles shifted towards lower drug concentration and the IC<sub>50</sub> value dropped to 0.4 µg/mL (see figure 5.18a).

This clearly shows that the cisplatin cytotoxicity increased 3 fold in presence of DOX; these data suggest synergistic cytotoxicity of TLN-DOX against MCF 7 cells. To confirm drug synergism in these nanoparticles, combination index (CI) analyses was carried out using below mentioned formula.<sup>44</sup>

$$CI = D_1/D_{m1} + D_2/D_{m2}$$

Where, D<sub>m1</sub> and D<sub>m2</sub> are the concentrations of the individual drugs and D1 and D2 are the concentrations of the drugs in dual loaded nanoparticles. 1= Cisplatin and 2 =DOX.

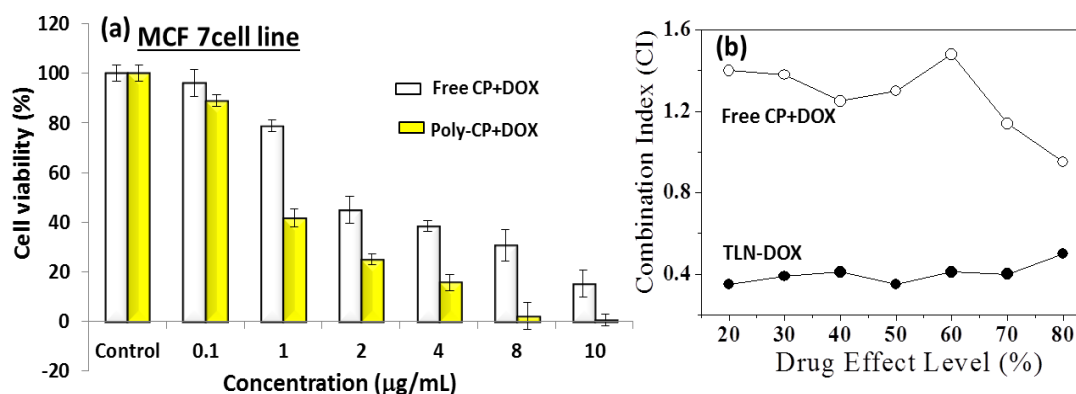


**Figure 5.18.** Histogram depicting cytotoxicity of cisplatin+DOX cocktail and dual drug loaded nanoparticles TLN-DOX (Poly-CP+DOX) (a) in MCF 7 at various concentrations. Combination index plots of cisplatin+DOX cocktail and dual drug loaded nanoparticles (b).

The CI plots, where combination index was derived from the dose-effect profiles of a given drug combination, was plotted against drug effect level. This plot can give quantitative information about the extent of drug interactions. Since, it is known that if CI values are lower than, equal to, or higher than 1, then they denote synergism, additivity, or antagonism, respectively. In this experiment dose level (cell death in %) plotted against CI values determined from above mentioned formula. As shown in figure 5.18b, CI plots for TLN-DOX clearly demonstrated efficient synergism against MCF 7 cells over the free drug combinations, which led to only additive effect. The enhanced potency of combination of drugs in TLN-DOX in MCF 7 human breast cancer cells might be attributed to the inhibition of DNA repair due to the presence of DOX. The reason for additivity or antagonistic effect in free drugs is due to differential availability of these drugs at the nuclear DNA whereas TLN-DOX is able to deliver both the drugs simultaneously to the site of action. The co-packaging of DOX and cisplatin in these nanoparticles rendered the drug combination synergistic: a highly attenuated CI value of 0.38 to 0.41 for various cytotoxicity levels was observed as compared to the 1.0 to 1.5 CI value of [CP + DOX] free drug combination at the same concentrations. The problems of drug resistance in MCF 7 cell were efficiently combated owing to the synergistic effect by combination therapy via co-delivery of cisplatin with DOX. Hence it can be concluded that the cisplatin chelated DOX encapsulated TLN-DOX provides proof for the need to conjugate cisplatin drugs with physical encapsulation of anthracyclines to slow-down the GSH detoxification and DNA repair in resistant breast cancer cells and for enhancing their efficacy. Though, the approach

has been demonstrated only for cisplatin and DOX, in principle, it can be extended to other platinum and anthracycline combinations. Currently, efforts are being taken to proceed in these directions to expand the triple layer nanoparticle strategy for various biomedical applications.

### 5.3.11. Cellular Uptake of Dual Loaded Nanoparticle (TLN-DOX)

The cellular internalization and intracellular drug release behaviour of dual loaded nanoparticles towards the MCF 7 cells was monitored using confocal laser scanning microscopy (CLSM). MCF 7 cells were incubated with free DOX, TB-DOX and TLN-DOX (for 8 h) at 37 °C. The red DOX fluorescence observed at  $\sim 590$  nm, was monitored through the red channel ( $\lambda = 568$  nm). As DOX has a propensity to gather at the nuclei, the diffusion and accumulation of DOX in the nucleus was probed by staining with DAPI. Blue fluorescence produced by the cell nuclei after DAPI staining was observed through the blue channel ( $\lambda = 405$  nm). In order to visualize the cell skeleton actin fibrils were stained with phalloidin, which was visualised through green channel ( $\lambda = 488$  nm).

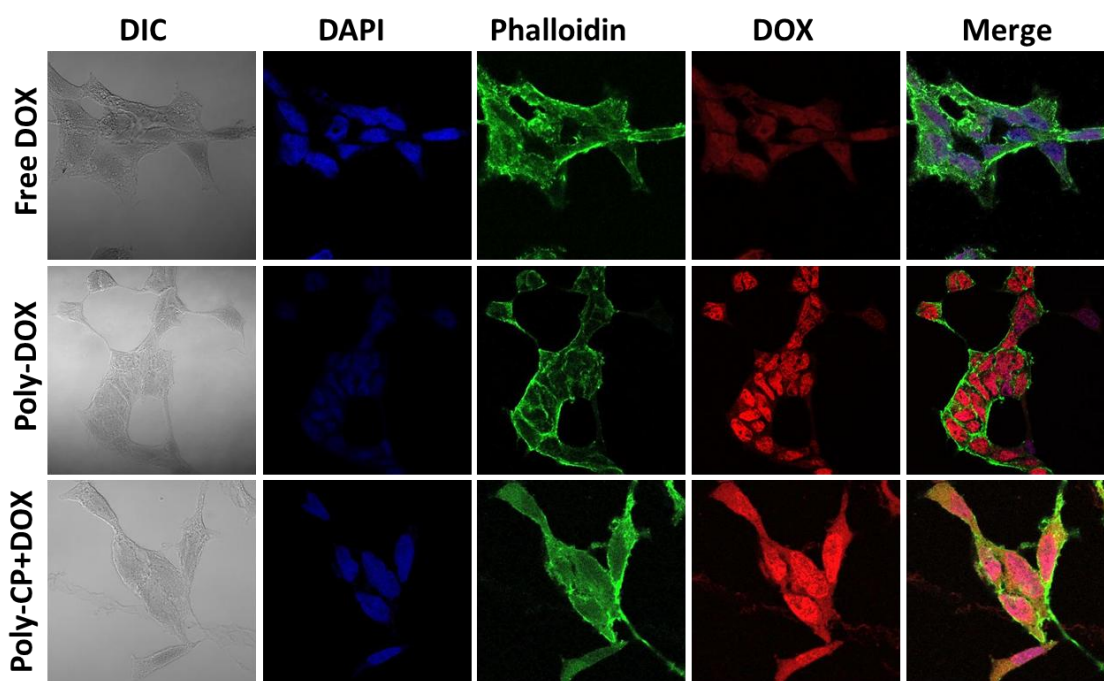


**Figure 5.19.** CLSM images of MCF-7 cells incubated with DOX, DOX loaded triblock (Poly-DOX) and DOX loaded TLN (TLN-DOX or Poly-CP+DOX) at 37 °C. For each panel, the images from the left to right show differential interference contrast (DIC), staining of cell nuclei by DAPI, phalloidin stained actin fibrils, DOX fluorescence in the cells, and an overlay of the three images.

The images corresponding to DIC (differential interference contrast), DAPI, phalloidin and DOX fluorescence in MCF 7 cells along with the merged image are shown in figure 5.15. In the case of free DOX the images were captured at 8h shown in first panel, where the nuclei were visible as blue rather than magenta color and very small red emission was found at the nuclei as an indication of lack of DOX accumulation at the nucleus. For TB-DOX and TLN-DOX images were captured after 8 h of incubation at 37 °C and are shown in second and third panels respectively, wherein strong DOX fluorescence was observed at the nuclei. This could, in principle, mean that the dual loaded nanoparticles efficiently internalize the drugs over the free drugs in MCF 7 cells. This enhanced intracellular accumulation of DOX enumerates the fact that degradation of nanoparticles occurs upon exposure to the lysosomal conditions inside the cells. Hence, it can be concluded that the biodegradable dual loaded nanoparticles undergo enzymatic cleavage at the intracellular compartments and release the drugs subsequently (only DOX was visualised as it is fluorescent in nature). This proves that nanoparticles travels towards the nucleus against cisplatin GSH detoxification in combination with DOX reaching to the nuclei and helping prevent the DNA-Pt adduct repair. This concept successfully demonstrated the co-delivery of cisplatin and DOX in order to achieve synergistic killing. This present investigation established the proof-of-concept of co-delivery of cisplatin with DOX to achieve highly efficient “synergism” in cisplatin resistant breast cancer cells, which could be extended to the other hydrophobic drugs too.

#### 5.4. Conclusion

In summary, the present work demonstrates co-delivery of cisplatin and DOX using biodegradable triple layer nanoparticles in order to achieve synergistic killing in resistant breast cancer cells. TLNs were designed using biocompatible PEG shell and biodegradable PCL and CPCL for multi-drug delivery. In fabrication of TLNs, cisplatin was chelated to COOH groups of CPCL block and DOX was physically encapsulated in to PCL layer. The TLNs were found to be very stable in water. In PBS > 90% of cisplatin and < 60 % of DOX was stabilised by the TLNs that is evidently attributed to the protection rendered by the middle PCL layer. *In vitro* drug release studies revealed that the PEG shell and PCL layer protected cisplatin drug against detoxification by the cytoplasmic thiol residues, i.e. GSH. Further, the biodegradable aliphatic PCL ester backbone was found to be ruptured upon exposure to esterase

enzyme at conditions identical to that of intracellular compartments, where cisplatin showed controlled release up to 48 h. Cytotoxicity of the polymer and dual drug loaded nanoparticles was tested in WT-MEF, HeLa and MCF 7 cell lines. The nascent polymers were found to be biocompatible and non-toxic to cells. In HeLa cell lines, both the free cisplatin drug and polymer-cisplatin core-shell nanoparticle showed almost identical cytotoxicity. Free cisplatin drug failed to kill all the cells in MCF 7 and more than 50 % of the cells were viable even at very high drug concentration. Over-expression of GSH in MCF 7 is responsible for poor killing by free cisplatin drug. This selective and enhanced cell killing in MCF 7 cells by the polymer nanoparticle was due to their resistance against drug detoxification by GSH. The dual drug loaded nanoparticles emanated in 3 fold excess cell killing over polymer-cisplatin conjugates, which can be attributed to the fact that DOX increased the stability of the DNA-Pt adduct and quenched the DNA repair mechanism efficiency. The dual loaded TLNs containing cisplatin and DOX act synergistically to promote killing of breast cancer cells. The CI values showed that the dual loaded nanoparticles exhibited synergistic killing, however when cisplatin and DOX were administered as a cocktail they showed antagonistic effect. Further the cellular uptake and nuclear localization of dual drug loaded nanoparticles (TLN-DOX) in MCF 7 cells was scrutinized using confocal microscopy. Thus, the novel custom designed dual loaded triple layer nanoparticles manifested as potent candidate to accomplish synergistic killing in cisplatin resistant breast cancer cells.

## **5.5. References**

1. Hoeschele, J. D. *Dalton Trans.* **2009**, 39, 10648–10650.
2. Martindale: The complete drug reference, ed. Sweetman, S. C. *Pharmaceutical Press, London*, **2007**, 35th edn.
3. Wang, X.; Liu, Q.; Hou, B.; Zhang, W.; Yan, M.; Jia, H.; Li, H.; Yan, D.; Zheng, F.; Ding, W.; Yi, C.; Wang, H. *PLoS One* **2013**, 8, e73942.
4. Holohan, C.; Van Schaeybroeck, S.; Longley, D. B.; Johnston, P. G. *Nat. Rev. Cancer* **2013**, 13, 714–726.
5. Longley, D. B.; Johnston, P. G. *J. Pathol.* **2005**, 205, 275–292.
6. Wang, D.; Lippard, S. J. *Nat. Rev. Drug Discovery* **2005**, 4, 307.
7. Jamieson, E. R.; Lippard, S. J. *Chem. Rev.* **1999**, 99, 2467.
8. Perry, R. R.; Mazzeta, J.; Levin, M.; Barranco, S. C. *Cancer* **1993**, 72, 783–787.
9. Kasherman, Y.; Sturup, S.; Gibson, D.; *J. Med. Chem.* **2009**, 52, 4319–438.
10. Syng-ai, C.; Kumari, A. L.; Khar, A. *Mol. Cancer Ther.* **2004**, 3, 1101–1107.
11. Kelland, L.; *Nat. Rev. Cancer*, **2007**, 7, 573–584.
12. Lehár, J.; Krueger, A. S.; Avery, W.; Heilbut, A. M.; Johansen, L. M.; Price, E. R.; Rickles, R. J.; Short, G. F.; Staunton, J. E.; Jin, X.; Lee, M. S.; Zimmermann, G. R.; Borisy, A. A. *Nat. Biotechnol.* **2009**, 27, 659–666.
13. Jia, J.; Zhu, F.; Ma, X.; Cao, Z. W.; Li, Y. X.; Chen, Y. Z. *Nat. Rev. Drug Discovery* **2009**, 8, 111–128.
14. Lee, J.; Park, J. O.; Kim, W. S.; Park, S. H.; Park, K. W.; Choi, M. S.; Lee, J. H.; Koh, K. C.; Paik, S. W.; Yoo, B. C.; Joh, J.; Kim, K.; Jung, C. W.; Park, Y. S.; Im, Y.-H.; Kang, W. K.; Lee, M. H.; Park, K. *Cancer Chemother. Pharmacol.* **2004**, 54, 385–390.
15. Thigpen, J. T.; Brady, M. F.; Homesley, H. D.; Malfetano, J.; DuBeshter, B.; Burger, R. A.; Liao, S. *J. Clin. Oncol.* **2004**, 22, 3902–3908.
16. Aapro, M. S.; van Wijk, F. H.; Bolis, G.; Chevallier, B.; van der Burg, M. E. L.; Poveda, A.; de Oliveira, C. F.; Tumolo, S.; Scotto di Palumbo, V.; Piccart, M.; Franchi, M.; Zanaboni, F.; Lacave, A. J.; Fontanelli, R.; Favalli, G.; Zola, P.; Guastalla, J. P.; Rosso, R.; Marth, C.; Nooij, M.; Presti, M.; Scarabelli, C.; Splinter, T. A. W.; Ploch, E.; Beex, L. V. A.; Huinink, W. B.; Forni, M.; Melpignano, M.; Blake, P.; Kerbrat, P.; Mendiola, C.; Cervantes, A. A.; Goupil; Harper, P. G.;

- Madronal, C.; Namer, M.; Scarfone, G.; Stoot, J. E. G. M.; Teodorovic, I.; Coens, C.; Vergote, I.; Vermorken, J. B. *Ann. Oncol.* **2003**, *14*, 441–448.
17. Nielsen, D.; Larsen, P. D. S. K.; Skovsgaard, O. P. H. T. *Cancer Chemother. Pharmacol.* **2000**, *46*, 459–466.
18. Martoni, A.; Bellucco, A.; Canova, N.; Pannuti, F. *Cancer. Oncology* **1989**, *46*, 109–116.
19. Nitiss, J. L. *Nat. Rev. Cancer* **2009**, *9*, 338–350.
20. Gomm, S. A.; Thatcher, N.; Cuthbert, A.; Chang, J.; Burmester, H. Hall, P. Carroll, K. B. *Br J Cancer.* **1991**, *63*, 293–297.
21. Kim, Y. H.; Shin, S. W.; Kim, B. S.; Kim, J. H.; Kim, J. G.; Mok, Y. J.; Kim, C. S.; Rhyu, H. S.; Hyun, J. H.; Kim, J. S. *Cancer* **1999**, *85*, 295–301.
22. Muggia, F. M.; Braly, P. S.; Brady, M. F.; Sutton, G.; Niemann, T. H.; Lentz, S. L.; Alvarez, R. D.; Kucera, P. R.; Small, J. M. *J. Clin. Oncol.* **2000**, *18*, 106.
23. Eder, J. P., Jr.; Chan, V. T. W.; Ng, S.-W.; Rizvi, N. A.; Zacharoulis, S.; Teicher, B. A.; Schnipper, L. E. *Cancer Res.* **1995**, *55*, 6109–6116.
24. Hu, C. M.; Aryal, S.; Zhang, L. F. *Ther. Delivery* **2010**, *1*, 323–334.
25. Davis, M. E.; Chen, Z.; Shin, D. M. *Nat. Rev. Drug Discovery* **2008**, *7*, 771–782.
26. Peer, D.; Karp, J. M.; Hong, S.; Farokhzad, O. C.; Margalit, R.; Langer, R. *Nat. Nanotechnol.* **2007**, *2*, 751–760.
27. Fang, J.; Nakamura, H.; and Maeda, H. *Adv. Drug Delivery Rev.*, **2011**, *63*, 136–151.
28. Shanmugam, V.; Chien, Y-H.; Cheng, Y-H.; Liu, T-Y.; Huang, C-C.; Su, C-H.; Chen, Y-S.; Kumar, U.; Hsu, H-F.; Yeh, C-S. *Appl. Mater. Interfaces* **2014**, *6*, 4382–4393.
29. Lee, S-M, O’Halloran, T. V.; Nguyen, S. B. T. *J. Am. Chem. Soc.* **2010**, *132*, 17130–17138.
30. Liao, L.; Liu, J.; Dreaden, E. C.; Morton, S.W.; Shopsowitz, K. E.; Hammond, P. T.; Johnson, J.A. *J. Am. Chem. Soc.* **2014**, *136*, 5896–5899.
31. Kang, H-C.; Cho, H.; Bae, Y-H. *Mol. Pharmaceutics* **2015**, *12*, 2845–2857.
32. Rainbolt, E. A.; Washington, K. E.; Biewer M.C.; Stefan, M.C. *Polym. Chem.*, **2015**, *6*, 2369–2381
33. Surnar, B.; Jayakannan, M.; *Biomacromolecules* **2013**, *14*, 4377–4387.

34. Surnar, B.; Pramod, P. S.; Jayakannan, M.; *Z. Anorg. Allg. Chem.* **2014**, *640*, 1119–1126.
35. Surnar, B.; Sharma, K.; Jayakannan, M. *Nanoscale* **2015**, *7*, 17964–17979.
36. Ski, R. W.; Kuduk-Jaworska, J.; Michalska, D. *J Mol Struc-Theochem.* **2006**, *758* 169–179.
37. Allen, A. D.; Theophanides, T. *Can. J. Chem.* **1964**, *42*, 1551-1554.
38. Xu, J.; Fu, Q.; Ren, J-M.; Bryant, G.; Qiao, G. G. *Chem. Commun.* **2013**, *49*, 33–35.
39. Todd, R. C.; Lovejoy, K. S.; Lippard, S. J. *J. Am. Chem. Soc.* **2007**, *129*, 6370-6371
40. Pramod, P. S.; Takamura, K.; Chaphekar, S.; Balasubramanian, N.; Jayakannan, M. *Biomacromolecules* **2012**, *13*, 3627–3640.
41. Min, Y.; Mao, C-Q.; Chen, S.; Ma, G.; Wang, J.; Liu, Y. *Angew. Chem. Int. Ed.* **2012**, *51*, 6742-6747.
42. K. Osada, H. Cabral, Y. Mochida, S. Lee, K. Nagata, T. Matsuura, M. Yamamoto, Y. Anraku, K. Kataoka, *J. Am. Chem. Soc.* **2012**, *134*, 13172-13175.
43. T. C. Johnstone, N. Kulak, E. C. Pridgen, O. C. Farokhzad, R. Langer, S.J. Lippard, *ACS NANO* **2013**, *7*, 5675-5683.
44. Chou, T.-C.; Talalay, P. *Trends Pharmacol. Sci.* **1983**, *4*, 450–454.



*Summary and Future Directions*

---

The thesis entitled “Polycaprolactone Block Copolymer Nano-scaffolds for Drug Delivery to Cancer Cells” deals with design and development of amphiphilic carboxylic polycaprolactone (CPCL) block copolymer nano-aggregates for drug delivery applications. The thesis is focused on the synthesis of PCL block copolymers with narrow molecular weights in order to further render precise control over the size and shape of the self-assembled nano-carriers such as micelles and vesicles. These biodegradable block copolymer nano-assemblies were demonstrated for delivering a wide range of anticancer drugs such as doxorubicin (DOX), cisplatin, camptothecin, and Ibuprofen, etc. The new polymer scaffolds were employed as oral delivery vehicles under gastrointestinal (GI) tract and also for the intracellular administration of drugs in cancer cells.

In chapter 2, a new carboxylic-functionalized caprolactone monomer was designed and synthesized from commercial starting materials and further subjected to ring opening polymerization. The carboxylic substituted PCL block copolymers PEG-*b*-CPCL<sub>x</sub> resulted in the production of water soluble 80-250 nm sized vesicles. The characterization of these PCL vesicles was carried out by various techniques such as DLS, SLS, FESEM, HR-TEM, WCA and so on. The pH responsiveness of these PCL vesicles was studied using zeta potential and DLS, which showed that the vesicles were stable upto pH < 6.0, however at neutral or basic pH ≥ 7.4 the carriers were ruptured causing the release of drug molecules. The loading and delivery of both water-soluble molecules such as Rh-B and hydrophobic drugs like IBU or CPT were investigated. *In vitro* drug release revealed that the drugs released exclusively under simulated intestinal fluid conditions that is similar to the physiological environment of the small intestine.

In chapter 3, new class of hydrogen bonded and enzyme-responsive (biodegradable) PCL diblock copolymer nanoparticles were designed and developed for loading and delivering anticancer drugs by tuning the biodegradability and hence the release mechanism as “burst” and “controlled” at the intracellular compartments in cervical (HeLa) and breast (MCF 7) cancer cells. New amide and ester substituted  $\omega$ -caprolactone monomers were tailor-made through multi-step synthesis starting from commercially available 1,4-cyclohexanol as the starting material. Their ring opening polymerization was carried out employing PEG 2000 mono methyl ether as an initiator in order to synthesize hydrogen bonded amide and non-hydrogen bonded ester PEG-*b*-PCL diblock copolymers. These polymers self-assembled as nanoparticles in water upon DOX loading. The nature of the linear or bulky substituent had great impact on the drug loading content of the diblock

copolymer nanoparticles. In order to study the hydrogen bonding interaction in the amide diblock in detail, variable temperature  $^1\text{H-NMR}$  analysis was performed. The *in vitro* drug release studies revealed that the aliphatic polyester PCL chain was readily degradable by lysosomal esterase enzyme in PBS at 37 °C to release the loaded drugs. The hydrogen bonded amide copolymer nanoparticles were very stable and as a result, they degraded slowly in the presence of enzyme to release drugs in a much more controlled manner over a prolonged period. On the other hand, the non-hydrogen bonded ester copolymers underwent burst uncontrolled release of drugs. This difference in the enzymatic degradation among the amide diblock copolymers (hydrogen bonded) and ester diblocks (non-hydrogen bonded) was further verified by determining their cell killing ability in HeLa and MCF 7 cell lines. The nascent polymer scaffolds were non-toxic to cells up to 40  $\mu\text{g/mL}$  as per the *in vitro* cytotoxicity tests. The DOX loaded nanoparticles accomplished more than 90 % cell killing in both HeLa and MCF 7 cells. Time-dependent *in vitro* cell studies further confirmed that the DOX loaded amide diblocks exhibited slower killing (20 % less) compared to the non-hydrogen bonded ester blocks. Both *in vitro* drug release profiles and *in vitro* cell line studies clearly stated that the hydrogen-bonding led to controlled drug delivery in the diblock copolymer design. The hydrogen bonding interaction was proven to play an important tool in controlling the drug release profiles of the anticancer drugs at the cancer cells. The cellular uptake of the DOX loaded polymer nanoparticles and their cleavage in the cytoplasm was further supported by the confocal microscope imaging.

In chapter 4, the concept of biodegradable diblock copolymer core-shell nanoparticle assemblies for cisplatin delivery against detoxification by cytoplasmic thiol residues was successfully demonstrated in breast cancer cells. The complexation of cisplatin aquo complex with the above said diblock copolymers produced core-shell nanoparticles. In this process, the core of the particles was fixed as 75 nm and the hydrophilic PEG shell was varied by varying the PEG chain length in the ROP process. The core-shell nanoparticles were found to be very stable in FBS and water. *In vitro* drug release studies in PBS and saline revealed that the drug stability increased with increase in the PEG shell protection layer, which could be attributed to the PEG shell protection rendered to the cisplatin drug against attack by the cytoplasmic thiol residues GSH and they were free from detoxification. Also the biodegradable aliphatic PCL ester backbone was found to provide additional shielding against GSH action on the cisplatin core and it ruptured only upon exposure to esterase

enzyme at conditions identical to that of intracellular compartments. Cytotoxicity of the polymer and polymer-cisplatin conjugates was tested in MCF 7 and HeLa cell lines. The nascent polymers were found to be biocompatible and non-toxic to cells. In HeLa cell lines, both the free cisplatin drug and polymer-cisplatin core-shell nanoparticle showed almost identical cytotoxicity. Free cisplatin drug failed to kill all the cells in MCF 7 and the cells were viable more than 50 % even at very high drug concentration. The poor killing by free cisplatin drug was attributed to over-expression of GSH in MCF 7. The polymer-cisplatin nanoparticles showed enhanced cell killing in MCF 7 and the cell viability was found to be < 10 % at 4 µg/mL drug concentration. This selective and enhanced cell killing in MCF 7 cells by the polymer nanoparticle was attributed to their resistance to drug detoxification by GSH. Cellular uptake of the nanoparticles in the cytoplasm and perinuclear environment assemblies was confirmed by confocal and fluorescence microscopic analysis using Nile red as a fluorophore.

In chapter 5, the combination delivery of cisplatin and DOX using triblock copolymer nanoparticles was carried out in order to achieve synergistic killing in resistant breast cancer cells. TLNs were designed using biocompatible PEG shell and biodegradable PCL and CPCL middle and inner core for multi-drug delivery. In the fabrication of TLNs, cisplatin was chelated to COOH groups of CPCL block and DOX was physically encapsulated into the PCL layer. The TLNs were found to be very stable in water. TLNs stabilized > 90% of cisplatin and < 60 % of DOX in PBS, which is evidently attributed to the protection rendered by the middle PCL layer. *In vitro* drug release studies revealed that the PEG shell and PCL layer protected cisplatin drug against detoxification by the cytoplasmic thiol residues, i.e. GSH. Further, the biodegradable aliphatic PCL ester backbone ruptured upon exposure to esterase enzyme at conditions identical to that of intracellular compartments, where cisplatin showed controlled release up to 48 h. Cytotoxicity of the polymer and dual drug loaded nanoparticles was tested in WT-MEF, HeLa, and MCF 7 cell lines. The nascent polymers were found to be biocompatible and non-toxic to cells. In HeLa cell lines, both the free cisplatin drug and polymer-cisplatin core-shell nanoparticle showed almost identical cytotoxicity. However, in MCF 7 cell lines, free cisplatin drug failed to kill all the cells and more than 50 % of the cells were viable even at very high drug concentration. Over-expression of GSH in MCF 7 is responsible for poor killing by free cisplatin drug. Polymer nanoparticles showed selective and enhanced cell killing

in MCF 7 cells, which was due to their resistance against drug detoxification by GSH. The dual drug loaded nanoparticles emanated in 3 fold excess cell killing over polymer-cisplatin conjugates, which can be attributed to the increased stability of the DNA-Pt adduct rendered by DOX that retards the DNA repair mechanism efficiency. The dual loaded TLNs containing cisplatin and DOX act synergistically to enhance the killing of breast cancer cells. The CI values showed that the dual loaded nanoparticles exhibited synergistic killing, however when cisplatin and DOX were administered as a cocktail they showed antagonistic effect.

### Future Directions

This thesis discusses in detail the synthesis of homopolymers, diblock copolymers and triblock copolymers of the novel carboxylic substituted caprolactone monomer. These polymers were completely characterized using standard techniques. These polymers self-assembled into vesicles and micelles that were found to be pH responsive and enzymatically degradable at conditions similar to the intracellular compartments. The polymeric scaffolds efficiently loaded drugs like Ibuprofen, CPT, DOX and cisplatin that could be orally and intravenously delivered at the tumor specific site respectively.

The pH responsive vesicles showed great potential in delivering drugs like IBU and CPT to the colon whilst protecting them against the harsh pH conditions of stomach. This approach could be extended to the delivery of multiple drugs for oral delivery applications. Around 20 different drugs (NSAIDS) face the problems of rapid systemic elimination causing shorter half-life and these are also known to interfere with the stomach's defence mechanisms. Proteins like insulin still lack efficient oral delivery carriers and hence, these polymeric scaffolds can be useful in protecting these drugs in the stomach and deliver only at the target specific site.

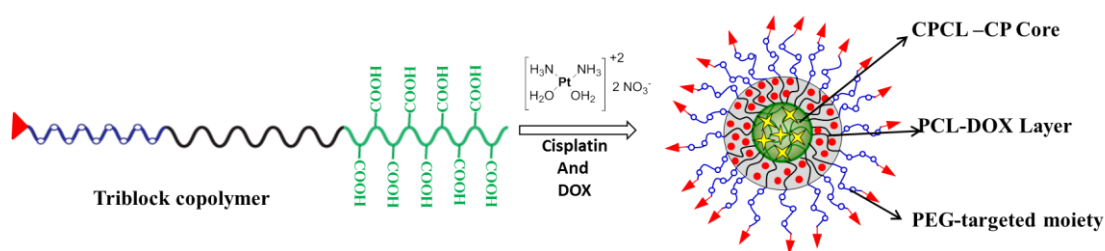


**Figure 6.1.** Future directions of thesis work: Schematic representation of new dual loaded triple layer nanoparticle attached with an imaging agent, cell penetrating peptide and targeting antibody

The carboxylic substituted polymers were able to chelate the anticancer drug cisplatin as well as bring about apoptosis in the breast cancer cells with the over expression of GSH. However, there is an urgent need to bring about target specificity in these scaffolds in order to overcome the various side effects associated with cisplatin delivery. The carboxylic side chain could be used to tag antibodies like Alemtuzumab for lymphocytic lymphoma, Rituximab for Hodgkin lymphoma, Trastuzumab for breast cancer, Cetuximab for colorectal tumor, Panitumumab for Metastatic colorectal tumor in order to enhance intracellular delivery and at the same time overcome side effects associated with non-specific delivery (see figure 6.1). This functional moiety could even be conjugated with drugs to generate prodrugs that deliver the active chemotherapeutic agent only at the specific tumor site.

The triblock cisplatin stitched nanoparticles brought about high levels of cytotoxicity in specifically the breast cancer cells. But the next level could be to tag these nanoparticles with fluorescent imaging dyes through which these particles could be monitored *in vivo*. All these aforementioned scaffolds need to be tested in mice models.

***List of Publications***

---

---

**Publications in International Journals:**

**List of Publications:**

1. **Surnar, B.;** Jayakannan, M. Stimuli-Responsive Poly(caprolactone) Vesicles for Dual Drug Delivery under the Gastrointestinal Tract. *Biomacromolecules* **2013**, *14*, 4377–4387.
2. **Surnar, B.;** Pramod, P. S.; Jayakannan, M. Z. Biodegradable Block Copolymer Scaffolds for Loading and Delivering Cisplatin Anticancer Drug. *Z. Anorg. Allg. Chem.* **2014**, *640*, 1119–1126.
3. **Surnar, B.;** Sharma, K.; Jayakannan, M. Core–shell polymer nanoparticles for prevention of GSH drug detoxification and cisplatin delivery to breast cancer cells. *Nanoscale* **2015**, *7*, 17964–17979.
4. Kulkarni, B.; **Surnar, B.;** Jayakannan, M. Dual Functional Nanocarrier for Cellular Imaging and Drug Delivery in Cancer Cells Based on  $\pi$ -Conjugated Core and Biodegradable Polymer Arms. *Biomacromolecules* **2016**, *17*, 1004–1016. (*This work is not included in thesis*).
5. Kashyap, S.; Nitish, S.; **Surnar, B.;** Jayakannan, M. Enzyme and Thermal Dual Responsive Amphiphilic Polymer Core–Shell Nanoparticle for Doxorubicin Delivery to Cancer Cells. *Biomacromolecules* **2016**, *17*, 384–398. (*This work is not included in thesis*).
6. **Surnar, B.;** Jayakannan, M. Hydrogen-Bond Controlled Drug Delivery to Cancer Cells by Programming the Enzyme Degradation in Block Copolymer Nano-assemblies. *Manuscript submitted*.
7. **Surnar, B.;** Jayakannan, M. Triple Layer Nanoparticle Approach for Cisplatin-Doxorubicin Combination Therapy. *Manuscript submitted*